UNIVERSITÉ DU QUÉBEC À TROIS-RIVIÈRES

ALLOCATION DE RESSOURCES OPTIMISÉE PAR IA POUR LES COMMUNICATIONS SANS FIL AMÉLIORÉES PAR LES RIS

THÈSE PRÉSENTÉE
COMME EXIGENCE PARTIELLE DU
DOCTORAT EN GÉNIE ÉLECTRIQUE

PAR
SAMANEH BIDABADI

NOVEMBRE 2024

UNIVERSITÉ DU QUÉBEC À TROIS-RIVIÈRES

DOCTORAT EN GÉNIE ÉLECTRIQUE (PH.D.)

Direction de recherche :

Prof. Messaoud Ahmed Ouameur	Directeur de recherche
Prof. Miloud Bagaa	Codirecteur de recherche

Jury d'évaluation:

Prof. Messaoud Ahmed Ouameur	Directeur de recherche
Prof. Miloud Bagaa	Codirecteur de recherche
Prof. Alben Cardenas	Président du jury
Prof. Abdellah Chehri	Évaluateur externe
Prof. Frederique Domingue	Évaluateur interne

Thèse soutenue le 1er novembre 2024.

Résumé

Les réseaux 6G (en anglais 6G, sixth generation) prévus présentent de nombreux défis et opportunités pour améliorer les débits de données, l'EE (en anglais EE, Energy Efficiency), la couverture mondiale, la fiabilité et la latence. Ces systèmes utilisent des technologies innovantes telles que les RIS (en anglais RIS, Reconfigurable Intelligent Surfaces), le MIMO (en anglais MIMO, Multiple Input Multiple Output) et les communications THz (en anglais THz, Terahertz Communications). Les canaux sans fil intelligents et adaptables proposés par la technologie RIS permettent un contrôle dynamique de la propagation du signal en manipulant l'environnement sans fil. Il est possible d'améliorer considérablement les performances du système en optimisant le déploiement et l'utilisation des systèmes de communication assistés par RIS. L'EE est un indicateur clé de performance, et la technologie RIS présente des perspectives prometteuses pour l'améliorer grâce à une consommation d'énergie réduite ainsi qu'à une meilleure amplification et couverture du signal. Cependant, pour obtenir ces bénéfices, il est essentiel de surmonter les défis liés à la répartition des ressources, à l'optimisation de la configuration des RIS, et à l'application de techniques d'optimisation avancées.

Dans cette thèse, notre principal but est de trouver des solutions aux limites des méthodes d'optimisation basées sur les modèles pour les systèmes de communication assistés par RIS. Deux nouvelles méthodes sont présentées dans notre travail pour aborder le problème du taux de convergence de la méthode de gradient, à savoir l'GAW (en anglais GAW, Gradient Algorithm with Wolfe Conditions) et la méthode de maximisation de l'EE basée sur la TR (en anglais TR, Trust Region Method). Ces méthodes optimisent le problème de l'EE dans un système MISO (en anglais, Multiple Input Single Output) à porteuse unique assisté par RIS avec plusieurs utilisateurs. Non seulement nos méthodes suggérées présentent des taux de convergence plus élevés, mais elles entraînent également

une amélioration de l'EE par rapport aux approches antérieures. En outre, notre attention se porte sur la transmission en bande large à l'aide de canaux sélectifs en fréquence dans un système à MUs (en anglais MUs, Multi-Users), un domaine qui a été peu exploré dans diverses études. Il est plus difficile de concevoir un système à plusieurs porteuses que celui à porteuse unique, car il faut optimiser en même temps les coefficients de réflexion du RIS, la planification de transmission des MUs et l'allocation des ressources. En exploitant les bénéfices de l'OFDMA (en anglais OFDMA, Orthogonal Frequency Division Multiple Access), qui permet une répartition variable des ressources, nous élaborons le problème de l'EE pour un système MUs assisté par RIS à SISO (en anglais SISO, Single Input Single Output)-OFDMA. Afin de faire face à la complexité computationnelle, nous suggérons une solution sub-optimale qui repose sur l'optimisation de la borne inférieure de l'EE, assurant ainsi une efficacité computationnelle tout en obtenant des performances satisfaisantes. L'autre objectif du travail est de réaliser une étude exhaustive de l'utilisation des EM (en anglais EM, electromagnetic waves) des RIS pour améliorer les systèmes de communication assistés par RIS. Bien que les publications sur le sujet soient peu nombreuses, il existe une forte volonté d'améliorer les formulations de problèmes existantes en intégrant des modèles EM des RIS. Dans notre étude, nous incorporerons des modèles EM de RIS dans les cadres existants pour exploiter les capacités avancées de formation de faisceaux des architectures à BD-RIS (en anglais BD-RIS, Beyond Diagonal RIS) , ce qui améliore la souplesse opérationnelle. L'intégration du BD-RIS avec l'ISAC (en anglais ISAC, Integrated Sensing and Communication) a été recherchée en raison de son succès dans différents contextes de communication, mettant en évidence sa supériorité par rapport aux RIS diagonaux traditionnels dans les applications de communication et de détection. L'ISAC constitue une méthode innovante qui combine les objectifs de communication et de détection en utilisant des stratégies de co-conception.

Notre étude se concentre sur l'implémentation du BD-RIS pour améliorer l'efficacité énergétique en utilisant des stratégies de formation de faisceaux passives et actives, garantissant ainsi une performance robuste en communication et en détection. Cette tâche est complexe en raison des contraintes inhérentes aux configurations BD-RIS, telles que l'orthogonalité, les inégalités quartiques et la nature fractionnaire de la fonction objective. Afin de faire face à ces difficultés, nous employons des méthodes d'RL (en englais RL, Reinforcement Learning) avancées, telles que le TD3 (en anglais TD3, Twin Delayed Deep Deterministic Policy Gradient). Selon les simulations, l'incorporation du BD-RIS entraîne des améliorations significatives en termes d'efficacité énergétique par rapport aux références qui utilisent des RIS diagonaux et des RIS avec des décalages de phase aléatoires. En outre, l'efficacité de la méthode TD3 pour l'optimisation du problème complexe d'efficacité énergétique est mise en évidence par sa convergence constante.

Dédicaces

À mon père, dont l'encouragement inébranlable a été la lumière qui m'a toujours guidée et inspirée à poursuivre mes rêves ; à ma mère, pour sa patience infinie et sa compréhension, endurant avec grâce les longues années de mon absence ; et à mes sœurs, pour leur amour inconditionnel et leur soutien indéfectible, rendant chaque étape de ce voyage plus supportable et plus belle.

Remerciements

Je souhaite exprimer ma profonde gratitude à mon directeur de recherche, le Professeur Messaoud Ahmed Ouameur, pour ses conseils précieux tout au long de ce projet. Son soutien et ses recommandations ont été essentiels pour mener à bien cette recherche. Je tiens également à remercier sincèrement mon codirecteur, le Professeur Miloud Bagaa, pour son soutien et ses contributions scientifiques tout au long de ma thèse.

Je suis particulièrement reconnaissante envers le Professeur Daniel Massicotte pour son soutien tout au long de cette expérience ; ce fut un privilège de collaborer avec lui. Je souhaite également adresser ma gratitude au Professeur Anas Chaaban et au Professeur Felipe De Figueiredo pour leur aide et leur contribution scientifique lors de la rédaction de mes articles.

Je remercie chaleureusement toutes les personnes qui ont contribué au succès de ce projet.

Table des matières

Liste des tableaux

Liste des figures

Liste des Abbreviations

5G cinquième génération

6G sixième génération

UIT-R WP5D Secteur des radiocommunications de l'Union internationale des télécommunications Groupe de travail 5D

URLLC Communications ultra-fiables et à faible latence

RIS Surface Intelligente Reconfigurable

EM Ondes électromagnétiques

mmWave Ondes millimétriques

EE Efficacité énergétique

MIMO Entrées Multiples, Sorties Multiples

ML Apprentissage automatique

PINN Réseaux de neurones informés par la physique

RL Apprentissage par renforcement

DRL Apprentissage par renforcement profond

SNR Rapport signal sur bruit

EMOs Objets électromagnétiques

FEM Méthode des éléments finis

FDTD Méthode des différences finies dans le domaine temporel

MoM Méthode des moments

EMF Exposition au champ électromagnétique

SAR Taux d'absorption spécifique

SIMO Entrée unique, sorties multiples

MISO Entrées multiples, sortie unique

ULA Réseau linéaire uniforme

DOA Direction d'arrivée

SISO Entrée unique, sortie unique

STAR Transmission et réflexion simultanées

DoFs Degrés de liberté

IDU Utilisateur décodeur d'informations

EHU Utilisateur récolteur d'énergie

LISs Grandes surfaces intelligentes

AO Optimisation alternée

MM Techniques de majorisation-minimisation

SCA Optimisation convexe successive

SDR Relaxation semi-définie

BCD Descente par coordonnées bloquées

CCP Procédure convexe-concave

GA Algorithme génétique

PSO Optimisation par essaim particulaire

BPSO Optimisation binaire par essaim particulaire

ACO Optimisation par colonies de fourmis

MOLACO Optimisation multi-objectif par colonies de fourmis paresseuses

FL Apprentissage fédéré

NNs Réseaux de neurones

MTS Surface métamatériau

ANN Réseaux de neurones artificiels

CNNs Réseaux de neurones convolutionnels

cDC-GAN Réseau antagoniste génératif convolutionnel profond conditionnel

cDC-VAE Autoencodeur variationnel convolutionnel profond conditionnel

AI Intelligence artificielle

SVM Machine à vecteurs de support

PIDL Apprentissage profond informé par la physique

SRR Résonateur à anneau fendu

MAE Erreur moyenne absolue

MI Information mutuelle

CSI Information de l'état du canal

DMT Compromis diversité-multiplexage

OMA Accès multiple orthogonal

NOMA Accès multiple non-orthogonal

PGM Méthode du gradient projeté

OP Probabilité de panne

EMI Interférence électromagnétique

IM Méta-surface d'information

EH Récolte d'énergie

OAM Moment angulaire orbital

ISAC Système Intégré de Détection et Communication

NTN Réseaux Non-Terrestres

THz Terahertz

MI Interférences Mutuelles

LOS Ligne de Visée

CUs Utilisateurs de Communication

MUI Interférences Multi-Utilisateurs

IS Surfaces Intelligentes

DMA Contrôle de Phase Dynamique

STAR-RIS Transmission et Réflexion Simultanées RIS

RIS Surface Intelligente Reconfigurable

SIM Configurations Empilées

KPI Indicateurs Clés de Performance

EM Ondes Électromagnétiques

BD-RIS RIS Au-Delà de la Diagonale

OFDMA Accès Multiple par Division de Fréquence Orthogonale

EE Efficacité Énergétique

MIMO Entrées Multiples, Sorties Multiples

SE Efficacité Spectrale

SISO Entrée Unique, Sortie Unique

MINLP Programmation Non Linéaire en Nombres Entiers Mixtes

AO Optimisation Alternée

DRL Apprentissage par Renforcement Profond

MU Multi-Utilisateurs

SINR Rapport Signal sur Interférence Plus Bruit

SGD Descente de Gradient Stochastique

SA Recuit Simulé

PSO Optimisation par Essaim Particulaire

GA Algorithme Génétique

AF Amplifier-et-Retour

GAW Algorithme de Gradient avec Conditions de Wolfe

TR Méthode de Région de Confiance

SCMs Modèles Causaux Structurels

5G Fifth generation

6G Sixth generation

ITU-R WP5D International Telecommunication Union Radiocommunication Sector Working Party 5D

URLLC Ultra-reliable low latency communications

RIS Reconfigurable Intelligent Surface

EM Electromagnetic waves

mmWave Millimeter wave

EE Energy Efficiency

MIMO Multiple Input, Multiple Output

ML Machine Learning

PINN Physics-Informed Neural Networks

RL Reinforcement Learning

DRL Deep Reinforcement Learning

SNR Signal-to-Noise Ratio

EMOs Electromagnetic Objects

FEM Finite Element Method

FDTD Finite Difference Time Domain

MoM Method of Moments

EMF Electromagnetic Field Exposure

SAR Specific Absorption Rate

SIMO Single Input, Multiple Outputs

MISO Multiple Inputs, Single Output

ULA Uniform Linear Array

DOA Direction of Arrival

SISO Single Input, Single Output

STAR Simultaneous Transmission and Reflection

DoFs Degrees of Freedom

IDU Information Decoder User

EHU Energy Harvesting User

LISs Large Intelligent Surfaces

AO Alternating Optimization

MM Majorization-Minimization Techniques

SCA Successive Convex Approximation

SDR Semi-Definite Relaxation

BCD Block Coordinate Descent

CCP Convex-Concave Procedure

GA Genetic Algorithm

PSO Particle Swarm Optimization

BPSO Binary Particle Swarm Optimization

ACO Ant Colony Optimization

MOLACO Multi-Objective Lazy Ant Colony Optimization

FL Federated Learning

NNs Neural Networks

MTS Metamaterial Surface

ANN Artificial Neural Networks

CNNs Convolutional Neural Networks

cDC-GAN Conditional Deep Convolutional Generative Adversarial Network

cDC-VAE Conditional Deep Convolutional Variational Autoencoder

DGMs Deep Generative Models

AI Artificial Intelligence

SVM Support Vector Machine

PIDL Physics-Informed Deep Learning

MAE Mean Absolute Error

IDBP Information-Driven Branch Pruning

ADC Analog-to-Digital Converters

MI Mutual Information

CSI Channel State Information

OAM Orbital Angular Momentum

NOMA Non-Orthogonal Multiple Access

PGM Projected Gradient Method

OP Outage Probability

EMI Electromagnetic Interference

IM Information Metasurface

EH Energy Harvesting

ISAC Integrated Sensing and Communication

NTN Non-Terrestrial Networks

THz Terahertz

MI Mutual Interference

LOS Line of Sight

CUs Communication Users

MUI Multi-User Interference

IS Intelligent Surfaces

DMA Dynamic Phase Control

STAR-RIS Simultaneous Transmission and Reflection RIS

RIS Reconfigurable Intelligent Surface

SIM Stacked Configurations

KPI Key Performance Indicators

EM Electromagnetic Waves

BD-RIS Beyond Diagonal RIS

OFDMA Orthogonal Frequency Division Multiple Access

EE Energy Efficiency

SE Spectral Efficiency

MINLP Mixed Integer Non-Linear Programming

AO Alternating Optimization

MU Multi-Users

SINR Signal to Interference Plus Noise Ratio

SGD Stochastic Gradient Descent

SA Simulated Annealing

PSO Particle Swarm Optimization

GA Genetic Algorithm

AF Amplify-and-Forward

GAW Gradient Algorithm with Wolfe Conditions

TR Trust Region Method

SCMs Structural Causal Models

Chapitre 1 - Introduction

1.1 Contexte générale de recherche

Le trafic de données mobiles mondial devrait croître à un rythme exponentiel d'ici 2030, dépassant les 5000 exaoctets par mois. Cela constitue un défi majeur pour les réseaux de la 5G (en anglais 5G, cinquième génération) actuels en termes de consommation d'énergie, de coûts et de complexité [7]. Les communautés académiques et industrielles mondiales, en collaboration avec des organisations de normalisation, se concentrent sur le développement des réseaux sans fil de la 6G (en anglais 6G, sixième génération) afin de répondre à cette demande croissante et d'encourager de nouvelles applications. Un travail préliminaire approfondi et un ensemble de propositions de normes ont été lancés par le programme de recherche mondial "6Genesis" en 2018 afin de déterminer le cadre de la 6G, les scénarios d'utilisation, les exigences techniques essentielles et les technologies habilitantes. À l'occasion de la 44e réunion du Secteur des radiocommunications de l'UIT-R WP5D (en anglais ITU-R WP5D, International Telecommunication Union Radiocommunication Sector Working Party 5D) en juin 2023, le groupe de promotion IMT-2030 a présenté une nouvelle perspective globale de la 6G. [4].

La 6G devrait surpasser la 5G dans certains domaines, comme l'illustre la Figure 1.1 [1]-[8]. Évoluant à partir de la 5G, la 6G est conçue pour garantir une couverture mondiale sans faille, étendre l'utilisation des ressources spectrales au-delà des bandes de fréquences mmWave (en anglais mmWave, millimeter wave) et créer un jumeau physique-numérique du monde pour soutenir une large gamme de nouvelles applications et services intelligents. Cette évolution vise à impulser la prochaine vague de croissance économique numérique et de transformations sociétales durables. En s'inspirant des

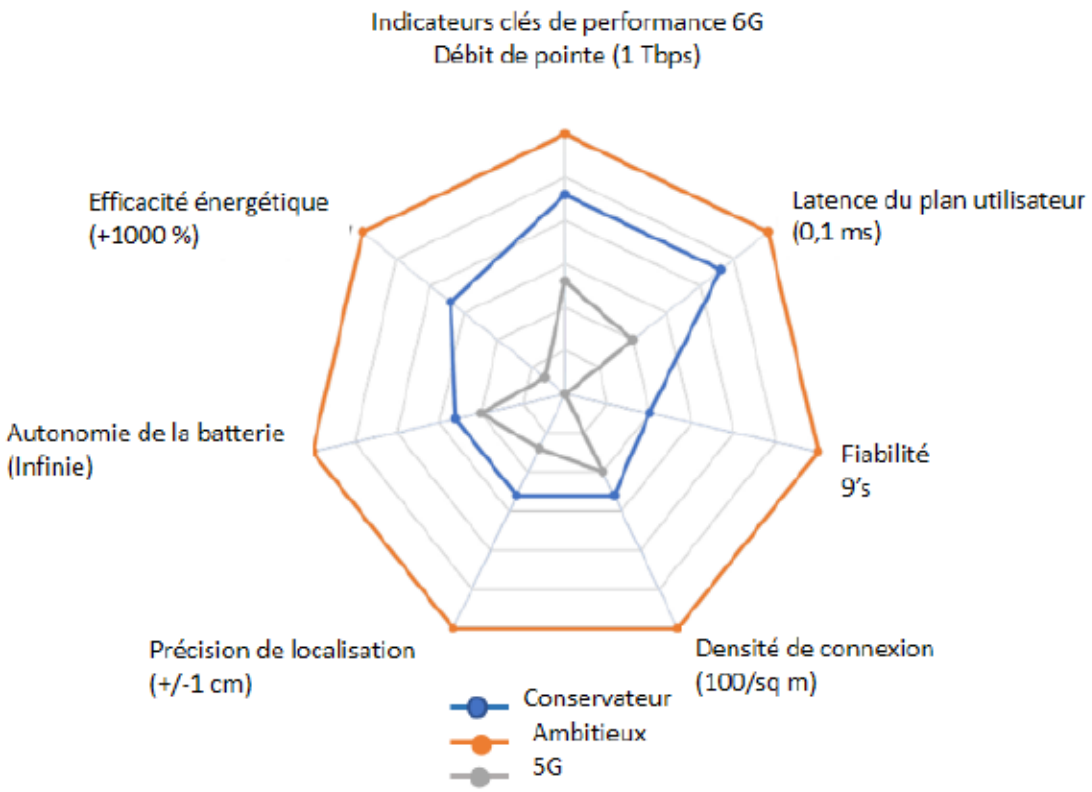

Figure 1.1 Spécifications pour les communications sans fil de prochaine génération [1].

expériences passées, les nouvelles recommandations pour la 6G élargissent les capacités de l'IMT-2020 et introduisent trois innovations clés, comme illustré dans la Figure 1.2 [2]. Les recommandations IMT-2030 pour la 6G améliorent les capacités de la 5G en faisant évoluer l'URLLC (en anglais URLLC, ultra-reliable low latency communications) vers l'HRLLC (en anglais HRLLC, hyper-reliable low latency communications), l'eMBB (en anglais eMBB, enhanced mobile broadband) vers la communication immersive, et le mMTC (en anglais mMTC, massive machine type communications) vers la communication massive. Elles introduisent des fonctionnalités innovantes telles que la virtualisation de réseau basée sur l'IA (en anglais AI, Artificial Intelligence), l'ISAC

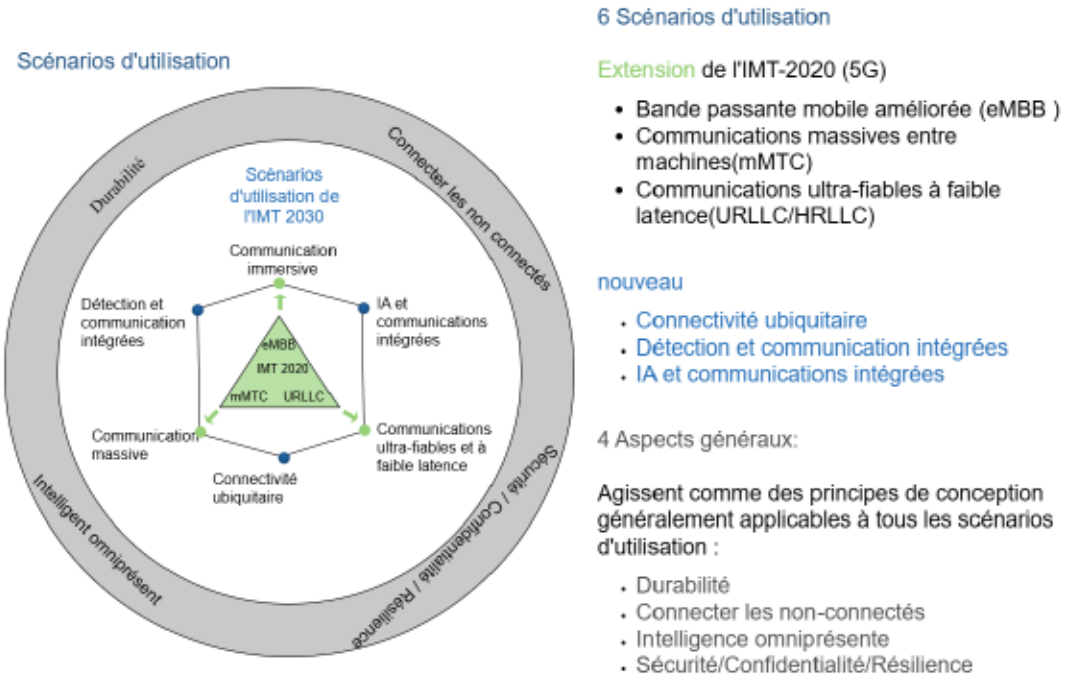

Figure 1.2 Illustration des capacités, extensions et défis associés à l'IMT 2030 [2].

(en anglais ISAC, Integrated Sensing and Communication), et l'NTN (en anglais NTN, Non-Terrestrial Networks) pour une connectivité omniprésente. Les principaux défis soulignés incluent l'assurance de la fiabilité de la transmission THz (en anglais THz, Terahertz), l'harmonisation des technologies cellulaires et non cellulaires, et la résolution des préoccupations liées à la confidentialité des données en raison de la dépendance du réseau aux algorithmes basés sur les données [2].

Une plus grande largeur de bande, des réseaux d'antennes massives et des bandes de fréquences plus élevées (du mmWave au THz) permettront un sondeur de haute résolution et de haute précision dans les systèmes de communication mobile 6G. Cela facilitera l'intégration de l'ISAC au sein d'un même système pour leur bénéfice mutuel [8]. Il existe différentes façons de combiner les fonctions de sensation et de communication. En les considérant comme des objectifs distincts, la

stratégie de coexistence agit conjointement pour minimiser les conflits et optimiser les performances. Toutefois, cela limite les degrés de liberté spatiotemporels et l'utilisation des ressources. Au-delà de la coexistence, l'idée fondamentale de l'ISAC est de concevoir les opérations de sensation et de communication de manière à permettre le partage des ressources telles que le matériel, l'énergie et la bande passante. La localisation ultra-haute précision, le suivi, l'imagerie, la cartographie, la reconstruction de l'environnement, la détection humaine augmentée et la reconnaissance des gestes/activités sont autant d'exemples d'applications de sensation [9]. L'un des nombreux obstacles à la mise en œuvre des systèmes ISAC est la possibilité d'interférences mutuelles (en anglais MI, mutual interference) entre les processus de communication et de détection. L'atténuation élevée de la propagation constitue un problème particulier pour les systèmes ISAC opérant dans la bande millimétrique, et le blocage de la ligne de visée (en anglais LOS, line of sight) entre la station de base (en anglais BS, base station) et les utilisateurs de communication (en anglais CUs, communication users) ou les cibles nuit considérablement à leurs performances. Une solution potentielle pour résoudre ces problèmes est d'utiliser les Surfaces Intelligentes Reconfigurables (en anglais RIS, reconfigurable intelligent surfaces). Grâce au placement stratégique des RIS entre la BS, les utilisateurs de la cellule (en anglais CUs, cell users) et les cibles, ainsi qu'à la commande adaptative des faisceaux, nous pouvons améliorer les signaux de communication et de détection, créer des connexions LOS, augmenter la couverture et réduire les IM et les interférences multi-utilisateurs (en anglais MUI, multi-user interference) [10].

La combinaison de l'intelligence artificielle et de la communication permettra de soutenir de nombreuses applications intelligentes, telles que l'interaction entre les êtres humains et les machines, la prédiction basée sur les jumeaux numériques et la prise

de décision, ce qui requiert un système de communication et de calcul axé sur l'IA. La connexion omniprésente a pour objectif de pallier les manques de couverture dans des environnements tels que les mers, les déserts et les forêts, ainsi que dans des environnements intérieurs complexes, offrant ainsi une expérience utilisateur cohérente à travers ces environnements [4].

La Figure 1.3 présente les facilitateurs de la 6G. Il est prévu que ces progrès jouent un rôle crucial dans la définition des capacités et des normes de performance des futurs réseaux 6G [11]. Les IS (en anglais IS, Intelligent Surfaces), et plus spécifiquement les RIS (en anglais RIS, Reconfigurable Intelligent Surfaces), jouent un rôle crucial dans l'avancement des applications 6G en améliorant les performances des communications sans fil. En utilisant des techniques telles que la réflexion, la réfraction, l'absorption, la division de faisceau, la manipulation de polarisation et la focalisation, les ISs réussissent à influencer activement la propagation du signal sur des surfaces passives. Les IS sont réputées pour leur efficacité, avec des capacités de traitement de signal à faible complexité, à faible consommation d'énergie et à faible latence, offrant ainsi des avantages importants aussi bien dans les milieux urbains que ruraux.

Envisagées dans le cadre des réseaux 6G définis par l'IMT-2030, les IS permettent des capacités cruciales telles que le soutien à des populations d'utilisateurs plus denses, l'atteinte de débits de données allant jusqu'à 1 Gbps, le maintien d'une latence inférieure à 1 milliseconde et la garantie d'une fiabilité exceptionnelle. Ces capacités sont essentielles pour améliorer de manière durable les performances du réseau et répondre efficacement aux exigences évolutives de la connectivité sans fil future [4].

Comme le montre la Figure 1.4, les surfaces intelligentes ont subi une évolution significative, en passant des antennes à réseau réflecteur (reflectarray) à des structures

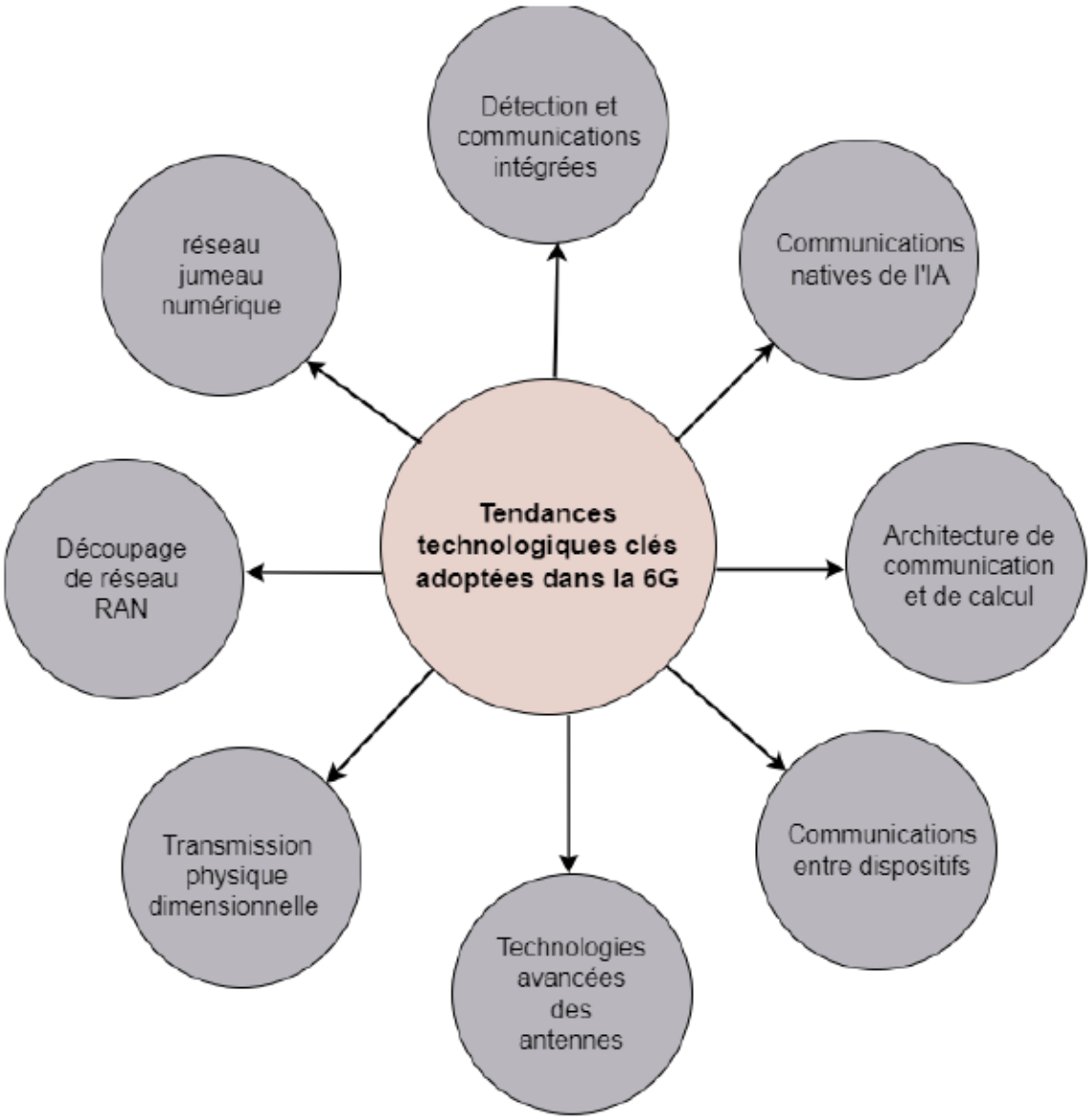

Figure 1.3 Tendances technologiques clés adoptées dans le Rapport ITU-R FTT M.2516 [3]

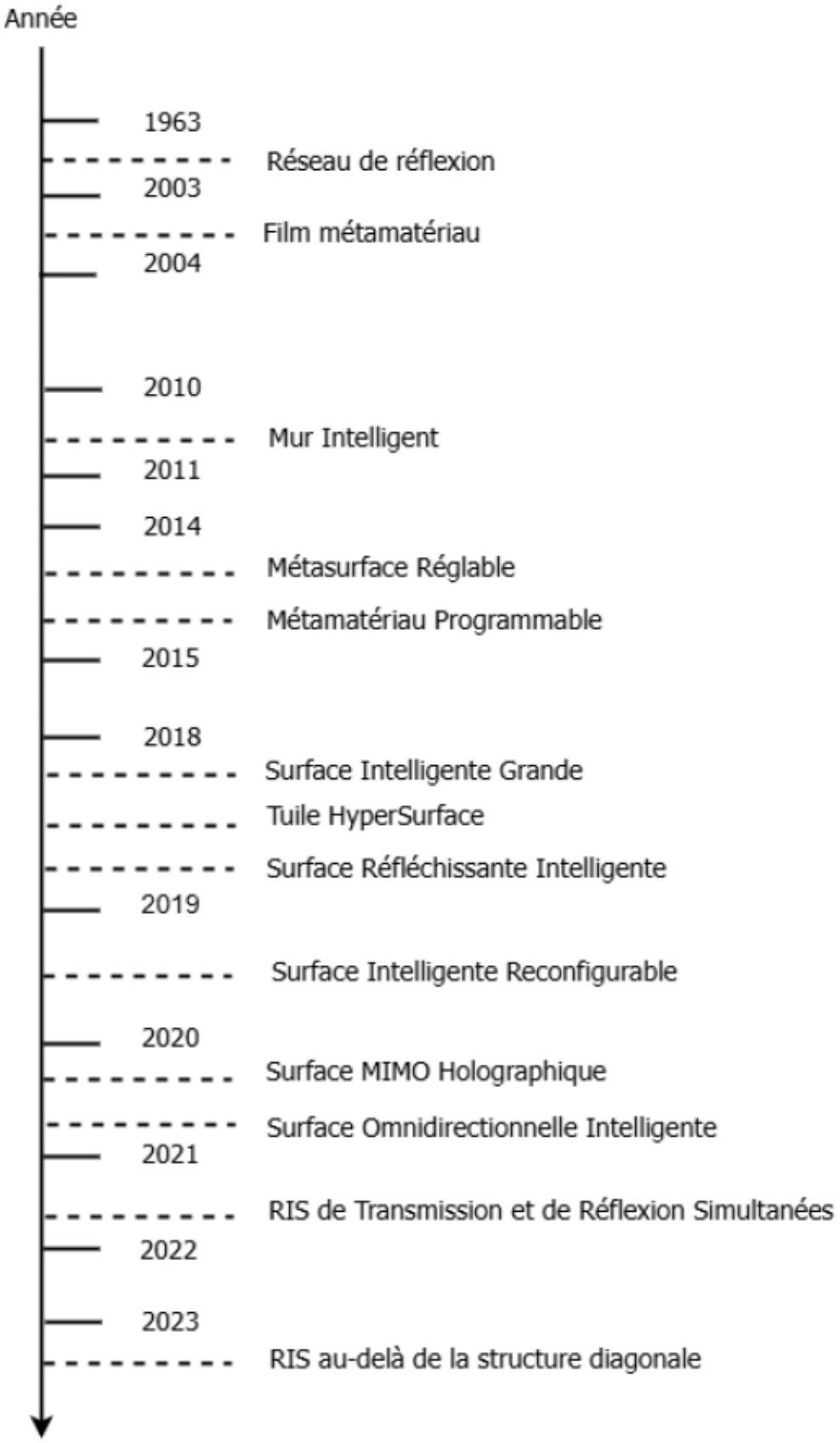

Figure 1.4 Développement historique des IS [4].

avancées à base de métamatériaux. Parmi ces avancées, on retrouve le DMA (en anglais DMA, dynamic metasurface antenna), le STAR-RIS (en anglais STAR-RIS, transmission et réflexion simultanée), le RIS actif, les SIM (en anglais SIM, stacked intelligent metasurfaces), les méta-lentilles, les méta-prismes et les matrices de phase non diagonales (Ris 2.0). Les nouvelles avancées permettent des améliorations cruciales dans le traitement du signal, l'adaptabilité et les performances des réseaux 6G, offrant ainsi la capacité de soutenir des populations d'utilisateurs plus denses, d'atteindre des débits de données allant jusqu'à 1 Gbps, de maintenir une latence inférieure à 1 milliseconde et d'assurer une fiabilité exceptionnelle, tout en réduisant la consommation de puissance. Il est essentiel d'utiliser des surfaces intelligentes pour créer des environnements radio intelligents qui garantissent une connectivité sans fil transparente de manière durable, en exploitant les ondes radio recyclées pour maximiser l'efficacité du réseau [4].

Comme illustré dans la Fig. 1.5, la communication assistée par IS est essentielle pour atteindre les objectifs ambitieux de la 6G définis par l'IMT-2030, tels que desservir des populations plus denses avec des débits de données plus élevés et une latence ultra-faible. En particulier, la 6G vise à accueillir jusqu'à 10 millions d'utilisateurs par km², offrir des vitesses de téléchargement de 1 Gbps et réduire la latence à moins de 1 ms, tout en garantissant une fiabilité de 99,99999% [5].

Pour garantir des réseaux sans fil respectueux de l'environnement et durables, l'efficacité énergétique mesurée en bits par joule est devenue un indicateur de performance crucial, comme le montre la Figure 1.1. Ainsi, plusieurs solutions sans fil écologiques en énergie ont été proposées pour la technologie 6G [12]. L'une des solutions potentielles pour une communication verte en 6G est le RIS, une avancée matérielle novatrice avec un potentiel croissant pour des économies significatives en consommation d'énergie.

Capacités des Communications Assistées par Surfaces Métas Intelligentes

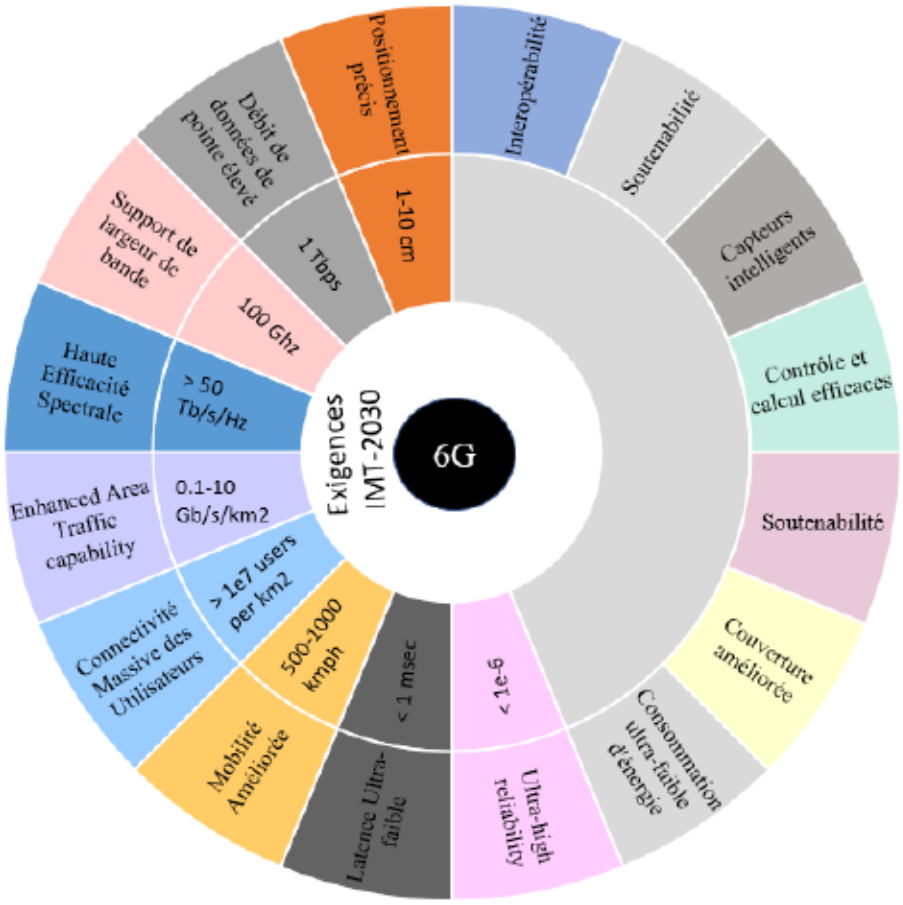

Figure 1.5 Exigences IMT-2030 et Capacités des IS. [5]

Il permet la création de systèmes sans fil intelligents et reconfigurables de manière économique [13]- [14].

Les RIS peuvent être réalisés en utilisant des technologies basées sur des métamatériaux ou des réseaux de patchs. Les RIS basés sur des métamatériaux sont appelés métasurfaces. Ils peuvent être installés à différents endroits et sont conçus pour agir comme des surfaces réfléchissantes/réfractantes entre la BS et l'utilisateur, ou comme des surfaces de guides d'ondes à la BS. Ces surfaces peuvent être reconfigurées de différentes manières, notamment électriquement, mécaniquement ou thermiquement. De plus, les RIS peuvent être classés en fonction de leur consommation d'énergie en tant que passifs-perdus, passifs-sans pertes ou actifs. Les capacités de performance de ces surfaces sont influencées par le niveau d'activité ou de passivité de ces surfaces, mais il convient de souligner que les RIS ne peuvent pas être totalement passifs en raison de leur nature configurable [15].

Les RIS passifs basés sur des métamatériaux sont constitués de plusieurs éléments réfléchissants passifs qui consomment très peu d'énergie pour ajuster programmatiquement les variations de phase et/ou les amplitudes des signaux incidents vers le RIS. En conséquence, contrairement aux techniques de communication sans fil traditionnelles utilisées pour les transcepteurs, les RIS peuvent directement remodeler le canal de propagation sans fil en faveur de la transmission des signaux (par exemple, en augmentant la puissance du signal reçu chez les utilisateurs ciblés et/ou en supprimant les interférences chez les utilisateurs non ciblés [13]- [14]). Cela offre une solution créative et pratique pour atteindre les indicateurs clés de performance (en anglais KPI, key performance indicators) de la 6G. En réalité, les RIS présentent un immense potentiel pour offrir une large gamme de fonctionnalités souhaitées et apporter des gains de performance

prometteurs pour la 6G de manière économique, sans avoir besoin de déployer de manière dense des BSs/APs énergivores [16]. Ces caractéristiques attrayantes placent les RIS comme une technologie économe en énergie et économiquement viable pour améliorer les performances système, et ils s'intègrent progressivement dans le courant principal des réseaux de communication.

Afin d'analyser les conséquences des RIS sur les communications sans fil, divers modèles de canaux physiques intégrant les RIS ont été suggérés. Ces modèles exploitent les champs et les ondes électromagnétiques (en anglais EM, electromagnetic waves) afin de décrire l'interaction des éléments RIS avec leur environnement, en intégrant la physique de la propagation, de la réflexion et de la diffusion des signaux. **Récemment, l'intérêt a grandi pour l'utilisation des paramètres d'impédance (Z), d'admittance (Y) et de diffusion (S) pour une description plus réaliste des RIS [17].** Dans [18], on a suggéré un cadre universel pour générer des modèles de communication compatibles avec l'EM pour les systèmes assistés par RIS. Les paramètres Z-, Y- et S- sont utilisés dans ce cadre pour définir diverses architectures RIS, ce qui offre une approche globale pour étudier les systèmes de communication assistés par RIS en utilisant les paramètres d'impédance et de diffusion [18].

Les BD-RIS (en anglais BD-RIS,beyond diagonal RIS) marquent une avancée significative dans la technologie des RIS. Contrairement aux RIS conventionnels, généralement représentés par des matrices de diffusion diagonales, les BD-RIS disposent de matrices de diffusion plus flexibles. Cette expansion englobe diverses architectures telles que les RIS groupés et entièrement connectés, ainsi que des innovations comme les STAR-RIS et les BD-RIS multi-sectoriels, offrant ainsi des performances améliorées et une couverture complète de l'espace. En outre, les RIS connectées à un groupe dynamique

et les matrices de déphasage non diagonales améliorent encore la flexibilité et les performances. Les BD-RIS entièrement connectés affichent des performances optimales malgré une complexité accrue des circuits [6].

1.1.1 Problématique de la thèse

Outre les avancées dans la technologie des RIS, plusieurs défis subsistent, notamment la caractérisation des performances et l'optimisation des réseaux. Il est essentiel de surmonter ces obstacles pour déployer efficacement **Des systèmes RIS efficaces en énergie** pour les communications sans fil de prochaine génération [19].

L'optimisation des réseaux a été largement abordée dans des articles récents pour améliorer différents éléments du système, tels que l'allocation de fréquence et de puissance dans un réseau OFDMA (en anglais, OFDMA, orthogonal frequency division multiple access) et le beamforming passif dans les systèmes RIS. Les méthodes les plus couramment utilisées pour améliorer l'EE (en anglais EE, energy efficiency) des réseaux sans fil sont classées dans les quatre domaines suivants: l'allocation des ressources, la planification et le déploiement des réseaux, la collecte et la transmission d'énergie, ainsi que les solutions matérielles. L'allocation des ressources peut améliorer les performances du système en modifiant dynamiquement la puissance de transmission, les coefficients d'allocation des sous-canaux, la bande passante disponible, etc. Cette étude aborde le défi de maximiser l'efficacité énergétique dans les réseaux de communication assistés par RIS, en combinant la technologie RIS et l'allocation des ressources pour atteindre simultanément un réseau plus respectueux de l'environnement.

Au cours du siècle dernier, les réseaux de communication ont principalement été développés dans le but d'améliorer des critères de performance tels que le débit et la

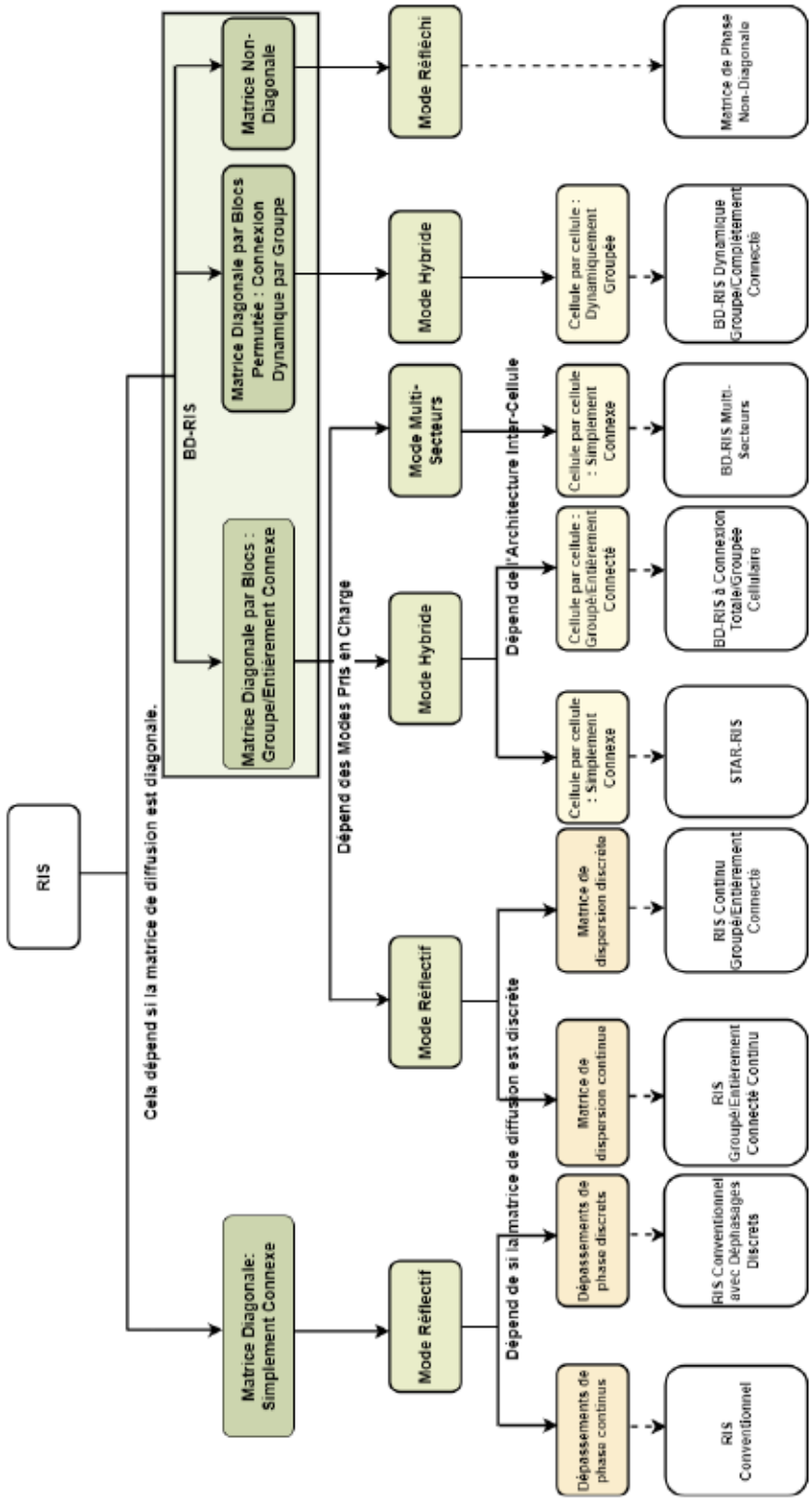

Figure 1.6 Arbre de classification des RIS [6].

latence. Toutefois, ces dix dernières années, l'EE, est devenue un élément de mérite important. Les RIS proposent une multitude de possibilités de conception des systèmes tout en utilisant une puissance très faible. Les RIS presque passifs, notamment, ne requièrent qu'une alimentation statique afin de reprogrammer les éléments réfléchissants sans utiliser de puissance radiofréquence. Les RIS presque passifs ont prouvé une consommation d'énergie réduite et une efficacité énergétique élevée, dépassant les technologies actives telles que les relais et les réseaux MIMO (en anglais, MIMO, multiple input multiple output) massifs [20].

L'objectif de cette étude est de concevoir et de répartir les ressources nécessaires pour les transmissions sans fil assistées par RIS. L'amélioration de l'SE (SE, spectral efficiency) et de l'EE reste un objectif central des systèmes de communication sans fil modernes. **En particulier, nous examinons deux types de RIS: le RIS conventionnel avec des décalages de phase continus, et le BD-RIS en mode réflexif avec une matrice de diffusion continue, comme illustré dans l'architecture présentée à la Fig. 1.6.** L'objectif de la 6G est d'atteindre des niveaux de SE 10 fois plus élevés et des niveaux d'EE 100 fois plus élevés que ceux des systèmes 5G [21, 22].L'indicateur de performance traditionnel, la SE, a fait l'objet d'une étude approfondie dans les systèmes assistés par RIS, en utilisant différentes méthodes d'optimisation. Toutefois, afin d'aborder la consommation d'énergie de manière plus efficace, les chercheurs ont opté pour l'EE, qui évalue le rapport entre la SE et la consommation totale d'énergie. L'optimisation de l'EE est plus complexe que l'optimisation de la SE en raison de sa nature fractionnaire, ce qui implique que les algorithmes d'optimisation de la SE ne peuvent pas être directement utilisés pour répondre aux défis de l'optimisation de l'EE [23].

En avançant, il est devenu évident que la plupart des travaux existants sur la

communication sans fil améliorée par RIS se sont principalement concentrés sur la maximisation de l'efficacité spectrale à travers la conception des coefficients de réflexion et l'allocation des ressources pour la transmission en bande étroite. Récemment, des études plus générales sur la transmission en bande large à travers des canaux sélectifs en fréquence ont été menées, tant pour les configurations à utilisateur unique que multi-utilisateur.

Dans ce travail, nous abordons le problème de la maximisation de l'EE dans les réseaux SISO (en anglais SISO, single input single output)-OFDMA assistés par RIS en direction descendante. **Nous proposons des techniques efficaces pour aborder l'optimisation du problème complexe formulé en programmation non linéaire en nombres entiers mixtes (en anglais MINLP, mixed integer non-linear programming) dans ce système.**

Les méthodes mathématiques traditionnelles comme l'AO (en anglais AO, alternating optimization) sont inadaptées pour résoudre les problèmes complexes inhérents aux réseaux de communication de haute dimension. Ces techniques conventionnelles d'allocation des ressources nécessitent un grand nombre d'itérations, d'ajustements des paramètres du système et d'échanges d'informations fréquents, les rendant moins adaptables aux environnements sans fil **réalistes**.

À cet égard, les techniques d'intelligence artificielle peuvent être utilisées pour résoudre efficacement le problème. Nous proposons donc une approche d'apprentissage par renforcement profond (en anglais DRL, deep reinforcement learning) pour optimiser conjointement les phases des RIS et les autres variables du système proposé.

1.2 Objectifs et contributions

Ce travail vise principalement à présenter des méthodes d'attribution de ressources énergétiquement efficaces pour les systèmes de communication assistés par RIS. Afin d'atteindre cet objectif, les objectifs sous-jacents suivants sont établis:

- Le premier sous-objectif consiste à revoir les méthodes actuelles de pointe pour l'attribution des ressources dans les communications assistées par RIS. L'objectif de cette revue est de donner une vision approfondie des contraintes des approches existantes, afin de proposer des méthodes innovantes qui s'attaquent à ces contraintes.
- L'objectif suivant vise à formuler et optimiser le problème de l'efficacité énergétique dans un système de communication MU (en anglais MU, Multi-Users) à SISO utilisant l'OFDMA. Selon nous, la maximisation de l'efficacité énergétique n'a pas été étudiée de manière approfondie dans les systèmes OFDMA assistés par RIS, qui comportent diverses variables d'optimisation telles que l'attribution des sous-canaux, l'allocation de puissance et les paramètres de décalage de phase du RIS. Une approche novatrice pour résoudre ce problème complexe consiste à utiliser une méthode sub-optimale qui utilise une borne inférieure du problème de maximisation de l'efficacité énergétique formulé pour les systèmes OFDMA assistés par RIS.
- Le sous-objectif numéro trois se focalise sur l'amélioration des communications assistées par RIS en termes d'EM. Une étude approfondie a été réalisée sur les travaux récents dans ce domaine, incluant les modèles électromagnétiques de RIS, les problèmes formulés et les solutions à ces modèles basées sur les EM du RIS.
- L'objectif final consiste à formuler et à résoudre le problème de l'EE pour un

système ISAC renforcé par un BD-RIS en utilisant **une méthode efficace de DL.** Malgré quelques recherches sur le BD-RIS dans les systèmes ISAC, ce domaine est encore peu étudié. Comme il est difficile de trouver une solution optimale, exploiter les bénéfices du DL offre une opportunité de recherche prometteuse.

La réalisation de ces objectifs a donné lieu à trois contributions principales

1. "AI-enabled Resource Allocation for BD-RIS Empowered ISAC Systems", S. Bidabadi, M.A. Ouameur, M. Bagaa, D. Massicotte, F.D. Figueiredo, and A. Chaaban, ***Digital Communications and Networks***, Nov. 2024. (submitted).
2. "Physically Consistent EM Models-Aware RIS-Aided Communication: A Survey", S. Bidabadi, M.A. Ouameur, M. Bagaa, D. Massicotte, F.D. Figueiredo, and A. Chaaban, ***Computer Networks Journal***, Nov. 2024. (accepted).
3. "Lower Bound Optimization of Energy Efficiency for an OFDMA SISO RIS-enabled System", S. Bidabadi, M.A. Ouameur, M. Bagaa, and D. Massicotte, ***MDPI Journal on Microwave and Wireless Communications***, Mar. 2024.
4. "Energy Efficient Resource Allocation for Reconfigurable Intelligent Surface-Assisted Wireless Networks", M.A. Ouameur, M. Bagaa, and D. Massicotte, ***EURASIP Journal on Wireless Communications and Networking***, Aug. 2023.

1.3 Méthodologie

Les systèmes de communication de prochaine génération sont confrontés à des défis de recherche ouverts, et les indicateurs clés de performance sont établis. Une variété de nouvelles technologies à différents niveaux permettra de rendre possibles les capacités de la prochaine génération de systèmes de communication. En raison de leur faible consommation d'énergie, les composants RIS passifs offrent des avantages significatifs

en termes d'efficacité énergétique pour l'infrastructure. Cependant, la mise en place de systèmes RIS écoénergétiques présente divers obstacles, allant de la détermination des performances à l'amélioration du réseau [24]. Cette étude vise à améliorer le réseau afin de maximiser l'efficacité énergétique du système. Afin d'atteindre cet objectif, on a établi les méthodologies suivantes.

Afin de parvenir à l'objectif initial, une analyse approfondie de la littérature des études récentes sur les communications assistées par RIS a été effectuée. Les dernières avancées et les méthodes d'optimisation proposées pour améliorer la performance des systèmes assistés par RIS ont été soulignées dans cette revue, tout en abordant également leurs limites. Un problème majeur repéré est que les algorithmes utilisant des gradients peuvent ne pas toujours être efficaces, car le problème de calcul de la taille du pas peut être concave. Afin de résoudre ce problème, deux techniques d'optimisation performantes ont été suggérées pour résoudre le problème de l'EE dans un système MISO à porteuse unique assisté par RIS: l'GAW (en anglais GAW, gradient algorithm with Wolfe conditions) et la TR (en anglais TR, trust region method). La méthode GAW tire parti des conditions de Wolf afin d'assurer une réduction adéquate de la fonction objectif en choisissant une taille de pas adéquate. La méthode TR, quant à elle, est reconnue pour ses performances supérieures par rapport aux méthodes de recherche de ligne, car elle trouve la solution optimale à chaque itération en explorant dans une zone de confiance.

Au sein du deuxième sous-objectif, nous avons repéré une disparité significative dans les études existantes sur l'amélioration de l'efficacité énergétique dans les systèmes de communication OFDMA assistés par RIS. Afin de résoudre ce problème, nous avons spécifié le problème de l'EE pour un système de communication downlink SISO-OFDMA activé par RIS. En raison de la difficulté du problème, qui résulte de diverses variables,

nous proposons un paramètre innovant qui simplifie la fonction EE en la découplant pour chaque utilisateur. En outre, dans ce contexte, nous identifions la borne inférieure du problème EE et proposons une solution sub-optimale qui exploite cette borne inférieure dans le cadre de l'optimisation alternée.

Nous avons étudié la littérature actuelle sur l'utilisation des modèles EM pour améliorer les systèmes de communication assistés par RIS dans le cadre du troisième sous-objectif. L'intérêt grandissant pour l'intégration des modèles basés sur EM est mis en évidence dans cette revue, dans le but d'améliorer les formulations de problème existantes. Malgré la rareté des recherches sur ce sujet, il est clair qu'il faut améliorer ces formulations à l'aide de modèles basés sur EM. Nous avons pour approche d'élargir la formulation de problème existante en intégrant des modèles EM du RIS. Grâce à cette approche, nous pouvons aborder de manière plus performante les défis pratiques liés à l'amélioration des systèmes de communication assistés par RIS.

Dans le but d'atteindre le quatrième sous-objectif, une analyse de la littérature sur les utilisations de l'IA et de l'apprentissage profond dans les systèmes de communication assistés par RIS met en évidence un intérêt grandissant pour ce projet. Dans les études actuelles, les méthodes d'optimisation convexe classiques ont été principalement employées afin de résoudre les problèmes complexes non convexes associés à ces systèmes. Toutefois, ces techniques classiques ont du mal à satisfaire les exigences de traitement en temps réel, notamment dans les réseaux de communication à grande échelle. En outre, les méthodes d'optimisation pour l'allocation des ressources font face à des difficultés majeures en raison du problème de la malédiction de la dimension lorsque le nombre de variables d'optimisation devient trop élevé. Afin de dépasser ces contraintes, nous suggérons d'adopter des méthodes d'apprentissage profond afin de formuler et

résoudre le problème de l'EE pour un système ISAC activé par BD-RIS. L'objectif de cette méthode novatrice est de faire face aux défis de complexité et d'évolutivité auxquels font face les méthodes d'optimisation classiques.

Les progrès récents dans le domaine du DL ont entraîné d'importantes améliorations dans différents secteurs, y compris les communications sans fil. Plus précisément, le TD3 (en anglais TD3, Twin Delayed Deep Deterministic Policy Gradient), une version du DDPG (en anglais DDPG, Deep Deterministic Policy Gradient), est une méthode d'apprentissage avancée basée sur le renforcement profond pour résoudre des problèmes complexes dans des environnements d'action continus.

Les modèles TD3 se révèlent efficaces dans des situations où il est difficile de disposer de CSI précis ou de connaissances détaillées sur les canaux de réflexion du RIS. À la différence des approches classiques d'apprentissage par Q, qui peuvent rencontrer des difficultés avec des espaces d'action continus et causer des divergences, les différentes versions de TD3 ont démontré leur efficacité dans de tels environnements. Ainsi, pour les systèmes ISAC activés par BD-RIS, le problème de l'EE est formulé, et l'algorithme TD3 est proposé comme une solution solide.

1.4 Structure du mémoire

Le travail entrepris dans cette thèse se concentre sur la proposition de techniques d'allocation des ressources écoénergétiques pour les communications assistées par RIS. Chaque chapitre contribue de manière significative à atteindre cet objectif. Voici un aperçu succinct de chaque chapitre :

1. Introduction (Chapitre 1) : Ce chapitre fournit une introduction générale à la thèse, en présentant le problème, les objectifs, les contributions et la méthodologie de

recherche. Il pose les bases pour comprendre le contexte global du travail.

2. État de l'art (Chapitre 2) : Ce chapitre passe en revue la littérature sur les différentes dimensions de recherche concernant les modèles EM des RIS dans les systèmes de communication sans fil. Il se concentre sur la formulation des problèmes d'optimisation du point de vue électromagnétique et explore les techniques d'optimisation et les méthodologies de solution conscientes des modèles EM adaptées pour tirer parti des capacités des réseaux assistés par RIS. L'objectif est de combler le fossé entre les perspectives théoriques et les mises en œuvre pratiques, fournissant des perspicacités sur la communication assistée par RIS consciente des modèles EM. Le contenu de ce chapitre est tiré de l'article « Modèles EM Physiquement Consistants pour les Communications Assistées par RIS : Un Survol ».
3. Présentation des Résultats par Articles (Chapitre 3) : Ce chapitre est divisé en trois sections détaillant les approches innovantes développées pour atteindre les objectifs fixés. La première section présente la maximisation de l'efficacité énergétique dans les systèmes de communication MISO assistés par RIS, illustrée par l'article « Allocation de Ressources Énergétiquement Efficace pour les Réseaux Sans Fil Assistés par Surface Intelligent Reconfigurable ». L'analyse met en évidence les lacunes des méthodes d'optimisation basées sur les modèles disponibles pour l'allocation des ressources dans les communications assistées par RIS, avec une évaluation des performances axée sur la convergence et la complexité. La deuxième section aborde le même problème pour les systèmes SISO-OFDMA, comme discuté dans l'article « Optimisation de la Borne Inférieure de l'Efficacité Énergétique pour un Système RIS-OFDMA SISO ». La troisième section explore le problème de maximisation de l'efficacité énergétique pour les systèmes ISAC

activés par BD-RIS, présenté dans l'article « Allocation des Ressources Activée par IA pour les Systèmes ISAC avec BD-RIS ». Cette section introduit une approche basée sur l'apprentissage par renforcement pour surmonter les défis rencontrés dans les sections précédentes en utilisant des approches basées sur les modèles, qui, bien que précises, peinent souvent avec la haute dimensionnalité de l'espace d'optimisation et nécessitent des simulations intensives en calcul.

4. Conclusions et Recommandations (Chapitre 4) : Le dernier chapitre synthétise les principales contributions, les limites de la recherche et propose des perspectives futures. Il conclut la thèse en présentant des conclusions solides tirées des résultats et offre des recommandations pour guider les développements et améliorations futurs.

Chapitre 2 - État de l'art

Développer des modèles précis pour décrire les propriétés de diffusion et de réflexion des systèmes assistés par RIS est essentiel pour leur analyse et leur optimisation. Il existe deux principales approches : l'une considère les RIS comme des surfaces continues régies par les équations de Maxwell pour déterminer les limites théoriques de performance, et l'autre modélise les RIS de manière discrète en sommant les réponses de diffusion des cellules élémentaires individuelles. Un modèle discret de base suggère que les cellules élémentaires modifient l'amplitude et la phase des ondes électromagnétiques entrantes. Dans un scénario où une source à antenne unique transmet à une destination à antenne unique, le RIS est représenté par une matrice diagonale de coefficients de réflexion et de décalages de phase. Le signal reçu à la destination est la somme des champs diffusés, exprimée par $y = \mathbf{h}_s^T \mathbf{\Theta} \mathbf{h}_i x$, où x, y, et $\mathbf{h}$ représentent respectivement le signal transmis, le signal reçu et les canaux [25].

Les modèles largement utilisés mentionnés ci-dessus sont généralement simplifiés pour faciliter l'analyse théorique et la simulation numérique. Une limitation significative des recherches actuelles est le manque de modèles physiquement précis et mathématiquement traitables pour décrire les comportements d'entrée/sortie des RIS. Les chercheurs doivent approfondir les modèles électromagnétiques pour mieux comprendre le comportement des RIS et optimiser la performance des systèmes en tenant compte de ces modèles.

Les défis clés incluent la gestion des effets de couplage mutuel entre les éléments RIS adjacents, les limites des modèles traditionnels de résolution des décalages de phase, et l'interférence électromagnétique incontrôlable dans des environnements dynamiques. De plus, des phénomènes tels que les modes de Floquet — réflexions non intentionnelles provenant de surfaces avec une impédance périodique — peuvent provoquer des

interférences et compromettre les performances du système. Pour déterminer les limites théoriques ultimes, une compréhension précise des phénomènes électromagnétiques fondamentaux est cruciale.

La conception des réseaux sans fil assistés par RIS nécessite de prêter attention à deux aspects importants. Tout d'abord, il est essentiel de considérer les conceptions basées sur l'EM, où les RIS effectuent des transformations fondamentales des ondes radio spécifiées au niveau électromagnétique. Dans ce paradigme, les ingénieurs optimisent les paramètres des RIS pour améliorer les performances du réseau. Ensuite, il est important de considérer les conceptions basées sur les communications, en mettant l'accent sur l'optimisation des RIS pour atteindre des objectifs de communication spécifiques, qui doivent nécessairement s'aligner avec les manipulations basées sur l'EM. Dans ce paradigme, l'optimisation est utilisée pour rendre les RIS polyvalents pour divers critères de performance tels que la capacité du canal et les schémas de modulation [26].

2.1 Modèles EM des RIS

2.1.1 Théorie des Réseaux Multiports

Dans les systèmes de communication sans fil, les RIS sont souvent simplifiés en tant que diffuseurs idéaux, négligeant des facteurs clés tels que le couplage mutuel et la corrélation phase-amplitude. Pour remédier à cela, les études récentes mettent l'accent sur des modèles électromagnétiques cohérents et des algorithmes d'optimisation avancés. La théorie des réseaux multiports a émergé comme une approche prometteuse pour modéliser les canaux assistés par RIS, capturant efficacement le couplage électromagnétique entre les éléments radiants étroitement espacés, crucial pour une efficacité énergétique élevée et des transformations d'ondes avancées [27].

Dans une configuration MIMO améliorée par un RIS, le système peut être modélisé à l'aide d'une configuration réseau à N ports, décrite à travers sa matrice d'impédance, d'admittance ou de diffusion pour une représentation détaillée des interactions [18,27–29].

Pour améliorer la flexibilité au-delà des implémentations traditionnelles de RIS, le concept de BD-RIS a été introduit, intégrant des composants d'impédance réglables pour interconnecter les éléments du RIS [30]. La classification des systèmes BD-RIS, en mettant l'accent sur les caractéristiques des matrices, les modes supportés et les conceptions architecturales, a été largement explorée dans les études récentes [6, 18, 30, 31].

2.1.2 Couplage Mutuel

Les modèles prenant en compte le couplage mutuel sont essentiels pour simuler et comprendre avec précision les interactions entre les éléments d'un RIS. Ces modèles permettent de prédire et d'optimiser précisément les performances des systèmes RIS dans divers scénarios de communication [32]. Il existe deux principaux types de modèles pour considérer le couplage mutuel : ceux utilisant des matrices d'impédance et ceux reposant sur des matrices de diffusion.

L'étude [33] examine un modèle de communication tenant compte du couplage mutuel, assisté par BD-RIS, utilisant des analyses des paramètres de diffusion et d'impédance. Le canal général assisté par RIS, $\mathbf{h}_{\mathrm{TR}}$, décrivant la relation entre la tension aux ports récepteur et émetteur, est donné par:

$$\mathbf{h}_{\mathrm{TR}} = (\mathbf{\Gamma}_R + \mathbf{I}_K)^{-1}\mathbf{T}_{\mathrm{RT}}(\mathbf{I}_N + \mathbf{\Gamma}_T\mathbf{T}_{\mathrm{TT}} + \mathbf{T}_{\mathrm{TT}})^{-1} \tag{2.1}$$

ou $\mathbf{T}_{\mathrm{TT}}$ et $\mathbf{T}_{\mathrm{RT}}$ sont des sous-matrices de $\mathbf{T} = \mathbf{S}(\mathbf{I}_L - \mathbf{\Gamma}\mathbf{S})^{-1}$, et $\mathbf{\Gamma} = \mathrm{blkdiag}(\mathbf{\Gamma}_T, \mathbf{\Theta}, \mathbf{\Gamma}_R)$.

Le modèle intègre les décalages d'antenne et le couplage mutuel au niveau de l'émetteur, du BD-RIS et du récepteur. Pour simplifier le modèle, des hypothèses telles que des impédances de source et de charge égales, l'approximation unilatérale et des antennes parfaitement appariées sont faites. Ces hypothèses conduisent au modèle de canal simplifié :

$$\mathbf{h}_{\mathrm{TR}} \approx \mathbf{S}_{\mathrm{RT}} + \mathbf{S}_{\mathrm{RI}}(\mathbf{I}_M - \boldsymbol{\Theta}\mathbf{S}_{\mathrm{II}})^{-1}\boldsymbol{\Theta}\mathbf{S}_{\mathrm{IT}} \tag{2.2}$$

Further simplification yields:

$$\mathbf{h}_{\mathrm{TR}} \approx \frac{1}{2Z_0}(\mathbf{Z}_{\mathrm{RT}} - \mathbf{Z}_{\mathrm{RI}}(\mathbf{Z}_{\mathrm{II}} + \mathbf{Z}_{\mathrm{I}})^{-1}\mathbf{Z}_{\mathrm{IT}}) \tag{2.3}$$

Les matrices $\mathbf{Z}_{\mathrm{RT}}$, $\mathbf{Z}_{\mathrm{RI}}$ et $\mathbf{Z}_{\mathrm{IT}}$ décrivent les canaux de l'émetteur au récepteur, du BD-RIS au récepteur, et de l'émetteur au BD-RIS, respectivement. La matrice $\mathbf{Z}_{\mathrm{II}}$ traite les effets de décalage et de couplage mutuel au niveau des éléments du RIS.

D'autres chercheurs ont également étudié les communications assistées par RIS en tenant compte du couplage mutuel [28, 34].

2.2 Formulation du problème en tenant compte des modèles électromagnétiques

Diverses formulations de problèmes d'optimisation pour les réseaux sans fil améliorés par RIS ont été largement étudiées par les chercheurs, en mettant l'accent sur les considérations électromagnétiques pour améliorer le gain de canal, la capacité, le SINR (en anglais SINR, signal to interference plus noise ratio), le débit total, l'efficacité énergétique et minimiser la consommation d'énergie, comme indiqué dans les tableaux 2-1, 2-2, 2-3 et 2-4.

Tableau 2-1 Maximisation du modèle EM basé sur le SNR/SINR dans les communications assistées par RIS

Réf.	Scénario	Objectif	Variables de conception	Algorithmes
[35]	SISO, MISO, SIMO assisté par BD-RIS	Maximisation du SNR	Matrice de décalage de phase du RIS	Solution analytique
[36]	SISO	Maximisation du SNR de bout en bout	Impédances réglables du RIS	Solution analytique
[37]	MUs SIMO	Maximisation du SINR de bout en bout	Vecteurs BF de réception à la BS, allocation de puissance de transmission aux utilisateurs, et conception du décalage de phase du RIS	Solution basée sur la descente de gradient projeté

Tableau 2-2 Minimisation de la puissance de transmission ou maximisation de la puissance reçue pour les modèles basés sur EM dans les communications assistées par RIS

Réf.	Scénario	Objectif	Variables de conception	Algorithmes
[38]	Réseau MU-MISO assisté par BD-RIS	Minimisation de la puissance de transmission	Formation de faisceaux de transmission Déphasages du BD-RIS	BCD
[39]	SU MISO coordonné assisté par BD-RIS	Maximisation de la puissance reçue	Formation de faisceaux de transmission Déphasages du RIS	AO, Solutions analytiques
[40]	MISO assisté par BD-RIS	Maximisation de la puissance reçue	Formation de faisceaux de transmission et déphasages du RIS	Solutions analytiques
[41]	RIS multi-bande MIMO multi-BS	Maximisation de la puissance reçue	Déphasages du RIS	Solutions analytiques
[42]	SU SISO, MISO, MIMO hybride BD-RIS	Maximisation de la puissance reçue	Déphasages du RIS	PDD
[43]	SISO	Maximisation de la puissance reçue	Formation de faisceaux de transmission , déphasages du RIS, orientation et position du RIS	AO, solutions analytiques
[44]	SISO	Maximisation de la puissance reçue	Formation de faisceaux de transmission et déphasages du RIS	AO, SOCP, algorithme de contrôle de phase optimal basé sur la géométrie
[45]	SISO	Maximisation de la puissance reçue	Impédances réglables au RIS	Algorithme basé sur le gradient
[46]	SISO	Maximisation de la puissance reçue	Déphasages discrets du RIS	Quantification de phase avec seuil dynamique (DTPQ) et quantification de phase à intervalle égal (EIPQ)
[47]	SISO	Maximisation de la puissance reçue	Déphasages discrets du RIS	Algorithme basé sur des groupes, solutions analytiques
[48]	STAR-RIS	Maximisation de la puissance reçue	Formation de faisceaux de transmission et déphasages du RIS	Solutions analytiques

Tableau 2-3 Maximisation du taux de somme avec des modèles physiquement cohérents pour le RIS dans les communications assistées par RIS

Réf.	Scénario	Objectif	Variables de conception	Algorithmes
[49]	MUs-MISO assisté par BD-RIS hybride	Maximisation du taux de somme	Formation de faisceaux de transmission, et matrice BD-RIS	Algorithme itératif, Solution analytique
[38]	Réseau SU-MISO assisté par BD-RIS	Maximisation du taux de somme	Formation de faisceaux de transmission Déphasages du BD-RIS	Méthode de montée en bloc (BCA)
[50]	MIMO	Maximisation du taux de somme	Formation de faisceaux active et passive	BCD, wMMSE
[51]	BD-RIS assisté SU/MUs-MISO	Maximisation du taux de somme	Composants d'impédance réglables du BD-RIS	Solution analytique
[52]	BD-RIS RSMA assisté MUs-MISO	Maximisation du taux de somme	Formation de faisceaux de transmission et configuration multi-sectorielle du BD-RIS	Méthode de majorisation-minimisation (MM) et méthode de décomposition pénalisante-duale (PDD)
[53]	Système ISAC MUs MISO FC BD-RIS	Maximisation du taux de somme	Filtre linéaire, formation de faisceaux de transmission, et configuration du BD-RIS	RCG (Gradient Conjugué Riemannien), Solution basée sur les variétés
[54]	MU-MIMO	Maximisation du taux de somme	Contraintes SAR	Algorithme itératif de remplissage d'eau
[55]	MISO	Maximisation du taux de somme	Impédances réglables des cellules unitaires du RIS, Formation de faisceaux passive	Algorithme itératif
[56]	RIS-aidé MUs-MISO SDMA/NOMA	Maximisation du taux de somme pondéré	Précodage d'accès multiple à la BS, et configuration du RIS	AO, Précodage WMMSE, ML non supervisé

Tableau 2-4 Maximisation de l'EE dans les communications assistées par RIS du point de vue EM

Réf.	Scénario	Objectif	Variables de conception	Algorithmes
[38]	Réseau MU-MISO assisté par BD-RIS	Maximisation de l'EE	Formation de faisceaux de transmission Déphasages du BD-RIS	Méthode de montée en bloc (BCA)
[57]	MISO assisté par RIS-SWIPT	Maximisation de l'EE	Paramètres d'impédance des éléments du RIS, Vecteurs de formation de faisceaux actifs	AO, SDR, SCA, et algorithme de Dinkelbach
[58]	MIMO	Maximisation de l'EE	Déphasages du RIS, formation de faisceaux de transmission, filtre de réception linéaire, et puissance de transmission	AO, Solutions analytiques
[59]	Réseau cellulaire mmWave assisté par LIS	Maximisation de l'EE	Nombre d'éléments LIS	Géométrie stochastique

2.3 Solution du problème en tenant compte des modèles électromagnétiques

2.3.1 Optimisation Basée sur des Modèles

Dans le contexte de cette étude, les approches basées sur des modèles se réfèrent à des algorithmes fondés sur des modèles d'optimisation spécifiques, soutenus par une compréhension approfondie du problème défini. De tels algorithmes nécessitent souvent des prérequis stricts en termes de caractéristiques de formulation du problème, telles que la convexité, la continuité et la différentiabilité. Parmi les algorithmes basés sur des modèles pour l'optimisation des modèles électromagnétiques physiquement cohérents et des communications assistées par RIS, on trouve des méthodologies telles que l'AO, les techniques de MM (en anglais MM, Majorization-Minimization), l'SCA (en anglais SCA, Successive Convex Approximation), la SDR (en anglais SDR, Semidefinite Relaxation), et la BCD (en anglais BCD, Block Coordinate Descent), comme indiqué dans les tableaux 2-1, 2-2, 2-3 et 2-4.

2.3.2 Stratégies Heuristiques

Ces stratégies reposent sur des règles heuristiques pour accélérer la résolution des problèmes, offrant des alternatives efficaces aux méthodes basées sur des modèles conventionnels. Bien qu'elles puissent sacrifier l'optimalité et la précision au profit d'une complexité réduite et de solutions rapides, les algorithmes heuristiques se révèlent essentiels, notamment pour aborder des problèmes NP-difficiles ou pour compléter d'autres algorithmes. Des algorithmes heuristiques tels que l'CCP (en anglais CCP, Convex-Concave Procedure), divers algorithmes méta-heuristiques, des algorithmes gloutons, et l'application de la théorie des appariements peuvent tous être employés pour améliorer l'optimisation des réseaux sans fil intégrant des RIS. Le travail de [60] a utilisé

des méthodes heuristiques pour résoudre des communications assistées par RIS en tenant compte des modèles électromagnétiques physiquement cohérents.

2.3.3 Optimisation Basée sur l'Apprentissage Automatique

Les techniques de ML (en anglais ML, Machine Learning) et de DL offrent des solutions prometteuses pour l'optimisation des systèmes de communication assistés par RIS, grâce à leur capacité à traiter des problèmes d'optimisation de haute dimension et non linéaires. Ces techniques apprennent des motifs à partir des données, permettant une exploration et une exploitation efficaces des solutions, et peuvent s'adapter à des environnements dynamiques grâce à un retour d'information en temps réel.

En revanche, les approches traditionnelles basées sur des modèles rencontrent des défis liés à l'intensité computationnelle et à la scalabilité [32]. Les algorithmes heuristiques offrent des mécanismes de recherche efficaces mais ne garantissent pas toujours l'optimalité [31]. Malgré ces défis, les méthodes ML/DL se distinguent par leur potentiel à révolutionner l'optimisation des technologies RIS en exploitant des paradigmes d'apprentissage avancés tels que l'apprentissage supervisé et non supervisé, l'RL (en anglais RL, Reinforcement Learning), l'FL (en anglais FL, Federated Learning), l'apprentissage par graphe, l'apprentissage par transfert etl'apprentissage hiérarchique.

Les recherches actuelles, bien que limitées, comme le travail de Peng et al. [56], ont exploré l'application du ML spécifiquement pour l'optimisation des systèmes de communication assistés par RIS en tenant compte des modèles électromagnétiques physiquement cohérents.

2.3.4 Droits d'auteur

Computer Networks 257 (2025) 110963

Contents lists available at ScienceDirect

Computer Networks

journal homepage: www.elsevier.com/locate/comnet

Survey paper

Physically-consistent EM models-aware RIS-aided communication — A survey

S. Bidabadi [a],*, M.A. Ouameur [a], M. Bagaa [a], D. Massicotte [a], F.D. Figueiredo [b], A. Chaaban [c]

[a] UQTR, Trois-Rivières, QC, Canada
[b] National Institute of Telecommunications – Inatel, Santa Rita do Sapucaí-MG, Brazil
[c] University of British Columbia Okanagan, Kelowna, Canada

ARTICLE INFO

Keywords:
Wireless communication
Reconfigurable intelligent surfaces
Electromagnetic models
Optimization techniques
Machine learning

ABSTRACT

The rapid development of reconfigurable intelligent surfaces (RISs) has sparked transformative advancements in wireless communication systems. These intelligent metasurfaces, adept at dynamically manipulating electromagnetic (EM) waves, hold vast potential for enhancing network capacity, coverage, and efficiency. However, to fully unleash the capabilities of RIS-aided communication systems, effective optimization is crucial. This article provides a recent development of RIS-assisted communication from the viewpoint of physically-consistent EM models. We delve into the realm of physically-consistent EM models, highlighting their pivotal role in achieving robust and efficient RIS designs. Furthermore, this paper offers a survey of the different optimization models utilized for RIS-assisted wireless communication systems, which consider various EM and physical aspects of RIS. We explore solution approaches aimed at optimizing different objectives like sum-rate/spectral efficiency and energy efficiency, spanning traditional optimization models to machine learning-based methods. Additionally, we discuss some open research issues in this field.

1. Introduction

Existing cellular generations will not be able to meet the extraordinary performance requirements needed by innovative applications anticipated in 2030, which will lead to a need for new technologies to enable 6G systems. 6G is expected to outperform 5G in various aspects, including ultra-high data rates, energy efficiency (EE), global coverage, connectivity, high reliability, and low latency, as illustrated in Fig. 1 [1–4]. While technologies like massive multiple-input multiple-output (MIMO), mmWave communication, and network densification have significantly advanced 5G performance, they face challenges such as increased hardware costs and energy consumption. These limitations highlight the need for new wireless technologies to efficiently achieve the key performance indicators (KPIs) of 6G, as listed in Fig. 2.

In this context, reconfigurable intelligent surfaces (RIS) have emerged as a promising solution, offering dynamic control over wireless environments and enhancing overall network performance for 6G. RIS are a natural evolution of earlier intelligent surface (IS) technologies [5]. The evolution of ISs can be traced back to reflectarrays, which used passive antennas for basic wave control. Metamaterials, with their ability to manipulate wave properties, further advanced the field. The concept of RIS emerged, enabling dynamic, programmable control of signal propagation. Subsequent innovations like large intelligent surfaces (LIS) and hybrid architectures expanded IS capabilities. More recently, the beyond-diagonal RIS (BD-RIS) architecture has emerged, offering even more sophisticated signal processing capabilities by encompassing previous IS architectures as special cases. This allows for enhanced control over signal propagation across IS elements. These advancements collectively pave the way for smarter, energy-efficient wireless networks [5–11].

Metasurfaces and patch-array designs represent two key approaches for implementing RIS technology. Metasurfaces consist of continuous, ultra-thin layers with sub-wavelength inclusions that manipulate electromagnetic (EM) waves in ways that natural surfaces cannot. They serve as two-dimensional equivalents of bulky metamaterials, providing similar capabilities to shape wave propagation while being more compact, easier to fabricate, and less lossy. This makes metasurfaces particularly effective for applications in wireless communications, where precise control of wave reflection, refraction, and scattering is crucial for optimizing signal transmission [12–18]. In contrast, many practical implementations of RISs use discrete components, such as patch antennas or PIN diodes, arranged in a grid-like structure. These elements can adjust the phase of impinging EM waves, similar to how reflectarrays operate. However, unlike conventional reflectarrays, which are typically static, RISs are equipped with tunable components

* Corresponding author.
E-mail address: samaneh.bidabadi@uqtr.ca (S. Bidabadi).

https://doi.org/10.1016/j.comnet.2024.110963
Received 25 June 2024; Received in revised form 9 November 2024; Accepted 28 November 2024
Available online 5 December 2024

Table 1
List of abbreviations.

Abbreviation	Description	Abbreviation	Description
ADC	Analog-to-Digital Converters	AI	Artificial Intelligence
ACO	Ant Colony Optimization	ANN	Artificial Neural Networks
AO	Alternating optimization	BC	Block Coordinate Descent
BPSO	Binary Particle Swarm Optimization	CCP	Convex-concave Procedure
CNNs	Convolutional Neural Networks	CR	Cutoff Rate
CSI	Channel State Information	cDC-GAN	Conditional Deep Convolutional Generative Adversarial Network
cDC-VAE	Conditional Deep Convolution Variational Autoencoder	DMT	Diversity-multiplexing tradeoff
DOA	Direction of Arrival	DRL	Deep Reinforcement Learning
DGMs	Deep Generative Models	DOFs	Degrees-of-Freedom
EHU	Energy Harvester User	EH	Energy Harvesting
EMI	Electromagnetic Interference	EMF	Electromagnetic Field Exposure
EM	Electromagnetic	EMOs	EM objects
FDTD	Finite-difference time-domain method	FEM	Finite Element Method
FL	Federated Learning	GA	Genetic Algorithm
IDBP	Information-Directed Branch-and-Prune	IDU	Information Decoder User
LHCP	Left-Handed Circular Polarization	LISs	Large Intelligent Surfaces
MAE	Mean Absolute Error	MEM	Mismatch Environment Model
MIMO	Massive Multiple-Input Multiple-Output	MI	Mutual Information
MISO	Multiple-input Single-output	ML	Machine Learning
MOLACO	Multi-Objective Lazy Ant Colony Optimization	MM	Majorization-Minimization Techniques
MTS	Metamaterial Surface	NOMA	Non-orthogonal Multiple Access
NNs	Neural Networks	OAM	Orbital Angular Momentum
OMA	Orthogonal Multiple Access	OP	Outage Probability
PIDL	Physics Informed Deep Learning	PINNs	Physics Informed Neural Networks
PGM	Projected Gradient Method	PSO	Particle Swarm Optimization
RL	Reinforcement Learning	SCA	Successive Convex Optimization
SAR	Specific Absorption Rate	SDR	Semidefinite Relaxation
SE	Spectral Efficiency	SIMO	Single-input Multiple-output
SISO	Single-input Single-output	SRR	Split-ring Resonator
SVM	Support Vector Machine	STAR	Simultaneous Transmission and Reflection
TEM	True Environment Model	ISAC	Integrated sensing and communication
SIMs	Stacked intelligent metasurfaces		

such as PIN diodes or varactors, enabling dynamic control of EM wave reflection. This software-defined control allows RISs to adapt in real-time to changing network conditions, providing flexibility in signal modulation and improving overall communication performance.

Despite the differences in hardware, both metasurface-based and patch-array-based RISs serve the same overarching purpose: they dynamically control the propagation of EM waves to optimize wireless communication environments. By adapting to varying network conditions and offering real-time configurability, RISs enable efficient signal management in next-generation communication systems, playing a critical role in the evolution toward 6G networks [12,13,19–25].

As the field of RIS-assisted communication systems rapidly evolves, it is essential to address the existing limitations and assumptions that have been prevalent in previous research efforts. For instance, the mutual coupling effects between adjacent RIS elements have been acknowledged as a critical consideration in the accurate modeling of RIS behavior. Likewise, the traditional phase shift resolution models, while providing valuable insights, often fail to capture the intricate nuances of real-world RIS scenarios [26]. Furthermore, the uncontrollable electromagnetic interference in dynamic environments introduces complexities that can significantly impact the performance of RIS-based communication systems. These challenges underscore the need for innovative solutions that can handle these practical constraints and push the boundaries of RIS deployment. Another instance of an often overlooked EM occurrence observed in intelligent surfaces involves what are known as Floquet modes. These are unintended reflections from surfaces that possess a periodic impedance, potentially causing interference at undesired angles and thus undermining system performance [27]. Furthermore, the quest to determine the ultimate theoretical boundaries cannot disregard the need for a precise understanding of the fundamental EM phenomena [28,29].

This comprehensive survey aims to provide an in-depth exploration of the various research dimensions concerning EM-based models of RIS in the context of wireless communication systems. Our focus centers on reviewing the formulation of optimization problems from EM perspectives. We also focus on investigating optimization techniques and EM-aware solution methodologies tailored to effectively harness the capabilities of RIS-assisted networks. By doing so, we strive to bridge the gap between theoretical insights and practical implementations and bring forward insights on EM model-aware RIS assisted communication.

In the pursuit of a comprehensive understanding, this survey draws from a wide range of literature sources and research contributions. It aims to provide researchers, practitioners, and decision-makers with valuable insights into the current state of EM-based RIS models and their implications for optimizing RIS-assisted communication systems.

Motivated by the importance of optimization techniques, in this paper we provide a comprehensive overview of optimization techniques for optimizing RIS-aided wireless communications from EM perspectives, including physics informed neural networks (PINN) approaches. There are several surveys devoted to the theory, design, analyses, and applications of RISs [26,31–38]. However, this work is different from existing surveys and tutorials since it systematically summarizes and analyzes EM-based models of RIS for optimizing RIS-aided communication systems. Specifically, as shown in Fig. 3, this paper focuses on the following aspects:

- First, the paper delves into the EM models of RIS employed in the literature to formulate and optimize EM-aware RIS-assisted communication problems.
- Second, the paper provides an extensive exploration of the various problem formulations related to optimizing RIS-enhanced wireless networks, all examined from the unique perspective of EM models. These formulations cover a wide range of objectives, including the maximization of sum-rate/capacity, energy efficiency, and the minimization of power consumption.
- Third, the paper presents a comprehensive review of model-centric, heuristic, and machine learning (ML) approaches used to optimize RIS-enhanced wireless networks from an EM perspective. The survey emphasizes the need for efficient optimization methods for solving the EM-based problems, notably

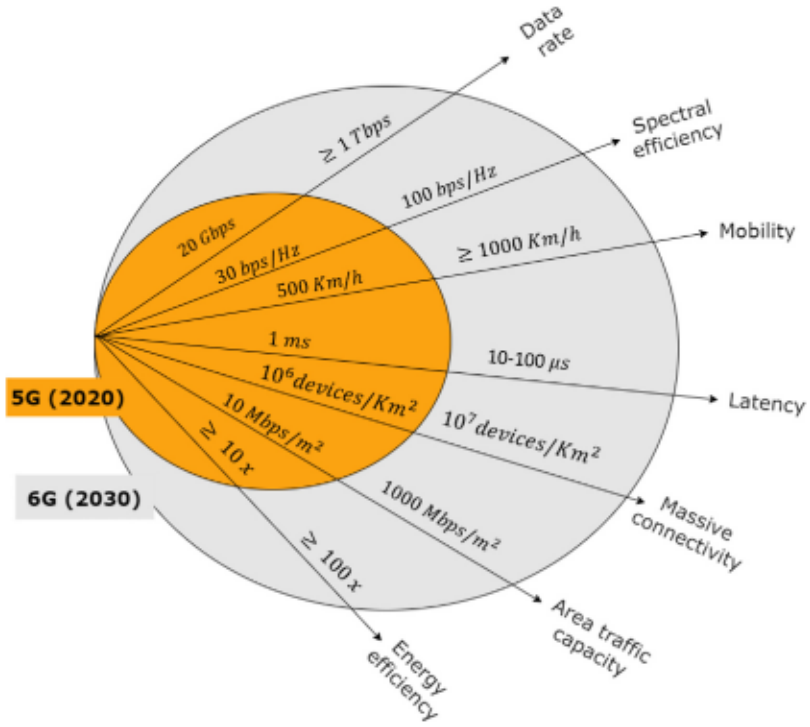

Fig. 1. Specifications for 6G wireless communication (© The Author(s) 2021, [1]).

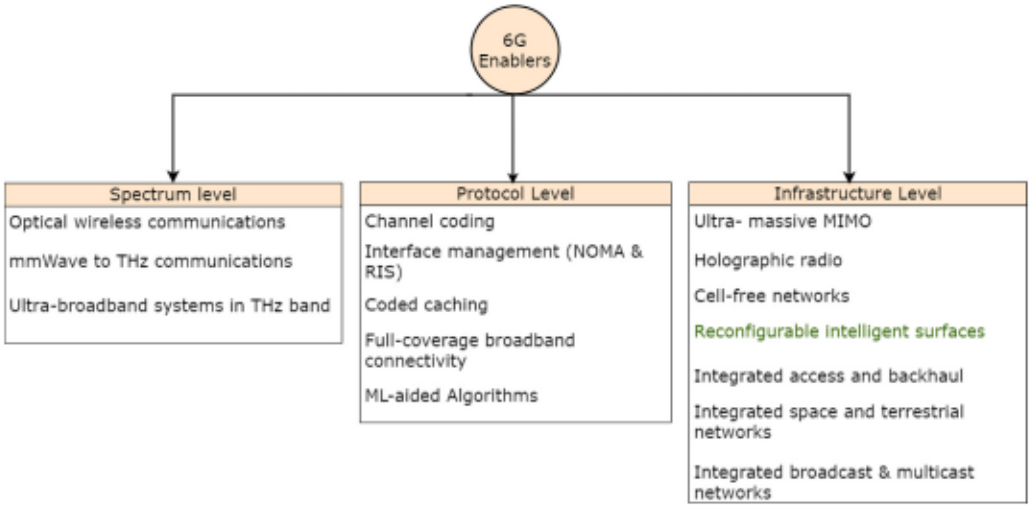

Fig. 2. 6G enablers (© 2021 IEEE, [30]).

highlighting PINN, which combines data-driven insights with governing differential equations to provide more realistic RIS behavior models.

Generally, the survey covers various aspects, including problem formulations, characteristics, and applications of different approaches, aiming to serve as a roadmap for researchers in this field. The paper is structured as follows: Section 2 reviews related work; Section 3 describes EM-based models of RIS; Section 4 presents EM model-aware problem formulations; and Section 5 reviews model-based, heuristic, and ML optimization algorithms used for optimizing RIS-assisted communications using physically consistent EM models of RIS. Section 6 discusses research gaps and identifies future challenges, and finally, Section 7 concludes the survey. The key themes of this paper are depicted in Fig. 3, and a comprehensive compilation of all abbreviations used in this survey can be found in Table 1.

2. Previous survey works and motivations

Numerous surveys have been dedicated to exploring the theory, design, analysis, optimization and practical applications of RISs and in particular meta-surfaces [26,31–34,34,34,36–41] as listed in Table 2. Some surveys delve into the exploration of physically-consistent EM models of RIS, while others examine RIS-aided communication without taking into account the physical models of RIS. This survey considers both perspectives, synthesizing them into a unified framework termed physically-consistent EM models-aware RIS-aided communication. The term "Physically-Consistent EM Models-Aware RIS-Aided Communication" is used to describe the integration of physically-consistent EM models with RIS-aided communication systems. This work aims to support researchers in wireless communication systems by offering more realistic communication models that incorporate the physical characteristics of RIS, which are essential for advancing future wireless

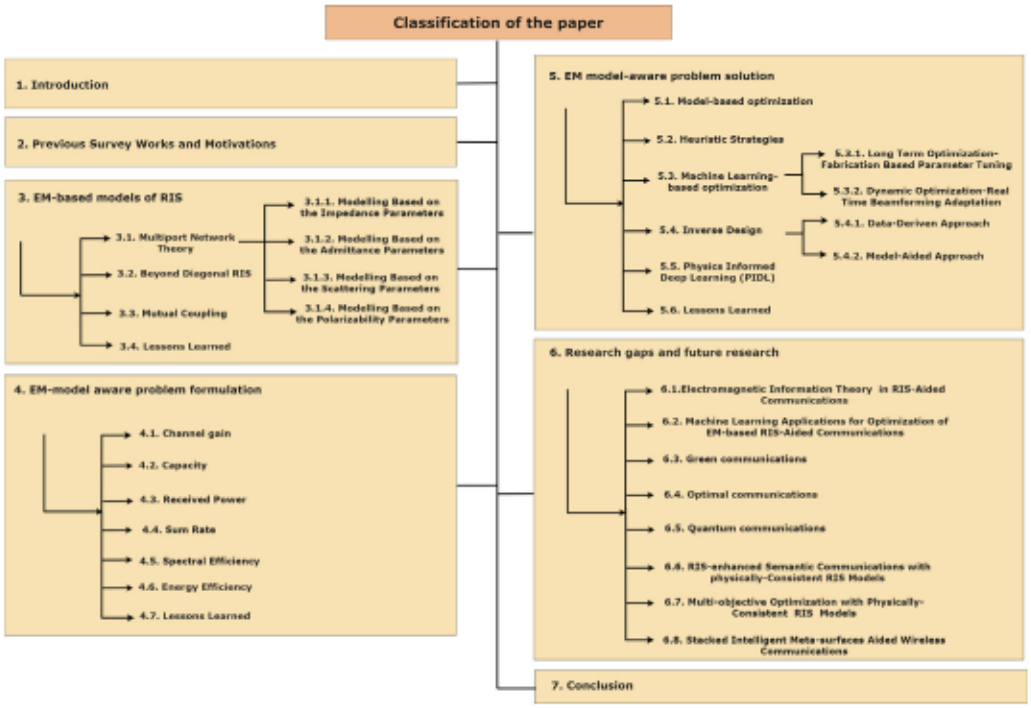

Fig. 3. The organization of this paper.

technologies, including 6G. We also find a gap in the existing literature that only focuses on the inverse design of metamaterials using ML and rarely studies EM-aware RIS-aided communication system optimization using ML techniques.

In [39], the authors investigate the potential applications of RIS technology for 6G communications. They begin with a comprehensive overview of RIS and then explore its various applications, including system and path loss models, asymptotic analysis, precoding techniques, channel state information (CSI) acquisition, prototypes, and its integration with other technologies, without focusing on EM-aware models of RIS. The paper provides practical examples to demonstrate the transformative impact of RIS on future wireless systems and highlights the potential benefits it offers. Furthermore, it identifies key challenges in the deployment and adoption of RIS technology and presents promising directions for future research. Authors in [26] provide a thorough review of RIS-assisted wireless communication, discussing fundamental principles like hardware architecture, control mechanisms, and channel models. They also analyze performance metrics to highlight the benefits of RIS deployment. They mention that, despite the advantages, the integration of RIS faces challenges due to its passive nature, including issues with channel estimation and deployment scenarios. However, the review does not cover physically-consistent EM models-aware RIS. The authors do identify mutual coupling as a significant research challenge and suggest it as a potential area for future exploration in RIS-aided wireless communication systems.

The survey in [31] offers a comprehensive exploration of machine learning algorithms applied to RIS-aided communications. It includes a concise introduction to RISs, a summarization of machine learning techniques used in RIS architecture, and a comparative analysis of these methods to elucidate their integration. The review, however, does not delve into physically-consistent EM Models of RIS in problem formulation and optimization. The authors do highlight that metasurfaces encounter challenges due to the absence of accurate models that consider their EM characteristics, which impacts their functionality beyond simple reflection. They identify this as a major research challenge and propose it as a promising avenue for future exploration in RIS-assisted wireless communication systems.

The work in [32] categorizes optimization techniques into model-based, heuristic, and ML algorithms, covering diverse problem formulations. It introduces model-based algorithms, heuristic optimization, and state-of-the-art ML applications, providing a comparative analysis across stability, robustness, and optimality. The survey also highlights RIS-aided applications in 6G networks and outlines emerging research challenges in this dynamic field, emphasizing RISs' pivotal role in shaping the future of wireless communication systems.

The survey in [33] offers a thorough overview of RISs and examines how reinforcement learning (RL) algorithms are used to optimize RIS parameters. This article specifically focuses on applying deep reinforcement learning (DRL) to improve aspects such as passive beamforming, phase shifting, and RIS placement. It also addresses various challenges in implementing RL algorithms for RIS technology in wireless communications and suggests possible solutions. Nevertheless, the study does not explore physically-consistent EM models of RISs in the problem formulation and restricts the optimization techniques to RL.

The work in [34] delves into the realm of optimizing RIS-aided wireless networks using a combination of heuristic algorithms and ML. It investigates various heuristic techniques, such as greedy algorithms, meta-heuristic algorithms, and matching theory, while also introducing innovative heuristic-ML hybrid approaches. These include heuristic DRL, heuristic-aided supervised learning, and heuristic hierarchical learning. Notably, the study demonstrates that heuristic DRL outperforms conventional DRL in terms of achieving higher data rates and faster convergence. The ultimate aim of the work is to present a novel perspective on optimizing RIS-aided wireless networks, capitalizing on the synergy between heuristic algorithms and ML methods.

The work in [35] discusses the combination of RISs with ML to enhance smart IoT systems, highlighting their use in managing radio propagation without traditional channel data. It examines specific ML techniques like deep reinforcement learning and federated learning, and their application in dynamic environments with challenges like user mobility and fluctuating wireless channels. The paper concludes with future challenges and the potential of RISs in next-generation IoT networks.

The work in [36] offers a comprehensive review of existing optimization techniques and artificial intelligence-driven methods employed to address the constraints associated with RISs. It conducts a

Table 2
Comparison of Related Surveys and Studies. [39][26][31][32][33][34][35][36][37][40][42][41][38].

Ref	Year	Main contributions	Physically-Consistent EM models	RIS-aided communication	Physically-consistent EM models-aware RIS-aided communication
[39]	2022	Provides an overview of RIS for 6G, including applications, system models, and future research directions.	○	●	○
[26]	2023	Comprehensive review of RIS-assisted wireless communication, covering hardware, control mechanisms, channel models, and highlighting challenges like channel estimation and deployment.	○	◐	○
[31]	2022	Comprehensive review of machine learning in RIS-aided communications, highlighting challenges with meta-surfaces due to the lack of accurate EM models and suggesting this as a key area for future research.	◐	●	○
[32]	2023	Explores model-based, heuristic, and ML optimization techniques for RIS-aided communication, provides a comparative analysis, and emphasizes emerging challenges and the critical role of RIS in future 6G networks.	○	●	○
[33]	2023	Examines deep reinforcement learning for optimizing RIS parameters and addresses implementation challenges.	○	◐	○
[34]	2023	Explores optimization of RIS-aided networks using heuristic and ML algorithms, highlighting the advantages of heuristic deep reinforcement learning over conventional DRL, and presents a novel approach combining heuristic and ML methods.	○	◐	○
[35]	2023	Explores RIS and ML integration for smart IoT systems, focusing on techniques like deep reinforcement learning and federated learning , and addresses future challenges in next-generation IoT networks.	◐	◐	○
[36]	2022	Reviews optimization and AI methods for RISs, compares solution quality and complexity, and addresses phase-shift optimization challenges.	○	●	○
[37]	2022	Examines state-of-the-art ML and DL techniques for RIS-enhanced communication, covering operational principles, channel estimation, and various ML applications in RIS-enhanced networks.	○	◐	○
[40]	2023	Provides a comprehensive review of STAR-RIS for 6G networks, covering fundamentals, protocols, applications, and performance metrics.	○	●	○
[42]	2024	Analyzes RIS control mechanisms and their optimization using AI, reviewing current methods, AI enhancements, and the challenges in meeting future network demands.	○	◐	○
[41]	2024	Comprehensive Review on advanced reconfigurable intelligent surfaces (ARIS), focusing on their advancements and applications in 6G networks. Examines various RIS technologies, their benefits, practical implementations, and identifies key research challenges and future directions.	○	◐	○
[38]	2022	Introduces a parametric model and optimization framework for RIS-assisted communications focusing on power maximization and surface impedance.	◐	◐	○
Current Survey	2024	Explores recent advancements in RIS-assisted communication through physically-consistent EM models, reviews optimization models for EM-aware RIS systems, including both traditional and ML-based approaches, and addresses open research issues in the field.	●	●	●

○ Not discussed in the paper.
◐ Mentioned in the paper, but not in detail.
● Discussed in detail in the paper.

comparative analysis, considering factors such as solution quality and computational complexity. Additionally, the paper outlines forthcoming challenges related to phase-shift optimization in the context of RISs and explores potential avenues for resolving these challenges.

Meanwhile, the survey in [37] offers a thorough examination of the current state-of-the-art in ML, with a particular emphasis on DL, within the context of RIS-enhanced communication. The review covers their operational principles, channel estimation (CE) techniques, and the diverse range of ML applications in RIS-enhanced wireless networks. Furthermore, it conducts a systematic survey of existing designs for RIS-enhanced wireless networks.

In [40], the authors deliver a comprehensive review of simultaneously transmitting and reflecting reconfigurable intelligent surface (STAR-RIS), with a particular emphasis on its applications in 6G networks. The paper begins by detailing the fundamentals of STAR-RIS, including its protocols, benefits, and various applications. The review categorizes STAR-RIS techniques across different use case scenarios, such as enhancing network coverage, improving physical layer security (PLS), maximizing sum rate, boosting EE, and reducing interference. It also explores various resource allocation strategies and performance evaluation metrics pertinent to STAR-RIS. However, the focus of this review is primarily on STAR-RIS. While it extensively surveys existing literature in this area, the paper does not delve into specific formulations or detailed solution approaches. Additionally, it does not address the EM-aware aspects of RIS, which is a key focus of our own work.

Another survey in [42] provides an in-depth analysis of RIS, focusing on the technology's control mechanisms and their optimization using artificial intelligence (AI). The paper reviews current RIS control methods, explores how AI can enhance performance, and highlights the limitations of AI-powered RIS control, as well as the significant challenges that must be addressed to meet future network demands.

A thorough examination of active RIS (ARIS) is given in [41], which highlights recent developments and their revolutionary effects on 6G networks. It provides a comparative examination of various schemes and solutions, covers numerous types and modes of RIS, and assesses ARIS applications for network parameter optimization. Additionally, it identifies key research challenges and future directions, highlighting ARIS's crucial role in advancing wireless communication, with a focus away from the physical aspects of RIS modeling and optimization.

Despite the extensive review of the works [26,31–34,34,34,36–41], there remains a gap in addressing the optimization of RIS-aided communications with an emphasis on EM-model-awareness. The work in [38] provides a thorough exploration of three pivotal communication models applied to RISs within wireless communication systems. These models are particularly relevant in scenarios involving in-homogeneous surface impedance boundaries, benefiting from their alignment with Maxwell's equations and consistent electromagnetic behavior, especially under practical approximations like physical optics. Delving deeper, the study navigates the intricacies of designing effective RISs, guided by local and global optimal criteria, and introduces an innovative approximate framework yielding reactive impedance boundaries. Supported by numerical examples, mathematical analysis, and simulations, the study offers a nuanced understanding of the models' strengths and limitations. A significant contribution lies in the introduction of a parametric model and optimization framework tailored for RIS-assisted communications, accommodating scenarios with gradually varying surface impedance while retaining the validity of the physical optics approximation. This model balances solution quality and implementation complexity through electromagnetic-consistent constraints. The study also emphasizes optimization scenarios where surface power efficiency is the objective, capturing optimal designs, corroborated by the power flux as a demonstrative measure of RIS steering capabilities. Placing findings within the context of wireless communications, the study paves the way for future research with streamlined numerical algorithms for electromagnetically consistent optimization problems and considerations for practical constraints in manufacturing-oriented applications. Ultimately, the study bridges theoretical models with tangible wireless communication systems, laying the groundwork for advancements that harmonize theory and application.

While the work in [38] presented a parametric model and an optimization framework for RIS-assisted communications, under the assumptions that the surface impedance changes slowly at the wavelength scale, and the physical optics approximation is valid, it did not extensively explore physically-consistent EM models-aware RIS-aided communication. The existing work focuss solely on the power maximization problem with respect to the surface impedance variable. In contrast, our work will address and comprehensively review EM-aware problems by taking into account both communication and physical variables.

Designing RIS-aided wireless networks requires paying attention to two important aspects. Firstly, it is important to consider EM-based designs where RISs perform fundamental radio wave transformations specified at the EM level. In this paradigm, engineers optimize RIS parameters to enhance network performance. Secondly, it is important to consider communication-based designs with focus on optimizing RISs to achieve specific communication goals, which must necessarily align with EM-based manipulations. In this paradigm, optimization is used to make RISs versatile for various performance metrics such as channel capacity and modulation schemes [12]. Compared to the surveys in Table 2, this comprehensive survey is dedicated to conducting a detailed exploration of the multifaceted research dimensions associated with RIS-aided networks while taking into account both aforementioned considerations. Our primary focus revolves around formulating optimization challenges concerning various objectives and constraints, including sum rate, received power, spectral efficiency (SE), and EE, all from an EM perspective. We also delve into the examination of the optimization techniques and methodologies applied to address these optimization challenges.

The exploration of RISs in wireless networks encompasses a diverse research landscape, spanning disciplines like communication theory, computer science, and electromagnetism. However, a significant drawback in the current state of RIS research lies in the absence of accurate models that effectively encapsulate the intricate EM characteristics of these adaptive meta-surfaces [43]. In the upcoming era, defined by the existence of reconfigurable EM environments, the primary goal will be to enhance system performance, potentially in real-time. This enhancement will be achieved by adjusting the parameters of EM objects (EMOs), such as the reflective properties of metasurface-based RISs. To achieve this goal, a holistic strategy is required, integrating physically-consistent models and design utilities that amalgamate signal processing with electromagnetic theory [44].

While existing studies often adopt a simplistic view of RISs as perfect reflectors, this oversimplification sidesteps crucial factors, such as incident angles, polarization, and material properties. To address these limitations and cultivate more realistic performance predictions, it is imperative to embrace physics and EM-compliant models [43].

In the pursuit of an accurate portrayal and optimization of RIS behavior, the incorporation of EM models proves indispensable. These models furnish a mathematical framework to decipher the intricate interplay between electromagnetic waves and the reconfigurable elements constituting the RIS. Physically-consistent EM models-aware RIS-aided communication approach, particularly demonstrated in the formulation of RIS-aided communication systems, offers significant advantages. These EM-aware models provide an accurate representation of the electromagnetic interactions between RIS elements and incoming waves, enabling more realistic predictions of RIS effects on signal propagation, reflection, and refraction, which is crucial for optimizing network performance. By incorporating these detailed aspects, the models enable precise tuning of RIS parameters, such as phase shifts and beamforming settings, resulting in improved performance metrics. This approach minimizes discrepancies between theoretical predictions and actual performance by accounting for real-world complexities. Additionally, EM models that integrate these concepts facilitate simulations of RIS-aided networks under realistic conditions, including environmental variations and complex wave interactions, which aids in assessing the feasibility of proposed solutions and making informed decisions about network deployment and configuration.

3. EM-based models of RIS

RIS are frequently reduced to perfect scatterers in optimization and signal processing designs for wireless communication systems. Nevertheless, because they ignore important details like phase–amplitude correlation in reflection coefficients and mutual coupling between scattering elements, these simplified models lack EM consistency. Incorporating realistic reradiation models that address the interaction between element-level scattering design and surface-level optimization is crucial, according to recent studies. Consequently, efforts are underway to develop electromagnetically consistent RIS models and efficient optimization algorithms. Traditionally, RIS behavior is analyzed using three main EM modeling approaches:

- Scattering (S-parameter) Model: This model describes how RIS elements scatter incoming signals, providing insights into the reflected signal's characteristics.
- Impedance (Z-parameter) Model: This model characterizes the impedance of the RIS elements, allowing analysis of how the elements interact with the incident signal in terms of impedance.

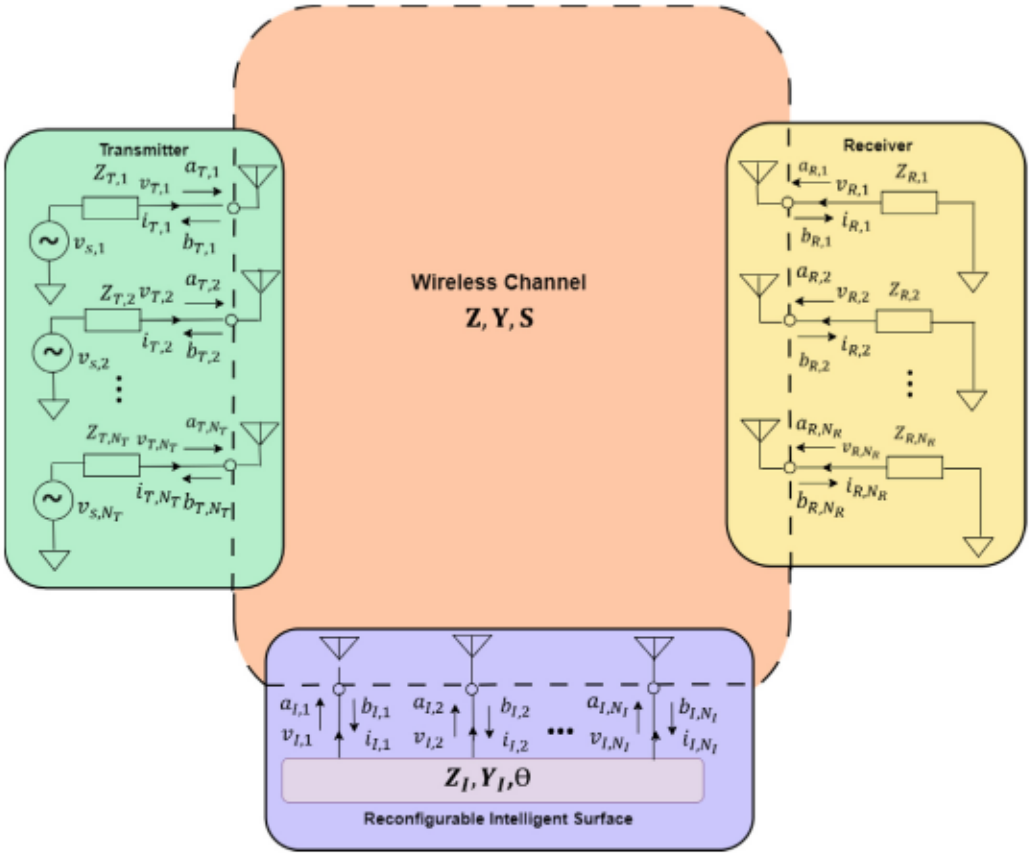

Fig. 4. Multiport representation of an RIS-assisted communication system (© 2024 IEEE, [46]).

- Admittance (Y-parameter) Model: This model describes the admittance characteristics of the RIS elements, offering an alternative perspective on how the elements interact with the incident signal.

All three models are ultimately derived from Maxwell's equations and provide equivalent descriptions of the RIS system.

Recently, another approach based on the polarizabilities of RIS elements has been proposed. The polarizability-based model offers simpler and more intuitive mathematical expressions, aligning better with the localized nature of RIS element reconfigurability. This approach complements the traditional models by providing a more flexible framework for RIS system analysis and design, particularly in capturing the interaction between RIS elements and electromagnetic waves.

3.1. Multiport network theory

Multiport network theory is emerging as a promising approach for modeling and optimizing RIS-aided channels due to its ability to capture electromagnetic coupling between closely spaced radiating elements, which is crucial for achieving advanced wave transformations with high power efficiency [45,46].

Consider a MIMO communication setup enhanced by an RIS, featuring N_T antennas at the transmitter, N_R antennas at the receiver, and N_I antennas at the RIS, as depicted in Fig. 4. The wireless channel is modeled as an N-port network, where $N = N_T + N_I + N_R$.

3.1.1. Modeling based on the impedance parameters

The wireless channel can be characterized by its impedance matrix $\mathbf{Z} \in \mathbb{C}^{N\times N}$, with the relationship:

$$\mathbf{v} = \mathbf{Z}\mathbf{i}, \tag{1}$$

where $\mathbf{v} \in \mathbb{C}^{N\times 1}$ and $\mathbf{i} \in \mathbb{C}^{N\times 1}$ are the voltages and currents at the N ports, respectively. We partition $\mathbf{v}$, $\mathbf{i}$, and $\mathbf{Z}$ as:

$$\mathbf{v} = \begin{bmatrix} \mathbf{v}_T \\ \mathbf{v}_I \\ \mathbf{v}_R \end{bmatrix}, \quad \mathbf{i} = \begin{bmatrix} \mathbf{i}_T \\ \mathbf{i}_I \\ \mathbf{i}_R \end{bmatrix}, \quad \mathbf{Z} = \begin{bmatrix} \mathbf{Z}_{TT} & \mathbf{Z}_{TI} & \mathbf{Z}_{TR} \\ \mathbf{Z}_{IT} & \mathbf{Z}_{II} & \mathbf{Z}_{IR} \\ \mathbf{Z}_{RT} & \mathbf{Z}_{RI} & \mathbf{Z}_{RR} \end{bmatrix}, \tag{2}$$

where $\mathbf{v}_i \in \mathbb{C}^{N_i\times 1}$ and $\mathbf{i}_i \in \mathbb{C}^{N_i\times 1}$ for $i \in \{T, I, R\}$ denote the voltages and currents at the antennas of the transmitter, RIS, and receiver, respectively. Besides, $\mathbf{Z}_{TT} \in \mathbb{C}^{N_T\times N_T}$ is the impedance matrix for the transmitting antennas, with off-diagonal entries indicating mutual coupling among the antennas. $\mathbf{Z}_{II} \in \mathbb{C}^{N_I\times N_I}$ represents the impedance matrix for the RIS elements, where the off-diagonal terms reflect mutual coupling between different RIS elements. $\mathbf{Z}_{RR} \in \mathbb{C}^{N_R\times N_R}$ denotes the impedance matrix for the receiving antennas, capturing mutual coupling among these antennas. The transmission impedance matrices include $\mathbf{Z}_{TI} \in \mathbb{C}^{N_I\times N_T}$, which describes the interaction from transmitting antennas to the RIS; $\mathbf{Z}_{IR} \in \mathbb{C}^{N_R\times N_I}$, representing the interaction from the RIS to the receiving antennas; and $\mathbf{Z}_{RT} \in \mathbb{C}^{N_R\times N_T}$, which covers the interaction from receiving antennas to transmitting antennas. For a reciprocal wireless channel:

$$\mathbf{Z}_{TR} = \mathbf{Z}_{RT}^T, \quad \mathbf{Z}_{TI} = \mathbf{Z}_{IT}^T, \quad \mathbf{Z}_{IR} = \mathbf{Z}_{RI}^T. \tag{3}$$

At the transmitter, each antenna n_T is connected in series with a source voltage $\mathbf{v}_{s,n_T}$ and a source impedance $\mathbf{Z}_{T,n_T}$, where:

$$\mathbf{v}_T = \mathbf{v}_{s,T} - \mathbf{Z}_T\mathbf{i}_T, \tag{4}$$

with $\mathbf{v}_{s,T}$ as the source voltage vector and $\mathbf{Z}_T$ as a diagonal matrix.

At the RIS, the N_I scattering elements are connected to an N_I-port reconfigurable impedance network, related by:

$$\mathbf{v}_I = -\mathbf{Z}_I\mathbf{i}_I, \tag{5}$$

where $\mathbf{Z}_I$ is the impedance matrix of the reconfigurable network.

At the receiver, each antenna n_R is connected in series with a load impedance $\mathbf{Z}_{R,n_R}$, related by:

$$\mathbf{v}_R = -\mathbf{Z}_R \mathbf{i}_R, \tag{6}$$

where $\mathbf{Z}_R$ is a diagonal matrix.

3.1.2. Modeling based on the admittance parameters

The channel can also be characterized by its admittance matrix $\mathbf{Y} \in \mathbb{C}^{N\times N}$, where:

$$\mathbf{i} = \mathbf{Y}\mathbf{v}. \tag{7}$$

The admittance matrix $\mathbf{Y}$ is the inverse of $\mathbf{Z}$:

$$\mathbf{Y} = \mathbf{Z}^{-1}. \tag{8}$$

Similar to $\mathbf{Z}$, $\mathbf{Y}$ can be partitioned as:

$$\mathbf{Y} = \begin{bmatrix} \mathbf{Y}_{TT} & \mathbf{Y}_{TI} & \mathbf{Y}_{TR} \\ \mathbf{Y}_{IT} & \mathbf{Y}_{II} & \mathbf{Y}_{IR} \\ \mathbf{Y}_{RT} & \mathbf{Y}_{RI} & \mathbf{Y}_{RR} \end{bmatrix}, \tag{9}$$

where $\mathbf{Y}_{ij} \in \mathbb{C}^{N_i\times N_j}$ for $i, j \in \{T, I, R\}$.

At the transmitter, receiver, and RIS, the currents $\mathbf{i}_T$, $\mathbf{i}_I$, and $\mathbf{i}_R$ and voltages $\mathbf{v}_T$, $\mathbf{v}_I$, and $\mathbf{v}_R$ are related by:

$$\mathbf{i}_T = \mathbf{i}_{s,T} - \mathbf{Y}_T\mathbf{v}_T, \quad \mathbf{i}_I = -\mathbf{Y}_I\mathbf{v}_I, \quad \mathbf{i}_R = -\mathbf{Y}_R\mathbf{v}_R, \tag{10}$$

where the source current vector $\mathbf{i}_{s,T}$ and diagonal matrix $\mathbf{Y}_T$ relate currents $\mathbf{i}_T$ and voltages $\mathbf{v}_T$ at the transmitter; the admittance matrix $\mathbf{Y}_I$ relates currents $\mathbf{i}_I$ and voltages $\mathbf{v}_I$ at the RIS; and the diagonal matrix $\mathbf{Y}_R$ relates currents $\mathbf{i}_R$ and voltages $\mathbf{v}_R$ at the receiver. Besides, the diagonal admittance matrices are related to the impedance matrices as $\mathbf{Y}_T = \mathbf{Z}_T^{-1}$, $\mathbf{Y}_I = \mathbf{Z}_I^{-1}$, and $\mathbf{Y}_R = \mathbf{Z}_R^{-1}$.

3.1.3. Modeling based on the scattering parameters

The channel can be characterized by its scattering matrix $\mathbf{S} \in \mathbb{C}^{N\times N}$, with the relationship:

$$\mathbf{b} = \mathbf{S}\mathbf{a}, \tag{11}$$

where $\mathbf{a} \in \mathbb{C}^{N\times 1}$ and $\mathbf{b} \in \mathbb{C}^{N\times 1}$ are the incident and reflected waves, respectively. The scattering matrix $\mathbf{S}$ can be partitioned as:

$$\mathbf{S} = \begin{bmatrix} \mathbf{S}_{TT} & \mathbf{S}_{TI} & \mathbf{S}_{TR} \\ \mathbf{S}_{IT} & \mathbf{S}_{II} & \mathbf{S}_{IR} \\ \mathbf{S}_{RT} & \mathbf{S}_{RI} & \mathbf{S}_{RR} \end{bmatrix}, \tag{12}$$

where $\mathbf{S}_{ij} \in \mathbb{C}^{N_i\times N_j}$ for $i, j \in \{T, I, R\}$.

The vectors $\mathbf{v}$ and $\mathbf{i}$ are related to $\mathbf{a}$ and $\mathbf{b}$ by:

$$\mathbf{v} = \mathbf{a} + \mathbf{b}, \quad \mathbf{i} = \frac{\mathbf{a} - \mathbf{b}}{Z_0} = Y_0(\mathbf{a} - \mathbf{b}), \tag{13}$$

where Z_0 is the characteristic impedance, and $Y_0 = \frac{1}{Z_0}$ is the characteristic admittance. The matrix $\mathbf{S}$ can be expressed in terms of $\mathbf{Z}$ as:

$$\mathbf{S} = (\mathbf{Z} + Z_0 I)^{-1}(\mathbf{Z} - Z_0 I). \tag{14}$$

At the transmitter, receiver, and RIS, the incident and reflected waves are related by:

$$\mathbf{a}_T = \mathbf{b}_{s,T} + \Gamma_T\mathbf{b}_T, \quad \mathbf{a}_I = \Theta\mathbf{b}_I, \mathbf{a}_R = \Gamma_R\mathbf{b}_R, \tag{15}$$

where $\mathbf{b}_{s,T}$ represents the source wave vector, Γ_T denotes the reflection coefficient matrix at the transmitter, Θ is the scattering matrix of the reconfigurable network at the RIS, and Γ_R is the reflection coefficient matrix at the receiver.

The summary of each model is presented in Table 3[45–49]. In the analysis of channel models utilizing Z, Y, and S parameters, several simplifications are applied under the assumptions of perfect matching and the absence of mutual coupling. Specifically, for the Z-parameters, the channel model simplifies to:

$$h = \frac{1}{2Z_0}\left[Z_{RT} - Z_{RI}(Z_I + Z_0 I)^{-1}Z_{IT}\right]. \tag{16}$$

For the Y-parameters, the model simplifies to:

$$h = \frac{1}{2Y_0}\left[-Y_{RT} + Y_{RI}(Y_I + Y_0 I)^{-1}Y_{IT}\right]. \tag{17}$$

For the S-parameters, the model is given by:

$$h = S_{RT} + S_{RI}(I - \Theta S_{II})^{-1}\Theta S_{IT}, \tag{18}$$

with further simplifications under the assumption of perfect matching at the RIS. The mappings between these parameter sets demonstrate that the simplified models are equivalent, confirming consistency across different parameter analyses [46,50].

3.1.4. Modeling based on the polarizability parameters

The majority of current signal-processing work makes the assumption that wireless channels and RIS configuration follow a linear relationship. But Maxwell's equations are frequently in conflict with this premise. A recently proposed physics-compliant model for RIS-parametrized channels focuses on expressing the reconfigurability of RIS elements through adjustable polarizability [51]. In this model, RIS elements and antennas are modeled as dipoles with tunable polarizabilities. An interaction matrix $\mathbf{M} \in \mathbb{C}^{N\times N}$ captures the local scattering characteristics of these dipoles along its diagonal and their interactions off-diagonal:

$$M_{i,j} = \begin{cases} \alpha_i^{-1} & \text{if } i = j \\ -G_{ij} & \text{if } i \neq j, \end{cases} \tag{19}$$

where $N = N_T + N_R + N_S$, with N_T transmitting antennas, N_R receiving antennas, and N_S RIS elements in the considered system model. Here, α_i denotes the polarizability of the ith dipole and G_{ij} is the Green's function, representing the electric field at the ith dipole due to a unit dipole moment at the jth dipole. The sub-indices T, R, A, and S denote the sets of indices associated with transmitting antennas, receiving antennas, all antennas, and RIS elements, respectively [52–56].

The vector $\mathbf{d}$ is defined as the vector of inverse polarizabilities for the RIS dipoles:

$$\mathbf{d} = \text{diag}(M_{SS}), \tag{20}$$

where $\mathbf{d}$ includes the diagonal elements of the matrix M_{SS}.

Assuming identical transmitting and receiving antennas, the channel matrix $\mathbf{h}$ is proportional to the RT block of the inverse of the interaction matrix:

$$\mathbf{h} \propto [\mathbf{M}]_{RT}^{-1}. \tag{21}$$

To compute this efficiently, the reduced interaction matrix $\bar{\mathbf{M}}$ is defined as:

$$\bar{\mathbf{M}} = \mathbf{M}_{AA} - \mathbf{M}_{AS}\left(\mathbf{M}_{SS}\right)^{-1}\mathbf{M}_{SA}. \tag{22}$$

Then, the RT block of the inverse of $\bar{\mathbf{M}}$ is given by:

$$\mathbf{H} \propto \left[\bar{\mathbf{M}}^{-1}\right]_{RT} = -\left[\bar{\mathbf{M}}_{RR} - \bar{\mathbf{M}}_{RT}\bar{\mathbf{M}}_{TT}^{-1}\bar{\mathbf{M}}_{TR}\right]^{-1}\bar{\mathbf{M}}_{RT}\bar{\mathbf{M}}_{TT}^{-1}. \tag{23}$$

3.2. Beyond diagonal RIS

Traditionally, RISs have been implemented by adjusting each RIS element through a tunable load, resulting in a diagonal phase shift matrix with limited flexibility. To address this constraint, the concept of BD-RIS has recently emerged [57]. The key innovation of BD-RIS lies in the integration of tunable impedance components that interconnect the RIS elements, enhancing its flexibility.

The classification of existing BD-RIS systems, which focuses on the characteristics of the BD-RIS matrix, the supported modes, and the architectural designs, has been extensively explored in various studies conducted by Hongyu et al. [46,57–59].

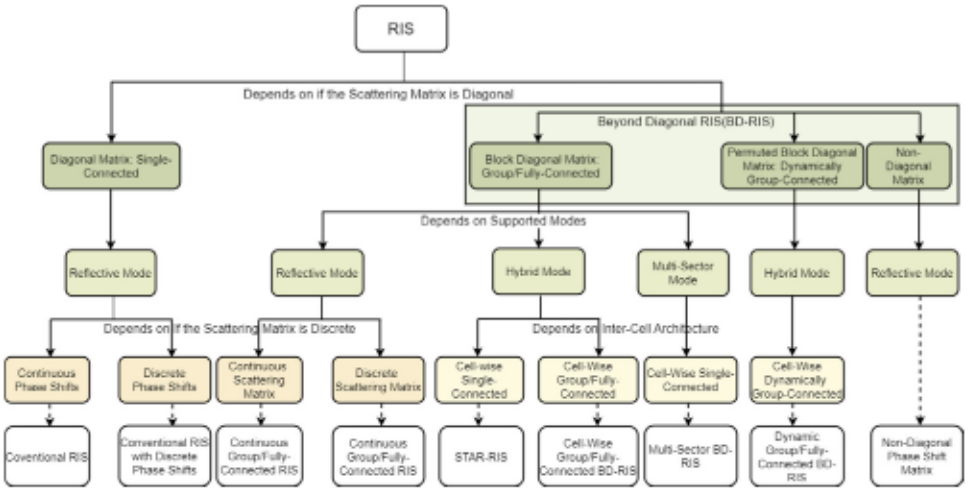

Fig. 5. RIS classification tree (© 2023 IEEE, [58]).

The three-layer classification scheme for BD-RIS systems, as described in [57], is depicted in Fig. 5. Each layer is explained in detail below.

First Layer: Characteristics of the Scattering Matrix Φ

1. **Diagonal Matrix-Single-Connected** The single connected RIS architecture, commonly found in the literature [13,60,61], follows a conventional approach. In this setup, each port of the reconfigurable impedance network connects to ground through a reconfigurable impedance and remains disconnected from the other ports.
2. **Block Diagonal Matrix:** This category involves dividing M antennas into G groups. Antennas within the same group are interconnected, but those across groups are not. This setup, known as group-connected RIS [57], employs a scattering matrix Φ structured as a block diagonal matrix. Each block is unitary, allowing manipulation of both phase and magnitude of incident waves. This configuration outperforms conventional RIS 1.0. When all antennas are connected (G = 1), it is termed fully connected RIS [57], resulting in a unitary scattering matrix. Single-connected RIS is a special case with M groups, having a diagonal scattering matrix [62].
3. **Permuted Block Diagonal Matrix:** Here, the grouping strategy adapts to channel state information (CSI), creating a permuted block diagonal matrix [59]. This flexibility enhances beam control compared to fixed group-connected RIS [63].
4. **Non-Diagonal Matrix:** Antennas are paired via phase shifters, causing signals on one antenna to purely reflect from another. This yields an asymmetric non-diagonal scattering matrix [46], offering higher power gain than conventional RIS 1.0 [64].

Second Layer: Supported Modes

1. **Reflective Mode:** Signals on one side of the RIS reflect toward the same side, covering half-space. Mathematically, it is characterized by a unitary constraint matrix Φ.
2. **Hybrid Mode:** In hybrid mode, the RIS allows signals to be partially reflected and transmitted to opposite sides, providing full-space coverage. This configuration, known as STAR-RIS or intelligent omni-surface (IOS), uses back-to-back antennas with unidirectional patterns, connected to a 2-port reconfigurable impedance network, to cover the entire space. Mathematically, the RIS operating in hybrid mode is described by two matrices, $\Phi_{\text{ref}} \in \mathbb{C}^{M/2\times M/2}$ and $\Phi_{\text{tms}} \in \mathbb{C}^{M/2\times M/2}$, satisfying the condition $\Phi_H^{\text{ref}}\Phi_{\text{ref}} + \Phi_H^{\text{tms}}\Phi_{\text{tms}} = I_{M/2}$ [59,65–69].
3. **Multi-Sector Mode:** This mode divides the full space into K sectors ($K \geq 2$), allowing signals impinging on one sector of the RIS to be partially reflected toward the same sector and partially scattered toward the other $K-1$ sectors . Each cell contains K antennas placed at each edge of an K-sided polygon, with each antenna having a unidirectional radiation pattern covering $1/K$ to avoid overlap among sectors. The K antennas are connected to an K-port fully-connected reconfigurable impedance network, resulting in coverage of the full space while providing higher performance gains than the hybrid mode. Mathematically, the RIS with multi-sector mode is characterized by K matrices, $\Phi_k \in \mathbb{C}^{M/K\times M/K}$, for $k = 1, \ldots, K$, which satisfy $\sum_{k=1}^{K} \Phi_k^H \Phi_k = I_M$ [57,66,70].

Third Layer: Inter-Cell Architecture

This layer considers how cells are connected in BD-RIS with hybrid/multi-sector modes, resulting in single/group/fully connected architectures, affecting the resulting scattering matrices [57].

The authors in [58] also explored designs of single, group, and fully-connected RIS with discrete values. Their findings indicate that while four resolution bits are required in single-connected RIS, only one resolution bit suffices in fully-connected RIS. This simplification significantly streamlines the future development of these promising RIS architectures.

3.3. Mutual coupling

Mutual coupling-aware models are crucial for accurately simulating and understanding the interactions between elements in a RIS. These models enable precise predictions and optimizations of RIS system performance across different communication scenarios [71]. The primary models for considering mutual coupling in communications are generally split into two types: those that use impedance matrices and those that rely on scattering matrices.

The study in [72] examines a mutual coupling-aware communication model assisted by BD-RIS, utilizing analyses of scattering and impedance parameters. The proposed general RIS-aided channel, denoted as $\mathbf{h}_{\text{TR}} \in \mathbb{C}^{K\times N}$, which describes the relationship between the voltage at receiver ports and transmitter ports, is expressed as follows:

$$\mathbf{h}_{\text{TR}} = (\Gamma_R + \mathbf{I}_K)^{-1}\mathbf{T}_{\text{RT}}(\mathbf{I}_N + \Gamma_T\mathbf{T}_{\text{TT}} + \mathbf{T}_{\text{TT}})^{-1} \tag{24}$$

where $\mathbf{T}_{\text{TT}} \in \mathbb{C}^{N\times N}$ and $\mathbf{T}_{\text{RT}} \in \mathbb{C}^{K\times N}$ are submatrices of $\mathbf{T} = \mathbf{S}(\mathbf{I}_L - \Gamma\mathbf{S})^{-1} \in \mathbb{C}^{L\times L}$ with $\Gamma = \text{blkdiag}(\Gamma_T, \Theta, \Gamma_R)$. Specifically, $\mathbf{T}_{\text{TT}} = [\mathbf{T}]_{1:N,1:N}$ and $\mathbf{T}_{\text{RT}} = [\mathbf{T}]_{N+M+1:L,1:N}$. Besides, Γ_T and Γ_R represents reflection coefficient matrix at the transmitter and receiver respectively.

Table 3
N-port network RIS-aided MIMO Communications using impedance, admittance, or scattering matrix [46].

Impedance parameters-based model	Scattering parameters-based model	Admittance parameters-based model
$\begin{bmatrix} \mathbf{v}_T \\ \mathbf{v}_I \\ \mathbf{v}_R \end{bmatrix} = \begin{bmatrix} \mathbf{Z}_{TT} & \mathbf{Z}_{TI} & \mathbf{Z}_{TR} \\ \mathbf{Z}_{IT} & \mathbf{Z}_{II} & \mathbf{Z}_{IR} \\ \mathbf{Z}_{RT} & \mathbf{Z}_{RI} & \mathbf{Z}_{RR} \end{bmatrix} \begin{bmatrix} \mathbf{i}_T \\ \mathbf{i}_I \\ \mathbf{i}_R \end{bmatrix}$	$\begin{bmatrix} \mathbf{b}_T \\ \mathbf{b}_I \\ \mathbf{b}_R \end{bmatrix} = \begin{bmatrix} \mathbf{S}_{TT} & \mathbf{S}_{TI} & \mathbf{S}_{TR} \\ \mathbf{S}_{IT} & \mathbf{S}_{II} & \mathbf{S}_{IR} \\ \mathbf{S}_{RT} & \mathbf{S}_{RI} & \mathbf{S}_{RR} \end{bmatrix} \begin{bmatrix} \mathbf{a}_T \\ \mathbf{a}_I \\ \mathbf{a}_R \end{bmatrix}$	$\begin{bmatrix} \mathbf{Y}_{TT} & \mathbf{Y}_{TI} & \mathbf{Y}_{TR} \\ \mathbf{Y}_{IT} & \mathbf{Y}_{II} & \mathbf{Y}_{IR} \\ \mathbf{Y}_{RT} & \mathbf{Y}_{RI} & \mathbf{Y}_{RR} \end{bmatrix}$
$\mathbf{v}_T = \mathbf{v}_{s,t} - \mathbf{Z}_T \mathbf{i}_T$	$\mathbf{a}_T = \mathbf{b}_{s,t} + \mathbf{\Gamma}_T \mathbf{b}_T$	$\mathbf{i}_T = \mathbf{i}_{s,T} - \mathbf{Y}_T \mathbf{v}_T$
$\mathbf{v}_I = -\mathbf{Z}_I \mathbf{i}_I$	$\mathbf{a}_I = \mathbf{\Theta} \mathbf{b}_I$	$\mathbf{i}_I = -\mathbf{Y}_I \mathbf{v}_I$
$\mathbf{v}_R = -\mathbf{Z}_R \mathbf{i}_R$	$\mathbf{a}_R = \mathbf{\Gamma}_R \mathbf{b}_R$	$\mathbf{i}_R = -\mathbf{Y}_R \mathbf{v}_R$
$\mathbf{Z}_T = \mathrm{diag}(Z_{T,1}, \dots, Z_{T,NT})$	$\mathbf{S} = (\mathbf{Z} + \mathbf{Z}_0\mathbf{I})^{-1}(\mathbf{Z} - \mathbf{Z}_0\mathbf{I})$	
$\mathbf{Z}_R = \mathrm{diag}(Z_{R,1}, \dots, Z_{R,NR})$	$\mathbf{\Gamma}_T = (\mathbf{Z}_T + \mathbf{Z}_0\mathbf{I})^{-1}(\mathbf{Z}_T - \mathbf{Z}_0\mathbf{I})$	
	$\mathbf{\Theta} = (\mathbf{Z}_I + \mathbf{Z}_0\mathbf{I})^{-1}(\mathbf{Z}_I - \mathbf{Z}_0\mathbf{I})$	
	$\mathbf{\Gamma}_R = (\mathbf{Z}_R + \mathbf{Z}_0\mathbf{I})^{-1}(\mathbf{Z}_R - \mathbf{Z}_0\mathbf{I})$	

The proposed channel model, outlined in Eq. (24), effectively encompasses the impacts of antenna mismatching and mutual coupling at the transmitter, BD-RIS, and receiver. Nonetheless, its complexity makes it challenging to clearly understand the function of BD-RIS. Then, to streamline the overall communication model, they introduce a simplifying set of assumptions. Firstly, they assume equal source and load impedances ($\mathbf{Z}_T = Z_0\mathbf{I}_N, \mathbf{Z}_R = Z_0\mathbf{I}_K$), ensuring optimal power matching at the transmitter and receiver. Secondly, they make the unilateral approximation, assuming negligible links between devices due to sufficiently large distances ($\mathbf{Z}_{TI} \approx 0, \quad \mathbf{Z}_{TR} \approx 0, \quad \mathbf{Z}_{IR} \approx 0$). Thirdly, they posit perfectly matched antennas at both ends, minimizing mutual coupling effects ($\mathbf{Z}_{TT} = Z_0\mathbf{I}_N$ and $\mathbf{Z}_{RR} = Z_0\mathbf{I}_K$)[72].

Based on the above assumptions, and the relationship $\mathbf{S} = (\mathbf{Z} + Z_0\mathbf{I}_L)^{-1}(\mathbf{Z} - Z_0\mathbf{I}_L)$, the transmission scattering matrices from the receiver to the transmitter approach zero, i.e., $\mathbf{S}_{\mathrm{TI}} \approx 0, \quad \mathbf{S}_{\mathrm{TR}} \approx 0, \quad \mathbf{S}_{IR} \approx 0$. Additionally, the scattering matrices at the antenna arrays of the transmitter and receiver also approach zero, i.e., ($\mathbf{S}_{\mathrm{TT}} \approx 0, \quad \mathbf{S}_{\mathrm{RR}} \approx 0$) Consequently, the following simplified channel is resulted:

$$\mathbf{h}_{\mathrm{TR}} \approx \mathbf{S}_{\mathrm{RT}} + \mathbf{S}_{\mathrm{RI}}(\mathbf{I}_M - \mathbf{\Theta}\mathbf{S}_{\mathrm{II}})^{-1}\mathbf{\Theta}\mathbf{S}_{\mathrm{IT}} \tag{25}$$

As the matrix $\mathbf{\Theta}$ of reflection coefficients introduces complexity by appearing both inside and outside the inverse, further simplifications by leveraging the relationship between nonzero sub-matrices of $\mathbf{S}$ and those of $\mathbf{Z}$ are introduced. So, a more tractable and convenient expression equivalent to is suggested as:

$$\mathbf{h}_{\mathrm{TR}} \approx \frac{1}{2Z_0}(\mathbf{Z}_{\mathrm{RT}} - \mathbf{Z}_{\mathrm{RI}}(\mathbf{Z}_{\mathrm{II}} + \mathbf{Z}_{\mathrm{I}})^{-1}\mathbf{Z}_{\mathrm{IT}}) \tag{26}$$

The matrices $\mathbf{Z}_{\mathrm{RT}}$, $\mathbf{Z}_{\mathrm{RI}}$, and $\mathbf{Z}_{\mathrm{TT}}$ describe the channels from the transmitter to the receiver, from the BD-RIS to the receiver, and from the transmitter to the BD-RIS, respectively. The matrix $\mathbf{Z}_{\mathrm{II}}$ addresses the mismatching and mutual coupling effects at the RIS elements, where its diagonal entries represent the self-impedance of the elements and the off-diagonal entries account for mutual coupling. This coupling is influenced by the spacing between the elements, with wider separations typically leading to less mutual coupling.

Several other researchers have investigated mutual coupling-aware RIS-aided communications [48,73].

3.4. Lessons learned

- The EM effects are commonly characterized using S parameters and/or Z parameters in communication systems.
- The introduction of BD-RIS has transformed the conventional approach to RIS implementation by incorporating tunable impedance components for interconnecting RIS elements. This innovation enhances the flexibility of RIS configurations beyond the limitations imposed by diagonal phase shift matrices, marking a significant departure from traditional RIS setups.
- Understanding and modeling mutual coupling effects between RIS elements is crucial in optimizing RIS performance and overall system efficiency, especially in scenarios where the proximity of elements leads to mutual interference and complex electromagnetic interactions.

4. EM model-aware problem formulation

This section delves into diverse problem formulations pertaining to the optimization of RIS-enhanced wireless networks. The emphasis is distinctly on EM factors and considerations. These formulations cover a broad spectrum of objectives, including the improvement of channel gain and capacity, enhancement of SINR and maximization of sum rate, enhancement of energy efficiency, and minimization of power consumption.

4.1. Channel gain

Maximization of channel gain in BD-RIS aided communications with considering the mutual coupling effects between RIS elements is studied in [72]. A SISO system with focuses on the optimization of block diagonal impedance matrix $\mathbf{Z}_I$ of group-connected architecture is considered. The channel gain maximization problem considering the channel model in Eq. (26) is formulated as follows:

$$\max_{\mathbf{Z}_I} \quad \left|\mathbf{Z}_{\mathrm{RT}} - \mathbf{Z}_{\mathrm{RI}}(\mathbf{Z}_{\mathrm{II}} + \mathbf{Z}_I)^{-1}\mathbf{Z}_{\mathrm{IT}}\right|^2 \tag{27a}$$

subject to

$$\mathbf{Z}_I = \mathrm{blkdiag}(\mathbf{Z}_{I,1}, \dots, \mathbf{Z}_{I,G}), \tag{27b}$$

$$\mathbf{Z}_{I,g} = \mathbf{Z}_{I,g}^T, \quad \Re\{\mathbf{Z}_{I,g}\} = 0, \quad \forall g \in \mathcal{G}. \tag{27c}$$

In this context, each block $\mathbf{Z}_{I,g} \in \mathbb{C}^{M' \times M'}$, for all $g \in \mathcal{G} = \{1, \dots, G\}$, is characterized by being symmetric and purely imaginary in the context of reciprocal and lossless reconfigurable impedance networks . In particular, when $G = 1$ and $G = M$, it corresponds to the fully-connected and single-connected architectures of BD-RIS, respectively [72]. An iterative optimization technique, incorporating the Neumann series approximation is employed to tackle the computational hurdle arising from matrix inversion within the objective function mentioned in Eq. (27a).

4.2. Capacity

RIS's dynamic control over the propagation environment enables it to improve link quality, extend coverage, and ultimately enhance the overall capacity of wireless communication systems.

The research presented in [74] addresses the gap concerning wideband communications with BD-RIS, a topic previously explored only in [75]. Prior studies assumed linear variations of RIS phase-shifts across subcarriers and proposed a quasi-Newton method to optimize channel capacity, lacking a derived system model and a problem-specific algorithm. This paper fills these gaps by deriving the OFDM system model from fundamental principles, resulting in a unique expression. Additionally, it introduces a specialized algorithm to optimize wideband capacity under specific constraints. The resulting capacity expression provides detailed insights into the impact of propagation paths on cascaded channel expressions. Simulation results demonstrate that employing BD-RIS significantly enhances wideband capacity, particularly in non-line-of-sight (NLOS) channels.

The capacity of the BD-RIS-assisted SISO OFDM system, given a reflection matrix $\mathbf{\Psi}$, is expressed as:

$$C = \frac{B}{N_c+T}\sum_{\nu=0}^{N_c-1}\log_2\left(1+\frac{p_\nu^{\text{opt}}|\bar{h}_\nu+\text{tr}(\mathbf{\Psi}\mathbf{H}_\nu)|^2}{N_0}\right)\ \text{bit/s} \tag{28}$$

where B denotes the bandwidth. Besides,

$$p_\nu^{\text{opt}} = \max\left(\mu - \frac{N_0}{|\bar{h}_\nu+\text{tr}(\mathbf{\Psi}\mathbf{H}_\nu)|^2}, 0\right), \quad \nu = 0,\dots,N_c-1 \tag{29}$$

Here, p_ν^{opt} denotes the power allocated to subcarrier ν using the water-filling method, and μ is chosen to meet the total power constraint $\sum_{\nu=0}^{N_c-1} p_\nu^{\text{opt}} = P_t N_c$. Moreover, P_t represents the total power available.

Considering the time and frequency domain representations of channels as follows:

$$c_s[\ell] = \sum_{i=1}^{L_s} a_{s,i}e^{-j2\pi f_c(\tau_{s,i}-\eta)}\text{sinc}\left(\ell + B(\eta-\tau_{s,i})\right), \tag{30}$$

$$c_{i,j}[\ell] = a_{r,1,j}a_{t,1,i}e^{-j2\pi f_c(\tau_{r,1,j}+\tau_{t,1,i}-\eta)} \times \text{sinc}\left(\ell + B(\eta-\tau_{r,1,j}-\tau_{t,1,i})\right), \tag{31}$$

$$\bar{c}_s[\nu] = \sum_{\ell=0}^{T} c_s[\ell]e^{-j2\pi\ell\nu/N_c}, \quad \nu = 0,\dots,N_c-1, \tag{32}$$

$$\bar{c}_{i,j}[\nu] = \sum_{\ell=0}^{T} c_{i,j}[\ell]e^{-j2\pi\ell\nu/N_c}, \quad \nu = 0,\dots,N_c-1, \tag{33}$$

where $a_{r,1,j}, a_{t,1,i} \in [0,1]$ represent the attenuations, and $\tau_{t,1,i}, \tau_{r,1,j} \geq 0$ represent the propagation delays of the impulse responses to and from RIS element 1. The following channel formulation is obtained:

$$\bar{h}_{\mathbf{\Psi}}[\nu] = \bar{c}_s[\nu] + \text{tr}(\mathbf{\Psi}\sum_{j=1}^{L_r}\sum_{i=1}^{L_t}\bar{c}_{i,j}[\nu]\mathbf{a}(\phi_{i,i},\theta_{i,i})\mathbf{a}^T(\phi_{o,j},\theta_{o,j})) \tag{34}$$

where

$$\bar{h}_\nu = \bar{c}_s[\nu], \tag{35}$$

$$\mathbf{H}_\nu = \sum_{j=1}^{L_r}\sum_{i=1}^{L_t}\bar{c}_{i,j}[\nu]\mathbf{a}(\phi_{i,i},\theta_{i,i})\mathbf{a}^T(\phi_{o,j},\theta_{o,j}), \tag{36}$$

The channel model includes several parameters: L_t and L_r denote the number of propagation paths from the transmitter to the RIS and from the RIS to the receiver, respectively. T represents the length determined by the delay spread and PAM pulse, crucial for OFDM modulation. ν and ℓ are indices representing frequency and time, essential for analyzing temporal and spectral dynamics. The angles $(\phi_{i,i},\theta_{i,i})$ and $(\phi_{o,j},\theta_{o,j})$ describe incident and outgoing paths relative to the RIS's broadside direction. Finally, N represents the number of phase shifts associated with each path, influencing the interactions within the RIS-assisted communication system. Besides, the vectors $\mathbf{a}(\phi_{i,i},\theta_{i,i})$ and $\mathbf{a}(\phi_{o,j},\theta_{o,j})$ are the array response vectors for the incident and outgoing paths at the RIS, respectively, capturing the phase shifts across array elements due to path differences for the specified angles. Then, the capacity in Eq. (28) is maximized respect to a fully connected BD-RIS phase shift constraint as follows:

$$\mathbf{\Psi} = \mathbf{\Psi}^T, \tag{37}$$

$$\mathbf{\Psi}\mathbf{\Psi}^H = \mathbf{I}_N \tag{38}$$

Due to the complexity arising from the reflection matrix $\mathbf{\Psi}$ impacting all subcarriers, they adopt a novel divide-and-conquer approach to address the maximization problem [74].

4.3. Received power

The minimization of transmit power or the maximization of received power is another widely investigated topic in RIS-aided wireless communications. Transmission power reduction not only saves the power consumption of wireless networks but also reduces the interference on adjacent cells. Several papers on maximizaing received power are listed in Table 4. The authors in [76] consider a multiple-input single-output (MISO) system in which a RIS is deployed to enhance wireless communication from the transmitter to the receiver, as depicted in Fig. 6. It is assumed that the direct link between the transmitter and the UE is blocked. The transmitter is equipped with M antennas, forming uniform linear array (ULA) while the user is equipped with a single antenna.

The channel between the transmitter (T) and the receiver (R) to RIS (I) is presented as $\mathbf{h}_{TI}^H \in \mathbb{C}^{N\times M}$ and $\mathbf{h}_{IR}^H \in \mathbb{C}^{1\times N}$ respectively and formulated as follows:

$$\mathbf{h}_{TI}^H = \begin{bmatrix} a_{TI,1,1}e^{\theta_{TI,1,1}} & \cdots & a_{TI,1,N}e^{\theta_{TI,1,N}} \\ \vdots & \ddots & \vdots \\ a_{TI,L,1}e^{\theta_{TI,L,1}} & \cdots & a_{TI,L,N}e^{\theta_{TI,L,N}} \end{bmatrix} \tag{39}$$

$$\mathbf{h}_{RI}^H = \begin{bmatrix} a_{IR,1}e^{\theta_{IR,1}} & \cdots & a_{IR,1,L}e^{\theta_{IR,L}} \end{bmatrix} \tag{40}$$

Where $a_{T_{I,p,q}}$, and $\theta_{T_{I,p,q}}$ denotes the gain and phase of channel from pth antenna of transmitter and the qth reflective element of RIS. In the context of far-field operation, it is reasonable to assume that the amplitude gains from various antenna elements to distinct RIS elements are equal. Thus, the following assumption holds true:

$$a_{\text{TI,p,q}} \simeq a_{\text{TI}}, a_{\text{IR,q}} \simeq a_{\text{IR}}, p = 1,\dots,M, q = 1,\dots,N. \tag{41}$$

and the final amplitude gain from the transmitter to the receiver through individual reflective element of the RIS is $a_{\text{TI}}a_{\text{IR}} \triangleq a_{\text{TIR}}$. The values of a_{TIR} from physical and electromagnetic perspectives is formulated as follows:

$$\begin{aligned} a_{\text{TIR}} &= \sqrt{\frac{\|E^r\|^2}{2Z_{\text{air}}}A_r} \\ &= \sqrt{\frac{Z_{\text{air}}G_t G d_x d_y F(\theta_t,\phi_t)F(\theta_r,\phi_r)\Gamma^2 d_{\text{TI}}^{-2}d_{\text{IR}}^{-2}}{16\pi^2 Z_{\text{air}}}\frac{G_r\lambda^2}{4\pi}} \\ &\cong \delta_{\text{TIR}}d_{\text{TI}}^{-1}d_{\text{IR}}^{-1}. \end{aligned} \tag{42}$$

where $F(\theta_t,\phi_t)F(\theta_r,\phi_r)$ is the normalized power radiation pattern of the RIS, Z_{air} is the characteristic impedance of the air, G_t is the transmitter antenna gains, Γ is the RIS gain, (θ,ϕ) are the elevation and azimuth angles from the reference point of the RIS to the transmitter and receiver, F is the normalized power radiation pattern, and μ_{TI} is the complement angle of the direction of arrival (DOA) of the RIS at the transmitter. Then, the phase changes in the channel $\boldsymbol{h}_{\text{TI}}^H$ are equivalently written as:

$$\theta_{\text{TI},q,p} = 2\pi\frac{d_{\text{TI},q,p}}{\lambda} \cong 2\pi\frac{d_{\text{TI}}+\Delta d_{\text{TI},q,p}}{\lambda}, \tag{43}$$

$$\theta_{\text{IR},q} = 2\pi\frac{d_{\text{IR},p}}{\lambda} \cong 2\pi\frac{d_{\text{IR}}+\Delta d_{\text{IR},q}}{\lambda}, \tag{44}$$

where λ is the carrier wavelength, $\Delta d_{TI,q,p}, d_{TI}$, corresponds to the distance between the pth antenna and the reference point of the transmitter and the distance from the pth antenna element to the qth RIS reflective element, and $a_{TI,p,q}, a_{IR,q}$, stands for the amplitude gains from various antenna elements to different RIS elements.

The received power and its maximization problem respect to transmit and passive beam forming vectors $\mathbf{v}$ and $\mathbf{\Theta}$, the position of the RIS $\mathbf{r}_{I,pos}$, and the orientation of the RIS, $\mathbf{r}_{I,ori}$, is formulated as follows:

$$P_r = |\mathbf{h}_{IR}^H\mathbf{\Theta}\mathbf{h}_{TI}^H\mathbf{v}|^2. \tag{45}$$

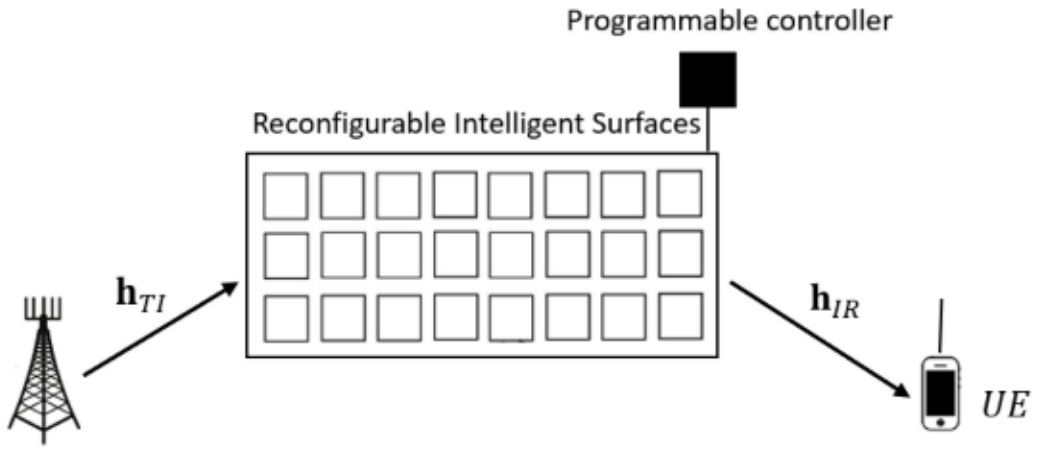

Fig. 6. Diagram of RIS-aided MISO communication system.

Table 4
Transmit power minimization or Received power maximization for EM-based models of RIS-assisted communications.

Ref.	Scenario	Objective	Design variables	Algorithms
[77]	BD-RIS aided MU-MISO network	Transmit power minimization	Transmit beamforming Phase shifts of the BD-RIS	BCD
[78]	Coordinated BD-RIS-aided SU MISO	Received power maximization	Transmit beamforming Phase shifts of the RIS	AO, Closed-form solutions
[79]	BD-RIS MISO	Received power maximization	Transmit beamforming and phase shifts of the RIS	Closed-form solutions
[80]	Multi-band RIS multi-BS MIMO	Received power maximization	phase shifts of the RIS	Closed-form solutions
[81]	Hybrid BD-RIS SU SISO, MISO,MIMO	Received power maximization	Phase shifts of the RIS	PDD
[76]	SISO	Received power maximization	Transmit beamforming ,phase shifts of the RIS, orientation and position of the RIS	AO, closed-form solutions
[82]	SISO	Received power maximization	Transmit beamforming and phase shifts of the RIS	AO, SOCP, geometry-based optimal phase control algorithm
[83]	SISO	Received power maximization	Tunable impedances at the RIS	Gradient-based algorithm
[84]	SISO	Received power maximization	Discrete phase shifts of RIS	Dynamic threshold phase quantization (DTPQ) and equal interval phase quantization (EIPQ)
[85]	SISO	Received power maximization	Discrete phase shifts of RIS	Group-based query algorithm, Closed-form solutions
[86]	STAR-RIS	Received power maximization	Transmit beamforming and phase shifts of the RIS	Closed-form solutions
[87]	BD-RIS-assisted SISO, MISO, SIMO	SNR maximization	RIS phase shift matrix	Closed-form solution
[88]	SISO	End-to-end SNR maximization	Tunable impedances of the RIS	Closed-form solution
[89]	MUs SIMO	End-to-end SINR maximization	Receive BF vectors at the BS, transmit power allocation at the users, and the RIS phase shift design	Projected gradient descent-based solution

$$\begin{aligned} \underset{\mathbf{v},\boldsymbol{\Theta},\mathbf{r}_{I,pos},\mathbf{r}_{I,ori}}{\text{maximize}} \quad & P_r \\ \text{subject to} \quad & \mathbf{v}^H\mathbf{v} \le P_t \\ & \boldsymbol{\Theta} \in \mathbb{B} \\ & \{\mathbf{r}_{I,pos}, \mathbf{r}_{I,ori}\} \in \mathbb{S}_0 \\ & \mathbf{r}_{I,pos} \in \mathbb{S}_1 \cap \mathbb{S}_2. \end{aligned} \tag{46}$$

where $\mathbb{S}_0$ is a set that guarantees the EM to propagate from transmitter to receiver through the RIS directly, which is specified by application environment, $\mathbb{S}_1$ can be expressed as $(d_{\mathrm{TI}} \ge r_0) \cap (d_{\mathrm{RI}} \ge r_1)$ where r_0 and r_1 are the minimum distance to guarantee the far-field condition, respectively, the region $\mathbb{S}_2$ defines the feasible area for fixing the RIS, while $\mathbb{B}$ characterizes the feasible set of $\boldsymbol{\Theta}$. It is assumed that the antennas in T and R are omni-directional.

The recent work in [78] proposes a coordinated RIS architecture that allows for optimized connection patterns between RIS elements and configurable impedances based on CSI. Unlike existing architectures, the coordinated RIS offers greater optimization flexibility. Simulation results show that it achieves higher power gain compared to

group-connected RIS, approaching the performance of fully-connected architectures while requiring fewer configurable impedances.

In [79], the authors introduces new BD-RIS models and architectures using graph theory, resulting in two efficient designs: tree-connected and forest-connected RIS. The tree-connected architecture, based on a tree graph, is the simplest yet reaches the performance peak for MISO systems. The forest-connected architecture offers a trade-off, reducing complexity more than the tree-connected model. For optimization, a closed-form solution is available for the tree-connected RIS, while the forest-connected RIS uses a simpler iterative method. Numerical tests show that the tree-connected RIS matches the performance of a fully-connected RIS and the forest-connected aligns with group-connected RIS, but with up to 16.4 times less complexity. Another work in [80] explores the frequency-dependent characteristics of BD-RISs, proposing a new reflection model for multi-band MIMO networks. It develops optimization strategies to enhance received power at various users connected to different base stations operating on separate frequencies. By leveraging matrix theory, the study derives simplified solutions for complex optimization challenges and implements these using codebook-based configurations. Simulation results demonstrate the effectiveness of BD-RISs over traditional models, particularly in their robustness to frequency variations, while also highlighting potential interference issues without proper synchronization between RISs and base stations. In [81], the authors present a closed-form solution for optimizing the scattering matrix in BD-RIS architectures, achieving theoretical performance limits across various channel setups. Initially developed for single-user SISO systems, the solution extends to MIMO and MISO configurations. The proposed algorithm simplifies and reduces the complexity compared to previous methods, scaling linearly with RIS elements in group connected architectures and cubically in fully connected ones.

The received power maximization is also studied in [83] [84,85]. The authors in [83] explore RISs using an EM-compliant model. Focusing on a SISO system with an RIS, the RIS is modeled as a collection of tunable load impedances controlling thin wire dipoles. A gradient-based algorithm is introduced to optimize the impedance of scattering elements in the presence of mutual coupling. The algorithm's convergence and computational complexity are analyzed, with numerical results demonstrating its superiority over a benchmark algorithm in terms of performance and convergence time.

The authors in [84] examine phase alignment and quantization for RIS in SISO systems. Their work uncovers phase distribution patterns that inform the discretization of phase shifts in the RIS. The study introduces dynamic threshold and equal interval phase quantization methods, demonstrating marked improvements in power gain, stability, and robustness over conventional methods. Additionally, the paper presents the first path loss scaling law under discrete phase shifts and validates these results through field trials. This research enhances RIS performance optimization and supports practical implementations in communication systems. In [85], the authors present a practical reflection coefficient model for RIS, departing from idealized assumptions. The model considers non-uniform amplitudes and limited phase shifts based on measurements. An algorithm is proposed to calculate the coefficients while accommodating these constraints, with analytical performance analysis. Simulation and experimental results validate the effectiveness of the algorithm, enhancing our understanding of RIS behavior and deployment possibilities. The work in [86] focus on metasurface-based RISs designed for simultaneous transmission and reflection (STAR). These structures, with tiny elements, differ from traditional patch-array RISs and are particularly suited for near-field scenarios. A continuous electric current distribution approach is employed for modeling their electromagnetic response. The research provides analytical insights for both single-user and multi-user settings. Notably, near-field channels offer higher degrees-of-freedom (DoFs) than far-field channels. STAR-RIS strategies are proposed and evaluated, showing the superiority of metasurface-based RISs and providing valuable insights into power scaling laws and optimal strategies for different scenarios. In [87], the authors discuss the use of BD-RIS architectures, which utilize unitary and symmetric RIS matrices to enhance wireless channel flexibility. The focus is on maximizing the SNR for single and multiple antenna systems using a BD-RIS. The problem of maximizing SNR is tackled by providing a solution in closed-form, achieved through the Takagi factorization of a complex symmetric matrix. This approach facilitates efficient resolution for SISO, SIMO, and MISO channel configurations. Besides, in [89], the authors presents a novel method for optimizing RIS in advanced communication systems. It uses channel statistics instead of instantaneous channel data, enhancing beamforming, user power allocation, and RIS phase adjustments to maximize the minimum SINR and ensure fairness among users. The problem is also formulated including electromagnetic field exposure (EMF)-aware constraints. The specific absorption rate (SAR), expressed in watts per kilogram of body weight (W/kg), gauges EMF in the immediate vicinity. It assesses how quickly the body absorbs energy when subjected to electromagnetic radiation.

The work in [88] introduces an optimization algorithm for RIS-assisted communications that maximizes end-to-end SNR by considering RIS tunable impedances and accounting for mutual coupling. The results show that this approach significantly improves SNR, primarily for single-antenna transceivers in the far-field.

4.4. Sum rate

Enhancing the sum-rate and channel capacity stands out as a prominent benefit of RIS. In contrast to direct transmission from the BS to the user, RISs offer an indirect line, potentially line-of-sight, resulting in reduced path loss and increased SINR [32].

In [90], the authors consider a MIMO interference channel that comprises N_T transmitter–receiver pairs. They adopt an electromagnetic-compliant communication model based on mutual impedances, particularly suited for RISs comprising thin wire dipoles made of perfectly conducting material. These dipoles are controllable through tunable load impedances, offering the flexibility to program and shape the scattered field within the RIS-assisted channel. The system model is shown in Fig. 7.

Under the following assumptions:

- The channel matrix between the jth transmitter and the kth receiver is determined by the internal impedances of the transmit antennas, the load impedances of the receive antennas, and the tunable impedances of the RIS.

- Denoting $\mathbf{Z}_I^{(i)} = \mathbf{Z}_{\text{tun}}^{(i)}$ as a $P \times P$ diagonal matrix representing the tunable impedances of the ith RIS, where $\boldsymbol{B}_i = \text{diag}(\boldsymbol{b}_i)$ is a diagonal matrix containing the adjustable impedances of all I RISs.

The following notation for channel matrices is derived:

$$\bar{\mathbf{h}}_{\text{TR},k,j} = (\boldsymbol{I}_L + \mathbf{Z}_{k,k}\mathbf{Z}_k^{-1})^{-1}\mathbf{Z}_{k,j}(\mathbf{Z}_{j,j} + \mathbf{Z}_j)^{-1} \in \mathbb{C}^{L\times M}, \tag{47a}$$

$$\bar{\boldsymbol{B}}_i = \mathbf{Z}_{i,i} \in \mathbb{C}^{P\times P}, \quad \boldsymbol{B}_i = \mathbf{Z}_I^{P\times P}, \tag{47b}$$

$$\bar{\mathbf{h}}_{\text{TR},k,i,j} = -\boldsymbol{T}_{k,i}(\bar{\boldsymbol{B}}_i + \boldsymbol{B}_i)^{-1}\boldsymbol{S}_{i,j} \in \mathbb{C}^{L\times M}, \tag{47c}$$

$$\mathbf{h}_{\text{TR},k,j}(\mathcal{B}) \sim \bar{\mathbf{h}}_{\text{TR},k,j} + \sum_{i=1}^{I} \bar{\mathbf{h}}_{\text{TR},k,i,j}(\mathcal{B}) \in \mathbb{C}^{L\times M}. \tag{47d}$$

where $\bar{\mathbf{h}}_{\text{TR},k,j}$ accounts for the line-of-sight link and $\bar{\mathbf{h}}_{\text{TR},k,i,j}$ accounts for the (virtual line-of-sight) link scattered by the ith RIS. To simplify notation, we use $\mathcal{B} = \{\boldsymbol{b}_1, \boldsymbol{b}_2, \dots, \boldsymbol{b}_I\}$ to collectively represent the I vectors b_i that are subject to optimization. Then, an EM-aware sum-rate maximization problem is formulated as follows:

$$\underset{\mathcal{V},\mathcal{B}}{\text{Max}} \quad \mathrm{R}_{\text{tot}}(\mathcal{V},\mathcal{B}) = \underset{\mathcal{V},\mathcal{B}}{\text{Max}} \sum_{k=1}^{N_T} \alpha_k R_k(\mathcal{V},\mathcal{B}) \tag{48a}$$

$$\text{subject to} \quad \text{tr}(\boldsymbol{V}_k\boldsymbol{V}_k^H) \le P_k, \quad \forall k = 1,\dots,N_T \tag{48b}$$

$$\Re(b_{k,p}) = R_{\text{resistance},0}, \quad \forall i = 1,\dots,I, \ p = 1,\dots,P \tag{48c}$$

$$\Im(b_{k,p}) \in \mathbb{R}, \quad \forall i = 1,\dots,I, \ p = 1,\dots,P \tag{48d}$$

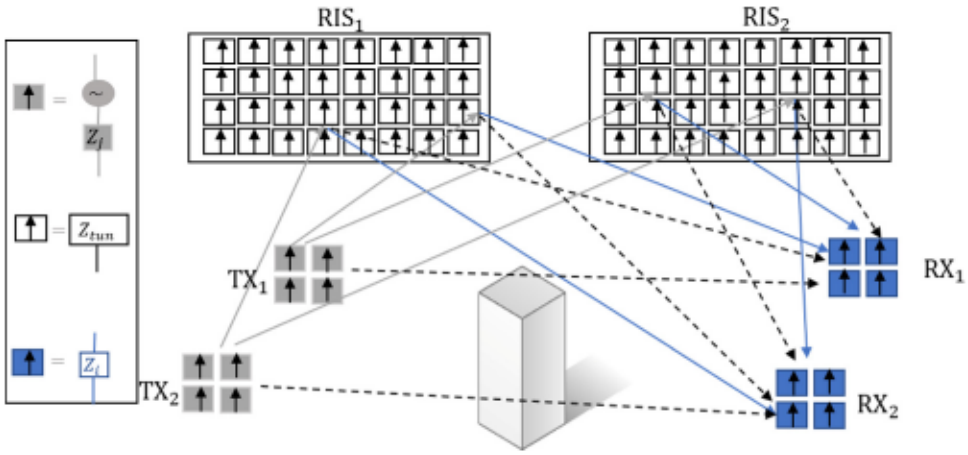

Fig. 7. Illustration of an RIS-assisted MIMO interference channel (© 2021 IEEE, [90]).

Table 5
Maximization of sum rate with physically-consistent models for the RIS in RIS-assisted communications.

Ref.	Scenario	Objective	Design variables	Algorithms
[63]	Hybrid BD-RIS-aided MUs-MISO	Sum rate maximization	Transmit beamforming , and BD-RIS matrix	Iterative algorithm, Closed form solution
[77]	BD-RIS aided SU-MISO network	Sum rate maximization	Transmit beamforming Phase shifts of the BD-RIS	block ascent (BCA) method
[90]	MIMO	Sum rate maximization	Active and passive beamforming	BCD, wMMSE
[91]	BD-RIS Aided SU/MUs-MISO	Sum rate maximization	Tunable impedance components of the BD-RIS	closed-form solution
[92]	BD-RIS RSMA Aided MUs-MISO	Sum rate maximization	Transmit beamforming and multi-sector BD-RIS configuration	Majorization-minimization (MM) and penalty-dual decomposition (PDD) method
[93]	FC BD-RIS MUs MISO ISAC system	Sum rate maximization	linear filter, transmit beamforming, and the BD-RIS configuration	RCG(Riemannian Conjugate Gradient), Manifold Based Solution
[94]	MU-MIMO	Sum rate maximization	SAR constraints	Iterative waterfilling algorithm
[95]	MISO	Sum rate maximization	Tunable impedances of the unit cells of the RIS, Passive beamforming	Iterative algorithm
[96]	RIS-aided MUs-MISO SDMA/NOMA	Weighted sum rate maximization	Multiple access precoding at the BS, and RIS configuration	AO, WMMSE precoding, Unsupervised ML

where

$$R_k(\mathcal{V},\mathcal{B}) = \log\det(\mathbf{I}_L + \mathbf{V}_k^H \mathbf{h}_{\mathrm{TR},k,k}^H(\mathcal{B})\bar{\mathbf{J}}_k^{-1}\mathbf{h}_{\mathrm{TR},k,k}(\mathcal{B})\mathbf{V}_k) \tag{49}$$

and the interference-plus-noise covariance matrix is formulated as:

$$\bar{\mathbf{J}}k = \sum_{j-1,j\neq k}^{N_u} \mathbf{h}_{\mathrm{TR},k,j}^H(\mathcal{B})\mathbf{V}j\mathbf{V}j^H\mathbf{h}_{\mathrm{TR},k,j}^H(\mathcal{B}) + \sigma_k^2\mathbf{I}_L \tag{50}$$

where $\mathcal{V} = \{\boldsymbol{V}_1, \boldsymbol{V}_2, \ldots, \boldsymbol{V}_{N_T}\}$ denotes the set of N_T precoding matrices.

Besides, $R_{\mathrm{resistance},0} \geq 0$ represents a resistance value that characterizes the losses within the tunable impedances of the RIS elements. Constraint (48c) is in place to guarantee that the RIS does not act as an amplifier for the incoming signal.

Table 5 summarizes sum-rate/channel capacity maximization works in RIS-aided wireless communications from EM perspectives, including scenario, objective, design variables, and algorithms.

The work in [91] explores optimizing the performance of group-connected BD-RIS. It introduces a static grouping strategy based on channel statistics to enhance performance while maintaining low circuit complexity. By solving optimization problems, the study demonstrates substantial performance improvements, particularly in scenarios with highly correlated channels, with up to a 60% increase in sum rate. On the other hand, the work in [63] introduces a new approach to enhance the performance of BD-RIS by dynamically adjusting antenna groupings based on CSI. Unlike existing static configurations, this dynamic grouping strategy optimizes the BD-RIS setup by adapting antenna subsets to variations in CSI, resulting in a more flexible and efficient system. The proposed method is evaluated using simulations, demonstrating its superiority over fixed group-connected architectures in multi-user multiple-input single-output systems.

In [93], the authors explore the use of fully-connected beyond-diagonal RIS (FC BD-RIS) to enhance the performance of integrated sensing and communication (ISAC) systems. The paper emphasizes the superior beamforming capabilities of BD-RIS compared to traditional diagonal RIS architectures. By applying the majorization-minimization (MM) and penalty-dual-decomposition (PDD) methods, the study develops an effective algorithm to address the challenges posed by orthogonality conditions and non-convex inequalities involving BD-RIS. The numerical results confirm the efficiency of the proposed solution and the advantages of incorporating BD-RIS in ISAC networks. The work in [92] investigates the combination of rate-splitting multiple access (RSMA) with a BD-RIS to enhance network performance and reduce antenna usage. Using a prism-shaped multi-sector BD-RIS in a multiuser system, the research develops joint transmit precoder and BD-RIS matrix designs under imperfect channel conditions. By transforming a

stochastic maximization problem into a deterministic one, the approach optimizes system performance iteratively. Simulations show that this integration outperforms traditional access methods and reduces the number of antennas needed.

In [94], the authors underscore the importance of incorporating user exposure constraints into the design of uplink transmission covariance matrices for advanced cellular systems such as 5G and beyond. The study emphasizes that ensuring near-field user exposure limitations impact the potential far-field data rates achievable by devices with multiple transmit antennas. The paper focuses on specific absorption rate (SAR) as a well-recognized metric for user exposure. It investigates a multi-user MIMO system, considering SAR restrictions at each user. The research analyzes the maximum achievable sum rates under different transmitter channel state information scenarios. The proposed SAR-aware MIMO transmission techniques, based on a modified waterfilling algorithm, are demonstrated to outperform conventional strategies for scenarios involving two users.

In [95], the authors focus on developing electromagnetic models for RISs, building upon a recent model involving mutually coupled loaded wire dipoles. The authors introduce an RIS-aided channel model suitable for more realistic scenarios. In this model, they represent scattering objects as loaded wire dipoles, allowing them to characterize the behavior of various natural and engineered materials by adjusting the dipole parameters. They also present an iterative algorithm that jointly optimizes RIS and transmitter configurations, aiming to maximize the system's overall data rate. Extensive numerical experiments confirm the considerable performance enhancements offered by their approach when compared to existing optimization methods.

In [96], Peng et al. employed ML techniques to WSR optimization of RIS-assisted communication systems, considering mutual coupling between RIS elements for the first time. The research begins by deriving an RIS-assisted channel model that incorporates mutual coupling effects. Subsequently, an unsupervised ML approach is proposed to optimize the RIS, utilizing a dedicated neural network architecture called RISnet with good scalability and desired symmetry. Furthermore, the study integrates ML-enabled RIS configuration with analytical precoding at the base station and introduces a variant of RISnet that requires partial channel state information from a subset of RIS elements [96].

4.5. Spectral efficiency

RISs are regarded as a promising technology for extending coverage and improving the spectral efficiency of wireless systems [97]. In a study by [98], the authors explore the design of SE maximization considering EM effects in multiuser MIMO uplink transmission assisted by RISs and digital metasurface antennas (DMAs). They propose a joint optimization of transmit precoding, RIS phases, and DMA weights to enhance SE while adhering to power and specific absorption rate (SAR) constraints at users. The system model is depicted in Fig. 8. The SE maximization problem concerning the transmission covariance matrix $\mathbf{Q}$ and EM exposure level is formulated as follows:

$$\underset{\mathbf{Q},\boldsymbol{\Phi},\boldsymbol{\Xi}}{\text{Maximize}} \quad \eta_{\text{SE}}(\mathbf{Q},\boldsymbol{\Phi},\boldsymbol{\Xi}) \tag{51a}$$

$$\text{subject to} \quad \text{tr}(\mathbf{Q}_k) \le P_{\max,k}, \quad \mathbf{Q}_k \succeq \mathbf{0} \tag{51b}$$

$$\text{tr}(\mathbf{R}_{k,i}\mathbf{Q}_k) \le D_{k,i}, \quad \forall k,i, \tag{51c}$$

$$\phi_n \in \mathcal{F}_1, \quad \forall n; \tag{51d}$$

$$\boldsymbol{\Xi} \in \mathcal{F}_3^{S\times M}. \tag{51e}$$

where $\varphi_n \in \mathcal{F}_1 = \{\varphi = e^{j\theta}, \theta \in [0, 2\pi)\}$. The DMA array is equipped at the BS consisting of M metamaterial units. These DMAs are composed of S microstrips, each of which contains L metamaterial units, i.e., $M = SL$. In practice, the DMA array can be regarded as a two-dimensional antenna array composed of a set of one-dimensional microstrips, and its configurable weight matrix $\boldsymbol{\Xi} \in \mathbb{C}^{S\times M}$ can be written as

$$\Xi_{s1,(s2-1)L+l} = \begin{cases} \xi_{s1,l} \in \mathcal{F}_2 & \text{for } s_1 = s_2 \\ \mathbf{0} & \text{otherwise} \end{cases} \in \mathcal{F}_3^{S\times M} \tag{52}$$

where $s_1, s_2 \in \{1,\dots,S\}$, $l \in \{1,\dots,L\}$, and $\{\xi_{s_1,l}\}_{\forall s_1,l}$ are the weights of the DMA elements, and the feasible set of weight matrices is denoted as $\mathcal{F}_{S\times M}^3$. $\xi_{s_1,l}$ often satisfies certain constraints, e.g., its feasible set represented by $\mathcal{F}_2$. The input–output relationship of the system between the transmit signals and DMA's output can be written as:

$$\mathbf{z} = \frac{1}{K}\sum_{k=1}^{K} \boldsymbol{\Xi}\mathbf{h}_{TI}\boldsymbol{\Phi}\mathbf{h}_{IR,k}\mathbf{x}_k + \tilde{\mathbf{n}} \in \mathbb{C}^{S\times 1}, \tag{53}$$

where the channel matrix from user k to the RIS is denoted as $\mathbf{h}_{IR,k} \in \mathbb{C}^{N_R\times N_k}$, and the channel matrix from the RIS to the BS as $\mathbf{h}_{TI} \in \mathbb{C}^{M\times N_R}$. $\tilde{\mathbf{n}} = \frac{1}{K}\boldsymbol{\Xi}\mathbf{n}$ is the equivalent channel noise. The constraints (51b) and (51c) keep the transmission power and EM exposure level below some specified values, and (51d) and (51e) prescribe the formats of RIS phase shift matrix $\boldsymbol{\Phi}$ and DMA weight matrix $\boldsymbol{\Xi}$, respectively.

4.6. Energy efficiency

Energy efficiency is a critical metric for green 5G and 6G networks. Different with power minimization problems, the objective of energy efficiency maximization includes both transmission rate and energy consumption metrics, which can better evaluate the power utilization efficiency. The main benefit of RISs lies in the capability of reshaping the signal propagation path with extremely low power consumption, making RISs a promising technique to improve energy efficiency. Energy efficiency maximization-related works are summarized in Table 6. In [99], a comprehensive model for MISO transmission with RIS assistance, incorporating both the end-to-end electromagnetic transfer model and the non-linear rectifier model is presented. The approach considers the hardware-related implications on EE, encompassing factors such as the radiation patterns of transmit antennas, the reflective properties of the RIS, and particularly the mutual coupling effects influenced by the arrangement of antenna arrays. The adopted model employs circuit impedances as optimization variables for configuring the RIS, making it more practical than ideal assumptions. The system model is shown in Fig. 9 and includes several separate information decoder user (IDU) and energy harvester user (EHU). Two kinds of users, IDUs and EHUs, are belong to the set $\mathcal{M}_I = \{1,\dots,M_I\}$ and $\mathcal{M}_E = \{1,\dots,M_E\}$, respectively. For the RIS-enhanced SWIPT network, the problem formulated to maximize the EE subject to the maximal transmitting power, the minimal rate of the IDU, the minimal DC output power of the EHU, and the hardware restrictions of the control circuit at the RIS. The formulated optimization problem is as follows:

$$\underset{\mathbf{w}_j,\mathbf{v}_l,\boldsymbol{\Omega}}{\text{Maximize}} \quad \eta_{\text{EE}}(\boldsymbol{\omega}_j,\mathbf{v}_l,\boldsymbol{\Omega}) \tag{54a}$$

$$\text{subject to} \quad R_j(\boldsymbol{\omega}_j,\boldsymbol{\Omega}) \ge R_j^{(D)}, \quad \forall j \tag{54b}$$

$$P_t(\boldsymbol{\omega}_j,\mathbf{v}_l) \le P_{\max}, \tag{54c}$$

$$P_{\text{RF},n}(\boldsymbol{\omega}_j,\mathbf{v}_l,\boldsymbol{\Omega}) \ge g_n(E_n^{(D)}), \quad \forall n; \tag{54d}$$

$$\Re(\Omega_q) = R_0 \ge 0, \quad \forall q \tag{54e}$$

$$\Im(\Omega_q) \in \mathbb{R}, \quad \forall q. \tag{54f}$$

where $\eta_{EE}(\boldsymbol{\omega}_j,\mathbf{v}_l,\boldsymbol{\Omega}) = \frac{\sum_{j=1}^{M_I} R_j(\boldsymbol{\omega}_j,\boldsymbol{\Omega})}{P(\boldsymbol{\omega}_j,\mathbf{v}_l)}$, $\boldsymbol{\omega}_j \in \mathbb{C}^{N_T\times 1}$ and $\mathbf{v}_l \in \mathbb{C}^{N_T\times 1}$ denote the transmitting beamforming vectors for the jth IDU and the lth EHU,(54), $R_j^{(D)}$ refers to the rate condition for the jth IDU. Regarding Eq. (54b), $P_{\max}$ represents the upper limit on the power budget for transmission. The value $E_n^{(D)}$ within Eq. (54c) signifies the minimum DC power output requirement for the nth EHU. Eq. (54c) and (54d) outline the constraints of the control circuit. In Eq. (54e), R_0 indicates the circuit's loss, with the requirement $R_0 \ge 0$ ensuring that the RIS functions in passive mode rather than active mode. Within the context of this paper, the reactances of the circuits mentioned in Eq. (54f) can be reconfigured, and we presume that their adjustable ranges encompass the real number set.

Furthermore, the total transfer model can be depicted by

$$\mathbf{h}(\boldsymbol{\Omega}) = \mathbf{h}_{\text{EM}}(\boldsymbol{\Omega}) + \mathbf{h}_{\text{Cluster}} \in \mathbb{C}^{1\times N_t} \tag{55}$$

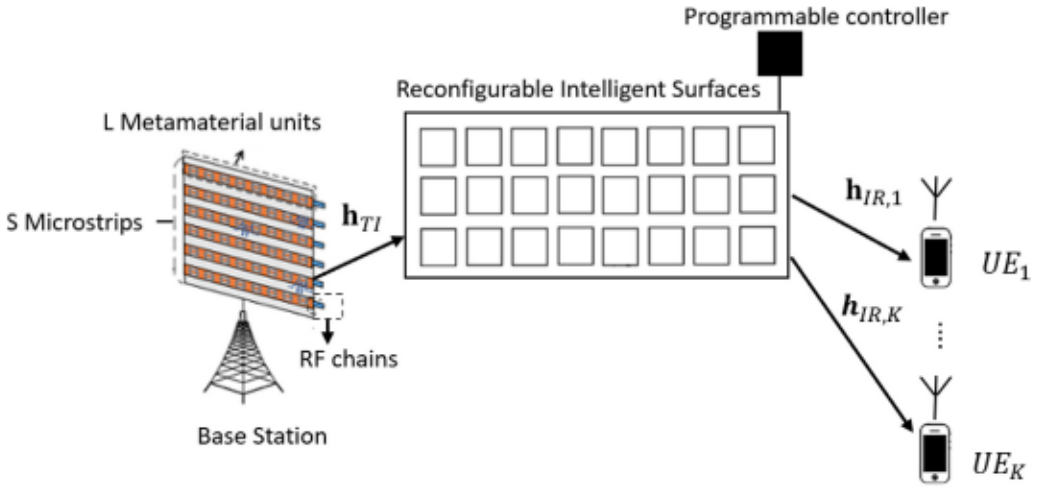

Fig. 8. Hybrid RIS and DMA assisted multiuser MIMO system (© 2022 IEEE, [98]).

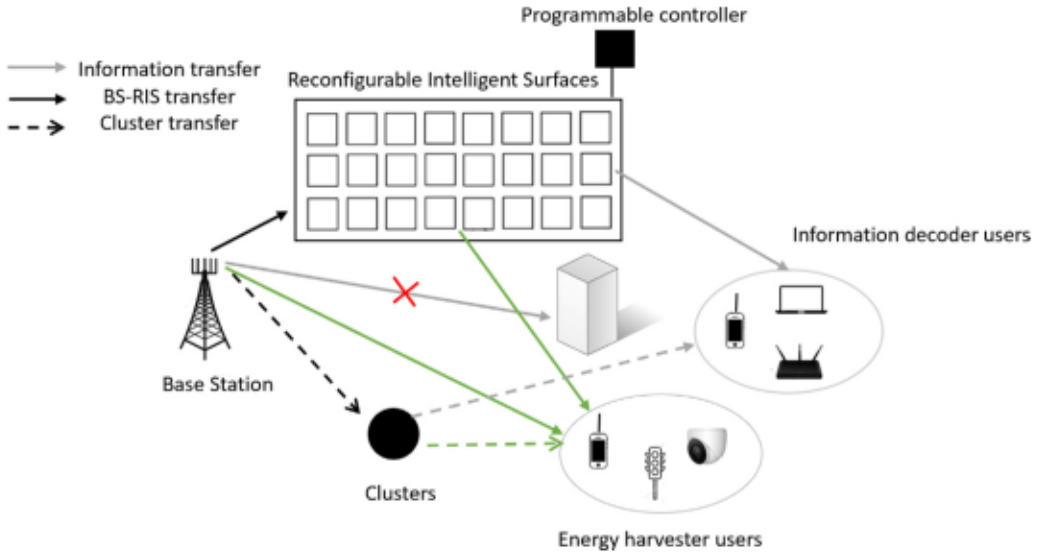

Fig. 9. The RIS-enhanced-SWIPT system (© 2023 IEEE, [99]).

where $\mathbf{h}_{\mathrm{EM}}$ is the electromagnetic physical transfer model and $\mathbf{h}_{\mathrm{Cluster}}$ is the clustered model. Regarding $\mathbf{h}_{\mathrm{EM}}$, its behavior is influenced by the tunable component matrix $\mathbf{\Omega} \in \mathbb{C}^{N_t \times N_t}$. This matrix has a specific structure, denoted as $\mathbf{\Omega} = \mathrm{diag}(\mathbf{\Omega}_1, \ldots, \mathbf{\Omega}_{N_t})$, with each entry representing the impedance of the backend circuits of the RIS elements. The choice of diodes or varactors allows for the configuration of $\mathbf{\Omega}$, with the RIS employing varactors to enable continuous adjustments of reactance. In more detail, the expression for $\mathbf{h}_{\mathrm{EM}}$ is as follows:

$$\mathbf{h}_{\mathrm{EM}}(\mathbf{\Omega}) = \frac{\mathbf{Z}_{\mathrm{L}}\mathbf{S}_{\mathrm{RT}}(\mathbf{\Omega})\left(\mathbf{Z}_{\mathrm{G}} + \mathbf{S}_{\mathrm{TT}}(\mathbf{\Omega})\right)^{-1}}{\mathbf{Z}_{\mathrm{L}} + \mathbf{S}_{\mathrm{RR}}(\mathbf{\Omega}) - \mathbf{S}_{\mathrm{RT}}(\mathbf{\Omega})\left(Z_{\mathrm{G}} + \mathbf{S}_{\mathrm{TT}}(\mathbf{\Omega})\right)^{-1}\mathbf{S}_{\mathrm{TR}}(\mathbf{\Omega})} \in \mathbb{C}^{1 \times N_t}. \tag{56}$$

where $\mathbf{Z}_{\mathrm{G}} \in \mathbb{C}^{N_t \times N_t}$ denotes the source impedance matrix, a diagonal matrix, $\mathbf{Z}_{\mathrm{L}}$ is the load impedance, and $\mathbf{S}_{\mathrm{RT}}, \mathbf{S}_{\mathrm{TT}}, \mathbf{S}_{\mathrm{RR}}, \mathbf{S}_{\mathrm{TR}}$ denote the transfer matrices between the transmitter, RIS, and receiver.

The author in [100] addresses the challenge of optimizing EE in a RIS-assisted MIMO communications. The optimization problem involves maximizing EE while adhering to power constraints and limiting end-users' electromagnetic radiation exposure. The work jointly optimizes RIS phase shifts, transmit beamforming, receive filters, and transmit power using two convergent and low-complexity algorithms. One algorithm is applicable to general scenarios but may not achieve global optimality, while the other is proven optimal for cases with isotropic EMF constraints. Numerical results demonstrate that the RIS maintains comparable EE to scenarios without EMF constraints.

The work in [101] investigates the impact of LISs in millimeter-wave networks, demonstrating their potential to boost capacity and energy efficiency. However, it also highlights limitations when the base station density exceeds that of the LISs, particularly due to reflected interference and phase-shift energy consumption, suggesting that LIS deployment may not be necessary in such cases.

In the following section, we provide an extensive overview of model-based, heuristic, and ML methodologies employed in the optimization of RIS-enhanced wireless networks, with a specific focus on EM considerations.

4.7. Lessons learned

- Various problem formulations have been explored in the context of EM-aware RIS-aided communications, aiming to achieve different objectives such as increasing channel gain, enhancing SINR, maximizing sum rate, improving energy efficiency, and minimizing power consumption.

Table 6
EE Maximization in RIS-assisted communications from EM perspective.

Ref.	Scenario	Objective	Design variables	Algorithms
[77]	BD-RIS aided MU-MISO network	EE maximization	Transmit beamforming Phase shifts of the BD-RIS	block ascent (BCA) method
[99]	RIS-aided-SWIPT MISO	EE maximization	Impedance parameters of the RIS elements, Active beamforming vectors	AO, SDR, SCA, and Dinkelbach's algorithm
[100]	MIMO	EE maximization	RIS phase shifts, the transmit beamforming, the linear receive filter, and the transmit power	AO, Closed form solutions
[101]	LIS-assisted mmWave cellular network	EE maximization	Number of LIS elements	Stochastic geometry

- Literature has employed various optimization methods to tackle these problems, including traditional optimization techniques and heuristic algorithms.
- Machine learning and deep learning methods have been relatively underutilized for solving EM-aware RIS-aided communications problems, with few studies exploring their potential in this domain.

5. EM model-aware problem solution

5.1. Model-based optimization

Within the context of this study, model-based approaches refer to algorithms grounded in specific optimization models, underpinned by a comprehensive grasp of the defined problem. Such algorithms often require stringent prerequisites in terms of problem formulation characteristics like convexity, continuity, and differentiability. Among the highlighted model-based algorithms for optimizing physically-consistent EM models-aware RIS-aided communication are methodologies such as alternating optimization (AO), majorization-minimization (MM) techniques, successive convex optimization (SCA), semidefinite relaxation (SDR), Block Coordinate Descent (BCD) as listed in Tables 4, 5, 6.

5.2. Heuristic strategies

These strategies rely on heuristic rules to expedite problem-solving, offering efficient alternatives to conventional model-based methods. Although they may sacrifice optimality and precision in favor of reduced complexity and rapid solutions, heuristic algorithms prove instrumental, especially for tackling NP-hard problems or complementing other algorithms. Heuristic algorithms such as the convex-concave procedure (CCP) algorithm, various meta-heuristic algorithms, greedy algorithms, and the application of matching theory can all be employed to enhance the optimization of wireless networks that incorporate RIS. The work in [102] used heuristic method to solve physically-consistent EM models-aware RIS-aided communication.

- Genetic Algorithm (GA): GA is a versatile optimization method inspired by the principles of natural selection. It uses a population-based approach and evolves solutions over generations to find optimal or near-optimal solutions to complex problems in various domains. GA has been widely applied in the creation of pixelated coded MTS designs [103].
- Particle Swarm Optimization (PSO): PSO is a nature-inspired optimization algorithm that simulates the behavior of a flock of birds or a swarm of particles. In PSO, individual solutions, represented as particles, move through a search space to find the best solution by adjusting their positions based on their own experience and the collective knowledge of the swarm. PSO has been utilized to model EM waves with pixelized coded MTSs [103], while in [104], binary particle swarm optimization (BPSO) was applied to achieve a reflecting MTS featuring both left-handed circular polarization (LHCP) and right-handed circular polarization (RHCP) beams.
- Ant Colony Optimization (ACO): ACO is a metaheuristic algorithm inspired by the foraging behavior of ants. It models the way ants find the shortest path between their nest and food source by simulating the pheromone-based communication and exploration of multiple paths, leading to the discovery of optimal solutions in complex optimization problems. In [103], an inverse design approach for MTS is executed utilizing multi-objective lazy ant colony optimization (MOLACO) to create 3-D nano-antenna configurations. These designs aim to achieve low-loss transmission performance and extensive phase tunability.

5.3. Machine learning-based optimization

The complexity of optimization models in RIS-assisted communication systems stems from various factors such as the large number of reconfigurable elements, mutual coupling effects, and dynamic environmental conditions. Model-based approaches, while accurate, often face challenges due to the high dimensionality of the optimization space and the need for computationally intensive simulations. Heuristic algorithms offer alternative strategies for tackling these complex optimization problems. These methods provide efficient search mechanisms to explore the solution space and can often find near-optimal solutions in a reasonable amount of time. However, heuristic algorithms may struggle with scalability and may not always guarantee convergence to the global optimum.

In contrast, ML/DL techniques offer promising avenues for optimization in RIS-assisted communication systems. ML/DL methods can effectively handle the high-dimensional and nonlinear nature of the optimization problems. By learning patterns and relationships from data, these techniques can provide insights into the underlying structure of the optimization space, enabling more efficient exploration and exploitation of solutions. Additionally, ML/DL approaches can adapt to dynamic environments and incorporate real-time feedback, allowing for continual improvement and optimization.

In the context of RIS-empowered wireless networks, advanced ML techniques encompass supervised and unsupervised learning, RL, federated learning (FL), graph learning, transfer learning, and hierarchical learning that widely used by the researchers for optimizing RIS-aided communications. To the best of our knowledge, and as indicated in Tables 4, 5, 6, limited work like [96] have explored the application of machine learning for the optimization of physically-consistent EM model-aware RIS-assisted communication systems. When optimizing an RIS for wireless communications, certain parameters, like circuit parameters, require long-term optimization, typically during the fabrication process. This means that these optimizations can be conducted offline. However, other optimizations, such as passive beamforming optimization, need to be performed dynamically, on the fly. In the upcoming sections, we will delve into recent literature concerning on applying ML/DL methods for the RIS design and optimization and shed light on these two distinct time scales of optimization.

5.3.1. Long-term optimization: Fabrication-based parameter tuning

Some literatures investigate using inverse design and PINN for metamaterial design generally not RIS. Metamaterials are artificially engineered materials designed to exhibit properties that are not found in naturally occurring materials. These materials are composed of sub-wavelength structures (often referred to as meta-atoms) that interact with electromagnetic waves in ways that lead to unique properties, such as negative refractive indices or extreme wave manipulation. Metamaterials can be designed to control the propagation, absorption, reflection, and transmission of electromagnetic waves across different frequency ranges. They find applications in various fields, including optics, antennas, cloaking devices, and imaging systems.

Metamaterials and RISs share some similarities in their ability to control electromagnetic waves, but they serve different purposes. Metamaterials focus on altering the inherent properties of materials to achieve specific electromagnetic behaviors, while RISs aim to actively control the propagation of existing electromagnetic signals. In some cases, metamaterials can be integrated into the design of RIS elements to enhance their performance, such as achieving more precise control over phase and amplitude adjustments.

5.3.2. Dynamic optimization: Real-time beamforming adaptation

To the best of our knowledge, the optimization of EM-model aware RIS-aided communication systems using ML/DL techniques has only been explored in the work by [96].

Peng et al. introduce a specialized NN architecture called RISnet, notable for its outstanding scalability and desired symmetry properties. They integrate ML-based RIS configuration with analytical precoding at the BS, leveraging pre-existing schemes. This work represents an early effort in combining ML techniques with domain knowledge in communication for NN architecture design. Problem-specific ML methods are shown to achieve higher performance, lower complexity, and enhanced symmetry compared to generic ML approaches. After formulating two optimization problem for two multiple access schemes, space-division multiple access (SDMA) and non-orthogonal multiple access (NOMA), problems optimization using proposed unsupervised ML presented. The framework of unsupervised ML begins by defining the problem representation Γ, which consists of CSI including the mutual coupling effect, user weights in SDMA, and rate requirements in NOMA. The solution sought is denoted by Φ, representing the RIS phase shifts aimed at maximizing the objective function f, expressed as $f(\Gamma, \Phi)$. This function is fully determined by Γ and Φ and can be expanded to $f(\Gamma, \Phi) = f(\Gamma, N_\theta(\Gamma); \theta)$, indicating the dependency on the parameters θ of neural network N_θ. The neural network maps Γ to Φ as $\Phi = N_\theta(\Gamma)$.

To optimize this setup, a large dataset D of Γ is collected, and the optimization problem is formulated as:

$$\max_\theta K = \sum_{\Gamma \in D} f(\Gamma, N_\theta(\Gamma); \theta). \tag{57}$$

The network N_θ is trained using gradient ascent, with the update rule:

$$\theta \leftarrow \theta + \eta \nabla_\theta K, \tag{58}$$

where η represents the learning rate. If N_θ is effectively trained, then for a new $\Gamma' \notin D$, $\Phi' = N_\theta(\Gamma')$ should also be a satisfactory solution, mimicking how humans apply experience to solve new but similar problems.

5.4. Inverse design

Inverse design techniques are increasingly recognized as powerful alternatives to traditional methods for developing intricate functional metasurfaces. In this section, we review the literature on the inverse design of metasurfaces.

5.4.1. Data-driven approach

In the domain of modern nanophotonic devices, characterized by intricate nanostructures engineered to achieve advanced functionalities, traditional design methodologies grounded in optimization face formidable challenges. These conventional approaches typically commence with the generation of random designs, followed by resource-intensive electromagnetic simulations to evaluate their performance. The iterative refinement process involves adjusting structural parameters, often necessitating a substantial number of simulations. This becomes particularly impractical for intricate and complex devices. However, the field is currently experiencing a transformative shift toward data-driven methods, prominently leveraging artificial neural networks (NNs) as a promising alternative.

NNs offer two primary modes of operation: first, forward-modeling networks, which expedite the design process by predicting electromagnetic responses from structural parameters, thereby replacing computationally expensive EM simulations; and second, inverse-design networks, which directly generate structures based on desired responses, eliminating the need for iterative optimization. Both modes require significant training data, which involves EM simulations and computational resources as a one-time investment. This approach offers a distinct advantage over conventional optimization, which consumes extensive simulations for each design iteration. This shift toward data-driven approaches extends to the optimization of intricate metasurfaces, showcasing their potential to streamline design processes efficiently.

Within this context, inverse design techniques are emerging as potent solutions to the challenges faced by conventional methodologies when crafting complex functional metasurfaces. Furthermore, emerging research trends, such as scaling up inverse design methodologies for larger aperiodic metasurfaces and exploring end-to-end inverse design by co-optimizing photonic hardware and post-image processing, are poised to shape the future of metasurface design. By integrating these trends, metasurface design stands to achieve new levels of efficiency and effectiveness in crafting advanced nanophotonic devices [103,105–111].

When inverse design employed in the context of metamaterial surface (MTS) design, deep learning networks offer a significant advantage by acquiring a deep understanding of complex and unconventional connections between the structure of a metamaterial surface and its EM behavior. This comprehension is achieved through a collection of training examples [112]. Leveraging these trained datasets containing transmission or reflection response information, the learning algorithms have the capability to generate tailored, customized MTS configurations, including arbitrary wave-front MTS or metagratings [113,114].

Several more Refs. [104,115–120] have utilized various neural network architectures for MTS inverse design. These architectures encompass artificial neural networks (ANN), convolutional neural networks (CNNs), conditional deep convolutional generative adversarial network (cDC-GAN), and conditional deep convolution variational autoencoder (cDC-VAE), contributing to different aspects of MTS inverse design.

5.4.2. Model-aided approach

Another method, topology optimization, leverages advanced algorithms and physics principles to efficiently adjust and re-evaluate parameters to achieve the desired goals. Typically applied to simple meta-surface structures, machine learning's precision relies on numerical algorithms and data set size. However, it might lead to non-unique solutions in inverse design scenarios. To address these challenges, physics-informed neural networks incorporate physical laws during training to predict electromagnetic responses accurately. Topology optimization, which considers physical laws and fabrication constraints, can also be employed for improved precision in designing structure size and shape. This method yields the highest accuracy when the physical model is precise during optimization. The computational time required by machine learning techniques depends largely on factors such as

dataset size, metasurface complexity, and the number of optimization parameters. Strategies to reduce computational time include minimizing the training dataset size, simplifying the structure, and reducing the number of optimized parameters. However, these approaches may lead to a limited number of design parameters, potentially decreasing the diversity of structure designs. In contrast, PINNs integrate mathematical and physical principles, enabling more efficient training with fewer data samples while accommodating a greater number of structure parameters. This approach enhances both time efficiency and design flexibility [121].

Inverse RIS design revolves around identifying the optimal configuration, spanning geometry and material properties, of RIS elements to achieve specific electromagnetic behaviors or functionalities. This approach involves tackling design challenges by pinpointing RIS parameters that align with desired electromagnetic responses, such as reflection, refraction, or absorption, for given input signals. As this methodology finds application in diverse domains, such as antenna design and metamaterial engineering, it aims to establish parameter sets that align with known material and structural properties to achieve precise and targeted outcomes. In [122], the authors offer a summary of progress in utilizing deep learning methods for the inverse design of metasurfaces. These advancements encompass various approaches, such as a target-focused deep learning inverse design method, the fuzzy inverse design approach, the freeform inverse design technique, and the application of machine learning to aid in inverse design.

The work in [123] presents a novel approach to radar-signature control using a diffusion-absorption hybrid metasurface. Unlike traditional random metasurfaces, this design offers flexible and precise scattering-field reduction by combining absorption and diffusion mechanisms. Multi-objective optimization is used to fine-tune the design, achieving a significant reduction in scattering-field across a wide bandwidth. Experimental results confirm the effectiveness of the approach, making it a promising solution for versatile wavefront manipulation in radar applications.

In [124], the authors introduce a method using machine learning to design versatile elastic metasurfaces for manipulating mechanical wavefronts efficiently. This approach reduces the need for trial-and-error and computationally intensive methods by establishing a mapping between input parameters and desired properties. The trained machine learning network accelerates the design process and can be extended to other types of wave manipulation.

In [125], the authors presents a synopsis of deep learning techniques for both inverse RIS design and RIS-assisted wireless systems. The work in [126] offer an overview of deep learning methods applied to the inverse design and optimization of RIS, aiming to achieve the desired EM response required for upcoming wireless networks. They mentioned that DL-based inverse design is versatile in accommodating various RIS unit structures. Deep Generative Models (DGMs) are particularly valuable due to their capacity to generate novel designs that have not been documented in existing literature. In the schematic representation of an inverse RIS design, machine learning algorithms acquire and generalize intricate electromagnetic relationships between the physical structure of the RIS (left column) and its corresponding spectral response (right column). This learning process is facilitated through training data, as depicted in Fig. 10. In [127], the authors demonstrate deep learning-based metasurface synthesis using conditional generative adversarial networks for inverse design and surrogate model prediction.

A novel approach called AMID is introduced in [128], which leverages artificial intelligence (AI) techniques, specifically a combination of a CNN, autoencoder, and optimized support vector machine (SVM), to enable inverse design of metasurface structures. Unlike traditional methods that require expert knowledge and simulation-based trial and error, AMID allows designers to input desired design targets directly, simplifying the design process. This method aims to utilize machine learning to establish connections between metasurface structures and electromagnetic properties, facilitating efficient and automated design. Compared to traditional methods, AMID reduces computational requirements and eliminates the need for extensive expertise, offering a more streamlined and accessible approach to metasurface design. The solution in [129] introduces a fast and accurate method for designing metasurfaces using transfer learning with a neural network. This approach can predict meta-atom phases with 90% accuracy. It is validated for 2D focusing and abnormal reflection functions, demonstrating high design accuracy in both simulations and experiments. This method streamlines functional metasurface design and can help create a versatile library of meta-atoms.

The approach in [130] suggests a new method for designing metasurfaces, which offer unique optical properties and practical advantages over traditional optical devices. Traditional metasurface design is slow and computationally intensive. The proposed approach uses deep tandem neural networks to speed up the design process. By connecting a pretrained forward prediction model with an inverse design model, this method allows for rapid creation of metasurface structures that meet specific spectral targets. It presents a promising way to streamline metasurface design and help researchers tailor optical properties more efficiently.

The work in [131] employs DNN to design metasurfaces for TE and TM polarized waves up to 45 GHz. It uses a confined output configuration to streamline the process, reducing calculations and speeding up learning. The DNN approach achieves a 92% accuracy and directly generates the desired metasurface structures, eliminating the need for time-consuming optimization. This simplifies inverse metasurface design, allowing designers to focus on their goals.

The work in [121] provides an overview of recent developments in using ML/DL for designing the physical layer of RIS. The authors in [121] discussed the basic principle of using machine learning for metasurface design as shown in Fig. 11. The figure outlines a two-part process using neural networks. Initially, datasets representing EM responses for various parameter combinations of a basic cylindrical structure are generated through forward solver algorithms. These datasets train a deep neural network designed to predict the EM response from given inputs, known as a forward network. Simultaneously, an inverse network is developed where the input is the desired EM response, and the output is the corresponding structural parameters. Furthermore, they present a diagram depicting the process of using physics-informed neural networks for metasurface design (Fig. 12). The datasets are generated by simulating the structure using a forward solver. However, by integrating fundamental physical principles like Maxwell's equations and electromagnetic boundary conditions into the neural networks, they manage to decrease the necessary dataset size. This reduction in dataset size results in a notable reduction in computational time.

5.5. Physics informed deep learning (PIDL)

Recent research has utilized deep learning to model complex relationships between metamaterials and their behaviors, often governed by Maxwell's equations in electromagnetics. This includes tackling inverse problems to determine desired properties. Physics-informed neural networks have emerged as a revolutionary approach, enabling the incorporation of physics directly into neural networks. PINNs bridge the gap between physics and machine learning, facilitating accurate predictions of complex physical phenomena with limited training data, advancing scientific computing and data-driven modeling.

Physics-informed neural networks are capable of solving general differential equations of the form:

$$\mathcal{F}(u(z);\gamma) = f(z), \quad z \in \Omega, \tag{59}$$

subject to boundary conditions:

$$\mathcal{B}(u(z)) = g(z), \quad z \in \partial\Omega, \tag{60}$$

where $z := [x_1, \ldots, x_{d-1}, t]$ represents the space–time coordinate vector, u is the unknown solution, γ denotes parameters related to the physics,

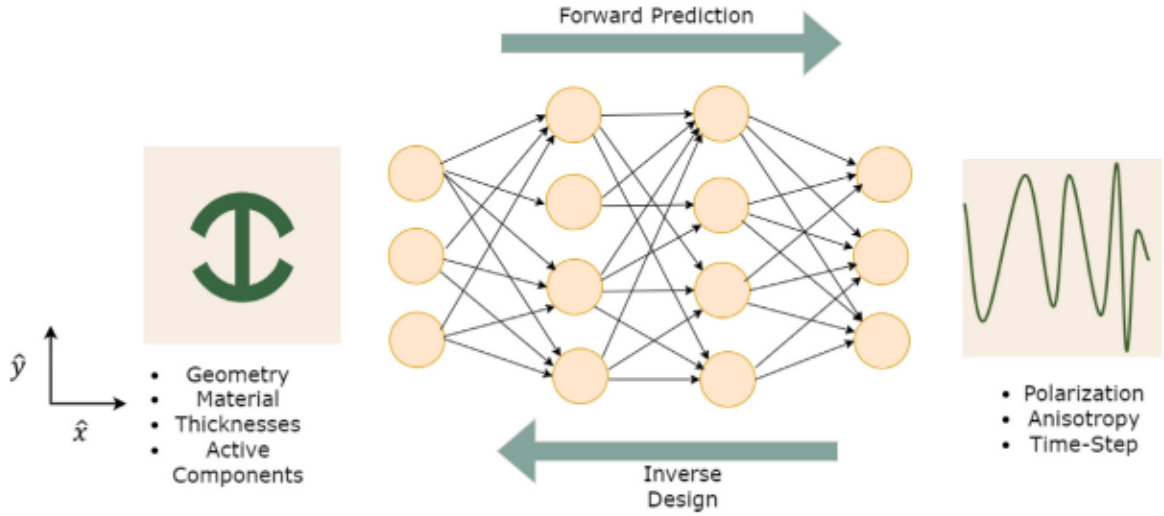

Fig. 10. Inverse RIS design: ML algorithms learn complex EM relationships between physical RIS structure (left) and spectral response (right) through training data (© The Author(s) 2022, [126]).

f is a function defining the problem's data, and $\mathcal{F}$ is a nonlinear differential operator. Besides, $\mathcal{B}$ represent the operator that signifies any unspecified initial or boundary conditions associated with the problem, and g denote the boundary function. In the PINN methodology, $u(z)$ is predicted computationally by a neural network parametrized by a set of parameters θ, leading to an approximation:

$$\hat{u}_\theta(z) \approx u(z;\theta), \tag{61}$$

where the notation $\hat{(\cdot)}_\theta$ signifies the neural network approximation performed using the parameters θ. In this context, the NN must learn to approximate the differential equations by determining the values of θ that define the NN. This is achieved by minimizing a loss function as follows:

$$\mathcal{L}(\theta) = \omega_{\text{physics}}\mathcal{L}_{\text{physics}} + \omega_{\text{Boundary}}\mathcal{L}_{\text{Boundary}} + \omega_{\text{data}}\mathcal{L}_{\text{data}} \tag{62}$$

$$\theta^* = \arg_\theta \min \mathcal{L}(\theta) \tag{63}$$

that includes three loss functions on:

1. **Labeled Data**

$$\mathcal{L}_{data}(\theta) = \text{MSE}_{\text{data}} = \frac{1}{N_{\text{data}}}\sum_{i=1}^{N_{\text{data}}} \left\|\hat{\mathbf{u}}_\theta(\mathbf{z}_i) - \mathbf{u}^*(i)\right\|^2 \tag{64}$$

2. **Boundary/ Initial Conditions**

$$\mathcal{L}_{\text{Boundary}}(\theta) = \text{MSE}_{\text{Boundary}} = \frac{1}{N_{\text{Boundary}}}\sum_{i=1}^{N_{\text{Boundary}}} \left\|\mathcal{B}(\hat{\mathbf{u}}_\theta(\mathbf{z}))\right\|^2 \tag{65}$$

3. **Residual on PDE Equations**

$$\mathcal{L}_{\text{physics}}(\theta) = \text{MSE}_{\text{physics}} = \frac{1}{N_{\text{physics}}}\sum_{i=1}^{N_{\text{physics}}} \left[\mathcal{F}(\hat{\mathbf{u}}_\theta(\mathbf{z}_i)) - \mathbf{r}_i\right]^2 = \frac{1}{N_{\text{physics}}}\left\|\sum_{i=1}^{N_{\text{physics}}} \left[\mathbf{r}_\theta(\mathbf{u}_i) - \mathbf{r}_i\right]\right\| \tag{66}$$

The PINN's building block is shown in Fig. 13. In Eq. (62), the initial term $\mathcal{L}_{\text{physics}}$ signifies the loss resulting from a discrepancy with the governing differential equations $\mathcal{F}$. It enforces the differential equation $\mathcal{F}$ at the collocation points, which can be uniformly or unevenly distributed over the domain Ω of Eq. (59). The remaining two losses aim to accommodate the known data within the neural network. The loss arising from a mismatch with the data (i.e., the measurements of u) is represented as $\mathcal{L}_{\text{data}}(\theta)$. The second term typically compels $\hat{u}_\theta$ to match the measurements of u at provided points (z, u^*), which can be either synthetic data or actual measurements. The weight ω_{data} can adjust for the quality of such measurements. The other term is the loss due to a mismatch with the boundary or initial conditions, $\mathbf{B}(\hat{\mathbf{u}}_\theta) = g$ from Eq. (59) [132–137].

In the context of RIS, PIDL can involve training deep neural networks to approximate the behavior of electromagnetic fields based on known physics principles, such as Maxwell's equations. By incorporating these physical constraints, the model can better generalize to unseen scenarios and provide insights into the underlying physical phenomena.

In [133], the authors employ PINNs to achieve the "homogenization" of distinct meta atom designs, specifically a disc and a split-ring resonator (SRR). The objective is to predict their effective electric permittivity distributions inversely based on simulated scattered electric fields. Homogenization aims to ensure that the resultant electric fields match those produced by a hypothetical continuous medium with equivalent material properties, aligning with the well-established 'effective medium theory'.

SRRs, which combine inductive and capacitive elements, function as oscillators. When the split-ring resonates with incident light's frequency, significant local fields occur in the gap region. The enhancement of these local fields is governed by the effective electric permittivity coefficient of these non-magnetic metamaterials. Notably, this work marks the first instance of showcasing the impact of PINN-based inverse model accuracy on the intricate and resonant behavior of SRRs. The electric field is determined as a function of the metasurface's spatial coordinates (denoted as x and y) by employing the Helmholtz wave equation in the frequency domain for linear, non-magnetic, weakly inhomogeneous materials. This equation is presented as follows:

$$\nabla \times \nabla \times E(x,y) - k_0^2\varepsilon_r E(x,y) = 0, \tag{67}$$

where, E represents the electric field, k_0 is the free space wave number, and ε_r signifies the relative electric permittivity distribution. Besides, $\nabla \times \nabla$ denotes the Laplacian operator. The mean squared error loss function, guided by physics principles, is derived from the residue of the Helmholtz equation and is computed as:

$$\text{MSE} = \frac{1}{N}\sum_{i=1}^{N}\left|F(x_i, y_i)\right|^2. \tag{68}$$

where, $F(x_i, y_i)$ is defined as:

$$F(x_i, y_i) = \frac{\partial^2 E(x_i, y_i)}{\partial x^2} + \frac{\partial^2 E(x_i, y_i)}{\partial y^2} + k_0^2\varepsilon_r E(x_i, y_i). \tag{69}$$

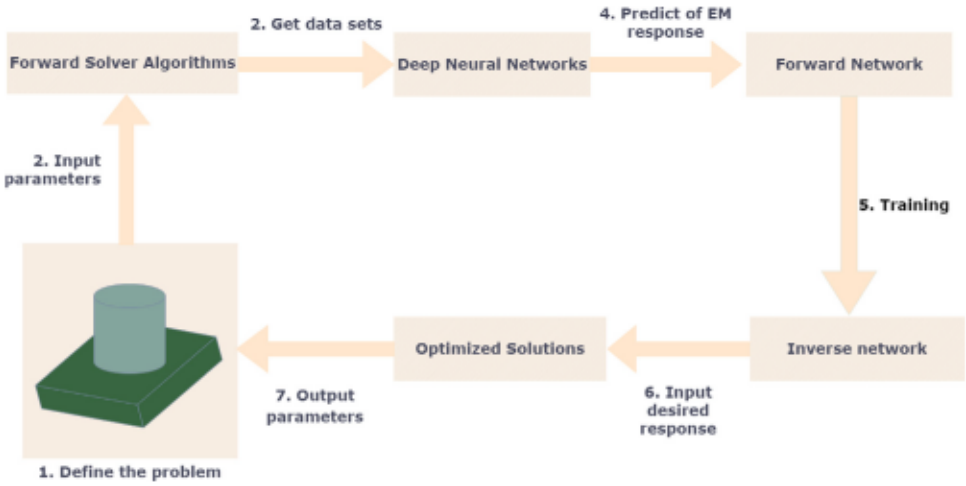

Fig. 11. Basic principle of using machine learning for metasurface design. Detailed steps are shown in the flowchart, including define the problem, collect data sets, pre-process data, train the model, validate the model, train inverse network, input desired response, iterate and optimization, and achieve desired performance (© The Author(s) 2023, [121]).

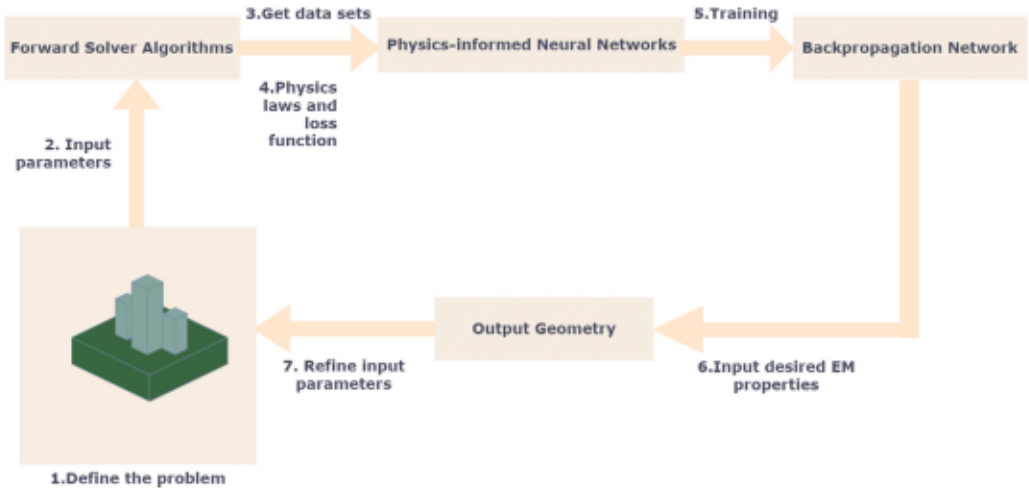

Fig. 12. Basic principle of using Physics-Informed Neural Networks for metasurface design. Detailed steps are demonstrated in the flowchart, including define the problem, create the training data, define physics principle and loss function, define the PINN architecture, validate the network, train backpropagation networks, input desired EM response, iterate the design process, and obtain desired metasurface designs (© The Author(s) 2023, [121]).

Eq. (68) is utilized to train the DNN and optimize its architecture to generate an effective spatial permittivity profile, resulting in an electric field that matches that of the original metasurface design. Fully connected feed-forward neural network, as shown in Fig. 14, with an input layer comprising of three neurons, namely, x, y, and normalized relative permittivity ε_r is employed. This is followed by 4 hidden layers of 250 neurons each and an output layer with a single neuron for the predicted E-field distribution $E(x, y)$. The input–output relationship of the network is denoted by $E(x, y, \theta)$ as a surrogate for the PDE solution to the Helmholtz equation, wherein θ is a vector containing the trainable weights and biases of the network.

One more paper [138] utilizes physical optics techniques to derive the pathloss expression for RIS configured to reflect waves toward a receiver in the far-field. The study highlights the limitations of using infinitely sized RISs and emphasizes the importance of coherent beamforming achieved through sub-wavelength-sized elements with unique phase shifts. The ideal phase shifts for beam creation follow the generalized Snell's law.

The work in [139] demonstrates the efficacy of a physics-guided deep learning approach with a tandem architecture (Fig. 15) for the efficient and interpretable design of metasurfaces in a supervised learning context. By harnessing neural networks' capabilities, they uncover the strong connection between device configuration and optical behavior. To address challenges posed by using deep neural networks for inverse problems, such as non-interpretability and non-uniqueness, they introduce a tandem architecture incorporating a physics-based constraint. Integrating both forward and inverse models in this architecture mitigates one-to-many prediction issues. By adding a physics-driven penalty term, their model generates interpretable and physically consistent predictions, while also enhancing generalizability and reducing data requirements. The physics penalty term is derived analytically by simplifying the metamaterial structure into a stratified medium, primarily applicable for sub-wavelength dimensions. To adapt the model to larger dimensions, they adjusted the physics-based loss function or employed a physics-guided deep learning architecture for prediction. The proposed model achieves high accuracy. The physics-guided DL framework that have developed to solve problem is shown in Fig. 16.

Tandem model structure consists of the forward EM equation approximated by a deep neural network and the inverse DL model. The networks are appended end-to-end so that the output of the inverse model is fed into the forward DL model. The inverse problem involves predicting the design based on a given response. In Fig. 16, the input of the pretrained forward DL model is connected to the output of the inverse model. This predicted design is then passed into the pretrained forward model to assess how well it can reconstruct

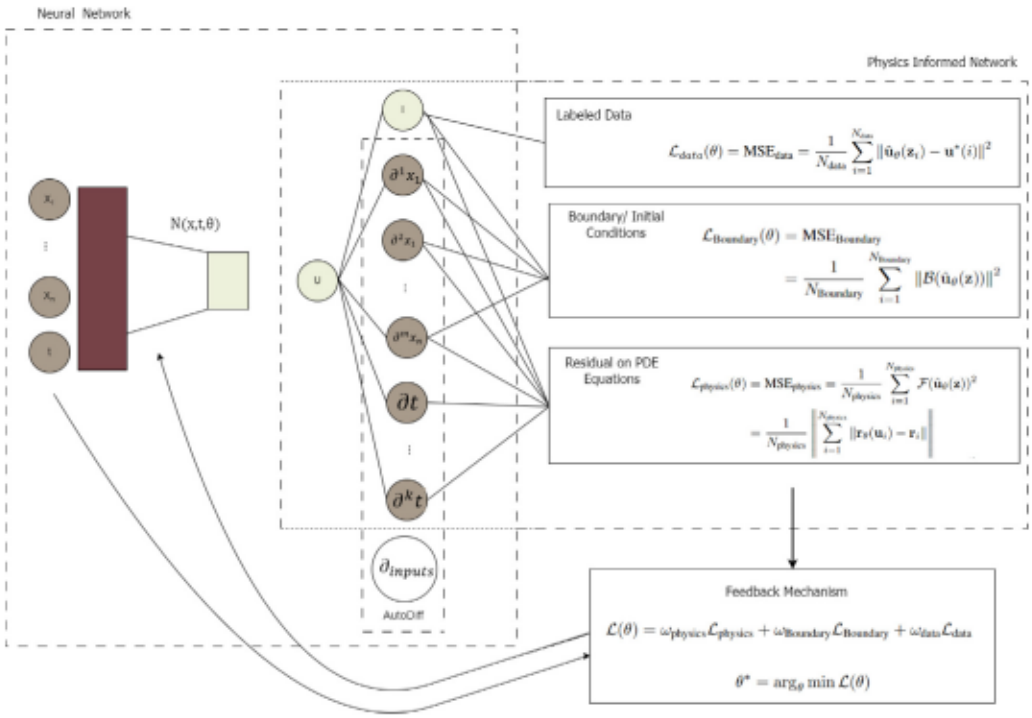

Fig. 13. The constituents of PINNs. PINNs are composed of residual terms derived from differential equations, as well as initial and boundary conditions. The network takes inputs, transforms them into field outputs (denoted as u), and is defined by parameters θ. The second component is the physics-informed network, which computes derivatives from the output field u based on provided equations. It also evaluates boundary and initial conditions (unless they are hardcoded in the neural network) and incorporates labeled data observations if available. The feedback mechanism is the final step, minimizing the loss with an optimizer and a specified learning rate to determine the NN parameters θ (© The Author(s) 2023, [137]).

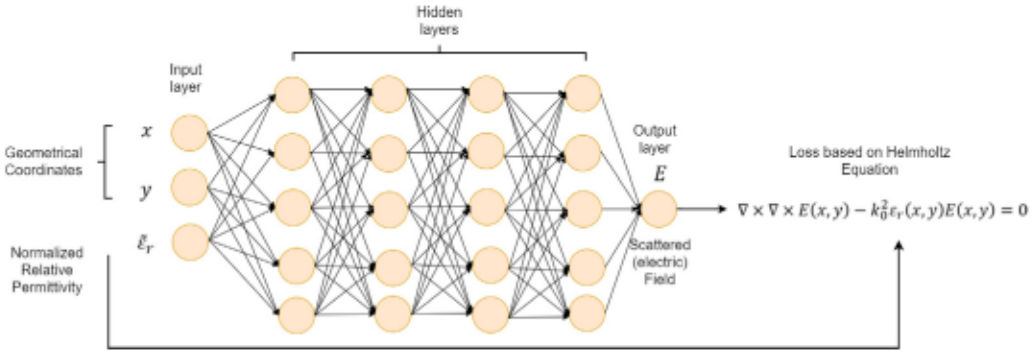

Fig. 14. Representative diagram of the physics-informed neural network model with 6 layers. Each hidden layer contains 250 neurons. A physics-driven loss function based on the Helmholtz equation is used to train the model (© The Author(s) 2020, [133]).

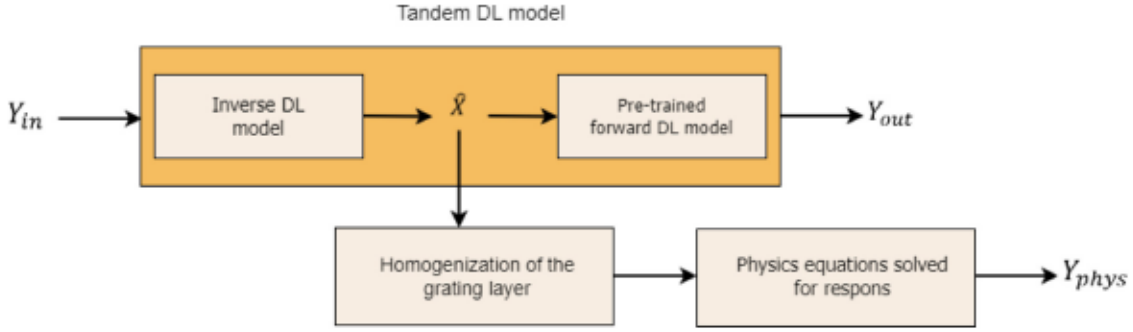

Fig. 15. Overview of the components of the physics-guided DL model. Y_{in} is the input optical response and the design, $\hat{X}$, predicted from the inverse model. The predicted design is then fed into a pre-trained forward model to ensure proper reconstruction of the optical response, Y_{out}. The structure of $\hat{X}$ is then simplified according to the homogenization principle and the physics equations are solved to obtain Y_{phys} that ensures physics guided learning (© The Author(s) 2023, [139]).

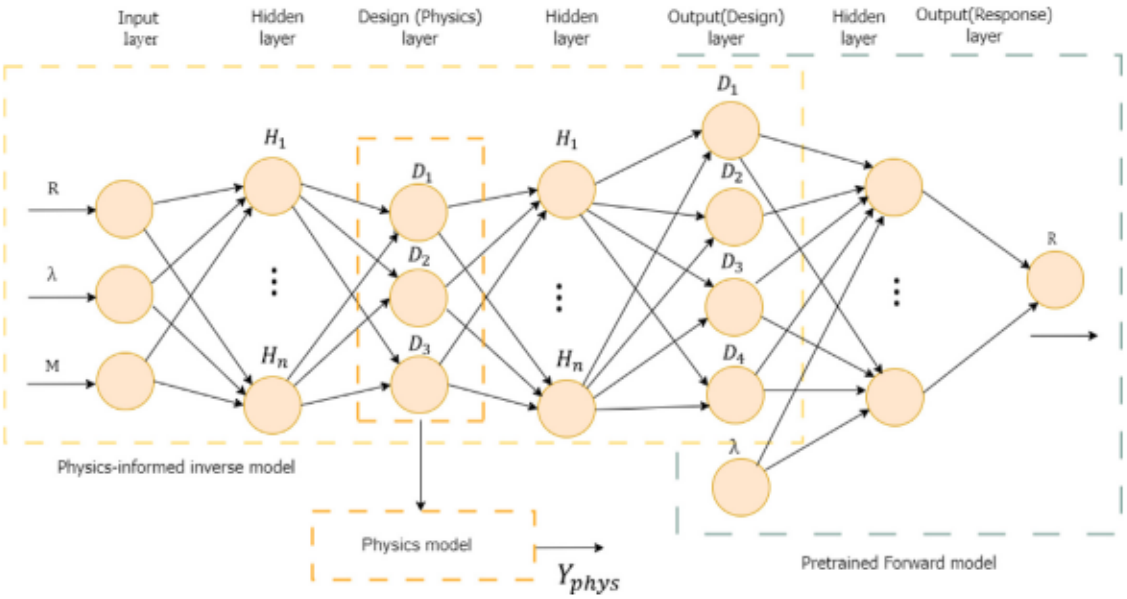

Fig. 16. Physics-informed DL architecture (PIA). The "Design (Physics) layer" includes intermediate variables that are consistent with the underlying physics. These variables are calculated based on the design parameters that result in a certain response, as predicted by the EM equations for the simplified homogenized structure. The "Output (Design) layer" then uses these intermediate variables to predict the original complex design parameters (© The Author(s) 2023, [139]).

the optical response. The entire structure, with the weights of the forward model fixed, undergoes training to minimize two key errors: the design prediction error (the deviation between the predicted design, denoted as $\hat{X}$, and the ground truth design, denoted as X) and the reconstruction error (the deviation between the response reconstructed by the predicted design, denoted as Y_{out}, and the ground truth response, denoted as Y_{in}).

Physics can be integrated into DL models through various approaches, including modifying the loss function, using residual modeling, initializing parameters, or adjusting the model architecture. In this study, the incorporation of physics was focusd on the loss function and DL architecture. By training a physics-guided DL model, the learning process adapts model parameters to align with physics principles, either for final or intermediate layer outputs. The inclusion of physics is manifested in Eq. (70) through a penalty term. This term is integrated either as a penalty for the final output layer or for the intermediate layer in the physics-guided loss function and the physics-guided architecture, respectively. This penalty corresponds to the disparity between the actual optical response, Y_{in}, and the response obtained through solving electromagnetic equations for a simplified design structure, denoted as Y_{phys}. The equation representing this incorporation is as follows:

$$\begin{aligned}\text{Objective} = &\omega_{\text{obs}_1}\text{Loss}(X;\hat{X}) \\ &+ \omega_{\text{obs}_2}\text{Loss}(Y_{\text{in}};Y_{\text{out}}) \\ &+ \omega_{\text{phys}}(X)\text{Loss}(Y_{\text{in}};Y_{\text{phys}}),\end{aligned} \tag{70}$$

In this context, the parameters ω_{obs_1}, ω_{obs_2}, and ω_{phys} represent the weighting of each loss term, acting as hyperparameters. The values for ω_{obs_1} and ω_{obs_2} are meticulously determined through grid search hyperparameter tuning to optimize the model's performance on the validation set. Simultaneously, ω_{phys} is directly proportional to $\frac{\lambda_0}{p}$, ensuring heightened emphasis on the physics-based loss function term when $\lambda_0 \gg p$, where the effective medium theory of homogenization holds true. Here, λ_0 denotes the wavelength, and p is a parameter associated with the metamaterial structure. The loss term in the equation corresponds to the mean absolute error (MAE) loss.

5.6. Lessons learned

- Model-based optimization techniques and heuristic algorithms often suffer from high computational complexity, scalability issues, and reliance on simplifying assumptions, limiting their effectiveness in solving complex EM-aware RIS optimization problems.
- In contrast, ML/DL methods offer advantages such as adaptability to dynamic environments, capability to handle large-scale optimization problems, and ability to learn complex patterns and relationships from data, making them promising for addressing the challenges of EM-aware RIS optimization in real-world communication scenarios.
- ML/DL methods has widely used for MTS design. However, dynamic optimization of EM-aware RIS-aided communications employing ML/DL algorithm rarely presented in the literatures.

6. Research gaps and future research

In this section, our goal is to delineate the areas of research that require further exploration and potential avenues for future research.

6.1. Electromagnetic information theory (EIT) in RIS-aided communications

In the realm of wireless communications, electromagnetic theory and information theory stand as fundamental principles, linked by antenna theory and wireless propagation channel modeling. While these concepts evolved separately until the era of 5G networks, the advent of 6G communication networks – spanning across space, air, ground, and sea – necessitates seamless coverage in three-dimensional space. This demands continuous acquisition of CSI and channel capacity calculation at any location and time. Electromagnetic theory enables precise modeling of how signals propagate through space, while information theory quantifies the capacity of these channels to carry information. By integrating these two theories, EIT provides a comprehensive framework that not only models the electromagnetic field distribution but also calculates the communication performance, allowing for more accurate and dynamic acquisition of CSI in 6G networks. Additionally, advanced 6G technologies like ultra-massive MIMO and holographic MIMO call for integrated modeling of antennas and wireless propagation environments. To address these challenges, the integration of electromagnetic theory, information theory, antenna theory, and wireless propagation channel modeling has become essential, leading to the emergence of EIT [140].

The classic electromagnetic theory, founded on Maxwell's equations, operates in continuous time and space, mainly addressing macroscopic fields. However, at microscopic scales, local field fluctuations become significant, especially in scenarios like high-mobility millimeter wave-aided wideband environments. Traditional Shannon's information theory, tailored for simple channels, lacks accuracy in complex, non-stationary settings demanded by emerging 6G technologies such as integrated sensing and communication (ISAC), RIS, massive MIMO, and holographic MIMO. Integrating electromagnetic theory with information theory expands the latter to encompass non-stationary channels, facilitating the evolution from discrete-space single-user information theory to continuous-space multi-user/network information theory. Continuous-space electromagnetic channel models, coupled with optimal antenna design, enhance channel capacity. By studying the mutual information between incident, reflected, transmitted, and scattered waves, Maxwell's equations find application in novel technologies like RIS, enabling precise performance and capacity descriptions. The concept of information metamaterials further integrates electromagnetic theory and information theory, aiming to manipulate electromagnetic waves within metamaterial structures for improved spectral efficiency and reduced system costs. However, conventional signal processing methods often fail to accurately characterize electromagnetic fields, underscoring the need for innovative approaches, such as leveraging RIS to understand electromagnetic wave interactions and realize end-to-end electromagnetic information transmission mechanisms in communication systems [140]. In [141], the concept of the digital metasurface, known as the information metasurface (IM), is introduced. The paper delves into its applications in wireless communications. IMs represent a significant paradigm shift, expanding the scope of metasurface research from the realm of physics into the realm of information.

Future research endeavors should aim to delve deeper into the possibilities and applications of EIT in RIS scenarios. This exploration could encompass theoretical developments, practical implementations, and experimentation to fully harness the potential benefits of EIT [142].

6.2. Machine learning applications for optimization of EM-based RIS-aided communications

Machine learning techniques for optimizing RIS-aided communications have been extensively examined in [32–35], all without the inclusion of physically consistent EM models. Machine learning techniques have yet to be thoroughly explored for optimizing RIS-aided communications from an EM perspective. While there are massive number of papers focusing on the inverse design of meta-surfaces using machine learning techniques (as discussed in Section 5), the optimization of EM-based RIS-aided communication and BD-RIS-assisted communication systems as a whole has been relatively untouched in the current literature. Furthermore, the integration of machine learning techniques into EIT-based RIS-aided communication systems is an uncharted territory in research. This represents a significant research gap that holds immense potential. Machine learning algorithms can play a pivotal role in enhancing the efficiency and accuracy of RIS-aided communications using EIT.

6.3. Green communications

In the evolving 5G and future 6G landscapes, the proliferation of network nodes is causing a surge in energy consumption and carbon emissions. Resource allocation, network planning and deployment, energy harvesting and transmission, and hardware solutions are the four areas under which the most popular methods for boosting the EE of wireless networks are categorized.

Energy harvesting (EH), which includes radio frequency (RF) energy harvesting, offers the dual advantage of supporting SWIPT while harnessing interference signals for energy collection. This concept has been explored in [99], as detailed in Section 4. When combined with SWIPT technology, RISs have the potential to enhance EH efficiency. Additionally, when integrated with orbital angular momentum (OAM) technology, RIS can serve the purpose of reflecting OAM waves obstructed by obstacles, establishing a direct path for OAM-based SWIPT. As a result, RIS-assisted OAM-SWIPT emerges as a promising technology for future wireless communication, offering energy and spectrum efficiency [143]. The works in [143–145] have delved into using OAM for RIS-assisted communications. Nonetheless, it is clear that additional research into the combined utilization of RIS and OAM technologies offers considerable potential for future advancements. To enable RIS to pass OAM waves effectively, RIS should be able to manipulate the electromagnetic field to accommodate the unique properties of OAM waves.

EM-aware resource allocation in RIS-assisted communications is another gap that should be addressed in future research. As elucidated in Section 4, the literature has offered several EM-aware problem formulations for RIS-assisted communications, addressing various aspects of this technology. These formulations have contributed significantly to our understanding and optimization of RIS deployments in diverse scenarios. However, one notable research gap pertains to resource allocation problems within the context of wideband communications. While existing studies have primarily focused on narrowband scenarios, the challenges and opportunities associated with wideband communication systems have yet to receive comprehensive attention. This represents a crucial area for further investigation, as wideband communications are increasingly prevalent in modern wireless networks, and tailored resource allocation strategies can significantly impact their performance and efficiency. In this regard, incorporating physical models of RIS systems into problem formulations can offer valuable insights and solutions.

By integrating physical models, researchers can develop resource allocation algorithms that are not only EM-aware but also consider the specific characteristics of RIS elements and their impact on wideband communication channels. This holistic approach, combining EM-awareness with physical realism, holds the potential to yield more robust and efficient resource allocation strategies for wideband RIS-aided communications.

6.4. Optical communications

The integration of optical communication with RIS-assisted communication presents a promising avenue for enhancing network performance and addressing modern communication challenges. Recent advancements, such as the introduction of optical simultaneous transmission and reflection reconfigurable intelligent surface (OSTAR-RIS), underscore the potential of this integration [146]. Authors in [147] seeks to bridge this gap by offering a comprehensive tutorial on indoor visible light communication (VLC) systems leveraging RIS technology. It delves into the fundamentals of VLC and RISs, explores the potential applications of optical RISs in mitigating line-of-sight blockages and device orientation issues, and proposes avenues for future research on integrating optical RISs with emerging technologies. However, there is currently limited exploration of RISs in optical wireless communication (OWC) systems. Novel BD-RIS architectures can be explored using the integration of optical communication. This integration can be as follows:

- Physical Consistency: Optical communication offers high-speed data transmission using light waves, which can be leveraged to accurately model the behavior of RIS elements. By considering the physical properties of light propagation, such as reflection, refraction, and diffraction, in conjunction with the characteristics of RIS surfaces, a more accurate and physically consistent model of RIS can be developed. This model can capture the intricate interactions between light waves and RIS elements, leading to improved performance predictions and optimization strategies.

- Innovative Architectures: The integration of optical communication with RIS-assisted communication opens up new possibilities for designing innovative RIS architectures, such as BD-RIS. By exploring the synergy between optical components and RIS elements, novel architectures that leverage both optical and electromagnetic properties can be proposed. For example, incorporating optical switches or modulators into RIS structures can enable dynamic reconfiguration of RIS elements, leading to enhanced flexibility and adaptability in network optimization.

6.5. Quantum communications

Quantum information science is rapidly advancing, promising enhanced security through quantum communication, transformative computational power with quantum computing, and revolutionary sensing capabilities. Digital metamaterials, also known as information metamaterials, enable the manipulation of digital data carried by electromagnetic waves, potentially revolutionizing information processing and high-performance wireless information systems. These metamaterials utilize binary coding for real-time control of electromagnetic waves, bridging the physical and digital realms. They offer significant potential for both fundamental science and engineering applications in the nonclassical electromagnetic field, closely tied to quantum information science. Electromagnetic metamaterials can further advance these quantum-inspired developments, giving rise to quantum metamaterials that extend classical concepts for manipulating and detecting nonclassical electromagnetic waves [148].

Viewing physical models of RIS from a quantum perspective introduces a fascinating and innovative dimension to the understanding of RIS. Quantum physics, with its principles of superposition, entanglement, and uncertainty, can provide new insights and possibilities in the design and operation of RIS.

To fully unlock the potential of RIS-enabled smart EM environments, it is essential to quickly identify the optimal configurations of the RIS to achieve specific objectives. While mathematical tools like generalized Snell's law aid in managing anomalous reflection, there is a lack of semi-analytical solutions for certain EM functionalities such as multi-beamforming, energy focusing, and diffusive scattering, as well as wireless functions like spatial diversity, data throughput, and physical-layer security. As a result, various optimization methods for RIS have been proposed, including genetic algorithms, impedance-based synthesis, electromagnetic inversion, machine learning, and dynamic optimization. However, despite these advancements, optimizing RIS configurations remains computationally challenging due to the vast number of possibilities, the complexity of EM scattering environments, and processing time constraints in wireless systems.

Recent progress in QC offers a promising solution to tackle these computational challenges. For EM applications, quantum algorithms like the quantum Fourier Transform have been applied to antenna array synthesis, while the Harrow/Hassidim/Lloyd (HHL) algorithm is used for characterizing interconnects. Variational quantum algorithms utilizing the finite difference method have also been developed for calculating waveguide modes. In the realm of wireless networks, quantum computing facilitates tasks such as multi-user MIMO detection, processing, and optimal resource allocation for 6G wireless networks [149].

Quantum communications and quantum computing for RIS-aided communications have been studied in some recent papers [149–152]. The possibilities of combining EM models-aware RIS-aided communication and quantum knowledge and computing is an interesting domain to be explored.

6.6. RIS-enhanced semantic communications with physically-consistent RIS models

Semantic communication, which prioritizes conveying the meaning of information rather than exact bit reconstruction, has garnered significant attention in recent years [153]. This approach revolutionizes the way we transmit and interpret data, focusing on the context and intent behind the information exchange. Recent studies have explored the integration of RIS in enhancing semantic communications, aiming to leverage their potential in shaping the electromagnetic environment for improved data transfer [153–156].

Despite these advancements, a promising avenue that remains largely unexplored is the incorporation of physically-consistent RIS models. These models, grounded in the principles of electromagnetic wave interactions, hold the key to achieving greater precision and efficiency in the context of RIS-enhanced semantic communications. By integrating EM models of RIS into the semantic communication framework, we can attain a deeper understanding of how RIS elements interact with electromagnetic waves and, in turn, impact the semantic content of the communication.

Such an integration offers numerous opportunities. It enables us to adapt RIS configurations dynamically, responding to real-time changes in the electromagnetic environment. This adaptability ensures that the conveyed meaning remains intact, even in the face of fluctuating signal quality and interference. Furthermore, physically-consistent RIS models facilitate the optimization of data transfer, allowing semantic content to be communicated with greater clarity and reliability.

6.7. Multi-objective optimization with physically-consistent RIS models

Developing a multi-objective optimization framework for RIS that integrates physically consistent models is crucial for enhancing RIS-based communication systems. This framework must balance optimizing communication capacity, minimizing interference, and conserving energy while adhering to the physical constraints and characteristics of RIS technology to ensure practical feasibility. Although significant strides have been made in multi-objective optimization for RIS, as noted in Refs. [157–162], there remains a notable opportunity to advance optimization strategies by incorporating EM phenomena.

In this context, recent research has expanded the scope of optimization by integrating RIS with ISAC systems. ISAC represents a paradigm shift that combines communication and sensing objectives into a unified framework through co-design approaches. This approach introduces a new dimension to the optimization problem, making it inherently multi-objective. Advanced signal processing techniques are being developed to design dual-functional waveforms that optimize both communication metrics—such as SINR and multi-user interference (MUI) and sensing metrics such as beam-pattern mean squared error (MSE), received echo power/signal-to-noise ratio (SNR), and Cramér–Rao bound (CRB) [163].

Further research can explore the advantages of EM-aware optimization in RIS-assisted ISAC systems. By incorporating a deeper understanding of EM phenomena into the optimization framework, this research avenue promises to unlock the full potential of RIS. It is likely to lead to more efficient and sophisticated applications of RIS in future wireless communication systems, paving the way for advanced solutions that better meet the demands of modern communication and sensing requirements.

6.8. Stacked intelligent metasurfaces aided wireless communication

Stacked intelligent metasurfaces (SIMs) represent a significant advancement in wireless communications by leveraging multiple layers of RIS to enhance signal processing. The study by Matteo and Clerckx [164] introduces a novel model utilizing multiport network theory to address SIM-assisted communications. Their approach provides a

physically consistent framework for understanding the EM coupling between transmitting antennas and metasurface layers, accurately predicting the transfer function of SIMs by considering the cascading effects of multiple metasurface layers on EM wave propagation. Despite this progress and some other limited recent literature [164–168], the exploration of SIMs remains limited, indicating a need for further investigation, particularly into their physical characteristics and modeling techniques.

7. Conclusion

In conclusion, the rapid evolution of RISs represents a remarkable leap forward in the realm of wireless communication systems. These adaptive metasurfaces, equipped with the ability to dynamically manipulate EM waves, hold great promise for enhancing network capacity, coverage, and efficiency. Throughout this survey, we have traversed the landscape of RIS-aided communication systems, exploring the multitude of EM-aware challenges and optimization avenues they present.

One key takeaway from our exploration is the pivotal role played by physically-consistent EM models. These models serve as the foundation for developing robust and efficient RIS designs, enabling precise control over EM wave propagation. By grounding our designs in these models, we can achieve superior performance and ensure the reliability of RIS-aided systems.

Furthermore, we have delved into the realm of machine learning approaches for RIS optimization. This exciting field has witnessed significant advancements, with recent developments showcasing the potential to simplify and expedite the design process. Machine learning techniques have the capacity to learn intricate relationships within RIS structures and EM responses, offering valuable tools for RIS engineers.

As we move forward, the integration of physically-consistent EM models with machine learning approaches promises to drive innovation in RIS-aided communications. These two paradigms, when harnessed synergistically, enable us to tackle complex EM-aware problems and optimize RIS performance effectively. However, it is important to remain cognizant of the challenges that lie ahead, including scalability, hardware constraints, and real-world deployment issues.

In essence, this survey paper has illuminated the path toward unlocking the full potential of RIS-aided communication systems. By embracing physically-consistent EM models and harnessing the power of machine learning, we can shape the future of wireless networks, ushering in an era of unprecedented capacity, coverage, and efficiency.

CRediT authorship contribution statement

S. Bidabadi: Writing – review & editing, Writing – original draft, Methodology, Conceptualization. **M.A. Ouameur:** Writing – review & editing, Supervision, Conceptualization. **M. Bagaa:** Writing – review & editing, Visualization, Supervision. **D. Massicotte:** Writing – review & editing, Validation. **F.D. Figueiredo:** Writing – review & editing. **A. Chaaban:** Writing – review & editing.

Declaration of competing interest

The authors declare that they have no known competing financial interests or personal relationships that could have appeared to influence the work reported in this paper.

Data availability

No data was used for the research described in the article.

Declaration of Generative AI and AI-assisted technologies in the writing process

During the preparation of this work, the authors used ChatGPT to check the grammar of the original manuscript and improve readability. After using this tool/service, the authors reviewed and edited the content as needed, taking full responsibility for the publication's content.

References

[1] Ahmad A.A. Solyman, Khalid Yahya, Key performance requirement of future next wireless networks (6G), Bull. Electr. Eng. Inform. 10 (6) (2021) 3249–3255.

[2] Keysight Technologies, Next-Generation Wireless: A Guide to the Fundamentals of 6G, Keysight Technologies, USA, 2023, June 13, 2023, 1–39.

[3] Walid Saad, Mehdi Bennis, Mingzhe Chen, A vision of 6G wireless systems: Applications, trends, technologies, and open research problems, IEEE Netw. 34 (3) (2019) 134–142.

[4] Samaneh Bidabadi, Messaoud Ahmed Ouameur, Miloud Bagaa, Daniel Massicotte, Energy efficient resource allocation for re-configurable intelligent surface-assisted wireless networks, EURASIP J. Wireless Commun. Networking 2023 (1) (2023) 1–22.

[5] Qingqing Wu, Beixiong Zheng, Changsheng You, Lipeng Zhu, Kaiming Shen, Xiaodan Shao, Weidong Mei, Boya Di, Hongliang Zhang, Ertugrul Basar, Lingyang Song, Marco Di Renzo, Zhi-Quan Luo, Rui Zhang, Intelligent surfaces empowered wireless network: Recent advances and the road to 6G, 2024, URL https://arxiv.org/abs/2312.16918.

[6] Moazzam Shah Bukhari Syed, Hafiz Muhammad Attaullah, Sundus Ali, Muhammad Imran Aslam, Wireless communications beyond antennas: The role of reconfigurable intelligent surfaces, Eng. Proc. 32 (1) (2023) 10.

[7] Xiaodan Shao, Changsheng You, Rui Zhang, Intelligent reflecting surface aided wireless sensing: Applications and design issues, 2023, arXiv preprint arXiv:2302.05864.

[8] Yuanwei Liu, Xiao Liu, Xidong Mu, Tianwei Hou, Jiaqi Xu, Marco Di Renzo, Naofal Al-Dhahir, Reconfigurable intelligent surfaces: Principles and opportunities, IEEE Commun. Surv. Tutor. 23 (3) (2021) 1546–1577.

[9] Shimin Gong, Xiao Lu, Dinh Thai Hoang, Dusit Niyato, Lei Shu, Dong In Kim, Ying-Chang Liang, Toward smart wireless communications via intelligent reflecting surfaces: A contemporary survey, IEEE Commun. Surv. Tutor. 22 (4) (2020) 2283–2314, http://dx.doi.org/10.1109/COMST.2020.3004197.

[10] Ertugrul Basar, Marco Di Renzo, Julien de Rosny, Merouane Debbah, Mohamed-Slim Alouini, Rui Zhang, Wireless communications through reconfigurable intelligent surfaces, 2019.

[11] Xiaojun Yuan, Ying-Jun Angela Zhang, Yuanming Shi, Wenjing Yan, Hang Liu, Reconfigurable-intelligent-surface empowered wireless communications: Challenges and opportunities, IEEE Wirel. Commun. 28 (2) (2021) 136–143.

[12] Marco Di Renzo, Alessio Zappone, Merouane Debbah, Mohamed-Slim Alouini, Chau Yuen, Julien De Rosny, Sergei Tretyakov, Smart radio environments empowered by reconfigurable intelligent surfaces: How it works, state of research, and the road ahead, IEEE J. Sel. Areas Commun. 38 (11) (2020) 2450–2525.

[13] Yuanwei Liu, Xiao Liu, Xidong Mu, Tianwei Hou, Jiaqi Xu, Marco Di Renzo, Naofal Al-Dhahir, Reconfigurable intelligent surfaces: Principles and opportunities, IEEE Commun. Surv. Tutor. 23 (3) (2021) 1546–1577, http://dx.doi.org/10.1109/COMST.2021.3077737.

[14] George C. Alexandropoulos, Geoffroy Lerosey, Merouane Debbah, Mathias Fink, Reconfigurable intelligent surfaces and metamaterials: The potential of wave propagation control for 6G wireless communications, 2020.

[15] Christopher L. Holloway, Edward F. Kuester, Joshua A. Gordon, John O'Hara, Jim Booth, David R. Smith, An overview of the theory and applications of metasurfaces: The two-dimensional equivalents of metamaterials, IEEE Antennas Propag. Mag. 54 (2) (2012) 10–35, http://dx.doi.org/10.1109/MAP.2012.6230714.

[16] Syed S. Bukhari, J. Vardaxoglou, William Whittow, A metasurfaces review: Definitions and applications, Appl. Sci. 9 (13) (2019) 2727.

[17] Mayurkumar Ladumor, Shreyas Charola, Shobhit K. Patel, Vigneswaran Dhasarathan, Graphene-based c-shaped metasurface broadband solar absorber, in: Physics and Simulation of Optoelectronic Devices XXVIII, vol. 11274, SPIE, 2020, pp. 7–12.

[18] Adnan Ali, Anirban Mitra, Brahim Aïssa, Metamaterials and metasurfaces: A review from the perspectives of materials, mechanisms and advanced metadevices, Nanomaterials 12 (6) (2022) 1027.

[19] Zhuqi Li, Yaxiong Xie, Longfei Shangguan, R. Ivan Zelaya, Jeremy Gummeson, Wenjun Hu, Kyle Jamieson, Programmable radio environments with large arrays of inexpensive antennas, GetMobile: Mob. Comput. Commun. 23 (3) (2020) 23–27.

[20] Chongwen Huang, Sha Hu, George C. Alexandropoulos, Alessio Zappone, Chau Yuen, Rui Zhang, Marco Di Renzo, Merouane Debbah, Holographic MIMO surfaces for 6G wireless networks: Opportunities, challenges, and trends, IEEE Wirel. Commun. 27 (5) (2020) 118–125.

[21] Marco Di Renzo, Konstantinos Ntontin, Jian Song, Fadil H. Danufane, Xuewen Qian, Fotis Lazarakis, Julien De Rosny, Dinh-Thuy Phan-Huy, Osvaldo Simeone, Rui Zhang, et al., Reconfigurable intelligent surfaces vs. relaying: Differences, similarities, and performance comparison, IEEE Open J. Commun. Soc. 1 (2020) 798–807.

[22] Marco Di Renzo, Alessio Zappone, Merouane Debbah, Mohamed-Slim Alouini, Chau Yuen, Julien de Rosny, Sergei Tretyakov, Smart radio environments empowered by reconfigurable intelligent surfaces: How it works, state of research, and road ahead, 2020.

[23] Haris Gacanin, Marco Di Renzo, Wireless 2.0: Toward an intelligent radio environment empowered by reconfigurable meta-surfaces and artificial intelligence, IEEE Veh. Technol. Mag. 15 (4) (2020) 74–82, http://dx.doi.org/10.1109/MVT.2020.3017927.

[24] Qingqing Wu, Rui Zhang, Towards smart and reconfigurable environment: Intelligent reflecting surface aided wireless network, IEEE Commun. Mag. 58 (1) (2019) 106–112.

[25] Cunhua Pan, Hong Ren, Kezhi Wang, Jonas Florentin Kolb, Maged Elkashlan, Ming Chen, Marco Di Renzo, Yang Hao, Jiangzhou Wang, A. Lee Swindlehurst, et al., Reconfigurable intelligent surfaces for 6G systems: Principles, applications, and research directions, IEEE Commun. Mag. 59 (6) (2021) 14–20.

[26] Saber Hassouna, Muhammad Ali Jamshed, James Rains, Jalil ur Rehman Kazim, Masood Ur Rehman, Mohammad Abualhayja, Lina Mohjazi, Tei Jun Cui, Muhammad Ali Imran, Qammer H Abbasi, A survey on reconfigurable intelligent surfaces: Wireless communication perspective, IET Commun. 17 (5) (2023) 497–537.

[27] Ana Díaz-Rubio, Sergei A. Tretyakov, Macroscopic modeling of anomalously reflecting metasurfaces: Angular response and far-field scattering, IEEE Trans. Antennas and Propagation 69 (10) (2021) 6560–6571, http://dx.doi.org/10.1109/TAP.2021.3076267.

[28] Özgecan Özdogan, Emil Björnson, Erik G. Larsson, Intelligent reflecting surfaces: Physics, propagation, and pathloss modeling, IEEE Wirel. Commun. Lett. 9 (5) (2020) 581–585, http://dx.doi.org/10.1109/LWC.2019.2960779.

[29] Davide Dardari, Communicating with large intelligent surfaces: Fundamental limits and models, IEEE J. Sel. Areas Commun. 38 (11) (2020) 2526–2537, http://dx.doi.org/10.1109/JSAC.2020.3007036.

[30] Nandana Rajatheva, Italo Atzeni, Simon Bicais, Emil Bjornson, Andre Bourdoux, Stefano Buzzi, Carmen D'Andrea, Jean-Baptiste Dore, Serhat Erkucuk, Manuel Fuentes, Ke Guan, Yuzhou Hu, Xiaojing Huang, Jari Hulkkonen, Josep Miquel Jornet, Marcos Katz, Behrooz Makki, Rickard Nilsson, Erdal Panayirci, Khaled Rabie, Nuwanthika Rajapaksha, MohammadJavad Salehi, Hadi Sarieddeen, Shahriar Shahabuddin, Tommy Svensson, Oskari Tervo, Antti Tolli, Qingqing Wu, Wen Xu, Scoring the terabit/s goal:Broadband connectivity in 6G, 2021, URL https://arxiv.org/abs/2008.07220.

[31] K.M. Faisal, Wooyeol Choi, Machine learning approaches for reconfigurable intelligent surfaces: A survey, IEEE Access 10 (2022) 27343–27367.

[32] Hao Zhou, Melike Erol-Kantarci, Yuanwei Liu, H Vincent Poor, A survey on model-based, heuristic, and machine learning optimization approaches in RIS-aided wireless networks, 2023, arXiv preprint arXiv:2303.14320.

[33] Annisa Anggun Puspitasari, Byung Moo Lee, A survey on reinforcement learning for reconfigurable intelligent surfaces in wireless communications, Sensors 23 (5) (2023) 2554.

[34] Hao Zhou, Melike Erol-Kantarci, Yuanwei Liu, H. Vincent Poor, Heuristic algorithms for RIS-assisted wireless networks: Exploring heuristic-aided machine learning, 2023, arXiv preprint arXiv:2307.01205.

[35] Sree Krishna Das, Fatma Benkhelifa, Yao Sun, Hanaa Abumarshoud, Qammer H. Abbasi, Muhammad Ali Imran, Lina Mohjazi, Comprehensive review on ML-based RIS-enhanced IoT systems: basics, research progress and future challenges, Comput. Netw. 224 (2023) 109581.

[36] Zongze Li, Shuai Wang, Qingfeng Lin, Yang Li, Miaowen Wen, Yik-Chung Wu, H. Vincent Poor, Phase shift design in RIS empowered wireless networks: from optimization to AI-based methods, Network 2 (3) (2022) 398–418.

[37] Mohammad Abrar Shakil Sejan, Md Habibur Rahman, Beom-Sik Shin, Ji-Hye Oh, Young-Hwan You, Hyoung-Kyu Song, Machine learning for intelligent-reflecting-surface-based wireless communication towards 6G: A review, Sensors 22 (14) (2022) 5405.

[38] Marco Di Renzo, Fadil H. Danufane, Sergei Tretyakov, Communication models for reconfigurable intelligent surfaces: From surface electromagnetics to wireless networks optimization, Proc. IEEE 110 (9) (2022) 1164–1209.

[39] Muhammad Zain Siddiqi, Talha Mir, Reconfigurable intelligent surface-aided wireless communications: An overview, Intell. Converged Netw. 3 (1) (2022) 33–63, http://dx.doi.org/10.23919/ICN.2022.0007.

[40] Manzoor Ahmed, Abdul Wahid, Sayed Shariq Laique, Wali Ullah Khan, Asim Ihsan, Fang Xu, Symeon Chatzinotas, Zhu Han, A survey on STAR-RIS: Use cases, recent advances, and future research challenges, IEEE Internet Things J. 10 (16) (2023) 14689–14711, http://dx.doi.org/10.1109/JIOT.2023.3279357.

[41] Manzoor Ahmed, Salman Raza, Aized Amin Soofi, Feroz Khan, Wali Ullah Khan, Syed Zain Ul Abideen, Fang Xu, Zhu Han, Active reconfigurable intelligent surfaces: Expanding the frontiers of wireless communication-a survey, IEEE Commun. Surv. Tutor. (2024).

[42] Kinza Shafique, Mohammad Alhassoun, Going beyond a simple RIS: Trends and techniques paving the path of future RIS, IEEE Open J. Antennas Propag. 5 (2) (2024) 256–276, http://dx.doi.org/10.1109/OJAP.2024.3360900.

[43] Filippo Costa, Michele Borgese, Electromagnetic model of reflective intelligent surfaces, IEEE Open J. Commun. Soc. 2 (2021) 1577–1589, http://dx.doi.org/10.1109/OJCOMS.2021.3092217.

[44] Jieao Zhu, Zhongzhichao Wan, Linglong Dai, Mérouane Debbah, H. Vincent Poor, Electromagnetic information theory: Fundamentals, modeling, applications, and open problems, 2022, arXiv preprint arXiv:2212.02882.

[45] Andrea Abrardo, Alberto Toccafondi, Marco Di Renzo, Design of reconfigurable intelligent surfaces by using S-parameter multiport network theory – Optimization and full-wave validation, 2023.

[46] Matteo Nerini, Shanpu Shen, Hongyu Li, Marco Di Renzo, Bruno Clerckx, A universal framework for multiport network analysis of reconfigurable intelligent surfaces, 2023, arXiv preprint arXiv:2311.10561.

[47] Josef A. Nossek, Dominik Semmler, Michael Joham, Wolfgang Utschick, Physically consistent modelling of wireless links with reconfigurable intelligent surfaces using multiport network analysis, 2023, arXiv preprint arXiv:2308.12223.

[48] Gabriele Gradoni, Marco Di Renzo, End-to-end mutual coupling aware communication model for reconfigurable intelligent surfaces: An electromagnetic-compliant approach based on mutual impedances, IEEE Wirel. Commun. Lett. 10 (5) (2021) 938–942, http://dx.doi.org/10.1109/LWC.2021.3050826.

[49] D.M. Pozar, Microwave Engineering, John Wiley & Sons, 2011.

[50] Andrea Abrardo, Alberto Toccafondi, Marco Di Renzo, Design of reconfigurable intelligent surfaces by using s-parameter multiport network theory–optimization and full-wave validation, IEEE Trans. Wireless Commun. (2024).

[51] Philipp Del Hougne, Load impedances vs polarizabilities: On the compactness of physics-compliant models of RIS-parametrized wireless channels, in: 2024 18th European Conference on Antennas and Propagation, EuCAP, IEEE, 2024, pp. 1–4.

[52] Rashid Faqiri, Chloe Saigre-Tardif, George C. Alexandropoulos, Nir Shlezinger, Mohammadreza F. Imani, Philipp del Hougne, PhysFad: Physics-based end-to-end channel modeling of RIS-parametrized environments with adjustable fading, IEEE Trans. Wirel. Commun. 22 (1) (2023) 580–595, http://dx.doi.org/10.1109/twc.2022.3196834.

[53] Chloé Saigre-Tardif, Philipp del Hougne, Self-adaptive RISs beyond free space: Convergence of localization, sensing, and communication under rich-scattering conditions, IEEE Wirel. Commun. (ISSN: 1558-0687) 30 (1) (2023) 24–30, http://dx.doi.org/10.1109/mwc.001.2200192.

[54] Philipp del Hougne, Physics-compliant diagonal representation of beyond-diagonal RIS, 2024, arXiv preprint arXiv:2403.17222.

[55] Philipp del Hougne, RIS-parametrized rich-scattering environments: Physics-compliant models, channel estimation, and optimization, 2023, URL https://arxiv.org/abs/2311.11651.

[56] Jérôme Sol, Hugo Prod'homme, Luc Le Magoarou, Philipp Del Hougne, Experimentally realized physical-model-based frugal wave control in metasurface-programmable complex media, Nature Commun. 15 (1) (2024) 2841.

[57] Hongyu Li, Shanpu Shen, Matteo Nerini, Bruno Clerckx, Reconfigurable intelligent surfaces 2.0: Beyond diagonal phase shift matrices, 2023.

[58] Matteo Nerini, Shanpu Shen, Bruno Clerckx, Discrete-value group and fully connected architectures for beyond diagonal reconfigurable intelligent surfaces, IEEE Trans. Veh. Technol. 72 (12) (2023) 16354–16368, http://dx.doi.org/10.1109/TVT.2023.3299882.

[59] Hongyu Li, Shanpu Shen, Bruno Clerckx, Beyond diagonal reconfigurable intelligent surfaces: From transmitting and reflecting modes to single-, group-, and fully-connected architectures, IEEE Trans. Wireless Commun. 22 (4) (2023) 2311–2324, http://dx.doi.org/10.1109/TWC.2022.3210706.

[60] Ertugrul Basar, Marco Di Renzo, Julien De Rosny, Merouane Debbah, Mohamed-Slim Alouini, Rui Zhang, Wireless communications through reconfigurable intelligent surfaces, IEEE Access 7 (2019) 116753–116773, http://dx.doi.org/10.1109/ACCESS.2019.2935192.

[61] Qingqing Wu, Rui Zhang, Towards smart and reconfigurable environment: Intelligent reflecting surface aided wireless network, IEEE Commun. Mag. 58 (1) (2020) 106–112, http://dx.doi.org/10.1109/MCOM.001.1900107.

[62] Shanpu Shen, Bruno Clerckx, Ross Murch, Modeling and architecture design of reconfigurable intelligent surfaces using scattering parameter network analysis, IEEE Trans. Wireless Commun. 21 (2) (2022) 1229–1243, http://dx.doi.org/10.1109/TWC.2021.3103256.

[63] Hongyu Li, Shanpu Shen, Bruno Clerckx, A dynamic grouping strategy for beyond diagonal reconfigurable intelligent surfaces with hybrid transmitting and reflecting mode, IEEE Trans. Veh. Technol. 72 (12) (2023) 16748–16753, http://dx.doi.org/10.1109/TVT.2023.3288690.

[64] Qingchao Li, Mohammed El-Hajjar, Ibrahim Hemadeh, Arman Shojaeifard, Alain A.M. Mourad, Bruno Clerckx, Lajos Hanzo, Reconfigurable intelligent surfaces relying on non-diagonal phase shift matrices, IEEE Trans. Veh. Technol. 71 (6) (2022) 6367–6383, http://dx.doi.org/10.1109/TVT.2022.3160364.

[65] Shuhang Zhang, Hongliang Zhang, Boya Di, Yunhua Tan, Zhu Han, Lingyang Song, Beyond intelligent reflecting surfaces: Reflective-transmissive metasurface aided communications for full-dimensional coverage extension, IEEE Trans. Veh. Technol. 69 (11) (2020) 13905–13909, http://dx.doi.org/10.1109/TVT.2020.3024756.

[66] Hongliang Zhang, Boya Di, Intelligent omni-surfaces: Simultaneous refraction and reflection for full-dimensional wireless communications, IEEE Commun. Surv. Tutor. 24 (4) (2022) 1997–2028, http://dx.doi.org/10.1109/COMST.2022.3202813.

[67] Jiaqi Xu, Yuanwei Liu, Xidong Mu, Joey Tianyi Zhou, Lingyang Song, H. Vincent Poor, Lajos Hanzo, Simultaneously transmitting and reflecting intelligent omni-surfaces: Modeling and implementation, IEEE Veh. Technol. Mag. 17 (2) (2022) 46–54, http://dx.doi.org/10.1109/MVT.2022.3157069.

[68] Hongliang Zhang, Shuhao Zeng, Boya Di, Yunhua Tan, Marco Di Renzo, Mérouane Debbah, Zhu Han, H. Vincent Poor, Lingyang Song, Intelligent omni-surfaces for full-dimensional wireless communications: Principles, technology, and implementation, IEEE Commun. Mag. 60 (2) (2022) 39–45, http://dx.doi.org/10.1109/MCOM.001.201097.

[69] Jiaqi Xu, Yuanwei Liu, Xidong Mu, Octavia A. Dobre, STAR-RISs: Simultaneous transmitting and reflecting reconfigurable intelligent surfaces, IEEE Commun. Lett. 25 (9) (2021) 3134–3138, http://dx.doi.org/10.1109/LCOMM.2021.3082214.

[70] Hongyu Li, Shanpu Shen, Bruno Clerckx, Beyond diagonal reconfigurable intelligent surfaces: A multi-sector mode enabling highly directional full-space wireless coverage, IEEE J. Sel. Areas Commun. 41 (8) (2023) 2446–2460, http://dx.doi.org/10.1109/JSAC.2023.3288251.

[71] Pinjun Zheng, Ruiqi Wang, Atif Shamim, Tareq Y. Al-Naffouri, Mutual coupling in RIS-aided communication: Model training and experimental validation, 2024.

[72] Hongyu Li, Shanpu Shen, Matteo Nerini, Marco Di Renzo, Bruno Clerckx, Beyond diagonal reconfigurable intelligent surfaces with mutual coupling: Modeling and optimization, IEEE Commun. Lett. 28 (4) (2024) 937–941, http://dx.doi.org/10.1109/LCOMM.2024.3361648.

[73] Ruoyan Ma, Jie Tang, Xiu Yin Zhang, Kai-Kit Wong, Jonathon A. Chambers, RIS-assisted SWIPT network for internet of everything under the electromagnetics-based communication model, IEEE Internet Things J. 11 (9) (2024) 15402–15415, http://dx.doi.org/10.1109/JIOT.2023.3347623.

[74] Özlem Tuğfe Demir, Emil Björnson, Wideband channel capacity maximization with beyond diagonal RIS reflection matrices, 2024.

[75] Hongyu Li, Matteo Nerini, Shanpu Shen, Bruno Clerckx, Wideband modeling and beamforming for beyond diagonal reconfigurable intelligent surfaces, 2024.

[76] Xin Cheng, Yan Lin, Weiping Shi, Jiayu Li, Cunhua Pan, Feng Shu, Yongpeng Wu, Jiangzhou Wang, Joint optimization for RIS-assisted wireless communications: From physical and electromagnetic perspectives, IEEE Trans. Commun. 70 (1) (2022) 606–620, http://dx.doi.org/10.1109/TCOMM.2021.3120721.

[77] Yuyan Zhou, Yang Liu, Hongyu Li, Qingqing Wu, Shanpu Shen, Bruno Clerckx, Optimizing power consumption, energy efficiency and sum-rate using beyond diagonal RIS — A unified approach, IEEE Trans. Wireless Commun. (2023) 1, http://dx.doi.org/10.1109/TWC.2023.3341262.

[78] Qingchao Li, Mohammed El-Hajjar, Ibrahim Hemadeh, Arman Shojaeifard, Lajos Hanzo, Coordinated reconfigurable intelligent surfaces: Non-diagonal group-connected design, IEEE Trans. Veh. Technol. (2024) 1–6, http://dx.doi.org/10.1109/TVT.2024.3376985.

[79] Matteo Nerini, Shanpu Shen, Hongyu Li, Bruno Clerckx, Beyond diagonal reconfigurable intelligent surfaces utilizing graph theory: Modeling, architecture design, and optimization, 2024.

[80] Arthur S. de Sena, Mehdi Rasti, Nurul H. Mahmood, Matti Latva-aho, Beyond diagonal RIS for multi-band multi-cell MIMO networks: A practical frequency-dependent model and performance analysis, 2024, arXiv preprint arXiv:2401.06475.

[81] Matteo Nerini, Shanpu Shen, Bruno Clerckx, Closed-form global optimization of beyond diagonal reconfigurable intelligent surfaces, IEEE Trans. Wireless Commun. 23 (2) (2024) 1037–1051, http://dx.doi.org/10.1109/TWC.2023.3285262.

[82] Zhuang Mao, Wei Wang, Qian Xia, Caijun Zhong, Xinhua Pan, Zhizhen Ye, Element-grouping intelligent reflecting surface: Electromagnetic-compliant model and geometry-based optimization, IEEE Trans. Wireless Commun. 21 (7) (2022) 5362–5376, http://dx.doi.org/10.1109/TWC.2021.3139611.

[83] Nemanja Stefan Perović, Le-Nam Tran, Marco Di Renzo, Mark F. Flanagan, Optimization of RIS-aided SISO systems based on a mutually coupled loaded wire dipole model, 2023.

[84] Jian Sang, Jifeng Lan, Mingyong Zhou, Boning Gao, Wankai Tang, Xiao Li, Xinping Yi, Shi Jin, Quantized phase alignment by discrete phase shifts for reconfigurable intelligent surface-assisted communication systems, 2023.

[85] Lin Cao, Haifan Yin, Li Tan, Xilong Pei, RIS with insufficient phase shifting capability: Modeling, beamforming, and experimental validations, 2023.

[86] Jiaqi Xu, Xidong Mu, Yuanwei Liu, Exploiting STAR-RISs in near-field communications, 2023.

[87] Ignacio Santamaria, Mohammad Soleymani, Eduard Jorswieck, Jesús Gutiérrez, SNR maximization in beyond diagonal RIS-assisted single and multiple antenna links, IEEE Signal Process. Lett. (2023).

[88] Xuewen Qian, Marco Di Renzo, Mutual coupling and unit cell aware optimization for reconfigurable intelligent surfaces, IEEE Wirel. Commun. Lett. 10 (6) (2021) 1183–1187.

[89] Athira Subhash, Abla Kammoun, Ahmed Elzanaty, Sheetal Kalyani, Yazan H. Al-Badarneh, Mohamed-Slim Alouini, Optimal phase shift design for fair allocation in RIS sided uplink network using statistical CSI, 2023.

[90] Andrea Abrardo, Davide Dardari, Marco Di Renzo, Xuewen Qian, MIMO interference channels assisted by reconfigurable intelligent surfaces: Mutual coupling aware sum-rate optimization based on a mutual impedance channel model, IEEE Wirel. Commun. Lett. 10 (12) (2021) 2624–2628, http://dx.doi.org/10.1109/LWC.2021.3109017.

[91] Matteo Nerini, Shanpu Shen, Bruno Clerckx, Static grouping strategy design for beyond diagonal reconfigurable intelligent surfaces, 2024.

[92] Hongyu Li, Shanpu Shen, Bruno Clerckx, Synergizing beyond diagonal reconfigurable intelligent surface and rate-splitting multiple access, IEEE Trans. Wireless Commun. (2024) 1, http://dx.doi.org/10.1109/TWC.2024.3353596.

[93] Zengrui Liu, Yang Liu, Shanpu Shen, Qingqing Wu, Qingjiang Shi, Enhancing ISAC network throughput using beyond diagonal RIS, IEEE Wirel. Commun. Lett. (2024) 1, http://dx.doi.org/10.1109/LWC.2024.3386155.

[94] Dawei Ying, David J. Love, Bertrand M. Hochwald, Sum-rate analysis for multi-user MIMO systems with user exposure constraints, IEEE Trans. Wireless Commun. 16 (11) (2017) 7376–7388, http://dx.doi.org/10.1109/TWC.2017.2748103.

[95] Placido Mursia, Sendy Phang, Vincenzo Sciancalepore, Gabriele Gradoni, Marco Di Renzo, SARIS: Scattering aware reconfigurable intelligent surface model and optimization for complex propagation channels, 2023.

[96] Bile Peng, Karl-Ludwig Besser, Shanpu Shen, Finn Siegismund-Poschmann, Ramprasad Raghunath, Daniel Mittleman, Vahid Jamali, Eduard A. Jorswieck, RISnet: A domain-knowledge driven neural network architecture for RIS optimization with mutual coupling and partial CSI, 2024.

[97] Bjorn Sihlbom, Marios I. Poulakis, Marco Di Renzo, Reconfigurable intelligent surfaces: Performance assessment through a system-level simulator, IEEE Wirel. Commun. (2022).

[98] Hanyu Jiang, Li You, Jue Wang, Wenjin Wang, Xiqi Gao, Hybrid RIS and DMA assisted multiuser MIMO uplink transmission with electromagnetic exposure constraints, IEEE J. Sel. Top. Sign. Proces. 16 (5) (2022) 1055–1069, http://dx.doi.org/10.1109/JSTSP.2022.3174701.

[99] Ruoyan Ma, Jie Tang, Xiuyin Zhang, Kai-Kit Wong, Jonathon A. Chambers, Energy efficiency optimization for mutual-coupling-aware wireless communication system based on RIS-enhanced SWIPT, IEEE Internet Things J. (2023) 1, http://dx.doi.org/10.1109/JIOT.2023.3241168.

[100] Alessio Zappone, Marco Di Renzo, Energy efficiency optimization of reconfigurable intelligent surfaces with electromagnetic field exposure constraints, IEEE Signal Process. Lett. 29 (2022) 1447–1451, http://dx.doi.org/10.1109/LSP.2022.3181532.

[101] Yongxu Zhu, Gan Zheng, Kai-Kit Wong, Stochastic geometry analysis of large intelligent surface-assisted millimeter wave networks, IEEE J. Sel. Areas Commun. 38 (8) (2020) 1749–1762, http://dx.doi.org/10.1109/JSAC.2020.3000806.

[102] Andrea De Jesus Torres, Luca Sanguinetti, Emil Björnson, Electromagnetic interference in RIS-aided communications, 2021.

[103] Sawyer D. Campbell, David Sell, Ronald P. Jenkins, Eric B. Whiting, Jonathan A. Fan, Douglas H. Werner, Review of numerical optimization techniques for meta-device design, Opt. Mater. Express 9 (4) (2019) 1842–1863.

[104] Qian Zhang, Che Liu, Xiang Wan, Lei Zhang, Shuo Liu, Yan Yang, Tie Jun Cui, Machine-learning designs of anisotropic digital coding metasurfaces, Adv. Theory Simul. 2 (2) (2019) 1800132.

[105] Zhaoyi Li, Raphaël Pestourie, Zin Lin, Steven G. Johnson, Federico Capasso, Empowering metasurfaces with inverse design: principles and applications, ACS Photonics 9 (7) (2022) 2178–2192.

[106] Dianjing Liu, Yixuan Tan, Erfan Khoram, Zongfu Yu, Training deep neural networks for the inverse design of nanophotonic structures, Acs Photonics 5 (4) (2018) 1365–1369.

[107] Sean Molesky, Zin Lin, Alexander Y. Piggott, Weiliang Jin, Jelena Vuković, Alejandro W. Rodriguez, Inverse design in nanophotonics, Nat. Photonics 12 (11) (2018) 659–670.

[108] Sunae So, Trevon Badloe, Jaebum Noh, Jorge Bravo-Abad, Junsuk Rho, Deep learning enabled inverse design in nanophotonics, Nanophotonics 9 (5) (2020) 1041–1057.

[109] Peter R. Wiecha, Arnaud Arbouet, Christian Girard, Otto L. Muskens, Deep learning in nano-photonics: inverse design and beyond, Photonics Res. 9 (5) (2021) B182–B200.

[110] Peter R. Wiecha, Alexander Yu Petrov, Patrice Genevet, Andrey Bogdanov, Inverse design of nanophotonics devices and materials, Photon. Nanostruct.: Fundam. Appl. (2022) 101084.

[111] Yurui Qu, Huanzheng Zhu, Yichen Shen, Jin Zhang, Chenning Tao, Pintu Ghosh, Min Qiu, Inverse design of an integrated-nanophotonics optical neural network, Sci. Bull. 65 (14) (2020) 1177–1183.

[112] Stefano Maci, Gabriele Minatti, Massimiliano Casaletti, Marko Bosiljevac, Metasurfing: Addressing waves on impenetrable metasurfaces, IEEE Antennas Wirel. Propag. Lett. 10 (2011) 1499–1502.

[113] Sandeep Inampudi, Hossein Mosallaei, Neural network based design of metagratings, Appl. Phys. Lett. 112 (24) (2018).

[114] Jiaqi Jiang, David Sell, Stephan Hoyer, Jason Hickey, Jianji Yang, Jonathan A Fan, Data-driven metasurface discovery, 2018, arXiv preprint arXiv:1811.12436.

[115] John Peurifoy, Yichen Shen, Li Jing, Yi Yang, Fidel Cano-Renteria, Brendan G. DeLacy, John D. Joannopoulos, Max Tegmark, Marin Soljačić, Nanophotonic particle simulation and inverse design using artificial neural networks, Sci. Adv. 4 (6) (2018) eaar4206.

[116] Tao Shan, Xiaotian Pan, Maokun Li, Shenheng Xu, Fan Yang, Coding programmable metasurfaces based on deep learning techniques, IEEE J. Emerg. Sel. Top. Circuits Syst. 10 (1) (2020) 114–125.

[117] Zhaocheng Liu, Dayu Zhu, Sean P. Rodrigues, Kyu-Tae Lee, Wenshan Cai, Generative model for the inverse design of metasurfaces, Nano Lett. 18 (10) (2018) 6570–6576.

[118] John A. Hodge, Kumar Vijay Mishra, Amir I. Zaghloul, RF metasurface array design using deep convolutional generative adversarial networks, in: 2019 IEEE International Symposium on Phased Array System & Technology, PAST, IEEE, 2019, pp. 1–6.

[119] Wei Ma, Feng Cheng, Yihao Xu, Qinlong Wen, Yongmin Liu, Probabilistic representation and inverse design of metamaterials based on a deep generative model with semi-supervised learning strategy, Adv. Mater. 31 (35) (2019) 1901111.

[120] Jiaqi Jiang, Jonathan A. Fan, Global optimization of dielectric metasurfaces using a physics-driven neural network, Nano Lett. 19 (8) (2019) 5366–5372.

[121] Wenye Ji, Jin Chang, He-Xiu Xu, Jian Rong Gao, Simon Gröblacher, H. Paul Urbach, Aurèle J.L. Adam, Recent advances in metasurface design and quantum optics applications with machine learning, physics-informed neural networks, and topology optimization methods, Light: Sci. Appl. 12 (1) (2023) 169.

[122] Junjie Hou, Jing Jin, Hai Lin, Zixin Liu, Jiaping Fu, Feng Feng, An overview of deep learning techniques for inverse design of metasurface, in: 2023 IEEE MTT-S International Conference on Numerical Electromagnetic and Multiphysics Modeling and Optimization, NEMO, IEEE, 2023, pp. 110–113.

[123] Zicheng Song, Ruicong Zhang, Pingping Min, Tianyu Wang, Wenxin Cao, Yurong He, Lin Wu, Jiaqi Zhu, Cheng-Wei Qiu, Inverse design of diffusion–absorption hybrid metasurfaces, Laser Photonics Rev. (2023) 2300280.

[124] Weijian Zhou, Shuoyuan Wang, Qian Wu, Xianchen Xu, Xinjing Huang, Guoliang Huang, Yang Liu, Zheng Fan, An inverse design paradigm of multi-functional elastic metasurface via data-driven machine learning, Mater. Des. 226 (2023) 111560.

[125] Kumar Vijay Mishra, Ahmet M. Elbir, Amir I. Zaghloul, Machine learning for metasurfaces design and their applications, 2022.

[126] John A. Hodge, Kumar Vijay Mishra, Amir I. Zaghloul, Deep inverse design of reconfigurable metasurfaces for future communications, 2021, arXiv preprint arXiv:2101.09131.

[127] John Adams Hodge II, Reconfigurable Intelligent Metasurfaces for Wireless Communication and Sensing Applications (Ph.D. thesis), Virginia Tech, 2022.

[128] Xin Shi, Tianshuo Qiu, Jiafu Wang, Xueqing Zhao, Shaobo Qu, Metasurface inverse design using machine learning approaches, J. Phys. D: Appl. Phys. 53 (27) (2020) 275105.

[129] Ruichao Zhu, Tianshuo Qiu, Jiafu Wang, Sai Sui, Chenglong Hao, Tonghao Liu, Yongfeng Li, Mingde Feng, Anxue Zhang, Cheng-Wei Qiu, et al., Phase-to-pattern inverse design paradigm for fast realization of functional metasurfaces via transfer learning, Nature Commun. 12 (1) (2021) 2974.

[130] Peng Xu, Jun Lou, Chenxia Li, Xufeng Jing, Inverse design of a metasurface based on a deep tandem neural network, J. Opt. Soc. Am. B 41 (2) (2024) A1–A5.

[131] Fardin Ghorbani, Javad Shabanpour, Sina Beyraghi, Hossein Soleimani, Homayoon Oraizi, Mohammad Soleimani, A deep learning approach for inverse design of the metasurface for dual-polarized waves, Appl. Phys. A 127 (11) (2021) http://dx.doi.org/10.1007/s00339-021-05030-6.

[132] Wei Peng, Jun Zhang, Weien Zhou, Xiaoyu Zhao, Wen Yao, Xiaoqian Chen, IDRLnet: A physics-informed neural network library, 2021.

[133] Prajith Pillai, Anirban Chaudhari, Parama Pal, Beena Rai, Physics-informed neural network for inversely predicting effective electric permittivities of metamaterials, in: Proceedings of the 35th Neural Information Processing Systems (NeurIPS) Machine Learning and the Physical Sciences Workshop, 2021.

[134] Tamara G. Grossmann, Urszula Julia Komorowska, Jonas Latz, Carola-Bibiane Schönlieb, Can physics-informed neural networks beat the finite element method? 2023, arXiv preprint arXiv:2302.04107.

[135] George Em Karniadakis, Ioannis G. Kevrekidis, Lu Lu, Paris Perdikaris, Sifan Wang, Liu Yang, Physics-informed machine learning, Nat. Rev. Phys. 3 (6) (2021) 422–440.

[136] Chuizheng Meng, Sungyong Seo, Defu Cao, Sam Griesemer, Yan Liu, When physics meets machine learning: A survey of physics-informed machine learning, 2022, arXiv preprint arXiv:2203.16797.

[137] Salvatore Cuomo, Vincenzo Schiano Di Cola, Fabio Giampaolo, Gianluigi Rozza, Maziar Raissi, Francesco Piccialli, Scientific machine learning through physics–informed neural networks: Where we are and what's next, J. Sci. Comput. 92 (3) (2022) 88.

[138] Steffen Limmer, Alberto Martinez Alba, Nicola Michailow, Physics-informed neural networks for pathloss prediction, 2022.

[139] Sulagna Sarkar, Anqi Ji, Zachary Jermain, Robert Lipton, Mark Brongersma, Kaushik Dayal, Hae Young Noh, Physics Guided Machine Learning for Inverse Design of Metamaterials, Department of Civil and Environmental Engineering, Carnegie Mellon University, 2022.

[140] Cheng-Xiang Wang, Yue Yang, Jie Huang, Xiqi Gao, Tie Jun Cui, Lajos Hanzo, Electromagnetic information theory: Fundamentals and applications for 6G wireless communication systems, 2024.

[141] Jun Yan Dai, Wankai Tang, Ming Zheng Chen, Chi Hou Chan, Qiang Cheng, Shi Jin, Tie Jun Cui, Wireless communication based on information metasurfaces, IEEE Trans. Microw. Theory Tech. 69 (3) (2021) 1493–1510.

[142] Zhongzhichao Wan, Jieao Zhu, Zijian Zhang, Linglong Dai, Chan-Byoung Chae, Mutual information for electromagnetic information theory based on random fields, IEEE Trans. Commun. 71 (4) (2023) 1982–1996.

[143] Runyu Lyu, Wenchi Cheng, Joint reflection and power splitting optimization for RIS-assisted OAM-SWIPT, in: GLOBECOM 2022 - 2022 IEEE Global Communications Conference, 2022, pp. 1073–1078, http://dx.doi.org/10.1109/GLOBECOM48099.2022.10001218.

[144] Decai Shen, Zijian Zhang, Linglong Dai, Joint beamforming design for RIS-assisted cell-free network with multi-hop transmissions, Tsinghua Sci. Technol. 28 (6) (2023) 1115–1127.

[145] Zhaohui Yang, Ye Hu, Zhaoyang Zhang, Wei Xu, Caijun Zhong, Kai-Kit Wong, Reconfigurable intelligent surface based orbital angular momentum: Architecture, opportunities, and challenges, IEEE Wirel. Commun. 28 (6) (2021) 132–137.

[146] Omar Maraqa, Sylvester Aboagye, Telex M.N. Ngatched, Optical STAR-RIS-aided VLC systems: RSMA versus NOMA, IEEE Open J. Commun. Soc. 5 (2024) 430–441, http://dx.doi.org/10.1109/OJCOMS.2023.3347534.

[147] Sylvester Aboagye, Alain R. Ndjiongue, Telex M.N. Ngatched, Octavia A. Dobre, H. Vincent Poor, RIS-assisted visible light communication systems: A tutorial, IEEE Commun. Surv. Tutor. 25 (1) (2023) 251–288, http://dx.doi.org/10.1109/COMST.2022.3225859.

[148] Jianwei You, Qian Ma, Lei Zhang, Che Liu, Jianan Zhang, Shuo Liu, Tiejun Cui, Electromagnetic metamaterials: From classical to quantum, Electromagn. Sci. 1 (1) (2023) 1–33.

[149] Qi Jian Lim, Charles Ross, Amitava Ghosh, Frederick Vook, Gabriele Gradoni, Zhen Peng, Quantum-assisted combinatorial optimization for reconfigurable intelligent surfaces in smart electromagnetic environments, IEEE Trans. Antennas and Propagation (2023).

[150] Takahiro Ohyama, Yuichi Kawamoto, Nei Kato, Resource allocation optimization by quantum computing for shared use of standalone IRS, IEEE Trans. Emerg. Top. Comput. (2023).

[151] Charles Ross, Gabriele Gradoni, Qi Jian Lim, Zhen Peng, Engineering reflective metasurfaces with ising Hamiltonian and quantum annealing, IEEE Trans. Antennas and Propagation 70 (4) (2021) 2841–2854.

[152] Charles Ross, Gabriele Gradoni, Zhen Peng, A hybrid classical-quantum computing framework for RIS-assisted wireless network, in: 2023 IEEE MTT-S International Conference on Numerical Electromagnetic and Multiphysics Modeling and Optimization, NEMO, 2023, pp. 99–102, http://dx.doi.org/10.1109/NEMO56117.2023.10202166.

[153] Jiajia Shi, Tse-Tin Chan, Haoyuan Pan, Tat-Ming Lok, Reconfigurable intelligent surface assisted semantic communication systems, 2023, arXiv preprint arXiv:2306.09650.

[154] Peiwen Jiang, Chao-Kai Wen, Shi Jin, Geoffrey Ye Li, RIS-enhanced semantic communications adaptive to user requirements, 2023, arXiv preprint arXiv:2307.16100.

[155] Yiru Wang, Wanting Yang, Pengxin Guan, Yuping Zhao, Zehui Xiong, STAR-RIS-assisted privacy protection in semantic communication system, 2023, arXiv preprint arXiv:2306.12675.

[156] Hongyang Du, Jiacheng Wang, Dusit Niyato, Jiawen Kang, Zehui Xiong, Junshan Zhang, Xuemin Shen, Semantic communications for wireless sensing: RIS-aided encoding and self-supervised decoding, IEEE J. Sel. Areas Commun. 41 (8) (2023) 2547–2562, http://dx.doi.org/10.1109/JSAC.2023.3288231.

[157] Mengke Li, Bai Yan, Jin Zhang, Evolutionary multi-objective optimization for RIS-aided MU-MISO communication systems, Soft Comput. 27 (12) (2023) 8091–8106.

[158] Arman Azizi, Arman Farhang, RIS meets aerodynamic HAPS: A multi-objective optimization approach, 2023, arXiv preprint arXiv:2301.10682.

[159] Abdelhamed Mohamed, A. Zappone, Marco Di Renzo, Bi-objective optimization of information rate and harvested power in RIS-aided SWIPT systems, IEEE Wirel. Commun. Lett. 11 (10) (2022) 2195–2199, http://dx.doi.org/10.1109/LWC.2022.3196906.

[160] Kefeng Guo, Min Wu, Xingwang Li, Houbing Song, Neeraj Kumar, Deep reinforcement learning and NOMA-based multi-objective RIS-assisted IS-UAV-TNs: Trajectory optimization and beamforming design, IEEE Trans. Intell. Transp. Syst. 24 (9) (2023) 10197–10210, http://dx.doi.org/10.1109/TITS.2023.3267607.

[161] Jian Chen, Sujie Wang, Jie Jia, Qinghu Wang, Leyou Yang, Xingwei Wang, Multi-objective oriented resource allocation in reconfigurable intelligent surface assisted HCNs, Ad Hoc Netw. 140 (2023) 103066.

[162] Junwei Chai, Yunhui Yi, Xiandeng He, Zicheng Xing, Yuanxinyu Luo, Xingcai Zhang, Rate optimization and interference suppression in RIS-assisted MIMO systems, in: Proceedings of the 2023 10th International Conference on Wireless Communication and Sensor Networks, 2023, pp. 103–109.

[163] Rang Liu, Ming Li, Qian Liu, A. Lee Swindlehurst, Joint waveform and filter designs for STAP-SLP-based MIMO-DFRC systems, IEEE J. Sel. Areas Commun. 40 (6) (2022) 1918–1931.

[164] Matteo Nerini, Bruno Clerckx, Physically consistent modeling of stacked intelligent metasurfaces implemented with beyond diagonal RIS, IEEE Commun. Lett. (2024).

[165] Jiancheng An, Marco Di Renzo, Mérouane Debbah, Chau Yuen, Stacked intelligent metasurfaces for multiuser beamforming in the wave domain, in: ICC 2023-IEEE International Conference on Communications, IEEE, 2023, pp. 2834–2839.

[166] Jiancheng An, Chau Yuen, Chao Xu, Hongbin Li, Derrick Wing Kwan Ng, Marco Di Renzo, Mérouane Debbah, Lajos Hanzo, Stacked intelligent metasurface-aided MIMO transceiver design, IEEE Wirel. Commun. (2024).

[167] Hao Liu, Jiancheng An, Xing Jia, Shining Lin, Xianghao Yao, Lu Gan, Bruno Clerckx, Chau Yuen, Mehdi Bennis, Mérouane Debbah, Stacked intelligent metasurfaces for wireless sensing and communication: Applications and challenges, 2024, arXiv preprint arXiv:2407.03566.

[168] Guojun Huang, Jiancheng An, Zhaohui Yang, Lu Gan, Mehdi Bennis, Mérouane Debbah, Stacked intelligent metasurfaces for task-oriented semantic communications, 2024, arXiv preprint arXiv:2407.15053.

Samaneh Bidabadi received her B.Sc. degree in Electrical Engineering from Yazd University, Yazd, Iran, in 2011, and her M.Sc. degree from Isfahan University of Technology, Isfahan, Iran, in 2014. She is currently pursuing a Ph.D. in the Department of Electrical and Computer Engineering at the Université du Québec à Trois-Rivières (UQTR), Québec, Canada. Her doctoral research focus on AI-enabled resource allocation for RIS-aided communications. Her research interests include the optimization of next-generation wireless networks and AI-enabled resource allocation.

Messaoud Ahmed Ouameur received a bachelor's degree in electrical engineering from the Institute national d'electronique et d" electricit' e (INELEC),' Boumerdes, Algeria, in 1998, the M.B.A. degree from the Graduate School of International Studies, Ajou University, Suwon, South Korea, in 2000, and the master's and Ph.D. degrees (Hons.) in electrical engineering from the Universite du Qu' ebec' a Trois- ' Rivieres (UQTR), QC, Canada, in 2002 and 2006, ' respectively. He has been a Regular Professor at UQTR since 2018. His research interests include embedded real-time systems, parallel and distributed processing with applications to distributed Massive MIMO, deep learning and machine learning for communication system design, and the Internet of Things with an emphasis on end-to-end systems prototyping and edge computing.

Miloud Bagaa (Senior Member, IEEE) received the engineering, master's, and Ph.D. degrees from the University of Science and Technology Houari Boumediene, Algiers, Algeria, in 2005, 2008, and 2014, respectively. From 2009 to 2015, he was a Researcher with the Research Center on Scientific and Technical Information, Algiers. From 2015 to 2016, he was a Postdoctoral Researcher with the Norwegian University of Science and Technology, Trondheim, Norway. From 2016 to 2019, he was a Postdoctoral Researcher with Aalto University. From 2019 to 2020, he was a Senior Researcher with Aalto University. Last but not least, he was a Visiting Researcher with Aalto University and a Senior System Cloud Specialist with CSC, from October 2020 to November 2022. He is currently a Professor with the Department of Electrical and Computer Engineering, Université du Québec à Trois-Rivières (UQTR).

Daniel Massicotte (S'91–M'94–SM'08) received the B.Sc.A. and M.Sc.A. degrees in electrical engineering and industrial electronics in 1987 and 1990 respectively from the Universite du Qu ' ebec ' a Trois-Rivi ' eres (UQTR), Qc, Canada. He obtained ' the Ph.D. degree in electrical engineering in 1995 at the Ecole Polytechnique de Montr ' eal, Qc, Canada. ' In 1994, he joined the Department of Electrical and Computer Engineering, Universite du Qu ' ebec ' a Trois-Rivi ' eres, where he is currently a Full Pro- ' fessor. He is Founder of the Laboratory of Signal and Systems Integration. Since 2001, he has been Founding President and Chief Technology Officer of Axiocom Inc. He has been Head of the Industrial Electronic Research Group from 2011 to 2018 and Head of the Electrical and Computer Engineering Department, since 2014. Head of the Research Chair in Signals and Intelligence of High-Performance Systems. He received the Douglas R. Colton Medal for Research Excellence awarded by the Canadian Microelectronics Corporation, the PMC-Sierra High Speed Networking and Communication Award and the Second place at the Complex Multimedia/Telecom IP Design Contest from Europractice. His research interests include advanced VLSI implementation, digital signal processing for wireless communications, measurement, medical, real-time simulation and control problems for linear/nonlinear complex systems. He has proposed many methods based on modern signal processing, such as machine learning, transform domain, and metaheuristics. He is author/cosuthor of more than 200 technical papers in international conferences and journals, as well as of 9 inventions. Dr. Massicotte is also member of the "Ordre des Ingenieurs du ' Quebec'' and "Microsystems Strategic Alliance of Quebec" (ReSMiQ).

Felipe A. P. de Figueiredo, received the B.Sc. and M.Sc. degrees in telecommunication engineering from the National Institute of Telecommunications (Inatel) Brazil, in 2004 and 2011, respectively. He received his first Ph.D. degree from the State University of Campinas (UNICAMP), Brazil, in 2019 and the second one from the University of Ghent (UGhent), Belgium, in 2021. He has been working on the research and development of telecommunication systems for more than 15 years. His research interests include digital signal processing, digital communications, mobile communications, MIMO, multicarrier modulations, FPGA development, and machine learning.

Anas Chaaban (SM'17) received the Mâitrise ès Sciences degree in electronics from Lebanese University, Lebanon, in 2006, the M.Sc. degree in communications technology from the University of Ulm, Germany, in 2009, and the Dr.Ing. (Ph.D.) degree in electrical engineering and information technology from the Ruhr-University of Bochum, Germany, in 2013. From 2008 to 2009, he was with the Daimler AG Research Group on Machine Vision, Ulm, Germany. He was a Research Assistant with the Emmy-Noether Research Group on Wireless Networks, University of Ulm, from 2009 to 2011, which relocated to the Ruhr-University of Bochum in 2011. He was a Post-Doctoral Fellow with the Ruhr-University of Bochum from 2013 to 2014, and with the King Abdullah University of Science and Technology, Saudi Arabia, from 2015 to 2017. He joined the School of Engineering, The University of British Columbia as an Assistant Professor in 2018. His research interests include information theory and wireless communications with focus on relaying, multi-user communications, and interference management.

Chapitre 3 - Présentation des résultats par articles

Trois publications distinctes regroupent les résultats de la méthodologie développée pour réaliser les objectifs du projet de recherche. La première concerne la mise en œuvre d'un modèle d'optimisation des systèmes de communication MISO assistés par RIS en bande étroite. La deuxième extension élargit la portée en incluant l'optimisation basée sur un modèle des systèmes SISO-OFDMA assistés par RIS. Finalement, le troisième article examine comment optimiser les systèmes ISAC assistés par BD-RIS en utilisant des techniques d'apprentissage profond.

3.1 Optimisation basée sur un modèle des systèmes de communication MISO assistés par RIS en bande étroite

3.1.1 Contexte

Cette section examine l'évolution des méthodes d'optimisation utilisant des modèles pour les systèmes de communication MISO assistés par RIS à bande étroite. L'objectif principal consiste à optimiser les déphasages du RIS afin de maximiser l'EE. En raison de problèmes de convergence, les méthodes classiques de descente de gradient font face à des obstacles pour atteindre une EE optimale. Afin de surmonter ces défis de façon efficace, cette étude présente des méthodes innovantes comme les méthodes GAW et TR. L'objectif de ces méthodes est d'optimiser les taux de convergence et la performance globale dans l'optimisation de l'efficacité énergétique au sein des configurations MISO supervisées par RIS. La mise en évidence du rôle essentiel des configurations RIS optimisées met en évidence leur contribution cruciale à la préservation de réseaux de communication sans fil efficaces et solides.

3.1.2 Méthodologie

La méthodologie a commencé par une revue de littérature complète axée sur les avancées récentes dans les communications assistées par RIS. Cette revue a mis en évidence diverses méthodes d'optimisation proposées pour améliorer les performances du système tout en soulignant également leurs limitations inhérentes. Un défi notable identifié était l'insuffisance potentielle des algorithmes basés sur les gradients en raison de la nature concave des problèmes de calcul de taille de pas. Pour remédier efficacement à ce problème, deux approches d'optimisation robustes ont été introduites pour optimiser l'EE dans les systèmes MISO à porteur unique assistés par RIS.

Dans un premier temps, nous avons suggéré un algorithme GAW afin de traiter le problème d'optimisation de l'EE en lien avec la création de faisceaux passifs du RIS dans le contexte de l'AO. La technique GAW utilise les conditions de Wolfe pour assurer une diminution significative de la fonction objectif, produisant ainsi un pas de taille convenable.

L'aspect de l'optimisation des déphasages du RIS, qui constitue la première phase de l'AO, peut être traité avec diverses techniques d'optimisation particulièrement pertinentes dans des situations d'optimisation avec ou sans contraintes. Parmi celles-ci, on retrouve la méthode de descente de gradient stochastique (en anglais, SGD, Stochastic Gradient Descent), la méthode de Newton, les méthodes quasi-Newton, le recuit simulé (en anglais, SA, Simulated Annealing), l'optimisation par essaims particulaires (en anglais, PSO, Particle Swarm Optimization), etc. Dans ce qui suit, nous comparons différentes méthodes [62, 63].

Bénéfices de l'emploi de la descente de gradient avec les conditions de Wolfe:

- Sélection de la taille de pas plus efficace:

  Un des bénéfices majeurs de l'utilisation de la méthode de descente de gradient fondée sur les conditions de Wolfe est la modulation dynamique de la taille du pas. Les conditions de Wolfe assurent que chaque mise à jour soit suffisamment efficace pour progresser (condition d'Armijo) et pas trop importante afin d'éviter une instabilité (condition de courbure). Toutefois, la descente de gradient standard peut rencontrer des problèmes de convergence si le taux d'apprentissage n'est pas correctement sélectionné. Un taux d'apprentissage trop faible entraîne une convergence lente, alors qu'un taux trop élevé risque de causer un dépassement, ce qui rend l'algorithme non convergent. Contrairement à d'autres techniques comme la descente de gradient stochastique qui emploie un pas constant ou déclinable, l'approche de Wolfe adapte de manière plus astucieuse la taille du pas, susceptible d'aboutir à des performances supérieures avec moins d'itérations.
- Convergence plus rapide (dans de nombreux cas):

  Le gradient à descente fondé sur les critères de Wolfe assure que l'amplitude du pas choisi lors de chaque itération est optimale pour la zone locale, ce qui pourrait favoriser une convergence plus rapide comparativement à la descente de gradient standard, qui peut exiger un ajustement précis du taux d'apprentissage. En comparaison avec les techniques de Newton ou quasi-Newton, qui nécessitent le calcul des dérivées de haut niveau (Hessienne), l'utilisation des conditions de Wolfe peut aboutir à une convergence plus rapide sans le coût computationnel associé aux informations d'ordre supérieur. La méthode permet aussi d'éviter l'approximation de l'Hessienne, à l'instar des techniques quasi-Newton [62].
- Meilleure stabilité et robustesse:

La condition de courbure contribue à éviter que la méthode ne fasse d'importants pas dans des directions où la fonction objective présente une forte courbure ou n'est pas convexe. Ceci peut renforcer la stabilité de l'algorithme et minimiser le risque de dériver ou de sauter vers des solutions qui ne sont pas optimales.

Dans les méthodes stochastiques telles que le SGD, le caractère aléatoire des tailles de pas peut engendrer des variations susceptibles de provoquer de l'instabilité. Par contre, la méthode de descente de gradient basée sur Wolfe se dispense de cette randomisation en privilégiant une stratégie plus maîtrisée pour la recherche de ligne [62].

- Pas besoin de dérivées d'ordre supérieur :

  À l'inverse de la démarche de Newton ou des approches Quasi-Newton, la descente de gradient qui s'appuie sur les conditions de Wolfe requiert uniquement des dérivées de premier ordre (à savoir le gradient). Cela la rend moins onéreuse en termes de calcul et plus simple à mettre en œuvre sur les problèmes où le calcul des dérivées d'ordre supérieur s'avère complexe, coûteux ou peu pratique. Dans les systèmes de communication sans fil, on constate fréquemment que les problèmes d'optimisation concernent des fonctions objectives complexes pour lesquelles le calcul des dérivées supérieures peut s'avérer ardu. L'emploi de méthodes de haut niveau, comme la méthode de Newton, pourrait engendrer une lourde exigence en termes de calcul.

- Fonctionne bien pour l'optimisation non convexe :

  Le gradient de descente Wolfe est performant dans les situations où les fonctions objectives sont non convexes, car il permet d'ajuster la direction de recherche en fonction de la courbure locale de la fonction objective. Un grand nombre de

problèmes de communication sans fil sont non convexes, et les minima locaux ou les points critiques peuvent représenter des défis pour les techniques basées sur le gradient. Tandis que des techniques comme le SA ou les algorithmes génétiques (en anglais GA,Genetic algorithm) ont été élaborées pour aborder la non-convexité et l'optimisation globale, l'approche du gradient de descente basée sur Wolfe propose une méthode plus directe et structurée pour se déplacer dans des espaces non convexes sans avoir besoin de coûteuses heuristiques de recherche à grande échelle.

- Exigences mémoire réduites :

  - La méthode de descente de gradient basée sur les conditions de Wolfe présente des besoins en mémoire moindres par rapport à des techniques comme le quasi-Newton ou l'PSO, qui demandent souvent le suivi de nombreux candidats à la solution ou l'estimation des matrices Hessiennes. Cela rend la première plus appropriée pour les problèmes d'optimisation d'envergure avec des moyens limités. C'est particulièrement essentiel dans les réseaux étendus sans fil où l'efficacité de traitement et l'exploitation de la mémoire sont primordiales [62, 63].

- Recherche locale pour des optima locaux efficaces:

  - L'optimisation locale efficace est obtenue de manière optimale en utilisant la méthode de descente de gradient basée sur les conditions de Wolfe, en particulier lorsqu'elle est associée à des initialisations judicieuses. Dans le domaine des communications sans fil, de nombreuses tâches d'optimisation, telles que l'allocation des ressources et la gestion de la puissance, nécessitent des solutions qui ne sont peut-être pas globalement optimales, mais suffisamment efficaces pour être mises en œuvre de manière pratique. Dans ce contexte, l'utilisation de la descente de gradient basée sur les conditions de Wolfe constitue un choix

stratégique, permettant d'atteindre des solutions proches du maximum tout en garantissant une efficacité et une stabilité computationnelles. Cela contraste avec des méthodes comme le SA, qui exigent souvent une exploration approfondie de l'espace des solutions à un coût computationnel nettement plus élevé.

Deuxièmement, nous avons introduit une approche novatrice en utilisant la méthode TR pour aborder le problème de l'EE associé à la conception des déphasages du RIS. Contrairement aux méthodes de recherche linéaire traditionnelles contraintes à des directions pré-définies, la méthode TR élargit l'espace de recherche du problème en explorant au sein d'une région de confiance. Cette amélioration stratégique permet à la méthode TR de naviguer efficacement loin des points de selle, montrant une performance supérieure par rapport à GAW et aux autres méthodes existantes dans nos simulations.

Comparaison entre la méthode de la région de confiance et la descente de gradient basée sur les conditions de Wolfe

Les techniques de la région de confiance et la descente de gradient fondée sur les critères de Wolfe se distinguent par leur méthode de choix de la taille du pas. Les techniques de la région de confiance se basent sur la limitation dynamique de l'étape à une zone déterminée autour du point actuel, assurant que les étapes demeurent dans une zone sûre de l'estimation du modèle. Cela favorise une stratégie équilibrée qui allie exploration et exploitation. Toutefois, la méthode de descente de gradient basée sur les conditions de Wolfe fait appel à des techniques d'exploration en ligne. Les conditions de Wolfe adaptent dynamiquement la taille du pas afin d'assurer non seulement une amélioration (condition d'Armijo), mais aussi une stabilité (condition de courbure). Les techniques de la région de confiance se montrent particulièrement performantes pour résoudre des problèmes d'optimisation complexes et fortement non convexes, où l'ajustement de la taille de la

région contribue à améliorer la solidité. L'optimisation par descente de gradient utilisant les conditions de Wolfe, elle, produit des résultats satisfaisants pour des problèmes plus lisses et peut aboutir à une convergence accélérée lorsqu'il existe des informations solides sur la courbure. Bien que les techniques de la région de confiance nécessitent des calculs supplémentaires pour établir et optimiser au sein de cette même région, elles se révèlent généralement plus stables pour des fonctions objectifs très irrégulières. La méthode de descente de gradient basée sur les critères de Wolfe, étant moins gourmande en calcul, est plus appropriée pour les situations où les gradients sont bien gérés et où les capacités de traitement sont restreintes. Dans les situations de communication sans fil, les deux stratégies sont importantes, cependant les techniques basées sur la région de confiance pourraient offrir des performances supérieures face aux problèmes complexes et non convexes [62].

La région de confiance comparée à d'autres méthodes d'optimisation

Les techniques de la région de confiance, par rapport à la SGD, montrent une meilleure stabilité et performance, particulièrement pour les problèmes non convexes. La descente de gradient stochastique est souvent confrontée à des problèmes liés aux variations causées par les gradients aléatoires et requiert une adaptation précise de la dimension des pas, alors que les techniques de la région de confiance ajustent intrinsèquement la taille des pas en fonction de la fiabilité du modèle. Par rapport à la méthode de Newton, les techniques de la région de confiance permettent d'éviter l'impact computationnel des dérivées secondes (calculs liés à la Hessienne), offrant une robustesse comparable sans les dépenses importantes. Cependant, la méthode de Newton peut offrir une convergence plus rapide pour des problèmes plus simples avec des Hessiennes lisses [62].

Lorsqu'on juxtapose les méthodes de la région de confiance avec des techniques

d'optimisation globale comme les algorithmes génétiques ou la recherche par optimisation par essaims de particules, les disparités sont notables. Les techniques de confiance régionale privilégient l'optimisation locale, ce qui les rend performantes en termes de calcul pour les problèmes à lissage, tandis que les algorithmes génétiques et la recherche par optimisation par essaims de particules sont plus adaptés aux missions d'optimisation globale. Ces approches fondées sur des ensembles de données examinant l'espace de recherche de façon étendue, mais impliquant un coût computationnel plus élevé et une demande en mémoire plus conséquente. Ainsi, les méthodes de la région de confiance se prêtent parfaitement aux situations où une solution locale est suffisante, notamment pour les problèmes d'optimisation des réseaux sans fil où l'efficacité du calcul revêt une grande importance.

Nous avons opté pour les techniques du Gradient à Condition de Wolfe et de la Région de Confiance plutôt que d'autres méthodes d'optimisation, en raison de leur harmonie entre rendement, stabilité et caractéristiques de convergence. La Condition de Wolfe assure un ajustement adaptatif de la taille du pas selon la courbure locale, ce qui contribue à prévenir les surcharges et à promouvoir une convergence plus rapide comparativement à la descente de gradient classique, surtout dans le cas de problèmes mal conditionnés ou non convexes. Malgré la nécessité de peaufiner les paramètres avec précision, l'habilité du Gradient à Condition de Wolfe à préserver la stabilité sans recourir aux dérivées secondes le rend efficace sur le plan computationnel. D'autre part, la méthode de la Région de Confiance adapte la taille du pas de recherche en fonction de la qualité du modèle local, offrant des garanties de convergence globale même dans des contextes non linéaires ou mal conditionnés. Bien que son coût en termes de calcul soit plus élevé par itération, la méthode TR est particulièrement efficace pour assurer une convergence fiable lorsque le paysage du problème est mal conditionné. Ces deux techniques sont utiles

dans des situations d'optimisation concrètes où les problématiques incluent fréquemment des fonctions objectives compliquées et non convexes, nécessitant une convergence stable sans le poids computationnel élevé associé aux méthodes de haut niveau comme celle de Newton. Leur capacité à s'adapter à différents types de problèmes, associée à des besoins en calculs maîtrisables, les rend largement utilisables pour des applications concrètes d'envergure.

3.1.3 Résultats

Dans la partie des résultats, nous examinons les différentes stratégies visant à optimiser l'efficacité énergétique des systèmes MISO assistés par RIS. La hausse de la puissance de transmission à la station de base permet d'améliorer l'efficacité spectrale, avec des améliorations notables observées à l'origine. Les systèmes de relais actifs à AF (en englais AF, Amplify-and-Forward) ont initialement surpassé les méthodes basées sur le RIS en raison de leur structure opérationnelle, mais ont démontré des avantages qui diminuaient à mesure que la puissance de transmission augmentait. Toutes les méthodes ont montré une relation non linéaire avec l'EE, les approches basées sur le RIS, notamment celles utilisant la méthode TR, ont systématiquement surpassé les méthodes assistées par relais AF. Les exigences en matière de QoS ont eu un effet bénéfique sur l'SE, mais ont tendance à diminuer l'EE lorsque plus de puissance de la station de base était allouée pour satisfaire aux standards. À propos de l'impact des éléments RIS, l'augmentation du nombre d'éléments de réflexion entraîne une augmentation de l'EE au départ, mais atteint une saturation au-delà d'une valeur optimale, ce qui suggère des limites pratiques pour l'évaluation. En outre, la méthode utilisant TR a démontré une rapidité de convergence vers les solutions optimales d'EE par rapport aux autres algorithmes, mettant en évidence son efficacité dans la gestion des performances des systèmes MISO assistés par RIS.

3.1.4 Droits d'auteur

Bidabadi *et al. J Wireless Com Network* (2023) 2023:89
https://doi.org/10.1186/s13638-023-02296-7

EURASIP Journal on Wireless Communications and Networking

RESEARCH Open Access

Energy efficient resource allocation for re-configurable intelligent surface-assisted wireless networks

Samaneh Bidabadi[1*], Messaoud Ahmed Ouameur[1*], Miloud Bagaa[1*] and Daniel Massicotte[1]

*Correspondence: samaneh.bidabadi@uqtr.ca; messaoud.ahmed.ouameur@uqtr.ca; miloud.bagaa@uqtr.ca

[1] Department of Electrical and Computer Engineering, University of Quebec at Trois-Rivieres, Trois-Rivieres, Canada

Abstract

This paper focuses on energy-efficient resource allocation in reconfigurable intelligent surface (RIS)-assisted multiple-input-single-output (MISO) communication systems. Specifically, it revisits the solution to the energy efficiency (EE) problem using the alternating optimization (AO) approach. In each AO iteration, the RIS phase optimization is achieved using the gradient descent method, which unfortunately does not guarantee convergence. To overcome this limitation, we propose two alternatives: the Wolfe-based gradient-descent (GAW) EE maximization Algorithm and the trust region (TR)-based EE maximization algorithm. Additionally, we use Dinkelbach's algorithm to obtain the optimal transmit power allocation. Our results demonstrate that the proposed methods outperform the existing approach that uses sequential fractional programming (SFP) for phase optimization and the traditional relay-based method.

Keywords: RIS-assisted Network, Power allocation, Energy efficiency, RIS phase design

1 Introduction

Existing cellular generations will not be able to meet the extraordinary performance demands, such as high spectral efficiency (SE) and massive connectivity, brought on by the innovative new applications anticipated for the 2030 era, which will lead to a need for 6G technology [1, 2]. 6G wireless networks are expected to support the connectivity of a huge variety of users and equipment through the dense deployment of multi-antenna base stations (BSs) and access points (APs). Consequently, the energy-efficiency (EE) behavior of 6G is a crucial topic [3–5]. One of the potential solutions for green communication in 6G is the reconfigurable intelligent surface (RIS), a recently emerging hardware technology with increasing potentiality for large energy consumption reductions [3]. In its simple form, an RIS is a meta-surface made up of numerous inexpensive passive antennas that may effectively reflect the electromagnetic waves impinging on it in a controllable way to favorably alter the propagation environment [5].

However, several obstacles, ranging from performance characterization to network optimization, must be overcome for the effective deployment of energy-efficient RIS systems [7]. Optimizing RIS-aided wireless networks involves employing various

approaches [6]. Model-based methods, such as alternating optimization (AO), decompose the joint optimization problem into smaller sub-problems. These are usually solved using techniques like successive convex approximation (SCA), fractional programming (FP), and branch-and-bound (BnB) techniques. These model-based algorithms offer the advantage of providing theoretical guarantees and insights into the optimality of their performance. However, they may be limited by the complexity of the problem and the need for full knowledge of the system. On the contrary, heuristic algorithms focus on local optima and offer low-complexity solutions. They provide a pragmatic approach to optimization but may not guarantee optimality or handle complex dynamic environments effectively. On the other hand, machine learning (ML) techniques, such as reinforcement learning (RL) and supervised learning, offer data-driven approaches that can adapt to dynamic wireless environments. ML techniques have the advantage of learning from data and capturing complex patterns and interactions, allowing them to potentially discover more efficient solutions. However, the effectiveness of ML techniques mainly depends on the quality and quantity of training data and the computational resources required for training and inference.

The use of RISs in wireless networks has been examined in some recent papers, including [4, 5, 9–17]. Among them, [4, 5, 15–17], focused on either power minimization or EE maximization in RIS-assisted wireless networks using model-based optimization methods that are briefly described in Table 1. On the other hand, the authors in [18] and [19–21] use heuristic and ML techniques, respectively, to solve the EE maximization problem in RIS-aided communications. The downlink sum-rate maximization of a wireless communication system with RIS assistance was examined in [9]. By jointly optimizing the transmit beamforming of the AP and the continuous phase shift of RIS's element, a joint beamforming problem is developed in [10] to maximize the received signal power at the user in RIS-assisted multiple input single output (MISO) system. The authors in [11] studied the RIS-enhanced MISO orthogonal frequency division multiplexing (OFDM) downlink system, whereby the RIS's passive beamforming and the BS's transmit power allocation is jointly optimized using the AO framework for increasing the downlink attainable rate. In [12], the use of several RISs to support mm-Wave MISO communications has been studied. The received signal power is maximized by jointly optimizing active and passive beamforming vectors. Meanwhile, the authors in [13] have suggested an element grouping approach of RIS elements, and then jointly optimized the RIS's

Table 1 Power minimization or EE maximization in RIS-assisted wireless networks

References	System setup	Objective	Design variables	Decoupling
[15]	MISO downlink	Min.transmit power	Transmit and passive beamforming	AO
[5]	MISO downlink-single carrier	Max. energy efficiency	Transmit and passive beamforming, On-off status of each RIS	AO
[16]	MISO downlink	Min.transmit power	Transmit beamforming, discrete phase control	AO
[17]	RIS-aided MISO downlink system	EE maximization	Active and passive beamforming	AO
[4]	MISO downlink-single carrier	Max. energy efficiency	Transmit and passive beamforming,	AO

passive beamforming and the BS's power distribution using the AO technique to increase the achievable rate. The authors in [14] integrate RIS into an orthogonal frequency division multiple access (OFDMA)-based multi-user (MU) downlink system. Joint optimization of the RIS's passive beamforming and OFDMA resource block (RB), as well as power allocations are leveraged to maximize the minimum user rate.

The goal of [15] is to minimize the AP's transmit power while taking into account the individual users' signal-to-interference-plus-noise ratio (SINR) restrictions by jointly optimizing the BS transmit beamforming and RIS's passive beamforming. The authors in [5] have used distributed RIS-enabled network to manage the RIS states. They investigate how to maximize EE by dynamically managing each RIS's on/off status and improving the reflection coefficients matrix of the RISs using two iterative techniques. In contrast, the paper proposed in [16] addresses the problem of minimizing transmit power in an RIS-aided wireless network with discrete phase shifts. The authors propose an AO technique as a suboptimal and low-complexity solution. Simulation results are provided to evaluate the performance compared to benchmark schemes. The authors in [17] present an optimization technique to maximize the EE of a RIS-aided system by jointly optimizing the BS's active beamforming and the RIS's passive beamforming. The proposed algorithm is shown to be effective through numerical results. The authors in [4] examined the maximization of EE in RIS-aided MISO systems. They tackled the problem by employing the gradient descent approach (GA). In each iteration of GA, they utilized a second-order approximation of the problem, assuming the convexity of the approximation. However, it is important to note that this assumption is not universally valid, as the objective function may not exhibit a shape resembling a second-order function. Therefore, to ensure that the optimization algorithm progresses in a decreasing manner, two line search strategies with the Wolfe condition and the trust region (TR) were employed in this paper. These strategies provide a guarantee of a monotonic decrease in the objective function values. Therefore, compared to the previously mentioned works, this paper addresses the limitations of existing optimization techniques when solving the EE problem in RIS-assisted communication networks. In this paper, we revisit the EE resource allocation problem in a RIS-assisted MISO communication system, focusing on overcoming the aforementioned limitations. As a result, the contributions of this paper can be summarized as follows:

- Due to concave nature of the problem at hand, the GA's success is not guaranteed. We, therefore, propose a Wolfe based gradient-descent algorithm (GAW) to solve the EE maximization problem with respect to RIS passive beamforming in the AO framework. The simulation results show that GAW improves the system's EE since using Wolf conditions in GAW guarantees a sufficient decrease in the objective function by producing an acceptable step size.
- We propose another novel approach using TR method for solving the EE problem with respect to RIS phase shifts design. By searching within a trust region, TR improves the search space of the problem compared to line search methods, which only search in a given direction. The improved search space helps TR to escape from saddle points [22, 23], resulting in better performance compared to GAW and other existing methods. Simulation results demonstrate the efficiency of the TR method.

Notation: The symbols A^T, A^H, A^{-1}, A^+, and $\|A\|_F$ stand for the transpose, hermitian (conjugate transpose), inverse, pseudo-inverse, and Frobenius norm of a matrix A, respectively. Besides, the functions $\mathcal{R}(\cdot)$, $\mathcal{I}(\cdot)$, $|\cdot|$, $(\cdot)^*$ and $\arg(\cdot)$ indicate distinct properties of a complex number, namely its real part, imaginary part, modulus, complex conjugate, and angle, in that order. The notation $\mathrm{tr}(\cdot)$ indicates the matrix trace, and I_n(with $n \geq 2$) refers to the $n \times n$ identity matrix. To represent the Hadamard and Kronecker products of matrices A and B, we use the symbols $A \circ B$ and $A \otimes B$, respectively. We use $vec(A)$ to denote a vector obtained by stacking all the columns of A, and $\mathrm{diag}(a)$ represents a diagonal matrix with entries from vector a.

$\mathbb{R}$ and $\mathbb{C}$ stand for the sets of real and complex numbers, respectively, and the notation $x \sim \mathcal{CN}(0, \sigma^2)$ indicates that the random variable x follows a complex circularly symmetric Gaussian distribution with zero mean and variance σ^2.

2 Methods

2.1 System description and problem formulation

In this section, we provide an overview of the system model used in the RIS-assisted downlink multi-user MISO system. We also describe the formulation of the EE problem, which involves jointly optimizing the transmit powers and the phase shifts of the RIS.

2.1.1 System description

The system model, depicted in Fig. 1, consists of an M-antenna base station communicating with K single-antenna users via an RIS comprising N elements [4]. The RIS is installed on the exterior surface of a building that is located near both communication endpoints. Owing to adverse propagation conditions, the direct path between BS

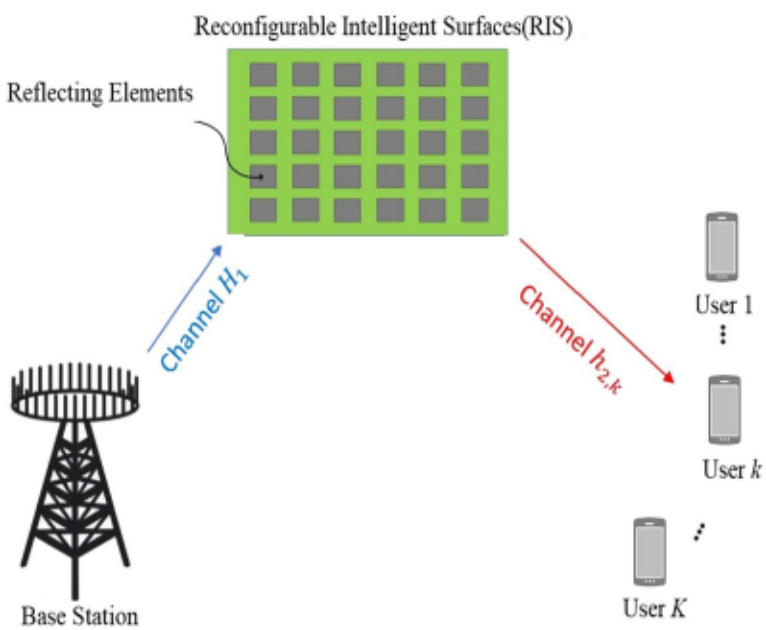

Fig. 1 The considered RIS-based multi-user MISO system

and mobile users is blocked. This RIS-assisted MISO communication model is widely described in [4, 11, 14].

The channel vector between the RIS and user k, the channel matrix between the BS and the RIS, and the diagonal matrix of RIS phase shifts, are denoted by $\boldsymbol{h}_{2,k} \in \mathbb{C}^{1\times N}$, $\boldsymbol{H}_1 \in \mathbb{C}^{N\times M}$, and $\boldsymbol{\Phi} = \text{diag}[\phi_1, \phi_2, \ldots, \phi_N]$, respectively, where $\phi_n = e^{j\theta_n}$ for all $n = 1, 2, \ldots, N$.

The transmitted signal is denoted by $\boldsymbol{x} = \sum_{k=1}^{K} \sqrt{p_k}\boldsymbol{g}_k s_k$, with p_k, s_k, and $\boldsymbol{g}_k \in \mathbb{C}^{M\times 1}$ representing, respectively, the transmit power, unit-power complex valued information symbol chosen from a discrete constellation set, and precoding vector of user k. The transmitted signal's power is also identified by $E[|\boldsymbol{x}|^2] = \text{tr}(\boldsymbol{P}\boldsymbol{G}^H\boldsymbol{G}) \leq P_{\max}$, where $\boldsymbol{G} = [\boldsymbol{g}_1, \boldsymbol{g}_2, \ldots, \boldsymbol{g}_K] \in \mathbb{C}^{M\times K}$ and $\boldsymbol{P} = \text{diag}[p_1, \ldots, p_K] \in \mathbb{R}^{K\times K}$.

Subsequently, $y_k = \boldsymbol{h}_{2,k}\boldsymbol{\Phi}\boldsymbol{H}_1\boldsymbol{x} + w_k$ denotes the discrete-time signal received by mobile user k, where $k = 1, 2, \ldots, K$. The thermal noise power at receiver k is represented by $w_k \sim \mathcal{CN}(0, \sigma^2)$.

Next, the formula for the experienced SINR for k-th mobile user and the associated SE in bps/Hz is as follows:

$$\gamma_k = \frac{p_k \left|\boldsymbol{h}_{2,k}\boldsymbol{\Phi}\boldsymbol{H}_1\boldsymbol{g}_k\right|^2}{\sum_{i=1, i\neq k}^{K} p_i \left|\boldsymbol{h}_{2,k}\boldsymbol{\Phi}\boldsymbol{H}_1\boldsymbol{g}_i\right|^2 + \sigma^2}. \tag{1}$$

$$\text{SE} = \frac{\sum_{k=1}^{K} \log_2(1 + \gamma_k)}{\text{B}}. \tag{2}$$

Consider the total power dissipation at an intelligent surface with N reflecting elements, denoted as P_{RIS}. It is given by the product of N and $P_n(b)$, where $P_n(b)$ represents the power consumption of a single phase shifter with b-bit resolution [4]. Therefore, the total power consumption of the system is represented as:

$$\mathcal{P}_{total} = \sum_{k=1}^{K} (\zeta p_k + P_{UE,k}) + P_{BS} + P_{\text{RIS}}, \tag{3}$$

where $\zeta = \nu^{-1}$ and ν represents the power amplifier's efficiency. Besides, $P_{UE,k}$, P_{BS}, P_{RIS} identifies the static power consumption of k-th user, BS, and RIS respectively.

2.1.2 Problem formulation

Consider $\boldsymbol{H}_2 = [\boldsymbol{h}_{2,1}^T, \boldsymbol{h}_{2,2}^T, \cdots, \boldsymbol{h}_{2,K}^T]^T \in \mathbb{C}^{K\times N}$. Then, assuming $M \geq K = N$, there exists a right inverse for $\boldsymbol{H}_2\boldsymbol{\Phi}\boldsymbol{H}_1$, which enables perfect interference suppression using the zero-forcing (ZF) beamforming scheme. The ZF precoding matrix $\boldsymbol{G} = (\boldsymbol{H}_2\boldsymbol{\Phi}\boldsymbol{H}_1)^+$ can then be used for this purpose. Substituting $\boldsymbol{G}$ in SINR formula (1, 2), the EE problem with respect to $\boldsymbol{P} = \text{diag}[p_1, p_2, \ldots, p_k]$ and $\boldsymbol{\Phi} = \text{diag}[\phi_1, \phi_2, \ldots, \phi_N]$ is formulated as follows:

$$\max_{\boldsymbol{\Phi}, \boldsymbol{P}} \quad \frac{\sum_{k=1}^{K} \log_2(1 + p_k\sigma^{-2})}{\xi \sum_{k=1}^{K} p_k + P_{BS} + KP_{UE} + P_{\text{RIS}}} \tag{4}$$

$$\text{subject to} \log_2\left(1+p_k\sigma^{-2}\right) \geq R_{min,k}, \forall k=1,2,\ldots,K, \tag{4a}$$

$$\mathrm{tr}((\mathbf{H}_2\Phi\mathbf{H}_1)^{+}\mathbf{P}(\mathbf{H}_2\Phi\mathbf{H}_1)^{+H}) \leq P_{max}, \tag{4b}$$

$$|\phi_n| = 1, \forall n = 1,2,\ldots,N, \tag{4c}$$

where the interference is thought to be completely suppressed by the ZF precoding matrix. The EE problem in Eq. (4) is not easy to solve due to the coupling of $\boldsymbol{P}$ and $\boldsymbol{\Phi}$ in the second constraint and unit modulus constraint on $\boldsymbol{\Phi}$. In order to obtain a sub-optimal solution, alternating optimization is applied by splitting the problem (4) to two sub-problems with respect to $\boldsymbol{P}$ and $\boldsymbol{\Phi}$. As depicted in Table 1, many works have relied on AO to solve the EE optimization problem. However, the novelty of this paper relies in investigating the limitation of such a scheme that mainly relies on GA with non-guaranteed convergence.

2.2 Problem solution

The alternating optimization algorithm is employed to solve the problem according to the following steps:

- Optimization with respect to the RIS elements values $\boldsymbol{\Phi}$
- Optimization with respect to transmitted power $\boldsymbol{P}$.

2.2.1 Optimization with respect to the RIS element values $\boldsymbol{\Phi}$

For the fixed values of $\boldsymbol{P}$, the problem (4) is converted to the following problem:

$$\max_{\boldsymbol{\Phi}} \quad C_o \tag{5}$$

$$\text{subject to} \quad \mathrm{tr}((\mathbf{H}_2\Phi\mathbf{H}_1)^{+}\mathbf{P}(\mathbf{H}_2\Phi\mathbf{H}_1)^{+H}) \leq P_{max}, \tag{5a}$$

$$|\phi_n| = 1, \forall n = 1,2,\ldots,N, \tag{5b}$$

within this context, C_o represents an arbitrary constant value. Then, Eq. (5) reformulated as an unconstrained problem as follows:

$$\begin{aligned}\min_{\boldsymbol{\Theta}} \mathcal{F}(\boldsymbol{\Phi}(\boldsymbol{\Theta})) &= \mathrm{tr}((H_2\boldsymbol{\Phi}(\boldsymbol{\Theta})H_1)^{+}P(H_2\boldsymbol{\Phi}(\boldsymbol{\Theta})H_1)^{+\mathrm{H}}) \\ &= \mathrm{vec}(\boldsymbol{\Phi}^{-1}(\boldsymbol{\Theta}))^{\mathrm{H}}(\overline{H}_2^{+\mathrm{H}} \otimes H_1^{+})^{\mathrm{H}}(\overline{H}_2^{+\mathrm{H}} \otimes H_1^{+})\mathrm{vec}(\boldsymbol{\Phi}^{-1}(\boldsymbol{\Theta})),\end{aligned} \tag{6}$$

where $\boldsymbol{\Theta} = \mathrm{diag}[\theta_1, \theta_2, ..., \theta_N]$, $\boldsymbol{\Phi} = \mathrm{diag}[e^{j\theta_1}, e^{j\theta_2}, ..., e^{j\theta_N}]$, $\boldsymbol{P} = \boldsymbol{Q}\boldsymbol{Q}^T$ and $\overline{H}_2 = \boldsymbol{Q}^{-1}H_2$. We proposed two efficient approach to solve the problem in Eq. (6) that will be described in the next subsections.

Gradient Descent Approach

The gradient descent method can be applied for solving the problem in Eq. (6) .

GA as a line search algorithm minimizes the linear approximation of $f(x)$ by first calculating a search direction, $s^{(t)}$, and then deciding how far to move in that direction. The GA iterates as follows:

$$x^{(t+1)} = x^{(t)} + \alpha^{(t)} s^{(t)}, \tag{7}$$

where $\alpha^{(t)}$ is step size. For the line search method to be effective, the direction $s^{(t)}$ and step length $\alpha^{(t)}$ must be carefully selected [22].

So, considering the problem in Eq. (6), the following matrices are defined:

$$A = (\overline{H}_2^{+H} \otimes H_1^{+})^H (\overline{H}_2^{+H} \otimes H_1^{+}) \in \mathbb{C}^{N^2 \times N^2}, \tag{8}$$

$$y = vec(\mathbf{\Phi}^{-1}(\mathbf{\Theta})) \in \mathbb{C}^{N^2 \times 1}, \tag{9}$$

so that,

$$\mathcal{F}(\mathbf{\Phi}(\mathbf{\Theta})) = y^H A y, \tag{10}$$

in which

$$y^H A y = \sum_{n=1}^{N} a_{l(n),l(n)} + 2\mathcal{R}\left\{ \sum_{n=1}^{N} \sum_{m \geq n}^{N} a_{l(n),l(m)} e^{j(\theta_n - \theta_m)} \right\}, \tag{11}$$

where $l(n)$ is the index map $l(n) = (n-1)N + n$, for all $n = 1, \ldots, N$, and $a_{l(n),l(m)}$ denotes the $l(n)$, $l(m)$-th element of A. By substituting $\alpha^{(t)}$ and $s^{(t)}$ in Eq. (7) with μ and $d^{(t)}$ respectively, the iteration of the gradient descent approach for the problem in Eq. (6) can be expressed as:

$$vec(\mathbf{\Theta})^{(t+1)} = vec(\mathbf{\Theta})^{(t)} + \mu d^{(t)}, \tag{12}$$

and

$$y^{(t+1)} = \exp(j \cdot \mathrm{vec}(\mathbf{\Theta})^{(t+1)}) \circ \mathrm{vec}(I_N) = y^{(t)} \circ \exp(j\mu d^{(t)}), \tag{13}$$

where $vec(\mathbf{\Theta})^{(t)}$ is the phase of y at iteration t [4].

The descent direction is updated using the Polak-Ribiere-Polyak conjugate gradient algorithm according to the following formula:

$$d^{(t+1)} = -q^{(t+1)} + \frac{(q^{(t+1)} - q^{(t)})^T q^{(t+1)}}{\|q^{(t)}\|^2} d^{(t)}, \tag{14}$$

where $q^{(t+1)}$ for the first iteration of the algorithm is obtained as follows:

$$\begin{aligned} -\nabla_{\mathbf{\Theta}}(y^H A y) = 2\mathcal{R}\Big\{ & j e^{j\theta_i} \sum_{m>i}^{N} a_{l(i),l(m)} e^{-j\theta_m} \\ & - j e^{-j\theta_i} \sum_{n<i}^{N} a_{l(n),l(i)} e^{j\theta_n} \Big\}. \end{aligned} \tag{15}$$

Next, to ensure that it is a descent direction, the following formula should be checked:

$$\boldsymbol{d}^{(t+1)} = \begin{cases} \boldsymbol{d}^{(t+1)} & : (\boldsymbol{q}^{(t+1)})^T \boldsymbol{d}^{(t+1)} < 0 \\ -\boldsymbol{q}^{(t+1)} & : (\boldsymbol{q}^{(t+1)})^T \boldsymbol{d}^{(t+1)} \geq 0. \end{cases} \tag{16}$$

In the subsequent subsections, two approaches based on Wolfe condition and trust region are proposed. The limitations of the GA is addressed in details in section IV.

Wolfe Condition Based GA

A common inexact line search condition mandates that $\alpha^{(t)}$ in Eq. (7) must first sufficiently reduce the objective function f. Wolfe conditions, including the Armijo condition and the curvature condition (CC), can be used to achieve this adequate reduction where their formulation is as follows [22]:

- Armijo Condition

$$\begin{aligned} \mathcal{F}(\boldsymbol{\Phi}(\boldsymbol{\Theta}^{(t+1)})) \leq \mathcal{F}(\boldsymbol{\Phi}(\boldsymbol{\Theta}^{(t)})) \\ + c_1 \mu (\boldsymbol{d}^{(t)})^T \nabla_{\boldsymbol{\Theta}} \mathcal{F}(\boldsymbol{\Phi}(\boldsymbol{\Theta}))|_{\boldsymbol{\Theta}=\boldsymbol{\Theta}^{(t)}}. \end{aligned} \tag{17}$$

- Curvature Condition

$$(\boldsymbol{d}^{(t)})^T \nabla_{\boldsymbol{\Theta}} \mathcal{F}(\boldsymbol{\Phi}(\boldsymbol{\Theta}))|_{\boldsymbol{\Theta}=\boldsymbol{\Theta}^{(t+1)}} \geq c_2 (\boldsymbol{d}^{(t)})^T \nabla_{\boldsymbol{\Theta}} \mathcal{F}(\boldsymbol{\Phi}(\boldsymbol{\Theta}))|_{\boldsymbol{\Theta}=\boldsymbol{\Theta}^{(t)}}. \tag{18}$$

Armijo condition ensures that the algorithm is making sufficient progress in each iteration towards the optimal solution. By requiring a minimum decrease in the objective function value, the algorithm avoids taking overly conservative steps that may converge slowly. The curvature condition ensures that the search direction points towards the optimal solution, rather than away from it. By requiring that the search direction is a descent direction, the algorithm ensures that it is moving towards the optimal solution in each iteration.

Trust-Region Method Trust-region methods use a quadratic model of the objective function to generate steps. These methods define a region around the current solution and trust that the model is a good representation of the objective function within this region. The method then simultaneously selects the direction and length of the step by approximating the minimizer of the model in this region. If the step is not acceptable, the trust region size is reduced and a new minimizer is found. The direction of the step changes whenever the size of the trust region is changed. The size of the trust region is critical to the effectiveness of the method because if it is too small, a significant step opportunity can be missed, and if it is too large, the model minimizer may be far from the objective function minimizer in the region, necessitating the reduction of the trust region size and go over another attempt. This method utilizes Algorithm 5 and applies it to the merit function:

$$F(\boldsymbol{\Phi}(\boldsymbol{\Theta})) = \frac{1}{2}\left\|(\overline{\boldsymbol{H}}_2^{+H} \otimes \boldsymbol{H}_1^{+}) vec(\boldsymbol{\Phi}^{-1}(\boldsymbol{\Theta}))\right\|_2^2 = \frac{1}{2}\left\|\boldsymbol{B}\boldsymbol{y}\right\|_2^2 = \frac{1}{2}\|\boldsymbol{r}(\boldsymbol{\Theta})\|_2^2, \tag{19}$$

where $B = (\overline{H}_2^{+H} \otimes H_1^{+}) \in \mathbb{C}^{N^2 \times N}$ and $y = vec(\mathbf{\Phi}^{-1}(\mathbf{\Theta})) \in \mathbb{C}^{N^2 \times 1}$. The model function $m^{(t)}(s)$ is usually defined as follows:

$$m^{(t)}(s) = \frac{1}{2}\left\| r^{(t)} + J^{(t)} s \right\|_2^2 = f^{(t)} + s^T (J^{(t)})^T r^{(t)} + \frac{1}{2} s^T (J^{(t)})^T J^{(t)} s^{(t)}, \tag{20}$$

Where $r^{(t)} = r(\mathbf{\Phi}(\mathbf{\Theta}))|_{\mathbf{\Theta}=\mathbf{\Theta}^{(t)}}$, $J^{(t)} = \nabla^T r^{(t)}(\mathbf{\Phi}(\mathbf{\Theta}))$ and $B^{(t)} = (J^{(t)})^T J^{(t)}$ is an approximation of the Hessian matrix. Considering $B = \left[b_{ij}\right] \in \mathbb{C}^{N^2 \times N}$, the Jacobian of the $r(\mathbf{\Theta})$ is formulated as follows:

$$J(\mathbf{\Phi}(\mathbf{\Theta})) = \left[-jb_{n,L(m)} \exp(-j\theta_m)\right], \tag{21}$$

where $L(m) = (m-1)N + m$.

Then, the step $s^{(t)}$ is obtained by solving the following sub-problem:

$$\min_s \quad m^{(t)}(s) \tag{22}$$

$$\text{subject to} \quad \|s\| \leq \overset{(t)}{\Delta}, \tag{22a}$$

where the scalar $\Delta > 0$ is called the trust-region radius. A crucial aspect in several trust-region algorithms is the ratio $\rho^{(t)}$, which represents the actual reduction to predicted reduction. Its value is determined as follows:

$$\rho_t = \frac{F(\mathbf{\Phi}(\mathbf{\Theta}^{(t)})) - F(\mathbf{\Phi}(\mathbf{\Theta}^{(t)} + s^{(t)}))}{m^{(t)}(0) - m^{(t)}(s^{(t)})}. \tag{23}$$

If the obtained $s^{(t)}$ does not result in a significant reduction in $F(\mathbf{\Phi}(\mathbf{\Theta}))$, it will result in a trust region being too large and shrink it before solving the problem in Eq. (22) again.

2.2.2 Optimization with respect to the transmitted power P

Solving the EE problem, with respect to the transmit power P for a fixed RIS phase shift matrix, rely on the Dinkelbach algorithm [4]. The Dinkelbach algorithm, known as a powerful fractional programming tool, is widely employed for optimizing wireless networks, as evidenced by its application in various studies [23–26].

The Backtracking line search algorithm, the trust region method, the GAW-based EE maximization algorithm, and the TR-based EE maximization algorithm are outlined in Tables 2, 3, 4, and 5, respectively.

Table 2 Backtracking line search

Algorithm 1. Backtracking Line Search
1. **Input**: $\overline{\mu} > 0, \rho \in (0,1), c_1 \in (0,1), c_2 \in (0,1)$.
2. Set $\mu_\ell = \overline{\mu}$,
3. If (17) and (18) are satisfied, stop and $\mu_\ell = \mu$.
4. Otherwise $\mu_\ell = \rho\mu$ and go to step 3.

Table 3 Trust region method

Algorithm 2. Trust Region Method
1. **Input**: $\overline{\triangle} > 0, \triangle^0 \in (0, \overline{\triangle})$, and $\eta \in [0, \frac{1}{4})$:
2. **For** $t = 0, 1, 2, \ldots$
3. Calculate $s^{(t)}$ as an (approximate) solution of (22).
4. Evaluate $\rho^{(t)}$.
5. **if** $\rho^{(t)} < \frac{1}{4}$
6. $\triangle^{(t+1)} = \frac{1}{4}\|s^{(t)}\|$.
7. **else**
8. **if** $\rho^{(t)} > \frac{3}{4}$ and $\|s^{(t)}\| = \triangle^{(t)}$
9. $\triangle^{(t+1)} = \min(2\triangle^{(t)}, \overline{\triangle})$.
10. **else**
11. $\triangle^{(t+1)} = \triangle^{(t)}$;
12. **end (if)**
13. **end (if)**
14. **if** $\rho^{(t)} > \eta$
15. $x^{(t+1)} = x^{(t)} + s^{(t)}$.
16. **else**
17. $x^{(t+1)} = x^{(t)}$.
18. **end (if)**
19. **end (for).**

Table 4 GAW-based EE maximization algorithm

Algorithm 3. GAW-based EE Maximization Algorithm
1. **Input**: $K, n, \eta, P_{\text{Bs}}, P_{\text{UE}}, P_n(b), P_{\text{max}}$,
σ^2, $\{R_{\text{min},k}\}_{k=1}^{K}$, $\mathbf{H}_2$, $\mathbf{H}_1$, $\epsilon > 0$,
2. **Initialization**: $p^0 = \frac{P_{\text{max}}}{K} \cdot I_K$, $\mathbf{\Phi}_0 = \frac{\pi}{2} \cdot I_N$,
$q_0 = \nabla_{\theta}((\mathbf{y}^0)^H \mathbf{A}\mathbf{y}^0)$, and $\mathbf{d}^0 = -\mathbf{q}^0$,
3. **While** $\left\|EE^{(l+1)} - EE^{(l)}\right\|^2 > \epsilon$, **do**
4. Given $\mathbf{P}$, update $\mathbf{\Phi}$,
5. **For** $t = 0, 1, 2, \cdots$ **do**,
6. Obtain step size μ_t using Algorithm 1,
7. $\mathbf{y}^{t+1} = \mathbf{y}^t \circ \exp^{j\mu\mathbf{d}^t} \circ \text{vec}(\mathbf{I}_N)$,
8. $\mathbf{q}^{t+1} = 2\text{Real}(-j(\mathbf{y}^*)^{t+1} \circ (\mathbf{A}\mathbf{y}^{t+1}))$,
9. $\mathbf{d}^{t+1} = -\mathbf{q}^{t+1} + \frac{(\mathbf{q}^{t+1} - \mathbf{q}^t)^T \mathbf{q}^{t+1}}{\|\mathbf{q}^t\|}\mathbf{d}^t$.
10. $\mathbf{d}^{t+1} = \begin{cases} \mathbf{d}^{t+1} & : (\mathbf{q}^{t+1})^T \mathbf{d}^{t+1} < 0 \\ -\mathbf{q}^{t+1} & : (\mathbf{q}^{t+1})^T \mathbf{d}^{t+1} \geq 0 \end{cases}$,
11. **Until** $\left\|\mathbf{\Phi}^{(t+1)} - \mathbf{\Phi}^t\right\|^2 < \epsilon$, Obtain $\mathbf{\Phi}^{(l+1)} = \mathbf{\Phi}^{(t+1)}$.
12. **end For**
13. Given $\mathbf{\Phi}$ update $\boldsymbol{P}$:
14. **if** $\text{tr}((\boldsymbol{H}_2\mathbf{\Phi}\boldsymbol{H}_1)^{+}\boldsymbol{P}(\boldsymbol{H}_2\mathbf{\Phi}\boldsymbol{H}_1)^{+H})$ evaluated at $\mathbf{\Phi}^{(l+1)}$ is lower than P_{max} **then**:
15: Update P by solving the following problem using Dinkelbach's Method: $\boldsymbol{P}^{l+1} = \arg max_{\boldsymbol{P} \in \mathcal{B}} \frac{\sum_{k=1}^{K} \log_2(1 + p_k \sigma^{-2})}{\xi \sum_{k=1}^{K} p_k + P_{BS} + KP_{UE} + NP_n(b)}$
16: **else** Break and declare infeasibility.
17: **end if**
18: **end while**
19: **Output**: $\mathbf{\Phi}$ and $\boldsymbol{P}$

Table 5 TR-based EE maximization algorithm

Algorithm 4. TR-based EE Maximization Algorithm
1. **Input**: $K, n, \eta, P_{Bs}, P_{UE}, P_n(b), P_{max}, \sigma^2, \{R_{min,k}\}_{k=1}^{K}$, $\boldsymbol{H_2}, \boldsymbol{H_1}$, $\epsilon > 0$.
2. **Initialization**: $p^0 = \frac{P_{max}}{K} * I_K, \boldsymbol{\Phi}_0 = \frac{\pi}{2} * I_N, q_0 = \nabla_{\boldsymbol{\theta}} = ((\boldsymbol{y}^0)^H \boldsymbol{A}\boldsymbol{y}^0)$, and$\boldsymbol{d}^0 = -\boldsymbol{q}^0$.
3. **While** $\left\|EE^{(l+1)} - EE^{(l)}\right\|^2 > \epsilon$, **do**
4. Given $\mathbf{P}$, update $\boldsymbol{\Phi}$ using Algorithm 5.
5. **Until** $\left\|\boldsymbol{\Phi}^{(t+1)} - \boldsymbol{\Phi}^t\right\|^2 < \epsilon$, Obtain$\boldsymbol{\Phi}^{(l+1)} = \boldsymbol{\Phi}^{(t+1)}$.
6. Given $\boldsymbol{\Phi}$ update $\boldsymbol{P}$:
7. **if** $\mathrm{tr}((\boldsymbol{H_2}\boldsymbol{\Phi}\boldsymbol{H}_1)^+\boldsymbol{P}(\boldsymbol{H_2}\boldsymbol{\Phi}\boldsymbol{H}_1)^{+H})$ evaluated at $\boldsymbol{\Phi}^{(l+1)}$ is lower than P_{max} then:
8: Update P by solving the following problem using Dinkelbach's Method: $\boldsymbol{P}^{(l+1)} = \arg max_{\boldsymbol{P}\in\mathcal{B}} \frac{\sum_{k=1}^{K}\log_2(1+p_k\sigma^{-2})}{\xi\sum_{k=1}^{K}p_k+P_{BS}+KP_{UE}+NP_n(b)}$
9. **else** Break and declare infeasibility.
10. **end if**
11. **end while**
12. **Output**: $\boldsymbol{\Phi}$ and $\boldsymbol{P}$

3 Results and discussion

In this section, we present the results of our study and provide a comprehensive discussion of the findings.

3.1 Discussion: Investigating the limitation of the GA and the convergence rate

In the following subsection, we analyze the drawbacks of the GA and conduct a comprehensive assessment of its convergence rate, shedding light on its effectiveness in solving the optimization problem.

3.1.1 Investigating the limitation of the GA

The gradient descent approach solves the following minimization problem to obtain the step length.

$$\min_{\mu>0} h(\mu) = (\boldsymbol{y}^{(t+1)})^H \boldsymbol{A}\boldsymbol{y}^{(t+1)}, \tag{24}$$

where

$$h(\mu) = \sum_{n=1}^{N} a_{l(n),l(n)} + 2\mathcal{R}\{\sum_{n=1}^{N}\sum_{m>n}^{N} a_{l(n),l(m)} e^{j(\theta_n^{(t)}-\theta_m^{(t)})} e^{j(d_m^{(t)}-d_n^{(t)})}\}. \tag{25}$$

In order to reduce the complexity, the authors in [4], consider a quadratic approximation of Eq. (25) by considering the second order Taylor expansion of the term $e^{j\mu(d_m^{(t)}-d_n^{(t)})}$ around $\mu = 0$, which yields the following approximation of $h(\mu)$:

$$\begin{aligned}\hat{h}(\mu) = \sum_{n=1}^{N} a_{l(n),l(n)} + 2\mathcal{R}\{\sum_{n=1}^{N}\sum_{m>n}^{N} a_{l(n),l(m)} e^{j(\theta_n^{(t)}-\theta_m^{(t)})} \\ \times(1 + j\mu(d_m^{(t)} - d_n^{(t)}) + \frac{(J\mu(d_m^{(t)} - d_n^{(t)}))^2}{2})\},\end{aligned} \tag{26}$$

Table 6 Limitations of GA in determining optimal step size

Monte Carlo #2, $N = 4$	Z_2	Monte Carlo, #2 $N = 20$	Z_2
AO #2	8.0169×10^{-6}	AO #2	0.0014
AO #2	5.1880×10^{-6}	AO #2	9.8480×10^{-4}
AO #2	2.7067×10^{-6}	AO #2	1.6767×10^{-4}
AO #3	8.1225×10^{-4}	AO #3	1.8284×10^{-6}
AO #3	4.1678×10^{-5}	AO #3	1.3191×10^{-6}

which can be expressed in a simple form as:

$$\hat{h}(\mu) = z_0 + z_1\mu - z_2\mu^2, \tag{27}$$

where the value of μ^* is given by $\mu^* = \frac{z_1}{(2z_2)}$. For μ^* to be a minimizer, the constraint $\mu > 0$ must be satisfied. This requires z_1 and z_2 to have the same sign. The relation between convexity of $\hat{h}(\mu)$ and the condition for μ^* to be a maximum or minimum is as follows:

$$\hat{h}''(\mu) = -2z_2 = \begin{cases} \hat{h}''(\mu) > 0 \text{ Minimizer,} \\ \hat{h}''(\mu) < 0 \text{ Maximizer,} \\ \hat{h}''(\mu) = 0 \text{ Indeterminate,} \end{cases} \tag{28}$$

where $\hat{h}''(\mu)$ is the second-order derivative of $\hat{h}(\mu)$. As a result, it is not appropriate to use the condition $\hat{h}''(\mu) < 0$ or $z_2 > 0$, as this may lead to incorrect results. Also, if $z_2 < 0$ but $z_1 > 0$, the resulting μ will be negative, even though a positive step size is acceptable.

While simulating the GA-based EE maximization algorithm, it was found that the case $z_2 > 0$ does occur, as shown in Table 6 for different number of RIS elements and AO iterations (Monte Carlo iterations). Moreover, the approximation of the exponential function with a second-order function may not be appropriate for obtaining the step size, as the values of the functions may be significantly different around $\mu = 0$.

3.1.2 Complexity and convergence rate

In this subsection, we discuss the comparsion of CPU time and convergence rate of the gradient descent, gradient descent with Wolfe condition, and trust region methods.

Gradient descent: Gradient descent is a widely used optimization algorithm that iteratively updates the solution by taking steps in the direction of the negative gradient of the objective function. The step size is usually determined by a fixed learning rate, which can be tuned for optimal performance. Gradient descent can be computationally efficient, but its convergence rate can be slow, especially for ill-conditioned or non-convex problems.

Gradient descent with Wolfe condition: Gradient descent with Wolfe condition is a variant of gradient descent that uses a line search to determine the step size at each iteration. The Wolfe condition ensures that the objective function decreases sufficiently at each iteration, which can improve the convergence rate compared to standard gradient

descent. However, the line search can add additional computational overhead, which can make this method slower than standard gradient descent.

Trust region methods: Trust region methods are a family of optimization algorithms that aim to find the optimal solution within a trust region around the current point. At each iteration, a quadratic model of the objective function is constructed and solved within the trust region. This approach can lead to faster convergence and better accuracy than gradient descent or gradient descent with Wolfe condition, especially for highly non-convex or ill-conditioned problems. However, the trust region sub-problem can be computationally expensive to solve, which can make this method slower than standard gradient descent or gradient descent with Wolfe condition.

The convergence rate and complexity of gradient descent with the Wolfe condition, as well as trust region method, are examined in the following through the utilization of mathematical theorems.

Gradient Descent

- Complexity For the nonconvex optimization problem, it is known that the gradient method finds an ϵ-stationary point (i.e., the point satisfies $\|\nabla\mathcal{F}\| \leq \epsilon$) after at most $o(\epsilon^{-2})$ iterations. When applied to convex optimization, the gradient method [27] drove an interation complexity bound $o(\epsilon^{-1})$.
- Convergence rate

Consider the following assumption:

Assumption 1 (i) The level set $\mathcal{L} := \{\boldsymbol{\Theta} : \mathcal{F}(\boldsymbol{\Phi}(\boldsymbol{\Theta})) \leq \mathcal{F}(\boldsymbol{\Phi}(\boldsymbol{\Theta}^{(0)}))\}$ is bounded. (ii) In some neighborhood $\mathcal{N}$ of $\mathcal{L}$, the objective function F is continuously differentiable, and its gradient is Lipschitz continuous i.e. there exists a constant $L > 0$ such that

$$||\nabla\mathcal{F}(\boldsymbol{\phi}(\boldsymbol{\theta})) - \nabla\mathcal{F}(\boldsymbol{\phi}(\tilde{\boldsymbol{\theta}}))|| \leq L||\theta - \tilde{\theta})||. \tag{29}$$

Theorem 1 [28] *Suppose that Assumptions 1 hold. Consider the Polak-Ribiere method with a line search satisfying the Wolfe conditions (17)-(18) and the sufficient descent condition* $\left\langle \boldsymbol{d}^{(t)}, \boldsymbol{q}^{(t)} \right\rangle \leq \sigma \left\|\boldsymbol{q}^{(t)}\right\|^2$ for some $0 < \sigma \leq 1$. *Then,*

$$\liminf_{t\to\infty} \mathcal{F}(\boldsymbol{\Phi}(\boldsymbol{\Theta}^{(t)}) = 0. \tag{30}$$

Regarding the rate of convergence of gradient descent with the Wolfe condition, many theories typically make the assumption that the line search is exact, meaning that:

$$\mu_k = \arg\min_{\mu}(\mathcal{F}(\boldsymbol{\Phi}(\boldsymbol{\Theta}^{(t+1)})), \tag{31}$$

where [29] shows that in fact:

$$\left\|\boldsymbol{\Theta}^{(t+n)} - \boldsymbol{\Theta}^*\right\| = O(\left\|\boldsymbol{\Theta}^{(t)} - \boldsymbol{\Theta}^*\right\|^2). \tag{32}$$

Trust region

- Complexity An early result of [30] shows that standard trust-region methods require $O(\epsilon_g^{-2})$ iterations to find an ϵ_g-stationary point; and given a (small) real positive tolerance ϵ_g, the algorithm terminate when it finds a point $\boldsymbol{\Theta}^{\epsilon}$ such that

$$\left\|\nabla\mathcal{F}(\boldsymbol{\Phi}(\boldsymbol{\Theta}^{\epsilon}))\right\| \leq \epsilon_g.$$

- Convergence rate The following theorem explains the global convergence of trust-region Newton methods.

Theorem 2 [22] *Let $\eta \in (0, \frac{1}{4})$ in step 1 of the algorithm presented in Table 3. Suppose that $||B^{(t)}|| \leq \beta$ for some constant β, that $\mathcal{F}$ is bounded below on the level set $S = \{\boldsymbol{\theta}|\mathcal{F}(\phi(\boldsymbol{\theta})) \leq \mathcal{F}(\phi(\boldsymbol{\theta}^{(0)}))\}$ and Lipschitz continuously differentiable in $S(R_0)$ for some $R_0 > 0$ (Eq. (34)), and that all approximate solutions $s^{(t)}$ of Eq. (20) satisfy the inequalities in Eq. (35) and $||s^{(t)}|| \leq \gamma\Delta^{(t)}$for some positive constants c and $\gamma \geq 1$. We then have*

$$\lim_{t\to\infty}\left(J^{(t)}\right)^T\gamma^{(t)} = 0. \tag{33}$$

$$S(R_0) = \{\boldsymbol{\theta}|\left\|\boldsymbol{\theta} - \bar{\boldsymbol{\theta}}\right\| < R_0 \quad \text{for some} \quad \bar{\boldsymbol{\theta}} \in S\}. \tag{34}$$

$$m^{(t)}(0) - m^{(t)}(s) \geq c\left\|(J^{(t)})^T\gamma^{(t)}\right\| \min\left(\Delta^{(t)}, \frac{\left\|(J^{(t)})^T\gamma^{(t)}\right\|}{\left\|B^{(t)}\right\|}\right). \tag{35}$$

The following theorem explains the local convergence of trust-region Newton methods.

Theorem 3 [[22]] *Let F be twice Lipschitz continuously differentiable in a neighborhood of a point $\boldsymbol{\theta}^*$ at which second-order sufficient conditions are satisfied. Suppose the sequence $\boldsymbol{\theta}^{(t)}$ converges to $\boldsymbol{\theta}^*$ and that for all t sufficiently large, the trust-region algorithm based on (22) chooses steps $s^{(t)}$ that satisfy Eq. (35) and are asymptotically similar to Newton steps $\mathbf{e}_k^N$ in (37) whenever $\left\|\mathbf{e}_k^N\right\| \leq \frac{1}{2}\Delta^{(t)}$, that is,*

$$\left\|s^{(t)} - \mathbf{e}_k^N\right\| = o\left(\left\|\mathbf{e}_k^N\right\|\right). \tag{36}$$

$$\mathbf{B}^{(t)}\mathbf{e}_k^N = -\left(\mathbf{J}^{(t)}\right)^T\boldsymbol{\gamma}^{(t)}. \tag{37}$$

Then the trust-region bound $\Delta^{(t)}$ becomes inactive for all t sufficiently large, and the sequence $\boldsymbol{\theta}^{(t)}$ converges superlinearly to $\boldsymbol{\theta}^*$.

3.2 Simulation results

In this sub-section, we investigate the performance of the RIS-assisted K-user MISO communication system. The channels are generated according to the 3GPP propagation environment described in [32]. An average of 10^3 independent realizations of the users' positions and channel realizations are used in the simulations. In addition, similar individual rate constraints for all K users are considered. $R_{\min,k} = R_{\min}$, for all k is considered where $R_{\min}$ is a fraction of the rate that each user would have in the genie case of mutually orthogonal channels and uniform power allocation. The genie rate is described as $R = \log_2(1 + \frac{P_{\max}}{K\sigma^2})$. Other simulation parameters are shown in

Table 7 Simulation parameters

Parameters	Values
Bandwidth of the BS B	180 KHz
Maximum transmit power of the AF relay P_R	20 dBm
Small scale fading model $\forall k, i,$ and j	$[\mathbf{H}_{1_{ij}}], [\mathbf{h}_{2_{kj}}] \sim \mathcal{CN}(0, 1)$.
Large scale fading model at distance d	$\frac{10^{-3.53}}{d^{3.76}}$
Circut power of the Bs P_B	39 dBm
Circut disspitated power coefficients at the Bs/AF relay νP_B	1.2
Circut power of each user P_k	10 dBm
Circut power of each RIS element P_R	10 dBm
Circut power of each AF relay transmit-receive antenna element P_A	10 dBm

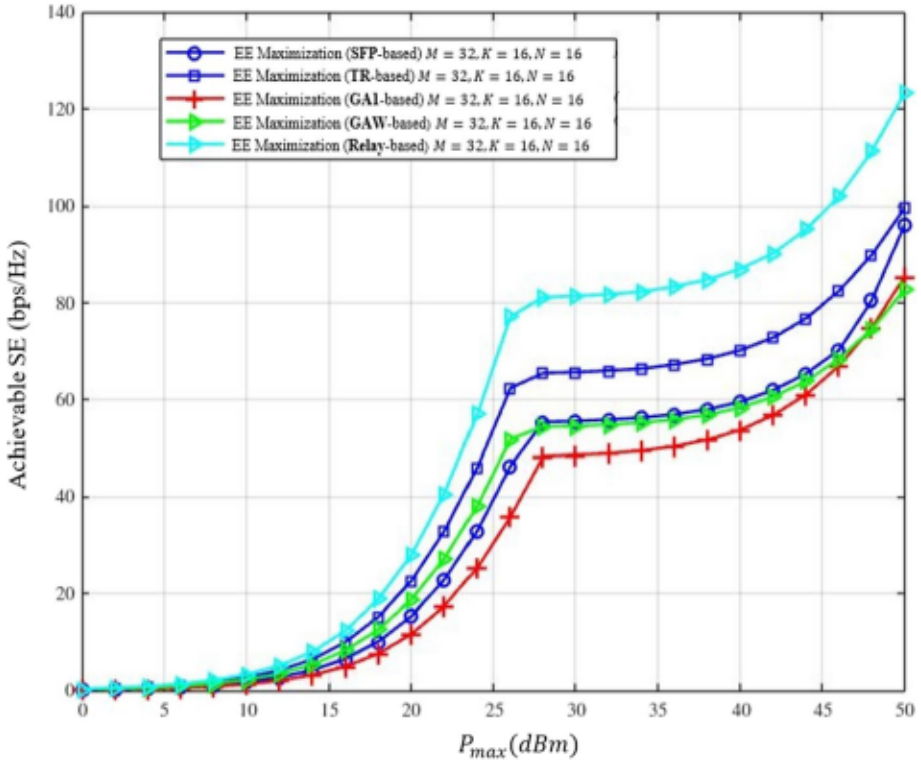

Fig. 2 Average SE using either RIS or AF relay versus $P_{\max}$ for $R_{\min} = 0.2$ bps/Hz and $M = 32, K = 16, N = 16$

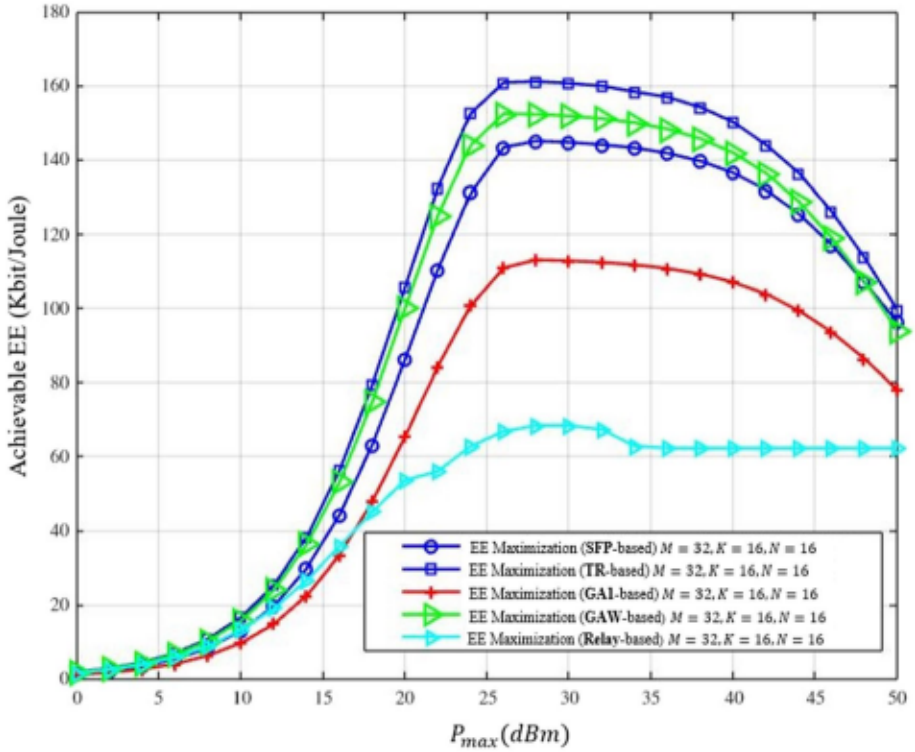

Fig. 3 Average EE using either RIS or AF relay versus $P_{\max}$ for $R_{\min} = 0.2$ bps/Hz and $M = 32, K = 16, N = 16$

Table 7. The achievable SE and EE performances as functions of $P_{\max}$ in dBm are illustrated in Figs. 2 and 3, respectively. We evaluated the proposed GAW- and TR-based approaches for EE maximization. Additionally, we considered the frequently referenced model-based benchmark approaches, such as the GA-based, SFP-based, and amplify-and-forward (AF) relay-based method [4] . In both figures, we have set the minimum QoS constraint as $R_{\min} = 0.2$ bps/Hz for all K users, and considered the setting $M = 32, K = 16,$ and$N = 16$. Figure 2 depicts the relationship between the SE and the maximum transmit power of BS. It also highlights that for low values of $P_{\max}$, the problem is almost always infeasible. This outcome is anticipated as the BS lacks sufficient transmit power to fulfill the rate requirements of the users, resulting in very low SE values. However, when $P_{\max} \geq 16$ dBm, the achievable SE begins to increase. The turning point is a result of optimizing for EE rather than SE. When maximizing SE, the objective is to fully utilize all available BS power, leading to a continuously increasing trend in SE. However, maximizing EE involves finding the optimal balance between spectral efficiency and power consumption, which require increasing the BS transmit power beyond a threshold value. Due to the active structure of the AF relay, as opposed to the passive reflecting structure of the RIS, the AF relay exhibits the best performance, as shown in Fig. 2. However, as $P_{\max}$ increases, the performance gap between the RIS and AF relay becomes smaller, as the SE is dominated by BS transmit power.

The EE performance is shown in Fig. 3. The result confirms the non-monotonicity of EE versus $P_{\max}$ for all the schemes. When $P_{\max} \geq 25$ dBm, the excess transmit power is not used since it will decrease the energy efficiency. Also, the proposed algorithms for

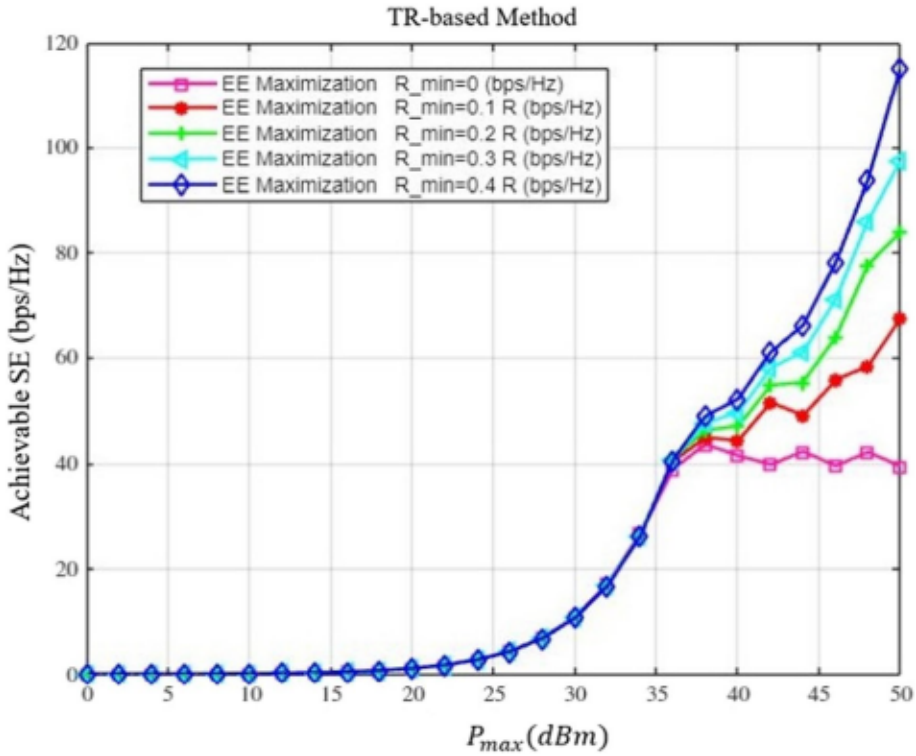

Fig. 4 Average SE using RIS versus P_{max} and $M = 32, K = 16, N = 16$ as well as different values for R_{min}

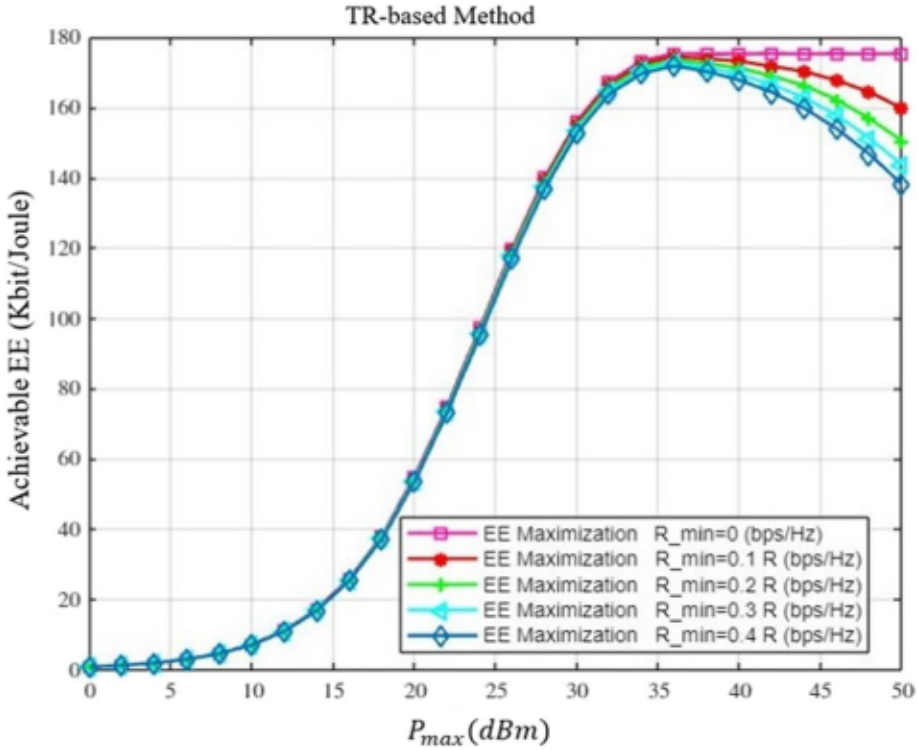

Fig. 5 Average EE using RIS versus P_{max} and $M = 32, K = 16, N = 16$ as well as different values for R_{min}

the RIS-based system case significantly outperform the AF relay-assisted one in terms of EE, as the RIS is a passive terminal. Moreover, the performance of TR-based algorithm is better than other methods as can be observed in both Figs. 2 and 3.

The effect of the different values for $R_{\min}$ in the TR-based algorithm's SE and EE versus $P_{\max}$ in dBm is depicted in Figs. 4 and 5, respectively. All of the schemes' SE values are extremely low for small $P_{\max}$ values at BS, which cannot meet the consumers' minimum rate requirements. However, increasing $R_{\min}$ values results in increasing the achievable SE for $P_{\max} > 37$ dBm. Increasing $R_{\min}$ leads to higher achievable SE, outperforming the unconstrained case of $R_{\min} = 0$bps/Hz. A larger $R_{\min}$ value result in a steeper slope in the SE curve.The performance behavior in Fig. 5 follows the same trend as in Fig. 4. It is shown that for larger $P_{\max}$, higher values of $R_{\min}$ results in faster reduction of the EE, since the extra BS transmit power is used to satisfy the user rate requirements. Besides, the achieved EE versus number of RIS reflecting elements N for different methods is shown in Fig. 6. The figure shows that, as the number of RIS reflecting elements N increases, the EE performance of all schemes initially improves, but it eventually reaches a saturation point for $N > 12$ values and it predicted to have a decreasing trend for a very large number of N. Therefore, there is an optimal number of reflecting elements for EE maximization problem.

We also compared the performance of different algorithms in terms of EE and CPU run time. Figure 7 illustrates that the TR-based method achieves faster convergence towards a highly accurate optimal solution, leading to its superior EE performance.

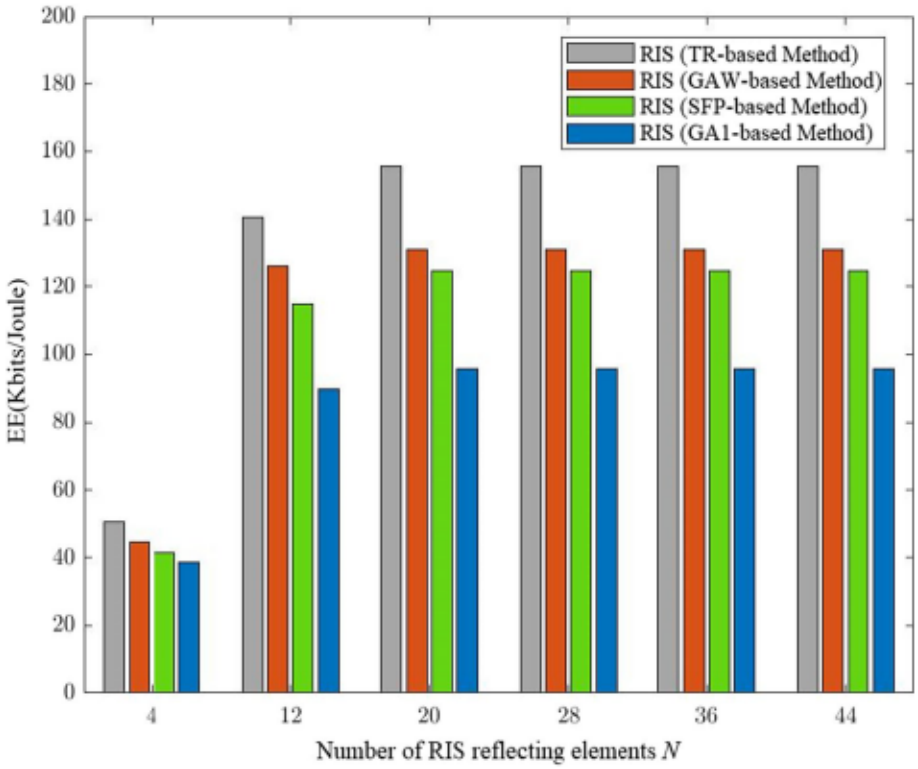

Fig. 6 EE using RIS versus N for SNR = 20dB and $R_{\min} = 0.2$ bps/Hz, as well as $P_n(b) = 0.01$dBm, $M = 64$, and $K = 16$

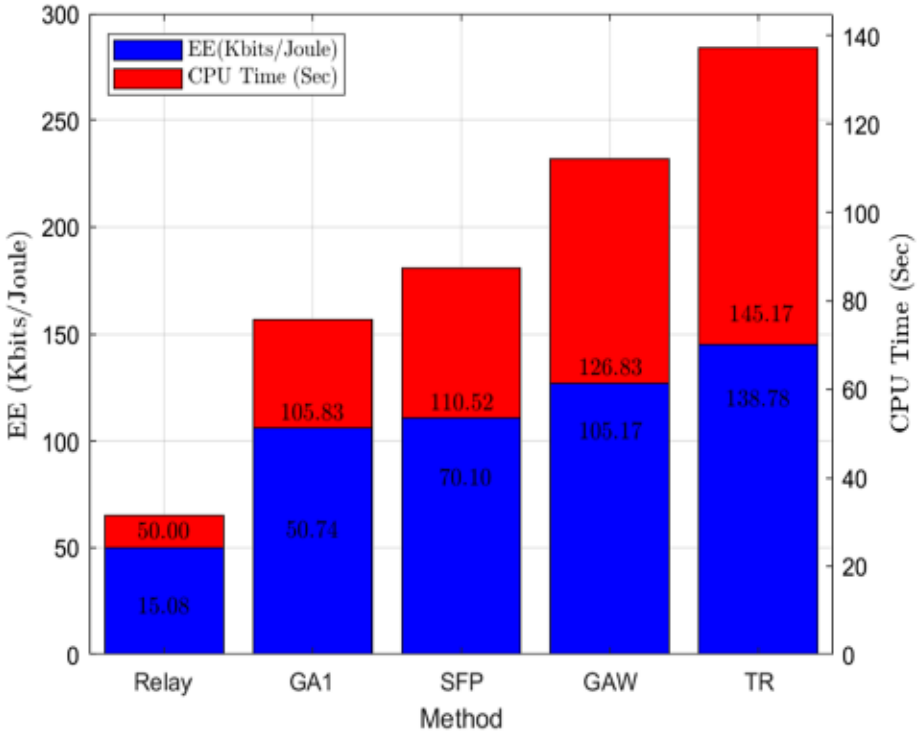

Fig. 7 EE and CPU time consumption of different algorithms for SNR = 20 dB and R_{min} = 0.2 bps/Hz, as well as $P_n(b)$ = 0.01 dBm, M = 64, and $K = N = 8$

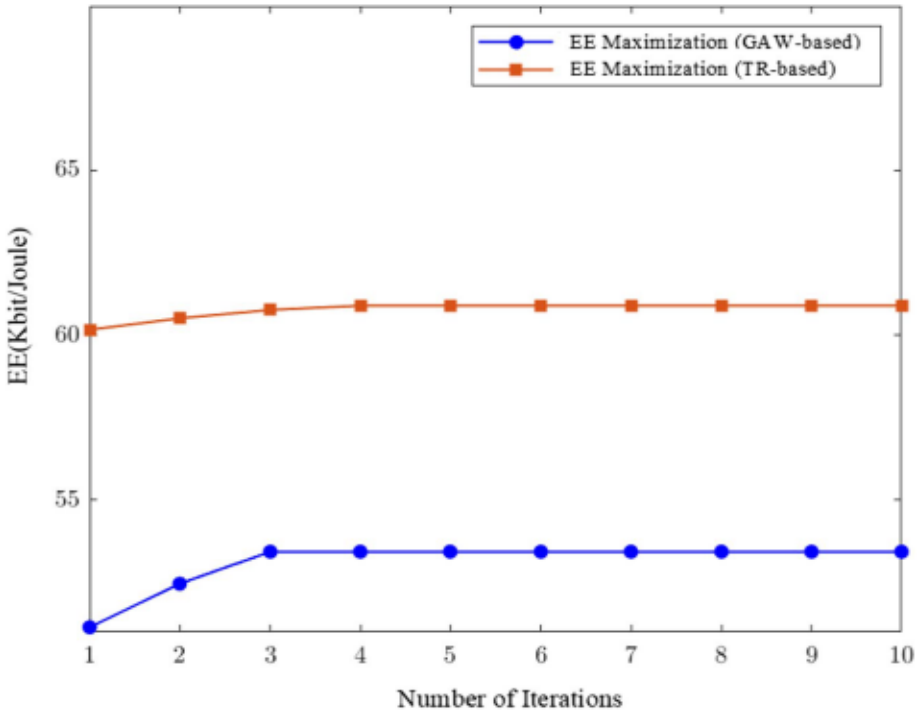

Fig. 8 EE versus number of iterations of different algorithms for SNR = 20 dB and R_{min} = 0.2 bps/Hz, as well as $P_n(b)$ = 0.01 dBm, M = 64, and $K = N = 8$

However, this advantage comes with the trade-off of requiring more CPU time compared to the other methods. Furthermore, Fig. 8 presents the convergence behaviors of the proposed methods. The EE is plotted against the number of iterations. The TR-based method demonstrates a faster convergence behavior compared to the GAW-based method. From the figure, it can be observed that the TR-based method converges rapidly in approximately one iteration. On the other hand, the GAW-based method takes more time to converge, reaching convergence after around three iterations.

4 CONCLUSION

In this paper, energy-efficient design and power allocation for RIS-based MISO networks in the downlink direction is investigated. After the introduction and formulation of the problem, RIS phase design and power allocation using TR- and GAW-based EE maximization methods are presented. Then, simulation results are compared with those of GA-based and SFP-based method and also a conventional method using the relay. Results show that TR- and GAW-based EE maximization method has improved energy efficiency in comparison to these methods.

This work primarily focuses on AO-based approaches for energy-efficient RIS-assisted MISO systems, leveraging the benefits of model-based optimization. However, we acknowledge the potential of ML techniques to further enhance our solutions by exploiting their adaptive capabilities and ability to capture complex system behaviors. Future work will explore advanced ML techniques and consider their integration with model-based algorithms to maximize the energy efficiency of RIS-aided wireless networks.

Abbreviations

UE	User
RF	Radio frequency
EE	Energy efficiency
SE	Spectral efficiency
RB	Resource block
GA	Gradient decent algorithm
QoS	Quality of Service
ZF	Zero-forcing
RIS	Reconfigurable intelligent surface
OFDM	Orthogonal frequency division multiplexing
OFDMA	Orthogonal frequency division multiple access
SISO	Single input single output
MISO	Multiple input single output
MIMO	Multiple input multiple output
APs	Access points
MU	Multiple user
SNR	Signal to noise ratio
AWGN	Additive white gussian noise
CSI	Channel state information
MC	Monte Carlo
AO	Alternating optimization
GA	Gradient-descent algorithm
GAW	Gradient-descent algorithm using Wolf conditions
TR	Trust Region
SCA	Successive convex approximation
FP	Fractional programming
BnB	Branch-and-bound
ML	Machine learning

Acknowledgements
The authors wish to convey their appreciation to every anonymous reviewer for their priceless feedback.

Author Contributions
SB conceived and designed the study, performed the simulations, and wrote the paper. MAO and MB have reviewed and discussed the technical details. All authors made suggestions for the improvements of the paper. All authors read, revised and approved the manuscript. SB and MAO oversaw the entire paper submission process. All authors read and approved the final manuscript.

Funding
This study received no external funding.

Availability of data and materials
Please contact the corresponding author at samaneh.bidabadi@uqtr.ca.

Declarations

Competing interests
The authors declare that they have no competing interests.

Received: 29 March 2023 Accepted: 22 August 2023
Published online: 05 September 2023

References

1. N. Rajatheva, I. Atzeni, E. Bjornson, A. Bourdoux, S. Buzzi, J.B. Dore, S. Erkucuk, M. Fuentes, K. Guan, Y. Hu, X. Huang, White paper on broadband connectivity in 6G. arXiv preprint arXiv:2004.14247. (2020)
2. W. Saad, M. Bennis, M. Chen, A vision of 6G wireless systems: applications, trends, technologies, and open research problems. IEEE Netw. **34**(3), 134–42 (2019)
3. Mitra P, Bhattacharjee R, Chatterjee T, De S, Karmakar R, Ghosh A, Adhikari T. Towards 6G Communications: Architecture, Challenges, and Future Directions. In2021 12th International Conference on Computing Communication and Networking Technologies (ICCCNT) 2021 Jul 6 (pp. 1–7). IEEE.
4. C. Huang, A. Zappone, G.C. Alexandropoulos, M. Debbah, C. Yuen, Reconfigurable intelligent surfaces for energy efficiency in wireless communication. IEEE Trans. Wirel. Commun. **18**(8), 4157–70 (2019)
5. Z. Yang, M. Chen, W. Saad, W. Xu, M. Shikh-Bahaei, H.V. Poor, S. Cui, Energy-efficient wireless communications with distributed reconfigurable intelligent surfaces. IEEE Trans. Wirel. Commun. **21**(1), 665–79 (2021)
6. H. Zhou, M. Erol-Kantarci, Y. Liu, H.V. Poor, A Survey on Model-based, Heuristic, and Machine Learning Optimization Approaches in RIS-aided Wireless Networks. arXiv preprint arXiv:2303.14320. (2023)
7. Q. Wu, G.Y. Li, W. Chen, D.W. Ng, R. Schober, An overview of sustainable green 5G networks. IEEE Wirel. Commun. **24**(4), 72–80 (2017)
8. B. Feng, J. Gao, Y. Wu, W. Zhang, X.G. Xia, C. Xiao, Optimization techniques in reconfigurable intelligent surface aided networks. IEEE Wirel. Commun. **28**(6), 87–93 (2021)
9. C. Huang, A. Zappone, M. Debbah, C. Yuen, Achievable rate maximization by passive intelligent mirrors. In 2018 IEEE International Conference on Acoustics, Speech and Signal Processing (ICASSP) (pp. 3714–3718). IEEE (2018)
10. Q. Wu, R. Zhang, Intelligent reflecting surface enhanced wireless network via joint active and passive beamforming. IEEE Trans. Wirel. Commun. **18**(11), 5394–409 (2019)
11. Y. Yang, S. Zhang, R. Zhang, IRS-enhanced OFDM: Power allocation and passive array optimization. In 2019 IEEE Global Communications Conference (GLOBECOM) (pp. 1–6). IEEE (2019)
12. P. Wang, J. Fang, X. Yuan, Z. Chen, H. Li, Intelligent reflecting surface-assisted millimeter wave communications: joint active and passive precoding design. IEEE Trans. Veh. Technol. **69**(12), 14960–73 (2020)
13. Y. Yang, B. Zheng, S. Zhang, R. Zhang, Intelligent reflecting surface meets OFDM: protocol design and rate maximization. IEEE Trans. Commun. **68**(7), 4522–35 (2020)
14. Y. Yang, S. Zhang, R. Zhang, IRS-enhanced OFDMA: joint resource allocation and passive beamforming optimization. IEEE Wirel. Commun. Lett. **9**(6), 760–4 (2020)
15. Q. Wu, R. Zhang, Intelligent reflecting surface enhanced wireless network via joint active and passive beamforming. IEEE Trans. Wirel. Commun. **18**(11), 5394–409 (2019)
16. Q. Wu, R. Zhang, Beamforming optimization for intelligent reflecting surface with discrete phase shifts. In ICASSP 2019-2019 IEEE International Conference on Acoustics, Speech and Signal Processing (ICASSP) (pp. 7830–7833). IEEE (2019)
17. F. Tan, X. Xu, H. Chen, S. Li, Energy-efficient beamforming optimization for MISO communication based on reconfigurable intelligent surface. Phys. Commun. **3**, 101996 (2023)
18. Z. Yang, M. Chen, W. Saad, W. Xu, M. Shikh-Bahaei, H.V. Poor, S. Cui, Energy-efficient wireless communications with distributed reconfigurable intelligent surfaces. IEEE Trans. Wireless Commun. **21**, 665–679 (2021)
19. O. Ozdogan, E. Bjornson, Deep learning-based phase reconfiguration for intelligent reflecting surfaces. In: Proceedings of Asilomar Conference on Signals, Systems, and Computers, pp. 707–711 (2020)
20. G. Lee, M. Jung, A.T.Z. Kasgari, W. Saad, M. Bennis, Deep reinforcement learning for energy-efficient networking with reconfigurable intelligent surfaces. In: Proceeings of IEEE International Conference on Communications (ICC), pp. 1–6 (2020)

21. X. Liu, Y. Liu, Y. Chen, H.V. Poor, RIS enhanced massive non-orthogonal multiple access networks: deployment and passive beamforming design. IEEE J. Sel. Areas Commun. **39**(4), 1057–1071 (2020)
22. S. Wright, J. Nocedal, Numerical optimization. Science. **35**(67–68), 7 (1999)
23. A. Zappone, L. Sanguinetti, G. Bacci, E. Jorswieck, M. Debbah, Energy-efficient power control: a look at 5G wireless technologies. IEEE Trans. Signal Process. **64**(7), 1668–83 (2015)
24. Zappone A, Jorswieck E, Energy efficiency in wireless networks via fractional programming theory. Found. Trends Commun. Inform. Theory. **11**(3-4), 185–396 (2015)
25. A. Magbool, V. Kumar, M.F. Flanaga, On Energy Efficiency and Fairness Maximization in RIS-Assisted MU-MISO mmWave Communications. arXiv preprint arXiv:2211.08224. (2022)
26. P. Guan, Y. Wang, H. Yu, Y. Zhao, Energy efficiency maximisation for STAR–RIS assisted full–duplex communications. IET Commun. (2023)
27. V. Nesterov, How to make the gradients small. OPTIMA MPS Newslett. **88**, 10–11 (2012)
28. J.C. Gilbert, J. Nocedal, Global convergence properties of conjugate gradient methods for optimization. SIAM J. Optim. **2**(1), 21–42 (1992)
29. K. Ritter, On the rate of superlinear convergence of a class of variable metric methods. Numerische Mathematik **35**, 293–313 (1980)
30. S. Gratton, A. Sartenaer, P.L. Toint, Recursive trust-region methods for multiscale nonlinear optimization. SIAM J. Optim. **19**, 414–444 (2008)
31. Y.X. Yuan, Recent advances in trust region algorithms. Math. Program. **151**, 249–81 (2015)
32. E. Björnson, L. Sanguinetti, J. Hoydis, M. Debbah, Optimal design of energy-efficient multi-user MIMO systems: is massive MIMO the answer? IEEE Trans. Wirel. Commun. **14**(6), 3059–75 (2015)

Publisher's Note

3.2 Optimisation basée sur un modèle des systèmes SISO-OFDMA assistés par RIS

3.2.1 Contexte

L'accent est mis sur l'amélioration de l'EE dans les systèmes SISO-OFDMA avec l'aide de RIS dans cette section. Les études antérieures se sont principalement concentrées sur l'EE dans des configurations plus basiques, en ignorant souvent les difficultés engendrées par l'allocation de fréquence des sous-porteuses en OFDMA et les paramètres de décalage de phase des RIS. Afin de pallier ce manque de recherche, notre étude pose le problème de maximisation de l'efficacité énergétique, en particulier pour les systèmes de communication downlink SISO-OFDMA agréés par RIS. Il est nécessaire de mettre en place des approches novatrices pour gérer efficacement la complexité computationnelle, telles que l'optimisation des variables telles que l'attribution des sous-porteuses, l'allocation de la puissance et les décalages de phase des RIS de manière optimale. Afin de faire face à ces défis, nous mettons en place des méthodes novatrices pour découpler la fonction EE pour chaque utilisateur et proposons une solution pratique qui repose sur une borne inférieure dans un contexte d'optimisation. Les performances de l'EE sont considérablement améliorées par cette approche par rapport aux méthodes traditionnelles, comme le démontrent nos évaluations numériques.

3.2.2 Méthodologie

Il semble qu'il y ait peu d'articles qui se sont penchés sur la conception du beamforming passif et l'attribution des ressources en vue de la communication multi-utilisateur à large bande. L'élaboration d'un système destiné à plusieurs utilisateurs est plus complexe que celle d'un système pour un seul utilisateur, étant donné qu'il faut

optimiser en même temps les coefficients de réflexion du RIS et organiser la transmission destinée à de multiples utilisateurs ainsi que la répartition des ressources. L'emploi du RIS dans les systèmes OFDMA, une version multi-utilisateur de la technique de modulation numérique familière qu'est la division de fréquence orthogonale (en englais OFDM, orthogonal frequency division multiplexing), fait l'objet d'une attention croissante dans la recherche. L'OFDMA offre l'avantage majeur d'une distribution variable des ressources, un facteur crucial pour optimiser l'efficacité énergétique des réseaux sans fil. L'élaboration d'algorithmes efficaces pour l'allocation de ressources, capables d'exploiter au mieux les ressources en main, constitue un enjeu majeur pour l'application des systèmes OFDMA améliorés par RIS. Face à ce défi, plusieurs chercheurs ont suggéré différentes méthodes d'optimisation, telles que l'apprentissage automatique, l'optimisation convexe et la théorie des jeux. Ces méthodes pourraient améliorer l'efficience énergétique du système en répartissant les ressources de la manière la plus optimale possible.

Des études récentes [65], [66]- [67], entre autres, ont exploré l'emploi des RIS dans les systèmes OFDMA, comme le montre le tableau 3-1. Les recherches de [65], [66]- [67] se sont focalisées sur l'optimisation du taux global dans un réseau OFDMA. L'étude de [65] suggère un système MIMO THz multi-utilisateur assisté par RIS et d'accès OFDM, dont l'objectif est d'optimiser le taux global pondéré par le biais d'un beamforming analogique/numérique conjoint à la station de base et une optimisation de la matrice réfléchissante au niveau du RIS. Selon [66], les chercheurs suggèrent un système innovant de communication en montée, faisant appel à un transcepteur RIS transmissif et au OFDMA pour plusieurs utilisateurs. Ils appliquent l'optimisation en alternance pour optimiser le débit global du système tout en respectant les exigences de QoS.

L'étude de [68] se penche sur la conception conjointe des beamformers à utilisateurs

multiples et des éléments réfléchissants programmables, également connus sous le sigle PRE (en englais PRE, programmable reflecting elements), dans le cadre des réseaux OFDM assistés par RIS, afin d'assurer une qualité de service optimale. Dans [69], les chercheurs suggèrent un algorithme de répartition des ressources pour les réseaux MISO OFDMA multicellulaires soutenus par RIS, visant les utilisateurs URLLC. Cet algorithme assure la QoS tout en cherchant à augmenter le débit du système via une méthode itérative sous-optimale.

Dans [70], les auteurs suggèrent un algorithme optimal de réflexion des faisceaux basé sur l'apprentissage fédéré (en englais OBR-FL, optimal beam reflection algorithm based on federated learning) pour les communications soutenues par RIS. Ils exploitent l'apprentissage fédéré pour perfectionner la réflexion des faisceaux en se basant sur le CSI clairsemé tout en protégeant la confidentialité des utilisateurs. L'étude de [67] introduit un beamforming passif dynamique pour les systèmes RIS intégrés OFDMA, qui optimise les coefficients de réflexion et les répartitions des ressources afin d'augmenter le débit partagé par les utilisateurs, tout en s'ajustant souplement aux changements du canal et surpassant les méthodes de beamforming passif fixe.

D'autre part, les auteurs de [71] ont étudié la maximisation de l'efficacité énergétique tout en garantissant l'équité dans un réseau sans cellule assisté par un RIS actif. Contrairement aux études mentionnées, les recherches récentes sont axées sur la formulation d'un problème d'efficacité énergétique dans la direction DL d'un système RIS-aidé SISO-OFDMA, en prenant en compte un RIS passif. La prise en compte d'une station de base à antenne unique et d'utilisateurs permet une simplification plus directe du problème proposé. Le problème présenté est complexe, impliquant des variables discrètes et continues de haute dimension. Compte tenu de cette complexité, suggérer une solution

optimale basée sur un modèle s'avère impraticable. Par ailleurs, le manque de données disponibles pour l'entraînement restreint l'application des techniques d'apprentissage automatique. Ainsi, par rapport aux autres solutions mentionnées dans la littérature et affichées dans le tableau 3-1, nous suggérons une solution suboptimale basée sur l'optimisation par borne inférieure du problème d'efficacité énergétique.

Tableau 3-1 Revue de la littérature.

Référence	Configuration du système	Objectif	Variables de conception	Découplage
[72]	Réseau RIS-aidé SISO OFDM multi-utilisateurs-UL	Max. taux global, et taux minimum	Allocation des ressources	Algorithme d'allocation max-min
[73]	Réseau RIS-aidé MISO OFDM multi-utilisateurs-DL	Max. taux-somme	Allocation des ressources, faisceau passif	Réseaux de Q profonds combinés (DQN) et gradient déterministe profond (DDPG)
[74]	Systèmes RIS-aidés SISO OFDM	Max. efficacité spectrale	Faisceau passif	DRL-DQN
[75]	Systèmes de communication D2D bidirectionnelle à deux voies multi-paires OFDM améliorés par RIS	Max. Min. taux pondéré somme-bidirectionnel	Allocation de sous-bandes, allocation de puissance, et conception de faisceau passif	SDR, méthode du sous-gradient projeté
[65]	Système RIS-aidé THz MIMO-OFDMA-DL	Max. taux pondéré somme	Faisceau analogique/numérique hybride à la station de base et matrice de réflexion au RIS	AO, SDR
[66]	Système multi-utilisateurs OFDMA avec transceiver RIS transmissif-Up	Max. taux-somme du système	Allocation de puissance, allocation de sous-porteuses, et coefficient RIS transmissif	AO, méthode de décomposition duale de Lagrange, SCA
[68]	Réseau RIS-aidé MIMO OFDM multi-utilisateurs-DL	Max. taux pondéré, taux somme, et moyenne géométrique du taux	Faisceau actif et passif	Algorithmes basés sur des formes fermées
[69]	Systèmes RIS-aidés OFDMA-URLLC	Max. taux-somme pondéré	Faisceau actif et passif	SCA, et approche itérative de minimisation de rang (IRMA)
[70]	Réseau RIS-aidé SIMO OFDMA multi-utilisateurs-DL	Max. taux des utilisateurs	Faisceau passif	Apprentissage fédéré (FL), Réseau neuronal profond (DNN)
[67]	Réseau RIS-aidé MIMO OFDMA multi-utilisateurs-DL	Max. taux commun (minimum) des utilisateurs	Faisceau passif, bloc de ressources temps-fréquence OFDMA ainsi que allocations de puissance	AO, dualité de Lagrange méthode, SCA
[71]	Réseau sans cellule RIS-aidé MISO OFDMA actif-Up	Max. EE	Faisceau passif et allocation des ressources	AO, FP
Ce travail	Réseau RIS-aidé SISO OFDMA multi-utilisateurs-DL	Max-EE	Allocation de sous-porteuses et de puissance, faisceau passif	AO, SQP , PSO

Les principales contributions de ce travail sont présentées ci-dessous:

- Nous formulons le problème de l'efficacité énergétique dans un système de

communication SISO OFDMA pour la direction descendante. Cette formulation prend en compte l'allocation des sous-canaux et de la puissance au sein du réseau OFDMA, ainsi que le décalage de phase du RIS. La relation complexe entre les variables d'optimisation rend le problème non convexe, posant un défi important pour trouver une solution optimale directement.

- Dans le cadre de l'AO, nous introduisons une stratégie de solution sous-optimale hautement efficace. Cette approche exploite la borne inférieure du problème d'EE en introduisant un nouveau paramètre dans la formule de l'EE. L'intégration de ce nouveau paramètre permet de décomposer la fonction objective complexe de l'EE en composants individuels pour chaque utilisateur. Par la suite, une méthode gourmande, appelée affectation des sous-porteuses en descente basée sur la borne inférieure de maximisation de l'efficacité énergétique (en englais MDSA, Maximizing-EE-Lower-Bound-Based Downlink Subcarrier Assignment), est proposée pour l'allocation des sous-canaux, garantissant une utilisation efficace des sous-canaux disponibles. Simultanément, l'approche utilise la méthode de programmation quadratique séquentielle (en englais SQP, Sequential Quadratic Programming) pour l'allocation de la puissance, une technique d'optimisation polyvalente. De plus, le décalage de phase du RIS est optimisé en utilisant l'algorithme de l'PSO, reconnu pour sa flexibilité dans la recherche de solutions optimales au sein de complexes espaces d'optimisation.

Suite à l'identification d'un vide dans les publications concernant l'optimisation de l'efficacité énergétique dans les systèmes de communication RIS-enabled OFDMA, nous avons formulé le problème de maximisation de l'EE spécifiquement adapté à ce scénario. Cette formulation intègre des variables telles que l'allocation des sous-canaux, la répartition de la puissance au sein du réseau OFDMA, et les décalages de phase introduits

par le RIS. La complexité inhérente résultant des interdépendances entre ces variables rend le problème non convexe, nécessitant des approches innovantes pour trouver des solutions efficaces.

3.2.3 Résultats

Dans notre recherche, nous avons examiné la performance d'une nouvelle méthode d'allocation conjointe des ressources en la comparant à deux schémas de référence : le beamforming passif aléatoire et un scénario sans RIS, où le premier schéma considère le lien direct BS-utilisateur et effectue l'allocation des ressources OFDMA. Selon nos résultats de simulation, il a été constaté que l'augmentation de la puissance de transmission maximale à la BS améliore initialement l'EE, mais des augmentations supplémentaires entraînent des rendements décroissants, mettant en évidence l'importance d'une allocation de puissance efficace. L'étude a également démontré que le nombre d'éléments RIS impacte significativement l'efficacité énergétique, avec des améliorations jusqu'à un seuil optimal, au-delà duquel des éléments supplémentaires réduisent les gains d'efficacité. En utilisant l'algorithme PSO pour le beamforming passif, nous avons surpassé d'autres techniques, illustrant les bénéfices de l'intégration de RIS dans des systèmes sans fil pour une meilleure EE et SE. Cette méthode équilibre efficacement la complexité informatique grâce à une approche suboptimale, simplifiant ainsi l'allocation de puissance et de sous-porteuses tout en garantissant une convergence solide et des améliorations de performance dans les systèmes de communication RIS. The approach effectively balances computational complexity through a sub-optimal method, simplifying power and subcarrier allocation while ensuring robust convergence and performance enhancements in RIS-enabled communication systems.

3.2.4 Validation du modèle et limitations

Nous avons simplifié notre modèle système par rapport aux scénarios réels. Des conditions réalistes, telles que les contraintes matérielles, l'information d'état de canal (en englais CSI, channel state information) imparfaite et les erreurs de quantification, peuvent entraîner une baisse de performance par rapport aux modèles idéalisés. Cependant, ces considérations offrent une représentation plus fidèle des déploiements pratiques, permettant le développement de systèmes robustes, adaptables et mieux adaptés aux applications concrètes. Bien que les modèles idéalisés puissent atteindre de meilleures performances théoriques, intégrer des hypothèses réalistes permet de trouver un équilibre entre performance et praticité, garantissant ainsi la fiabilité et la faisabilité dans des environnements réels. Pour aborder cela, nous proposons d'incorporer les hypothèses réalistes suivantes dans notre travail afin d'en améliorer la praticité et l'applicabilité face aux défis de déploiement réels.

- Bien que les systèmes SISO soient plus simples et plus faciles à optimiser, intégrer les communications MISO/SIMO/MIMO permettrait de proposer un modèle plus représentatif de la réalité. Ces systèmes augmentent le nombre de variables à considérer, mais ils peuvent offrir des améliorations significatives en matière de performance en exploitant pleinement la diversité spatiale et les configurations multi-antennes. Il est essentiel de soigneusement évaluer le compromis entre complexité et gain de performance, car l'ajout de couches d'optimisation supplémentaires peut considérablement renforcer la robustesse et les capacités du système dans des déploiements pratiques.
- L'abandon de l'hypothèse d'une résolution infinie des décalages de phase ($2^b \gg 1$) introduit des contraintes pratiques dues à la nature discrète des décalages de phase

dans les dispositifs RIS réels. Cette quantification de la résolution des décalages de phase entraîne des écarts entre les coefficients de réflexion idéaux et réels, provoquant un désalignement des signaux. En conséquence, le gain de formation de faisceau est réduit, et les signaux réfléchis peuvent ne pas s'additionner de manière entièrement constructive au niveau du récepteur. Cette dégradation de la qualité du signal impacte négativement des paramètres clés du système, tels que l'efficacité spectrale, l'efficacité énergétique et la fiabilité globale des communications.

- Une connaissance imparfaite des canaux de communication (par exemple, $h_{k,R,n}$ et $H_{T,n}$) met en évidence les défis pratiques liés à l'estimation précise des canaux dans des environnements bruyants ou riches en interférences. Un CSI incomplet ou inexact peut conduire à une optimisation sous-optimale des motifs de réflexion du RIS, entraînant une dégradation des performances de formation de faisceau, une réduction de l'efficacité spectrale et énergétique, ainsi qu'une fiabilité diminuée du réseau global. Ces inexactitudes peuvent avoir un impact significatif sur la capacité du système à atteindre ses objectifs de performance. Bien que la prise en compte de ces imperfections ajoute une complexité supplémentaire, elle permet des évaluations de performance plus réalistes, reflétant les scénarios de déploiement pratiques. De plus, une estimation précise des canaux est essentielle pour s'adapter aux conditions de canal dynamiques, telles que la mobilité des utilisateurs et les changements environnementaux, garantissant ainsi un fonctionnement robuste et fiable dans des environnements réels.

3.2.5 Droits d'auteur

electronics

MDPI

Article

Energy-Efficient RIS-Enabled SISO-OFDMA Communication via Lower Bound Optimization

Samaneh Bidabadi *, Messaoud Ahmed Ouameur *, Miloud Bagaa and Daniel Massicotte

Department of Electrical and Computer Engineering, University of Quebec at Trois-Rivieres, Trois-Rivieres, QC G8Z 4M3, Canada; miloud.bagaa@uqtr.ca (M.B.); daniel.massicotte@uqtr.ca (D.M.)
* Correspondence: samaneh.bidabadi@uqtr.ca (S.B.); messaoud.ahmed.ouameur@uqtr.ca (M.A.O.)

Abstract: The pursuit of energy-efficient solutions in the context of reconfigurable intelligent surface (RIS)-assisted wireless networks has become imperative and transformative. This paper investigates the integration of RIS into an orthogonal frequency-division multiple access (OFDMA) framework for multi-user downlink communication systems. We address the challenge of jointly optimizing RIS reflection coefficients alongside OFDMA frequency and power allocations, with the aim of maximizing energy efficiency. This optimization is subject to specific quality-of-service (QoS) requirements for each user equipment (UE) and a constraint on transmission power and the RIS phase shift matrix. To address this complex optimization problem, we propose a novel practical and low-complexity approach that is based on optimizing a computationally efficient and numerically tractable lower bound on energy efficiency. The numerical results highlight the effectiveness of our approach, demonstrating a substantial increase in energy efficiency compared to scenarios without RIS, with random RIS integration, and with the scheme using the Genetic Algorithm (GA).

Keywords: RIS-assisted network; OFDMA; energy efficiency; RIS phase design

check for updates

Citation: Bidabadi, S.; Ouameur, M.A.; Bagaa, M.; Massicotte, D. Energy-Efficient RIS-Enabled SISO-OFDMA Communication via Lower Bound Optimization. *Electronics* **2024**, *13*, 1040. https://doi.org/10.3390/electronics13061040

Academic Editor: Eneko Iradier

Received: 2 February 2024
Revised: 6 March 2024
Accepted: 7 March 2024
Published: 11 March 2024

1. Introduction

Energy efficiency (EE) has become a crucial topic in the research and development of next-generation wireless networks, particularly in sixth generation (6G). However, the deployment of 6G in the industry is quite challenging. Due to non-line of sight (NLOS), the energy efficiency and throughput of the network decrease. NLOS also gives rise to multipath fading, attenuation, and interference due to reflection and refraction. To overcome this problem, reconfigurable intelligent surface (RIS) is the primary solution. RIS reduces attenuation and improves network performance [1].

A RIS is a meta-surface made up of numerous inexpensive passive antennas that may effectively reflect the electromagnetic waves impinging on it to improve performance [2]. In wireless communication networks with RIS assistance, a base station (BS) communicates control signals to a RIS controller to enhance incident wave characteristics and user communication quality. As a reflector, the RIS does not engage in any digitization processes. Therefore, if implemented properly, a RIS promises to use substantially less energy than conventional amplify-and-forward (AF) relays [2,3].

When using a RIS in wireless communications, radio resource allocation to optimize the network performance is a prime concern [4]. Effective resource allocation can aid to further enhance a RIS-assisted wireless network's energy efficiency.

1.1. Related Works

The design of reflection coefficients (or passive beamforming) for narrowband transmission over frequency-flat channels was the main focus of earlier studies on RIS-enhanced wireless communication [3,5]. However, more recent studies in [6–14] have looked at the more general broadband transmission over frequency-selective channels for the case of a single-user setup.

In [6], the authors proposed a majorization–minimization (MM)-based iterative approach for optimizing RIS passive beamforming in an OFDM system, achieving near-optimal performance with lower computational complexity compared to the existing sine cosine algorithm (SCA). The work in [7] introduces a scalable framework for channel estimation and reflection optimization in RIS-enhanced OFDM systems, achieving improved rate performance with reduced training overhead and computational complexity. The authors in [8] proposed a practical transmission protocol for RIS-enhanced OFDM systems under frequency-selective channels, optimizing the achievable rate through a joint optimization of transmit power allocation and RIS passive array reflection coefficients while reducing training overhead. The work in [9] addresses the ergodic achievable rate optimization in RIS-assisted mmWave MIMO-OFDM systems with statistical CSI, utilizing majorization theory and alternating optimization for the joint design of the transmit covariance matrix and RIS reflection coefficients. The work in [10] proposed a framework for integrating RIS technology into wireless networks by leveraging localization information for robust user multiplexing, minimizing the overhead of channel estimation and phase shift optimization in OFDM systems. The authors in [11] suggested an intelligent resource allocation scheme utilizing reinforcement learning (RL) for maximizing the sum-rate in RIS-enhanced OFDM systems, considering both primary and secondary user scenarios, and demonstrated significant transmission rate improvements compared to benchmark schemes. The work in [12] investigates spectral efficiency improvement in an OFDM system with a 1-bit resolution RIS, utilizing a deep RL algorithm for optimizing reflection phase shifts, leading to significant performance gains and reduced calculation delay. The work in [13] addresses the optimization of RIS-enhanced two-way D2D OFDM systems, maximizing the bidirectional sum-rate via sub-band, power, and discrete phase shift optimization. In [14], the authors presented joint optimization of the UAV trajectory, RIS scheduling, and resource allocation in OFDMA systems to maximize the sum-rate while considering heterogeneous QoS requirements, showing promising performance gains with RIS deployment in UAV-based communication.

To the best of our knowledge, very few articles have examined a passive beamforming design and resource allocation for multi-user broadband communication. The multi-user system design is more complex than the single-user case because the RIS reflection coefficients must be concurrently optimized with the multi-user transmission scheduling and resource allocation. The use of RIS in orthogonal frequency-division multiple access (OFDMA) systems, a multi-user variant of the well-known orthogonal frequency-division multiplexing (OFDM) digital modulation method, has been the subject of an expanding body of study. The fundamental benefit of OFDMA is that it enables variable resource allocation, which is essential for enhancing wireless networks' energy efficiency. Designing efficient resource allocation algorithms that can effectively use the available resources is one of the major issues in putting RIS-assisted OFDMA systems into practice. To tackle this problem, many scholars have suggested numerous optimization strategies, including machine learning, convex optimization, and game theory. These techniques have the potential to increase the system's energy efficiency by allocating resources as efficiently as possible.

Recent publications [15–20], among others, have looked at the usage of RISs in OFDMA systems, as listed in Table 1. The works in [15–20] have focused on maximizing the sum-rate in an OFDMA network. The work in [15] proposes a RIS-aided multi-user THz MIMO system with OFDM access, aiming to maximize the weighted sum-rate via joint analog/digital beamforming at the base station and reflection matrix optimization at the RIS. In [16], the authors propose a novel uplink communication system with a transmissive RIS transceiver, employing OFDMA for multiple users, and utilize alternating optimization to maximize the system sum-rate while meeting QoS constraints. The work in [17] investigates the joint design of MU beamformers and RIS's programmable reflecting elements (PREs) for quality-of-service in RIS-aided OFDM networks. In [18], the authors propose a resource allocation algorithm for RIS-aided MISO OFDMA multicell networks targeting URLLC

users, ensuring QoS while maximizing system throughput through a sub-optimal iterative approach. The authors in [19] propose the optimal beam reflection based on the the federated learning (OBR-FL) algorithm for RIS-assisted communications, utilizing federated learning to optimize beam reflection based on sparse CSI while preserving user privacy. The work in [20] proposes dynamic passive beamforming for RIS-integrated OFDMA systems, optimizing reflection coefficients and resource allocations to maximize users' common rate while flexibly adapting to channel variations and outperforming fixed passive beamforming approaches. On the other hand, the authors in [21] delve into the investigation of maximizing energy efficiency fairness in an active RIS-aided cell-free network. In contrast to the studies mentioned, recent research is oriented towards formulating an energy-efficient problem in the DL direction of a RIS-aided single input single output (SISO) OFDMA system, taking passive RIS into account. The consideration of a single-antenna BS and users allows for a more straightforward simplification of our proposed problem. The presented problem is intricate, involving high-dimensional discrete and continuous variables. Given the complexity, suggesting a model-based optimal solution proves impractical. Additionally, the unavailability of accessible data for training hinders the utilization of machine learning methods. Consequently, in comparison to other solutions outlined in the literature and presented in Table 1, a sub-optimal solution is advocated by us through the lower-bound optimization of the EE problem.

Table 1. Literature review.

Reference	System Setup	Objective	Design Variables	Decoupling
[10]	Multi-user RIS-aided SISO OFDM network-UL	Max. overall rate, and minimum rate	Resource allocation	Max–min allocation algorithm
[11]	Multi-user RIS-aided MISO OFDM network-DL	Max. sum-rate	Resource allocation, passive beamforming	Combined deep Q networks (DQN) and deep deterministic policy-gradient (DDPG)
[12]	RIS-aided SISO OFDM systems	Max. spectral efficiency	Passive beamforming	DRL-DQN
[13]	RIS-enhanced two-way D2D multi-pair OFDM communication systems	Max. Min. bidirectional weighted sum-rate	Sub-band allocation, the power allocation, and passive beamforming design	SDR, projected sub-gradient method
[15]	RIS-aided THz MIMO-OFDMA system-DL	Max. weighted sum-rate	Hybrid analog/digital beamforming at the BS and reflection matrix at the RIS	AO, SDR
[16]	Multi-user OFDMA system with transmissive RIS transceiver-Up	Max. system sum-rate	Power allocation, subcarrier allocation, and transmissive RIS coefficient	AO, Lagrangian dual decomposition method, SCA
[17]	Multi-user RIS-aided MIMO OFDM network-DL	Max. weighted rate, sum-rate, and geometric mean of rate	Active and passive beamforming	Closed form-based algorithms
[18]	RIS-aided OFDMA-URLLC systems	Max. weighted sum throughput	Active and passive beamforming	SCA, and iterative rank minimization approach (IRMA)
[19]	Multi-user RIS-aided SIMO OFDMA network-DL	Max. users' rate	Passive beamforming	Federated learning (FL), Deep Neural Network(DNN)
[20]	Multi-user RIS-aided MIMO OFDMA network-DL	Max. users' common (minimum) rate	Passive beamforming, OFDMA time-frequency resource block as well as power allocations	AO, Lagrange duality method, SCA
[21]	Active RIS-aided cell-free network-MISO OFDMA-Up	Max. EE	Passive beamforming and resource allocation	AO, FP
This work	Multi-user RIS-aided SISO-OFDMA network-DL	Max-EE	Subcarrier and power allocations, passive beamforming	AO, Riemannian gradient method (RGM), PSO

1.2. Contributions

The key contributions of this work are outlined below:

- The EE problem in the SISO-OFDMA communication system for the DL direction is formulated by us. This formulation takes into account THE subchannel and power allocation within the OFDMA network, as well as the phase shift of the RIS. The intricate relationship among the optimization variables renders the problem non-convex, posing a significant challenge to finding an optimal solution directly.
- Within the framework of AO, a highly efficient sub-optimal solution strategy is introduced by us. This approach capitalizes on the lower bound of the EE problem by introducing a novel parameter into the EE formula. The integration of this new parameter allows for the dissection of the intricate objective function of EE into individual components for each user. Subsequently, a resourceful greedy method called the maximizing-EE-lower-bound-based downlink subcarrier assignment (MDSA) is proposed by us for subcarrier allocation, ensuring the effective utilization of available subchannels. Simultaneously, the approach employs the sequential quadratic programming method (SQP) for power allocation, a versatile optimization technique. Furthermore, the RIS phase shift is optimized using the particle swarm optimization (PSO) algorithm, recognized for its adaptability in finding optimal solutions within complex optimization spaces.
- The simulation results demonstrate that the proposed low-complexity sub-optimal method, employing MDSA and PSO, enhances the performance of RIS-enabled SISO-OFDMA communication systems compared to benchmark methods.

Notation: In this paper, vectors and matrices are denoted by bold-face lower-case and upper-case letters, respectively. Sets are designated by upper-case calligraphic letters. Additionally, the functions $\mathcal{R}(\cdot)$, $\mathcal{I}(\cdot)$, $|\cdot|$, $(\cdot)^*$, and $\arg(\cdot)$ indicate distinct properties of a complex number, namely, its real part, imaginary part, modulus, complex conjugate, and angle, in that order. $\mathbf{I}_M$ denotes the identity matrix of size $M \times M$, and $\mathbf{e}_m$ denotes the m_{th} column of $\mathbf{I}_M$. $\text{diag}(\boldsymbol{x})$ denotes a square diagonal matrix with the elements of $\boldsymbol{x}$ on the main diagonal. $\|.\|$ denotes the l_2 norm. The distribution of a circularly symmetric complex Gaussian (CSCG) random variable with mean μ and variance σ^2 is denoted by $\mathcal{CN}(\mu, \sigma^2)$. Some other notations used in the paper are defined in Table 2.

Table 2. Notations used.

Notation	Description
$H_{T,n}$	The channel from the transmitter to the RIS
$h^k_{R,n}$	The channel from kth receiver to the RIS
ϱ_k	Set of subcarriers assigned to the kth user
$\rho_{k,n}$	Subcarrier n assigned to the kth user
$p_{k,n}$	Transmit power assigned to the kth user on subcarrier n
R	Total data rate of the system, where $R = \sum_{k=1}^{K} \sum_{n=1}^{N} r_{k,n}$
$\alpha_{k,\text{RIS}}$	Hypothetical static circuit power allocated to the k_{th} UE and n_{th} RIS element

2. System Model and Problem Formulation

2.1. System Model

The depicted system model can be observed in Figure 1, illustrating the interaction between a single-antenna base station and K single-antenna users. These entities establish communication through the intermediary of a RIS comprising M elements.

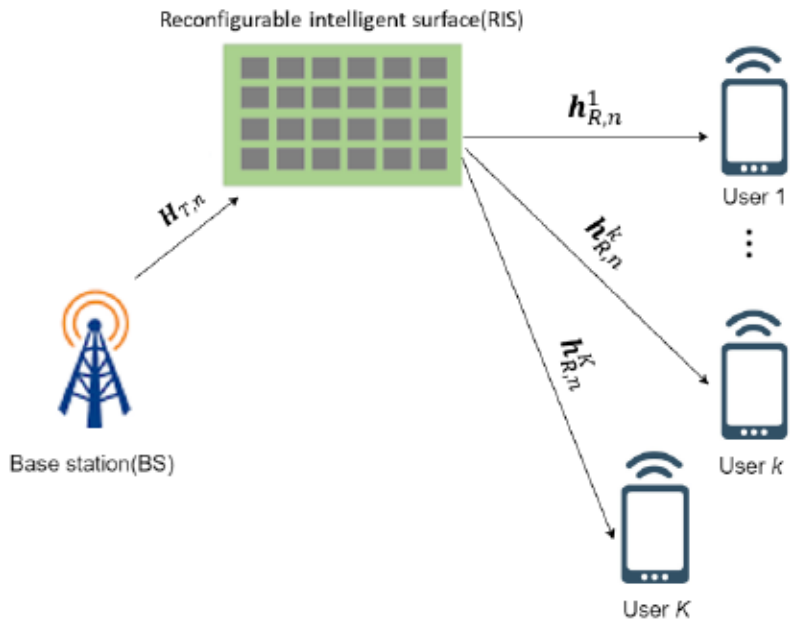

Figure 1. The considered RIS-based multi-user SISO-OFDMA system.

The channel model is based on an OFDM with N subcarriers. The channels from the transmitter and the kth user to the RIS are defined as $\boldsymbol{H}_{T,n} \in \mathbb{C}^{M\times 1}$ and $\boldsymbol{h}_{R,n}^{k} \in \mathbb{C}^{M\times 1}$, respectively, where $n = 1, 2, \ldots, N$ and $k = 1, 2, \ldots, K$. x_n^k is denoted as the transmitting signal from the transmitter to the kth user over the nth subcarrier.

In particular, the direct line-of-sight (LOS) link between the transmitter and the receiver is blocked (i.e., occlusion due to buildings). Thus, the received signal at the kth receiver is given as

$$y_n^k = ((\boldsymbol{h}_{R,n}^{k})^T \boldsymbol{\Phi}_n^k \boldsymbol{H}_{T,n}) p_{k,n} x_n^k + w_n^k,$$

where $\boldsymbol{\Phi}_n^k = \mathrm{diag}[\phi_1, \phi_1, \ldots, \phi_M] \in \mathbb{C}^{M\times M}$ is the RIS configuration matrix describing the phase shift effect of the RIS on the incident signal. Note that the amplitude of the incident signal does not change, which means $\phi_m = e^{j\theta_m}$ for any $m = 1, 2, \ldots, M$ and $\theta_m \in [0, 2\pi]$. Furthermore, $w_n^k \sim \mathcal{CN}(0, \sigma_n^2)$ denotes the additive white Gaussian noise (AWGN) at the receivers.

The signal-to-noise ratio (SNR) perceived by the kth user on the nth subcarrier is formulated as follows:

$$\mathrm{SNR}_{k,n} = \frac{\left|(\boldsymbol{h}_{R,n}^{k})^T \boldsymbol{\Phi}_n^k \boldsymbol{H}_{T,n}\right| p_{k,n}}{N_0 W}. \tag{1}$$

In this context, $N_0 = \sigma^2$ represents the variance of the AWGN noise. The total bandwidth, B, is divided into N subcarriers, each with a bandwidth of $W = \frac{B}{N}$.

Next, the maximum achievable data rate of the kth user on the nth subcarrier, $r_{k,n}$, and the overall rate of the system, R, can be expressed as:

$$r_{k,n} = W \log_2(1 + \mathrm{SNR}_{k,n}) \tag{2}$$

$$\mathrm{R} = \sum_{k=1}^{K} \sum_{n=1}^{N} \rho_{k,n} \log_2(1 + \mathrm{SNR}_{k,n}). \tag{3}$$

Also, $\rho_{k,n} \in \{0, 1\}$ indicates whether or not the nth subcarrier is assigned to the kth user. A feasible subcarrier assignment indictor matrix, $\boldsymbol{\rho} = [\rho_{k,n}]_{K\times N}$, should satisfy:

$$\boldsymbol{\rho} \in \varrho = \{[\rho_{k,n}]_{K\times N} | \sum_{k\in\mathcal{K}} \rho_{k,n} \leq 1, \forall n \in \mathcal{N}; \\ \rho_{k,n} \in \{0,1\}, \forall k \in \mathcal{K}, n \in \mathcal{N}\}, \tag{4}$$

where $\mathcal{N} = \{1, 2, \cdots, N\}$ and $\mathcal{K} = \{1, 2, \cdots, K\}$ represent the sets of all subcarriers and all UEs, respectively. To minimize interference between users, each subcarrier is assigned exclusively to one user at a time. Also, the total power consumption of the system is represented as:

$$\mathcal{P}_{total} = \zeta P + P_{BS} + KP_{UE} + MP_m(b), \tag{5}$$

where $P = \sum_{k\in\mathcal{K}} \sum_{n\in\mathcal{N}} p_{k,n}$, and $\mathbf{P} = [p_{k,n}]_{K\times N}$ denotes any possible power allocation matrix and should be subject to:

$$\mathbf{P} \in \mathcal{P} = \left\{ [p_{k,n}]_{K\times N} \middle| p_{k,n} \geq 0, \forall k \in \mathcal{K}, \forall n \in \mathcal{N}; \sum_{k\in\mathcal{K}} \sum_{n\in\mathcal{N}} p_{k,n} \leqslant P_{\max} \right\}. \tag{6}$$

In this context, P_{BS}, P_{UE}, and $P_m(b)$, respectively, represent the circuit power of the base station, the power consumption of users, and the power consumption of the m-th element of RIS. In addition, $\zeta = \nu^{-1}$, and the parameter ν is used to describe the drain efficiency of the power amplifier at the side of the transmitter.

2.2. Problem Formulation

The expression for the generalized EE in downlink transmission is given as the ratio of the total delivered bits to the total consumed energy, represented mathematically as:

$$\mathrm{EE} = \frac{\mathrm{R}}{\mathcal{P}_{total}}. \tag{7}$$

To ensure quality-of-service (QoS) for each user equipment (UE), we consider the generalized EE while incorporating minimum rate requirements $\hat{R}_k$ and the peak transmit power $P_{\max}$. To simplify the problem, we assume an infinite resolution for the reflectors' phase shifting ($2^b >> 1$). Furthermore, we assume perfect knowledge of all communication channels ($\boldsymbol{h}_{R,n}^k$ and $\boldsymbol{H}_{T,n}$) by the BS for all $k = 1, \cdots, K$.

Therefore, we can express the optimization problem for maximizing the EE in downlink transmission through the following formula:

$$(P1) \quad \max_{\boldsymbol{\Phi}, \boldsymbol{\rho}\in\varrho, \mathbf{P}\in\mathcal{P}} \quad \frac{\sum_{k=1}^{K}\sum_{n=1}^{N} \rho_{k,n} r_{k,n}}{\xi \sum_{k=1}^{K} p_{k,n} + P_{BS} + KP_{UE} + MP_m(b)} \tag{8}$$

$$\text{subject to} \quad \sum_{n\in\mathcal{N}} \rho_{k,n} r_{k,n} \geq \hat{R}_k, \quad \forall k = 1, 2, ..., K, \tag{8a}$$

$$|\phi_m| = 1, \quad \forall m = 1, 2, ..., M, \tag{8b}$$

where $\hat{R}_k$ denotes the individual QoS constraint of the k_{th} user. Also, constraint (8b) accounts for the fact that each RIS reflecting element can only provide a phase shift, without amplifying the incoming signal.

3. Proposal Method and Discussion

The EE optimization problem presented in (8) poses a significant computational challenge due to its NP-hard nature. This difficulty arises from the discrete variable $\boldsymbol{\rho}$ and the unit modulus constraint imposed on $\boldsymbol{\Phi}$. Finding optimal solutions for such problems is generally infeasible within reasonable time frames. To address these complexities, we propose a sub-optimal solution strategy using an AO framework.

In our AO-based approach, we iteratively optimize two sets of variables: the OFDMA resources $\rho_{k,n}$ and $p_{k,n}$ and the RIS reflection coefficients $\boldsymbol{\Phi}$. Crucially, we keep one set of

variables fixed while optimizing the other. This alternating optimization scheme allows us to tackle the intricate EE problem more effectively.

In the initial stages of our approach, we employ sub-optimal solutions. This choice is motivated by the computational expense associated with obtaining closed-form optimal solutions for all variables simultaneously. Instead, by initially focusing on one set of variables, we streamline the optimization process. Subsequently, in the following step of our AO framework, we introduce the PSO algorithm to further enhance the optimization process.

3.1. Optimization Respect to Subcarrier and Power Allocations

It is difficult to optimize the original objective function in (8) directly, but it may be possible to optimize a surrogate objective function that is easier to handle. In this case, the lower bound of the objective function can be used as a surrogate objective function to facilitate the optimization process. The surrogate objective function is then optimized instead of the original objective function, and the solution obtained using the surrogate objective function is used as a lower bound on the optimal value of the objective function.

Based on the insights from the work conducted in [22], the following theorem and corollary are established.

Theorem 1. *By considering a fixed value for the RIS phase shifts and introducing a new parameter* $\boldsymbol{\alpha}_{k,RIS} = \boldsymbol{\alpha}_{k,UE} \times \boldsymbol{\alpha}_{m,RIS}$ *into Equation (8), the optimal EE is given by:*

$$(P2) \quad \hat{EE} = \max_{\substack{\rho\in\varrho, \boldsymbol{P}\in\mathcal{P},\\ \boldsymbol{\alpha}\in\boldsymbol{\alpha}}} \min_{k\in\mathcal{K}} \frac{\sum_{k\in\mathcal{K}}\sum_{n\in\mathcal{N}} \rho_{k,n} r_{k,n}}{\sum_{k\in\mathcal{K}}\sum_{n\in\mathcal{N}} \zeta p_{k,n} + \alpha_{k,RIS} \times P_c} \tag{9}$$

$$s.t. \sum_{n\in\mathcal{N}} \rho_{k,n} r_{k,n} \geqslant \hat{R}_k, \quad \forall k = 1, 2, \ldots, K. \tag{9a}$$

where $\boldsymbol{\alpha}_{k,RIS} = \{[\alpha_{k,UE}]_{K\times 1}, [\alpha_{m,RIS}]_{M\times 1} \mid \sum_{k\in\mathcal{K}}\sum_{n\in\mathcal{N}} \alpha_{k,RIS} = 1; \alpha_{k,RIS} \in \mathbb{R}\}$ *and* $P_c = P_{BS} + KP_{UE} + MP_m(b)$. *The structure of the optimal solution, as demonstrated in Theorem 1 presented in Appendix A, can be depicted in a split form. This split form provides valuable insights that enable the derivation of Corollary 1.*

Corollary 1. *For any fixed* $\boldsymbol{\alpha}_{k,RIS} \in \alpha_{k,RIS}$, *the optimal energy efficiency* ($\hat{EE}$) *in (9) is bounded from below by:*

$$(P3) \quad \hat{EE} \geq \max_{\rho\in\varrho, \boldsymbol{P}\in\mathcal{P}} \min_{k\in\mathcal{K}} \left\{ \frac{\sum_{k\in\mathcal{K}}\sum_{n\in\mathcal{N}} \rho_{k,n} r_{k,n}}{\sum_{k\in\mathcal{K}}\sum_{n\in\mathcal{N}} \zeta p_{k,n} + \alpha_{k,RIS} \times P_c} \right\} \tag{10}$$

$$\textit{subject to} \quad \sum_{n\in\mathcal{N}} \rho_{k,n} r_{k,n} \geq \hat{R}_k, \forall k = 1, 2, \ldots, K. \tag{10a}$$

Assuming that $\boldsymbol{\alpha}_{k,\mathrm{RIS}}{}^{\mathrm{opt}} = [\alpha_{k,\mathrm{RIS}}^{\mathrm{opt}}]_{K\times 1}$ corresponds to the optimal energy efficiency ($\hat{EE}$) in Equations (8) and (9), $\alpha_{k,\mathrm{RIS}}^{\mathrm{opt}}$ can be interpreted as the portion of static circuit power individually allocated to the k_{th} UE and the m_{th} RIS element when aiming for maximum EE.

This decomposition allows us to split the complex optimization objective in Equation (8) into a set of relatively independent and simpler objectives in Equation (10). Consequently, we can employ sub-optimal methods for efficient problem-solving.

3.1.1. Subcarrier Allocations

Utilizing a heuristic algorithm is advantageous in this scenario since the maximum achievable energy efficiency of the k_{th} UE, $\hat{EE} = \frac{\sum_{n\in\mathcal{N}} \rho_{k,n} r_{k,n}}{\sum_{n\in\mathcal{N}} \zeta p_{k,n} + \alpha_{k,\mathrm{RIS}} P_c}$, depends solely on its own parameters and the subcarriers it occupies, without being influenced by the power adaptation strategies of other users. To simplify, we assume there is no difference in the RIS configuration matrix between subcarriers of the same user, meaning $\boldsymbol{\Phi}_1^k =, \cdots, = \boldsymbol{\Phi}_m^k = \boldsymbol{\Phi}^k$.

Additionally, constant values for $\boldsymbol{\alpha}_{k,\mathrm{RIS}}$ are considered for further simplification. Negative values of $\boldsymbol{\alpha}_{k,\mathrm{RIS}}$ may arise due to the nature of $\alpha_{k,\mathrm{RIS}} P_c$, representing the hypothetical

static circuit power allocated to the k_{th} UE and n_{th} RIS element. It is important to note that this value serves as a conceptual representation rather than a concrete physical reality. In practice, the total static circuit power remains constant at P_c.

To solve the optimization problem in Equation (10), we employ a heuristic algorithm called MDSA [22]. The power allocation is optimized using the SQP method, which is integrated into the MDSA algorithm.

The central concept behind the MDSA algorithm is to iteratively assign subcarriers, with the aim of maximizing the minimum individual EE, denoted as $\hat{\text{EE}}$, while ensuring that QoS requirements are met. Initially, each UE virtually receives its worst subcarrier, a conservative starting point. In this scenario, an individual EE is optimized under the QoS constraint using the algorithm employed for the power allocation, as described in Lines 2 to 5.

In each iteration, the UE with the lowest individual EE selects its preferred subcarrier from the pool of unassigned subcarriers. The UE then optimizes its individual EE under the QoS requirements using the SQP method. This iterative process continues until all subcarriers have been assigned, as outlined in lines 7 to 12 of Algorithm 1.

Algorithm 1: MDSA Maximizing-EE-lower-bound-based downlink subcarrier assignment.

1. **Input**: $\boldsymbol{\rho} = [\rho_{k,n}]_{K\times N} \leftarrow 0_{K\times N}$; $\varrho_k \leftarrow \emptyset, \forall k \in \mathcal{K}$; $\boldsymbol{\alpha}_{k,\text{RIS}} \leftarrow \alpha^{\text{ini}}_{k,\text{RIS}}$
2. **Output**: $\boldsymbol{\rho}, \boldsymbol{P}$
3. **For** each UE $k \in \mathcal{K}$
4. Find the subcarrier $\check{n}_k \leftarrow \arg\min_{n\in\mathcal{N}} \text{SNR}_{k,n}$
5. Calculate EE $\leftarrow \max_{P_k \geq R_k^{-1}} \frac{R_k(\check{n}_k, P_k)}{\zeta P_k + \alpha_{k,\text{RIS}} P_c}$
6. **End**
7. **While** $\mathcal{N} \neq \phi$
8. Find the UE $\check{k} \in \mathcal{K}$ such that $\check{k} \leftarrow \arg\min_{k\in\mathcal{K}} \text{EE}$
9. Find the UE $\hat{n} \in \mathcal{N}$ such that $\hat{n} \leftarrow \arg\max_{n\in\mathcal{N}} \text{SNR}_{k,n}$
10. Set $\rho_{\check{k},\hat{n}} \leftarrow 1$; $\varrho_{\check{k}} \leftarrow \varrho_{\check{k}} \cup \hat{n}_{\check{k}}$; $\mathcal{N} \leftarrow \mathcal{N} \setminus \{\hat{n}_{\check{k}}\}$
11. Calculate EE $\leftarrow \max_{P_k \geq R_k^{-1}(\varrho_k, R_k)} \frac{R_k(\varrho_k, P_k)}{\zeta P_k + (\alpha_{k,\text{RIS}} P_c)}$
12. **End**

Notably, the MDSA algorithm does not impose a total transmit power constraint explicitly. However, this constraint is likely to be automatically satisfied during subcarrier allocation for several reasons:

By appropriately choosing the parameter $\alpha_{k,\text{RIS}}$, the eventually optimized individual EEs tend to converge to similar values. If a UE initially requires excessive power to meet its QoS, it likely has a lower individual EE and will request more subcarriers later. This allows the UE to reduce its transmit power and increase its EE. In this work, a fixed set of parameters $\boldsymbol{\alpha}_{1,\text{RIS}}, \boldsymbol{\alpha}_{2,\text{RIS}}, \ldots, \boldsymbol{\alpha}_{K,\text{RIS}}$ is employed for more simplification.

When the EE improvement achieved by the energy-efficient design compared to the spectral-efficient design is substantial, the actual transmit power used for the energy-efficient design should be significantly lower than the maximum transmit power, ensuring efficient power utilization.

In the following, we delve into the SQP method employed to optimize power allocations.

3.1.2. Power Allocations

The sequential quadratic programming method is an iterative optimization technique used to solve constrained optimization problems, often encountered in mathematical modeling and engineering applications. SQP combines principles from both Newton's method and Lagrange multipliers to find the optimal solution within a feasible region defined by constraints.

In the context of SQP, the following subproblems should be defined:

$$\min_{\mathbf{P}\in\mathcal{P}} \quad g(\mathbf{P}) \tag{11}$$

$$\text{subject to} \quad b(\mathbf{P}) \leq 0, \quad \forall k = 1, 2, ..., K, \tag{11a}$$

where

$$g(\mathbf{P}) = -\left\{ \frac{\sum_{n\in\mathcal{N}} \rho_{k,n} r_{k,n}}{\xi \sum_{n=1}^{N} \rho_{k,n} p_{k,n} + \alpha_{k,\text{RIS}} \times P_c} \right\} \tag{12}$$

and

$$b(\mathbf{P}) = -\sum_{n\in\mathcal{N}} \rho_{k,n} r_{k,n} + \hat{R}_k \quad \forall k = 1, 2, ..., K. \tag{13}$$

The primary idea behind the SQP method is to use a second-order subproblem at the current point $\mathbf{P}^{(t)}$ and minimize this subproblem to determine the new point $\mathbf{P}^{(t+1)}$.

In its simplest form, the SQP method defines the second-order subproblem in the t_{th} iteration as follows:

$$\min_{\mathbf{P}} \quad \frac{1}{2} d^T \nabla^2_{\mathbf{PP}} L(\mathbf{P}^{(t)}, \lambda^{(t)}) d + \nabla^T g(\mathbf{P}^{(t)}) d + g^{(t)} \tag{14}$$

$$\text{s.t.} \quad \nabla^T b(\mathbf{P}^{(t)}) d + b(\mathbf{P}^{(t)}) = 0, \tag{14a}$$

$$\nabla^T b(\mathbf{P}^{(t)}) d + b_i(\mathbf{P}^{(t)}) \leq 0. \tag{14b}$$

Here, $\nabla^2_{\mathbf{PP}} L(\mathbf{P}^{(t)}, \lambda^{(t)})$ is the Hessian matrix (second-order partial derivatives matrix) of the Lagrange function for the problem (11), $\nabla^T g(\mathbf{P}^{(t)})$ denotes the gradient of the objective function at point $\mathbf{P}^{(t)}$, $\nabla^T b(\mathbf{P}^{(t)})$ represents the gradient of the constraints, and d is the direction of motion.

$$L(\mathbf{P}^{(t)}, \lambda^{(t)}) = g(\mathbf{P}^{(t)}) + \lambda * b(\mathbf{P}^{(t)}) \tag{15}$$

Solving this second-order subproblem yields the solution $(d^{(t)}, \lambda)$, which, under Karush–Kuhn–Tucker (KKT) conditions, is valid for the problem. A merit function is designed to assess solution suitability and balance the decrease rate of the objective function with respect to the established problem constraints.

The iterations continue until an acceptable answer is acquired [11]. The SQP algorithm is presented in Algorithm 2.

3.2. Optimization with Respect to RIS Phase Shift Matrix

Consider the optimized values for the vectors $\boldsymbol{\rho}$ and $\boldsymbol{P}$ obtained in the first step of the AO algorithm. The EE optimization problem with respect to RIS phase shifts is formulated as follows:

$$\underset{\mathbf{\Phi}}{\text{maximize}} \quad \text{EE} = \frac{\sum_{k=1}^{K} \sum_{n=1}^{N} \rho_{k,n} r_{k,n}}{\xi \sum_{k=1}^{K} p_k + P_{\text{BS}} + KP_{\text{UE}} + MP_m(b)} \tag{16}$$

$$\text{subject to} \quad |\phi_m| = 1, \quad \forall n = 1, 2, \ldots, M. \tag{16a}$$

In this problem, *EE* represents Energy Efficiency, $\mathbf{\Phi}$ is the RIS phase shift matrix, and the constraints in (16a) ensure that the phase shifts have unit magnitude. This EE maximization problem can be transformed into a rate maximization problem with respect to the RIS phase shift variables.

$$\underset{\mathbf{\Phi}}{\text{maximize}} \quad R_{\text{EE}} = \sum_{k=1}^{K} \sum_{n=1}^{N} \rho_{k,n} r_{k,n} \tag{17a}$$

$$\text{subject to} \quad |\phi_m| = 1, \quad \forall n = 1, 2, \ldots, M. \tag{17b}$$

To tackle this optimization problem, we employ the PSO algorithm, renowned for its versatility in solving complex optimization tasks. PSO maintains a population of particles, each associated with a phase shift vector, and efficiently explores the solution space to find optimal solutions. Here is a more detailed breakdown of the key operations and parameters in the PSO algorithm.

Algorithm 2: Sequential fractional programming algorithm.

1. Choose parameters $\eta \in (0, 0.5), \tau \in (0, 1)$, and an initial pair $(x^{(0)}, \lambda^{(0)})$;
2. Evaluate $g^{(0)}, \nabla g^{(0)}, b^{(0)}, A^{(0)}$;
3. If a quasi-Newton approximation is used, choose an initial $n \times n$ symmetric positive definite Hessian approximation $B^{(0)}$, otherwise compute $\nabla^2_{xx}\mathcal{L}^{(}0)$;
4. **repeat** until a convergence test is satisfied
5. Compute $d^{(t)}$ by solving (14); let $\hat{\lambda}$ be the corresponding multiplier;
6. Set $d_\lambda \leftarrow \lambda - \lambda^{(t)}$;
7. Choose $\mu^{(t)}$ to satisfy $\mu \geq \frac{\nabla f_k^T p_k + \frac{\sigma}{2} p_k^T \nabla^2_{xx} L_k p_k}{(1-\rho)\|c_k\|_1}$ with $\sigma = 1$;
8. Set $\alpha^{(t)} \leftarrow 1$;
9. **while** $O(x^{(t)} + \alpha^{(t)} d^{(t)}; \mu^{(t)}) \leq O(x^{(t)}; \mu^{(t)}) + \eta \alpha^{(t)} D(O(x^{(t)}; \mu^{(t)}), d^{(t)})$
10. Reset $\alpha^{(t)} \leftarrow \tau^{(t)} \alpha^{(t)}$ and $\lambda^{(t+1)} \leftarrow \lambda^{(t)} + \alpha^{(t)} d_\lambda$;
11. **end(while)**
12. $x^{(t+1)} \leftarrow x^{(t)} + \alpha^{(t)} d^{(t)}$ and $\lambda^{(t+1)} \leftarrow \lambda^{(t)} + \alpha^{(t)} d_\lambda$;
13. Evaluate $g^{(t+1)}, \nabla g^{(t+1)}, b^{(t+1)}, A^{(t+1)}$, (and possibly $\nabla^2_{xx}\mathcal{L}^{(t+1)}$);
14. If a quasi-Newton approximation is used, set
15. $d^{(t)} \leftarrow \alpha^{(t)} d^{(t)}$ and $y^{(t)} \leftarrow \nabla_x \mathcal{L}(x^{(t+1)}, \lambda^{(t+1)}) - \nabla^x \mathcal{L}(x^{(t)}, \lambda^{(t+1)})$,
16. and obtain $B^{(t+1)}$ by updating $B^{(t)}$ using a quasi-Newton formula;
17. **repeat**

The PSO algorithm, outlined in Algorithm 3, efficiently explores the solution space by maintaining a population of particles with associated phase shift vectors. The algorithm's complexity is proportional to the product of the population size L and the maximum number of iterations T.

For each particle $i = 1, 2, \ldots, L$ at time t, it is associated with a $1 \times M$ phase shift vector $\boldsymbol{\theta}_i^{(t)} = (\theta_{i1}, \theta_{i2}, \ldots, \theta_{iM})$, where each component is limited within $[-v_{\max}, v_{\max}]$. The fitness value of each particle is evaluated using the fitness function $R'_{\mathrm{EE}}(\boldsymbol{\theta})$, which can be defined as follows:

$$R'_{\mathrm{EE}}(\boldsymbol{\theta}) = -R_{\mathrm{EE}}. \tag{18}$$

Finding the maximum value of R_{EE} in Equation (17) is equivalent to finding the minimum value of $R'_{\mathrm{EE}}(\boldsymbol{\theta})$. $\boldsymbol{q}_{\mathrm{best},i}^{(t)}$ and $z_{\mathrm{best}}{}^{(t)}$ are defined as the optimal position of particle i and the optimal position of the entire population after t iterations. The following equations update, at each current iteration $t+1$, the velocity v and position of $\boldsymbol{\theta}$ of each particle i as:

$$\mathbf{v}_i^{(t+1)} = \omega \mathbf{v}_i^{(t)} + \boldsymbol{k}_1 \mathbf{u}_1 (\mathbf{q}_{\mathrm{best},i} - \boldsymbol{\theta}_i^{(t)}) + \boldsymbol{k}_1 \mathbf{u}_2 (\mathbf{z}_{\mathrm{best}}^t - \boldsymbol{\theta}_i^{(t)}), \tag{19}$$

$$\boldsymbol{\theta}_i^{(t+1)} = \boldsymbol{\theta}_i^{(t)} + \mathbf{v}_i^{(t+1)}. \tag{20}$$

In the context of our optimization process, we denote $\mathbf{v}$ as the velocity vector, and ω is employed as the inertia weight to carefully balance between local exploitation and global exploration. To introduce stochasticity, we utilize $\mathbf{u}_1$ and $\mathbf{u}_2$ as random vectors uniformly distributed within the interval [0, 1] for each dimension of the search space (where D

represents the dimensionality or size of the problem). Additionally, we incorporate k_1 and k_2, which we refer to as acceleration coefficients, as positive constants [23–25].

Algorithm 3: Particle swarm optimization algorithm.

1. Initialize $L, T, \omega, u_1, u_2, k_1, k_2$;
2. **for** $i = 1, 2, \ldots, L$ **do**
3. **Initialize** $\boldsymbol{\theta}_i^{(0)}, \mathbf{v}_i^{(0)}, \mathbf{q}_{\text{best},i}^{(0)} = \boldsymbol{\theta}_i^{(0)}$;
4. **end for**
5. Find $\acute{R}_{\text{EE}}(\mathbf{q}_{\text{best}}^{*(0)}) = \min\{\acute{R}_{\text{EE}}(\mathbf{q}_{\text{best},1}^{*(0)}), \ldots, \acute{R}_{\text{EE}}(\mathbf{q}_{\text{best},L}^{(0)})\}$, and set $\mathbf{z}_{\text{best}}^{(0)} = \mathbf{q}_{\text{best},1}^{*(0)}$;
6. **while** $t \leq T$ **do**
7. **for** $i = 1, 2, \ldots, L$ **do**
8. Update the velocity and position of particles using Equations (19) and (20):
9. Evaluate fitness value;
10. Calculate the historical optimal position of particle i:
11. $\mathbf{q}_{\text{best},i}^{(t+1)} = \begin{cases} \mathbf{q}_{\text{best},i}^{(t)}, & \acute{R}_{\text{EE}}(\mathbf{q}_{\text{best},i}^{(t)}) \leq \acute{R}_{\text{EE}}(\boldsymbol{\theta}_i^{(t+1)}), \\ \boldsymbol{\theta}_i^{(t+1)}, & \acute{R}_{\text{EE}}(\mathbf{q}_{\text{best},i}^{(t)}) > \acute{R}_{\text{EE}}(\boldsymbol{\theta}_i^{(t+1)}); \end{cases}$
12. Find $\acute{R}_{\text{EE}}(\mathbf{q}^{*(t+1)}) = \min\{\acute{R}_{\text{EE}}(\mathbf{q}_1^{(t+1)}), \ldots, \acute{R}_{\text{EE}}(\mathbf{q}_L^{(t+1)})\}$;
13. **end for**
14. Calculate the historical optimal position of the population:
15. $\mathbf{z}_{\text{best}}^{(t+1)} = \begin{cases} \mathbf{z}_{\text{best}}^{(t)}, & \acute{R}_{\text{EE}}(\mathbf{z}_{\text{best}}^{(t)}) \leq \acute{R}_{\text{EE}}(\mathbf{q}_{\text{best}}^{*(t+1)}), \\ \mathbf{q}_{\text{best}}^{*(t+1)}, & \acute{R}_{\text{EE}}(\mathbf{z}_{\text{best}}^{(t)}) > \acute{R}_{\text{EE}}(\mathbf{q}_{\text{best}}^{*(t+1)}); \end{cases}$
16. Adjust adaptive parameter shown in Algorithm 4;
17. Set $t \leftarrow t + 1$.
18. **end while**

The PSO algorithm proceeds through the outlined stages as detailed in Algorithm 3.

- In lines 2–4, we initialize each particle's position, velocity, and historical best position.
- In line 5, we find the best position among all particles and update the historical best position of the entire population, denoted as $\mathbf{z}_{\text{best}}^{(t)}$. This is the position with the best fitness value.
- The iterative optimization process starts in line 6 and continues until the maximum number of iterations T is reached.
  - Within each iteration:
    - In lines 7–17, we perform operations for each particle i in the population.
    - Lines 7–8 update the velocity and position of the particle based on its previous position, the best position it has encountered ($\mathbf{q}_{\text{best},i}$), and the best position in the entire swarm ($\mathbf{z}_{\text{best}}$). This helps particles explore the solution space.
    - Line 9 evaluates the fitness value of the particle's current position.
    - Lines 10–11 update the historical best position of the particle based on whether the current position or the previous best position is better. This helps particles remember their best-performing positions.
    - After evaluating and updating each particle, we find the best position among all particles in line 12 and update the historical best position of the entire population ($\mathbf{z}_{\text{best}}^{(t+1)}$) in line 15.
    - The adaptive parameter is adjusted in lines 16 based on the performance of the swarm according to Algorithm 4.
    - The dynamic adjustment of ω aims to strike a balance between exploration and exploitation during the PSO algorithm's execution. It helps fine-tune the search process to improve convergence and find optimal solutions effectively.

The AO algorithm is presented in Algorithm 5.

Algorithm 4: Adjust adaptive parameter.

Initialize $c = 0$;
if $\mathbf{z}_{\text{best}}^{(t+1)} < \mathbf{z}_{\text{best}}^{(t)}$
  $flag = 1$;
else
  $flag = 0$;
end if
if $flag = 0$
  $c = c + 1$;
else
  $c = \max\{c - 1, 0\}$;
  if $c < 2$
    $\omega = 2\omega$;
  else if $c > 5$
    $\omega = \omega/2$;
  end if
end if

Algorithm 5: Alternating optimization algorithm.

Input: $K, N, M, \eta, P_{Bs}, P_{UE}, P_m(b), P_{max}, \sigma^2, \{R_{min,k}\}_{k=1}^{K}, \boldsymbol{h}_{R,n}^{k}, \boldsymbol{h}_{T,n}, \epsilon > 0$;
Output: $\rho^\star, \boldsymbol{P}^\star$, and $\boldsymbol{\Phi}^\star$
repeat
Fixing the RIS coefficients $\boldsymbol{\Phi} = \boldsymbol{\Phi}_0 = \frac{\pi}{2} \cdot \boldsymbol{I}_N$
Find the $\rho, \boldsymbol{P}$ according to MDSA Algorithm and SQP Algorithm
Fixing the power allocation $\rho, \boldsymbol{P}$, given initial $\boldsymbol{\Phi}_0$, update the RIS coefficients $\boldsymbol{\Phi}$ via PSO Algorithm
Until the objective value of (P1) with the obtained $\rho, \boldsymbol{P}$, and $\boldsymbol{\Phi}$ reaches convergence.
$\rho^\star = \rho, \boldsymbol{P}^\star = \boldsymbol{P}$, and $\boldsymbol{\Phi}^\star = \boldsymbol{\Phi}$

4. Simulation Results

In this section, we present the results of our proposed algorithm's performance evaluation through numerical simulations for downlink communications. All simulations were conducted using MATLAB 2019b. The simulation setup is based on an OFDM system with $N = 72$ subcarriers. The multiple single-antenna mobile users are considered to be randomly and uniformly distributed within the 100 m $\times$ 100 m rectangular region on the right-hand side of the RIS in the x–y plane. All the provided illustrations represent averaged outcomes obtained from 10^3 independent scenarios involving variations in users' positions and channel characteristics. These scenarios were generated following the 3GPP propagation environment detailed in [26], and the relevant parameters are outlined in Table 1. The performance of our proposed joint resource allocation was compared with two benchmark schemes, random passive beamforming and without RIS, where the first scheme considers the BS-user direct link and performs the OFDMA resource allocation. The results also compared with the optimization approach using the genetic algorithm (GA) for phase shift optimization [27]. However, detailed information regarding these schemes are omitted in this context. The specific simulation parameters are outlined in Table 3.

Table 3. Simulation parameters.

Parameters	Values
Bandwidth of the BS B	180 KHz
Maximum transmit power at BS P_{max}	20 dBW
Circut power of the Bs P_B	39 dBm
Power amplifier efficiency at the Bs ν	0.8
Circut power of each user P_k	10 dBm
Circut power of each RIS element $P_m(b)$	10 dBm

It is noteworthy to point out that a majority of the papers listed in Table 1 primarily concentrate on optimizing the sum-rate. This poses a challenge when attempting to compare our results with the aforementioned papers. Moreover, the study in [21] focuses on maximizing EE and incorporates an active RIS in the system model, presenting a distinction from the system model considered in our work.

The graph in Figure 2 illustrates the performance of achievable EE with respect to variations in P_{max} in dBm. In this depiction, we have set the minimum QoS constraint as $R_{min} = 2.5$ bps/Hz and fixed $\alpha_{k,RIS}$ to 0.25 for all K users. Our study considers system parameters $M = 4$, $K = 4$, and $N = 72$. As depicted in Figure 2, an increase in P_{max} correlates with an increase in EE. Nevertheless, around $P_{max} = 12$ dBm, there is an underutilization of excess transmit power, resulting in a decline in energy efficiency. This can be attributed to the fact that the EE function does not exhibit a strictly increasing trend with the maximum BS transmit power, P_{max}. Instead, it reaches a finite maximizer. It is essential to emphasize that the proposed algorithm for passive beamforming optimization using PSO outperforms the one using GA, random passive beamforming optimization, as well as the scenario without RIS in terms of EE. Moreover, Figure 3 illustrates the average SE versus P_{max} for different schemes. It can be observed that with an increase in P_{max}, there is an enhancement in the achievable SE for all the schemes. It also underscores that for low values of P_{max}, the problem is frequently infeasible. This is expected since the BS lacks adequate transmit power to meet the rate requirements of the users, leading to significantly low SE values. Nevertheless, as P_{max} increases, the attainable SE starts to rise. Additionally, similar to the trend in Figure 2, the proposed algorithm for passive beamforming optimization using PSO outperforms other schemes. Besides, Figure 4 portrays the performance of EE concerning the number of RIS elements, denoted as M. As observed, when M is relatively small, i.e., $M \leq 10$, all designs except for the without-RIS scheme, exhibit the same trend. Particularly, EE performance increases as M increases. However, as M assumes moderate to intermediate values and beyond, EE undergoes a reduction, substantiating the existence of an optimal M for the maximization of EE objectives [28]. The proposed scheme exhibits a significant improvement when contrasted with a random passive beamforming mechanism. Conversely, the performance of the without-RIS scheme remains unaffected by the number of RIS elements in the system, implying the enhancement achievable through RIS in the wireless communication environment.

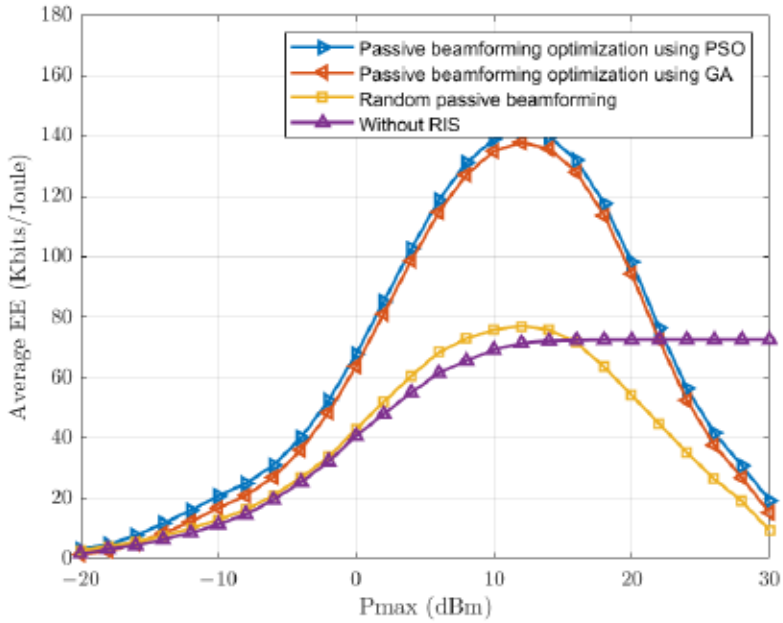

Figure 2. Average EE versus P_{max} for $R_{min} = 2.5$ bps/Hz, $\alpha_{k,RIS} = 0.25$, and $M = 4, K = 4, N = 72$.

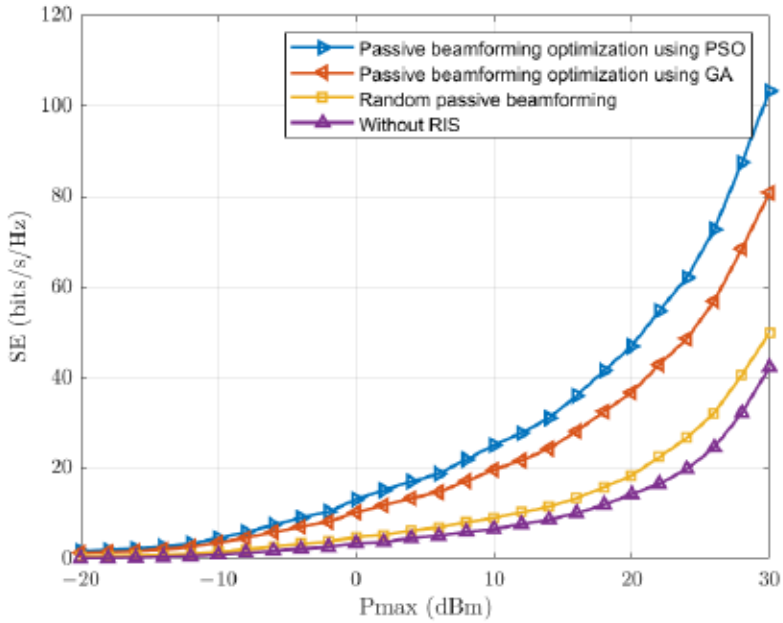

Figure 3. Average SE versus P_{max} for $R_{min} = 2.5$ bps/Hz, $\alpha_{k,RIS} = 0.25$, and $M = 4, K = 4, N = 72$.

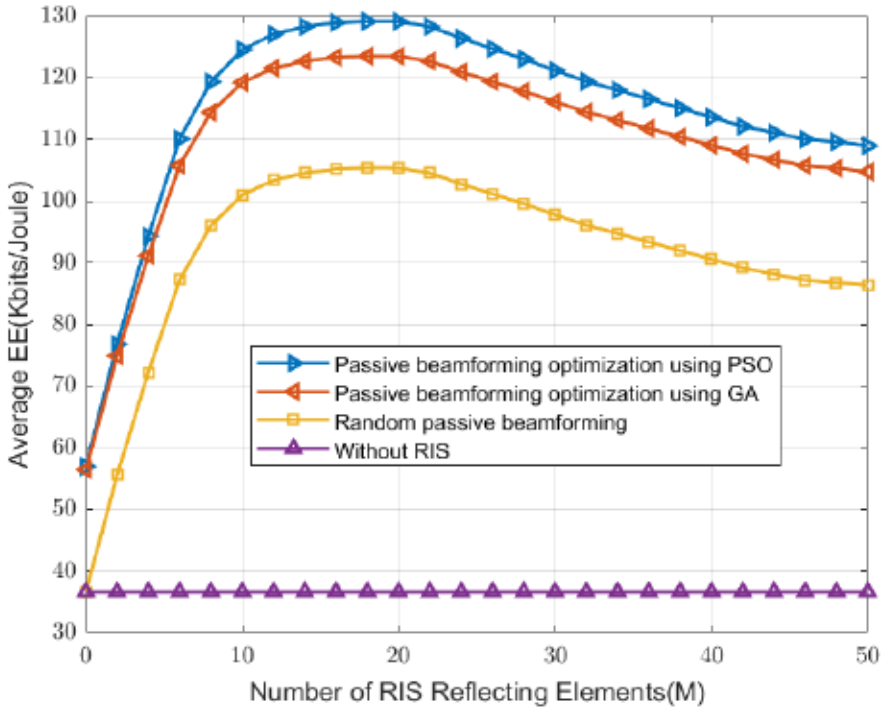

Figure 4. Average EE versus number of RIS elements, M for $R_{\min} = 2.5$ bps/Hz, $\alpha_{k,\mathrm{RIS}} = 0.25$, $P_{\max} = 20$ dBm, and $K = 4$, $N = 72$.

Remark

- Complexity
  Securing the optimal solution for problem (P1) requires the application of a power allocation algorithm to each feasible subcarrier assignment that meets the constraint in Equation (4) and subsequently selecting the assignment with the highest EE. Its computational complexity depends on the number of optimizing variables, which can be large if the number of subcarriers and/or the number of UEs is large. Nevertheless, the associated complexity proves excessively high, rendering it impractical for real-world scenarios.
  In contrast, the proposed sub-optimal solution, facilitated by the MDSA algorithm, eliminates the need to optimize a joint and intricate objective in each step. Subcarrier assignment becomes more manageable with this pragmatic approach. This is because, for each UE, the maximum of its individual EE is contingent solely upon its parameters and the subcarriers it will occupy, without reliance on the power adaptation strategies of other UEs. The complexity of the MDSA algorithm for a given $\boldsymbol{\alpha}_{k,\mathrm{RIS}}$ is roughly $\mathcal{O}((N_{OL}N)$ times that of the SQP method, where N_{OL} is the number of iterations in the outer layer, and N is the total number of subcarriers.
  The complexity of the SQP algorithm is dependent on the QP subproblem. By using modern interior-point (IP) methods for solving subproblems, a polynomial bound of computational complexity results [29]. Additionally, it is observed that the computational complexity of the PSO algorithm mainly involves the computation of fitness values of L passive beamformers for K users. Thus, the computational complexity is $\mathcal{O}((LK\log(L))$. It is clear that the complexity of the PSO algorithm is only linearly increasing with the number of particles L.
- Convergence
  The iterative alternating algorithm for solving the EE maximization problem (P3) is given in Algorithm 5. Since the updates through SQP and PSO all maximize the objective function at each iteration, the iterations in Algorithm 5 lead to a monotone in-

crease of the objective function of problem (P3). Since the objective function under the power and amplitude reflection coefficient constraints are bounded, the convergence of the alternating maximization algorithm can be guaranteed with the monotonic convergence theorem [30].

5. Conclusions and Future Work

This study seamlessly integrates RIS technology into multi-user downlink OFDMA communication systems, optimizing RIS reflection coefficients, OFDMA frequency allocations, and power distributions. Guided by stringent QoS requirements and transmission power constraints, as well as unit modulus constraint on the RIS phase shifts, the efficiency-focused methodology systematically address these multifaceted optimizations. These strategies redefine the original problem, deriving computationally accessible lower bounds on energy efficiency while striking a harmonious balance between performance enhancement and real-world feasibility. At its core, the AO algorithm, featuring the MDSA, SQP, and PSO approaches, effectively addresses complex challenges in energy-efficient wireless networks. Robust numerical results confirm substantial energy efficiency improvements compared to non-RIS scenarios. Our current work focuses on the simplicity of the SISO system, avoiding the complexities introduced by MISO and MIMO systems. For future research, we propose the exploration of the application of multiple antennas at both transmitter and receiver ends, anticipating a deeper understanding and a broader scope of findings.

Author Contributions: Conceptualization, S.B. and M.A.O.; methodology, S.B.; software, S.B.; validation, S.B., M.A.O., M.B. and D.M.; formal analysis, S.B.; investigation, S.B.; resources, S.B.; data Creation, S.B.; writing—original draft preparation, S.B.; writing—review and editing, S.B., M.A.O., M.B. and D.M; visualization, S.B.; supervision, M.A.O. and M.B.; project administration, S.B.; funding acquisition, S.B., M.A.O. and M.B. All authors have read and agreed to the published version of the manuscript.

Funding: This study received no external funding.

Data Availability Statement: Please contact the corresponding author at samaneh.bidabadi@uqtr.ca.

Conflicts of Interest: The authors declare no conflicts of interest.

Acronyms

RF	Radio Frequency
EE	Energy Efficiency
SE	Spectral Efficiency
RB	Resource block
GA	Gradient decent algorithm
RL	Reinforcement Learning
QoS	quality-of-service
ZF	Zero-Forcing
RIS	Reconfigurable Intelligent Surface
OFDM	Orthogonal Frequency Division Multiplexing
OFDMA	Orthogonal Frequency Division Multiple Access
SISO	Single Input Single Output
MISO	Multiple Input Single Output
MIMO	Multiple Input Multiple Output
APs	access points
MU	Multiple User
SNR	Signal to Noise Ratio
SINR	Signal to Interference Plus Noise Ratio
AWGN	Additive White Gussian Noise
CSI	Channel State Information
SCA	sine cosine algorithm

MM	Majorization–Minimization
OBR-FL	optimal beam reflection based on federated learning
MC	Monte Carlo
AO	Alternating Optimization
KKT	Karush Kuhn Tucker
SQP	Sequential Programming Method
PSO	Particle Swarm Optimization

Appendix A. Proof of Theorem 1

Proof. Consider the optimal subcarrier and power allocation matrices, denoted as $\boldsymbol{\rho}^{opt}$ and $\boldsymbol{P}^{opt}$, respectively, for (8). In this context, $\hat{\mathrm{EE}}$ represents the energy efficiency defined as $\hat{\mathrm{EE}} = \frac{\sum_{k\in K}\sum_{n\in N}\rho_{k,n}^{opt} r_{k,n}^{opt}}{\zeta\sum_{k\in K}\sum_{n\in N}p_{k,n}^{opt}+P_c}$.

For any fixed values of $\boldsymbol{\rho} \in \varrho$ and $\boldsymbol{P} \in \mathcal{P}$, we can express the energy efficiency, denoted as EE, as follows:

$$\begin{aligned}\mathrm{EE} &= \frac{\sum_{n\in N}\sum_{k=1}^{K}\rho_{k,n}r_{k,n}}{\sum_{n\in N}\sum_{k=1}^{K}(\zeta p_{k,n}+\alpha_{k,\mathrm{RIS}}P_c)} \\ &\geq \min_{k\in\mathcal{K}}\frac{\sum_{n\in N}\rho_{k,n}r_{k,n}}{\sum_{n\in N}(\zeta p_{K,n}+\alpha_{K,\mathrm{RIS}}P_c)}.\end{aligned} \tag{A1}$$

Here, $\boldsymbol{\alpha}_{K,\mathrm{RIS}} \in \alpha_{K,\mathrm{RIS}}$, and equality holds if and only if:

$$\frac{\sum_{n\in N}\rho_{1,n}r_{1,n}}{\sum_{n\in N}\zeta p_{1,n}+\alpha_{1,\mathrm{RIS}}P_c} = \cdots = \frac{\sum_{n\in N}\rho_{K,n}r_{K,n}}{\sum_{n\in N}\zeta p_{K,n}+\alpha_{K,\mathrm{RIS}}P_c}. \tag{A2}$$

This equality condition implies that $\alpha_{k,\mathrm{RIS}}$ can be expressed as $\alpha_{k,\mathrm{RIS}} = \frac{\sum_{n\in\mathcal{N}}\rho_{k,n}r_{k,n}}{\hat{\mathrm{EE}}P_c} - \frac{\sum_{n\in\mathcal{N}}\zeta p_{k,n}}{P_c}$.

Furthermore, it is evident that:

$$\hat{\mathrm{EE}} = \max_{\rho\in\varrho,\boldsymbol{P}\in\mathcal{P}}\mathrm{EE} \geq \max_{\rho\in\varrho,\boldsymbol{P}\in\mathcal{P}}\left\{\min_{k\in\mathcal{K}}\frac{\sum_{n\in\mathcal{N}}\rho_{k,n}r_{k,n}}{\sum_{n\in\mathcal{N}}\zeta p_{k,n}\alpha_{k,\mathrm{RIS}}P_c}.\right\} \tag{A3}$$

In this equation, $\boldsymbol{\alpha}_{K,\mathrm{RIS}} \in \alpha_{K,\mathrm{RIS}}$. Therefore, the right-hand side (RHS) cannot exceed the left-hand side (LHS) for any $\boldsymbol{\alpha}_{K,\mathrm{RIS}} \in \alpha_{K,\mathrm{RIS}}$. Additionally, equality always holds if the RHS uses the same $\boldsymbol{\rho}$ and $\boldsymbol{P}$ as $\boldsymbol{\rho}^{opt}$ and $\boldsymbol{P}^{opt}$ that achieve the LHS. This requires setting $\{\alpha_{k,\mathrm{RIS}}\}$ such that $\alpha_{k,\mathrm{RIS}} = \alpha_{k,\mathrm{RIS}}^{opt} \triangleq \frac{\sum_{n\in\mathcal{N}}\rho_{k,n}^{opt}r_{k,n}^{opt}}{\hat{\mathrm{EE}}P_c} - \frac{\sum_{n\in\mathcal{N}}\zeta p_{k,n}^{opt}}{P_c}$. It becomes apparent that through a straightforward substitution of $\alpha_{k,\mathrm{RIS}}^{opt}$ in the expression for $\hat{\mathrm{EE}}$, $\hat{\mathrm{EE}} = \frac{\sum_{k\in K}\sum_{n\in N}\rho_{k,n}^{opt}r_{k,n}^{opt}}{\zeta\sum_{k\in K}\sum_{n\in N}p_{k,n}^{opt}+P_c}$; we can draw the conclusion that the sum of the optimized $\alpha_{k,\mathrm{RIS}}^{opt}$ values for all k in $\mathcal{K}$ equals 1.

This concludes the proof. □

References

1. Jamil, S.; Rahman, M.; Abbas, M.S.; Fawad. Resource Allocation Using Reconfigurable Intelligent Surface (RIS)-Assisted Wireless Networks in Industry 5.0 Scenario. *Telecom* **2022**, *3*, 163–173. [CrossRef]
2. Yang, Y.; Zhang, S.; Zhang, R. IRS-enhanced OFDM: Power allacation and passive array optimization. In Proceedings of the IEEE Global Commun. Conf. (Globecom), Waikoloa, HI, USA, 9–13 December 2019; pp. 1–6. Available online: https://arxiv.org/abs/1905.00604 (accessed on 9 December 2019).
3. Bidabadi, S.; Ouameur, M.A.; Bagaa, M.; Massicotte, D. Energy efficient resource allocation for re-configurable intelligent surface-assisted wireless networks. *EURASIP J. Wirel. Commun. Netw.* **2023**, *2023*, 89. [CrossRef]
4. Lee, G.; Jung, M.; Kasgari, A.T.; Saad, W.; Bennis, M. Deep reinforcement learning for energy-efficient networking with reconfigurable intelligent surfaces. In Proceedings of the IEEE International Conference on Communications (ICC), Dublin, Ireland, 7–11 June 2020; pp. 1–6.

5. Tan, F.; Xu, X.; Chen, H.; Li, S. Energy-efficient beamforming optimization for MISO communication based on reconfigurable intelligent surface. *Phys. Commun.* **2023**, *3*, 101996. [CrossRef]
6. He, Z.; Shen, H.; Xu, W.; Zhao, C. Low-cost passive beamforming for ris-aided wideband ofdm systems. *IEEE Wirel. Commun.* **2022**, *11*, 318–322. [CrossRef]
7. An, J.; Wu, Q.; Yuen, C. Scalable channel estimation and reflec- tion optimization for reconfigurable intelligent surface-enhanced ofdm systems. *IEEE Wirel. Commun. Lett.* **2022**, *11*, 796–800. [CrossRef]
8. Yang, Y.; Zheng, B.; Zhang, S.; Zhang, R. Intelligent Reflecting Surface Meets OFDM: Protocol Design and Rate Maximization. June 2019. Available online: https://arxiv.org/pdf/1906.09956 (accessed on 9 December 2019).
9. Li, R.; Sun, S.; Tao, M. Ergodic achievable rate maximization of RIS-assisted millimeter-wave MIMO-OFDM communication systems. *IEEE Trans. Wirel. Commun.* **2022**, *22*, 2171–2184. [CrossRef]
10. Saggese, F.; Kansanen, K.; Popovski, P. Localization-based OFDM framework for RIS-aided systems. *arXiv* **2023**, arXiv:2303.12763.
11. Wu, W.; Yang, F.; Zhou, F.; Wu, Q.; Hu, R.Q. Intelligent Resource Allocation for IRS-Enhanced OFDM Communication Systems: A Hybrid Deep Reinforcement Learning Approach. *IEEE Trans. Wirel. Commun.* **2023**, *22*, 4028–4042. [CrossRef]
12. Chen, P.; Li, X.; Matthaiou, M.; Jin, S. DRL-Based RIS Phase Shift Design for OFDM Communication Systems. *IEEE Wirel. Commun. Lett.* **2023**, *12*, 733–737. [CrossRef]
13. Pradhan, C.; Li, A.; Song, L.; Li, J.; Vucetic, B.; Li, Y. Reconfigurable Intelligent Surface (RIS)-Enhanced Two-Way OFDM Communications. *IEEE Trans. Veh. Technol.* **2020**, *69*, 16270–16275. [CrossRef]
14. Wei, Z.; Cai, Y.; Sun, Z.; Ng, D.W.K.; Yuan, J.; Zhou, M.; Sun, L. Sum-Rate Maximization for IRS-Assisted UAV OFDMA Communication Systems. *arXiv* **2020**, arXiv:2008.09939.
15. Hao, W.; Sun, G.; Zeng, M.; Chu, Z.; Zhu, Z.; Dobre, O.A.; Xiao, P. Robust Design for Intelligent Reflecting Surface-Assisted MIMO-OFDMA Terahertz IoT Networks. *IEEE Internet Things J.* **2021**, *8*, 13052–13064. [CrossRef]
16. Li, Z.; Chen, W.; Wu, Q.; Zhu, X.; Qin, H.; Wang, K.; Li, J. Towards Transmissive RIS Transceiver Enabled Uplink Communication Systems: Design and Optimization. *IEEE Internet Things J.* **2023**, *11*, 6788–6801. [CrossRef]
17. Yu, H.; Tuan, H.D.; Nasir, A.A.; Dutkiewicz, E.; Hanzo, L. Rate-Fairness-Aware Low Resolution RIS-Aided Multi-User OFDM Beamforming. *IEEE Trans. Veh. Technol.* **2024**, *73*, 2401–2415. [CrossRef]
18. Ghanem, W.R.; Jamali, V.; Schober, R. Joint Beamforming and Phase Shift Optimization for Multicell IRS-aided OFDMA-URLLC Systems. In Proceedings of the 2021 IEEE Wireless Communications and Networking Conference (WCNC), Nanjing, China, 29 March–1 April 2021; pp. 1–7. [CrossRef]
19. Ma, D.; Li, L.; Ren, H.; Wang, D.; Li, X.; Han, Z. Distributed Rate Optimization for Intelligent Reflecting Surface with Federated Learning. In Proceedings of the 2020 IEEE International Conference on Communications Workshops (ICC Workshops), Dublin, Ireland, 7–11 June 2020; pp. 1–6. [CrossRef]
20. Yang, Y.; Zhang, S.; Zhang, R. IRS-enhanced OFDMA: Joint resource allocation and passive beamforming optimization. *IEEE Wireless Commun. Lett.* **2020**, *9*, 760–764. [CrossRef]
21. Wang, Y.; Peng, J. Energy Efficiency Fairness of Active Reconfigurable Intelligent Surfaces-Aided Cell-Free Network. *IEEE Access* **2023**, *11*, 5884–5893. [CrossRef]
22. Xiong, C.; Li, G.Y.; Zhang, S.; Chen, Y.; Xu, S. Energy-Efficient Resource Allocation in OFDMA Networks. *IEEE Trans. Commun.* **2012**, *60*, 3767–3778. [CrossRef]
23. Gad, A.G. Particle swarm optimization algorithm and its applications: A systematic review. *Arch. Comput. Methods Eng.* **2022**, *29*, 2531–2561. [CrossRef]
24. Dai, J.; Wang, Y.; Pan, C.; Zhi, K.; Ren, H.; Wang, K. Reconfigurable intelligent surface aided massive MIMO systems with low-resolution DACs. *IEEE Commun. Lett.* **2021**, *25*, 3124–3128. [CrossRef]
25. Pedersen, M.E. *Good Parameters for Particle Swarm Optimization*; Hvass Laboratories: Luxembourg, 2010.
26. Björnson, E.; Sanguinetti, L.; Hoydis, J.; Debbah, M. Optimal design of energy-efficient multi-user MIMO systems: Is massive MIMO the answer? *IEEE Trans. Wireless Commun.* **2015**, *14*, 3059–3075. [CrossRef]
27. Peng, Z.; Li, T.; Pan, C.; Ren, H.; Xu, W.; Renzo, M.D. Analysis and optimization for RIS-aided multi-pair communications relying on statistical CSI. *IEEE Trans. Veh. Technol.* **2021**, *70*, 3897–3901. [CrossRef]
28. Zappone, A.; Renzo, M.D.; Xi, X.; Debbah, M. On the optimal number of reflecting elements for reconfigurable intelligent surfaces. *IEEE Wireless Commun. Lett.* **2021**, *10*, 464–468. [CrossRef]
29. Błaszczyk, J.; Karbowski, A.; Malinowski, K. Object Library of Algorithms for Dynamic Optimization Problems: Benchmarking SQP and Nonlinear Interior Point Methods. *Int. J. Appl. Math. Comput. Sci.* **2007**, *17*, 515–537. [CrossRef]
30. Grippo, L.; Sciandrone, M. On the convergence of the block nonlinear Gauss–Seidel method under convex constraints. *Oper. Res. Lett.* **2000**, *26*, 127–136. [CrossRef]

3.3 Optimisation des systèmes ISAC assistés par BD-RIS grâce à l'IA

3.3.1 Contexte

Cette section examine l'application des techniques d'optimisation basées sur l'IA pour améliorer les systèmes ISAC assistés par RIS, en mettant en avant les contributions les plus récentes de cette thèse. Nous explorons le déploiement de BD-RIS pour améliorer l'efficacité énergétique à travers des stratégies de formation de faisceau passives et actives, tout en assurant une performance fiable en communication et en détection. Cette tâche est complexe en raison des contraintes inhérentes aux configurations BD-RIS, telles que l'orthogonalité, les inégalités quartiques et la nature fractionnaire de la fonction objective. Pour relever ces défis de manière efficace, nous utilisons des techniques de renforcement profond de pointe, en particulier le modèle de TD3. Les résultats de simulation montrent des améliorations significatives des performances en termes d'efficacité énergétique par rapport aux méthodes traditionnelles. Les validations numériques confirment l'efficacité de notre approche proposée et soulignent les avantages de l'intégration de BD-RIS dans les systèmes ISAC.

3.3.2 Méthodologie

Nous avons commencé par examiner la littérature existante sur les systèmes de communication assistés par BD-RIS et les systèmes ISAC équipés de BD-RIS afin d'identifier les limites de l'état de l'art actuel, comme suit:

Systèmes de communication assistés par BD-RIS

Dans [77,78], les auteurs explorent un canal descendant MISO multi-utilisateurs assisté par un BD-RIS multi-secteurs, où les matrices RIS pour chaque cellule sont à connexions

simples et donc diagonales. L'optimisation des coefficients du BD-RIS multi-secteurs est réalisée sur la variété sphérique complexe. Les travaux de [79] examinent des modèles de BD-RIS plus généraux, y compris des architectures entièrement connectées avec des BD-RIS hybrides (réflectifs et transmissifs), et optimisent la matrice BD-RIS sur la variété de Stiefel. Dans [80], des techniques d'optimisation pour les BD-RIS avec une architecture à connexions groupées de taille deux ont été proposées, en utilisant la procédure convexe-concave pour rendre la contrainte unitaire convexe. Les travaux de [81, 82] présentent des solutions fermées pour les BD-RIS entièrement connectés, visant à maximiser le gain de canal équivalent pour les configurations SISO ainsi que MISO/SIMO. Ces solutions reposent sur différentes factorizations symétriques et unitaires de la matrice BD-RIS mais restent par ailleurs équivalentes. Plus récemment, une solution approximative visant à maximiser la somme des gains de canal équivalents lorsque le canal direct n'est pas bloqué dans un scénario MU-MISO a été décrite dans [83]. Cette solution sous-optimale consiste à résoudre un problème relâché (sans les contraintes d'unicité et de symétrie), puis à projeter la solution obtenue sur l'ensemble des matrices symétriques et unitaires, pour lequel une solution fermée existe. L'article [83] aborde l'optimisation d'un BD-RIS afin d'augmenter la puissance reçue par les utilisateurs dans un contexte MU-MISO. Ce travail adopte un modèle BD-RIS dépendant de la fréquence, avec une optimisation effectuée à une fréquence prioritaire. De plus, [83] ne contraint pas le BD-RIS à être sans pertes, ce qui permet à la matrice BD-RIS d'être symétrique sans être nécessairement unitaire. L'optimisation d'une liaison MIMO soutenue par un BD-RIS pour maximiser la capacité est traitée dans les recherches de [84]. En ajustant alternativement la matrice de covariance de transmission et la matrice de diffusion BD-RIS symétrique et unitaire, ils développent un algorithme efficace qui améliore systématiquement les performances par rapport à un RIS diagonal.

Les systèmes ISAC équipés de BD-RIS

Les systèmes ISAC équipés de BD-RIS ont fait l'objet de plusieurs études récentes [41]–[45], où le BD-RIS joue un rôle central dans l'optimisation des performances du réseau grâce à des stratégies de beamforming passives et actives [85–89]. Dans [85], Liu et *al.* ont conjointement conçu des filtres linéaires, un beamforming d'émission et des réponses de phase afin de maximiser le débit global des systèmes ISAC équipés de BD-RIS. Les travaux de [86] explorent l'utilisation du BD-RIS pour minimiser la puissance d'émission de la station de base dans les réseaux ISAC tout en maintenant la qualité des communications et des fonctions de détection, en employant une méthode de décomposition duale pénalisée pour gérer efficacement les contraintes. Par ailleurs, la matrice de diffusion du BD-RIS dans un système ISAC a été étudiée dans [87] afin de maximiser la somme pondérée des SNR au niveau du récepteur radar et des utilisateurs de communication. De plus, les travaux de [88] explorent l'optimisation de l'estimation des paramètres dans les systèmes ISAC activés par RIS en utilisant une combinaison de précodage d'émission de la station de base et de beamforming actif de réflexion RIS sous des contraintes de SINR, en utilisant un algorithme efficace basé sur l'optimisation alternée, la SDR et les méthodes MM. Dans [89], une nouvelle architecture d'émetteur assistée par BD-RIS est proposée pour améliorer les performances ISAC en ondes millimétriques en optimisant le taux de somme de communication et les valeurs propres de la matrice CRB de détection à travers un algorithme en deux étapes, montrant des améliorations significatives par rapport aux configurations conventionnelles de DRIS. Récemment, les méthodes de DRL ont gagné une attention considérable dans divers domaines scientifiques en tant qu'outils puissants pour l'optimisation des ressources. Le DRL a été largement utilisé pour optimiser la communication assistée par RIS [90], mais son application à l'optimisation des systèmes ISAC assistés par

RIS reste limitée [91–93]. Le travail présenté dans [91] utilisant un algorithme de méta-apprentissage par renforcement (en englais MRL, Meta-Reinforcement Learning) étudie les systèmes ISAC en duplex intégral assistés par STAR-RIS. L'objectif est d'optimiser les matrices de déphasage au niveau du STAR-RIS pour maximiser le taux de somme en présence d'informations imparfaites sur l'CSI. L'article [92] introduit un algorithme de méta-apprentissage basé sur la descente de gradient pour optimiser le beamforming dans les systèmes ISAC assistés par RIS, visant à minimiser la puissance d'émission de la station de base tout en respectant les contraintes de SINR et de la matrice CRB.

De plus, [93] propose un nouveau cadre de localisation et de communication simultanées (en englais SLAC, Simultaneous Localization and Communication) exploitant les systèmes ISAC assistés par RIS et les réseaux d'accès radio en nuage (en englais C-RAN, Cloud Radio Access Networks) pour améliorer l'efficacité de la localisation et des communications. Il utilise un algorithme hybride d'apprentissage par renforcement profond pour optimiser les performances globales du système.

Cette section explore l'application des techniques d'optimisation avancées basées sur l'IA pour améliorer les systèmes ISAC assistés par RIS, en mettant principalement l'accent sur le déploiement du BD-RIS pour améliorer l'EE. Ce travail représente la première tentative d'intégration de la technologie BD-RIS dans les systèmes ISAC tout en abordant la tâche complexe d'optimiser l'EE axée sur la communication. Ici, l'EE est défini comme le rapport entre le taux de communication réalisable et la consommation totale d'énergie, un indicateur clé qui garantit des opérations durables et performantes. Contrairement aux études précédentes qui ont abordé des problèmes d'optimisation plus simples, cette recherche traite d'un scénario plus complexe, où le problème d'optimisation de l'EE inclut

des termes fractionnaires dans sa fonction objective, combinés à des contraintes strictes liées à la précision de la détection (borne de Cramér-Rao, CRB) et à la fiabilité de la communication (rapport signal-sur-bruit plus interférence, SINR).

Pour relever ces défis, un cadre de modélisation complet pour les systèmes ISAC équipés de BD-RIS est développé en utilisant l'analyse des paramètres de diffusion du réseau. Ce modèle capture de manière précise les caractéristiques physiques clés, telles que les désaccords d'impédance et les effets de couplage mutuel entre l'émetteur, le RIS et le récepteur, garantissant une représentation physiquement cohérente du système. Le modèle inclut également des conditions idéales avec une correspondance parfaite et aucun couplage mutuel, se concentrant sur l'optimisation des matrices de beamforming d'émission et passives. De plus, nous développons des modèles de signal pour les utilisateurs de communication, les cibles et la station de base, nous permettant de calculer des métriques clés telles que le SINR pour la communication et la CRB pour l'estimation de la direction d'arrivée (DoA) pour la détection radar. Ces éléments sont intégrés dans un cadre d'optimisation unifié, visant à maximiser l'efficacité énergétique tout en satisfaisant diverses contraintes, y compris l'orthogonalité de la configuration du BD-RIS, les limites de puissance et la configuration du BD-RIS, y compris l'orthogonalité.

Étant donné la complexité du problème d'optimisation, cette recherche exploite des techniques avancées de DRL, en particulier l'algorithme TD3. L'algorithme TD3 est utilisé pour optimiser à la fois les stratégies de beamforming passif et actif, abordant la nature non linéaire et de haute dimension du problème. D'importantes simulations numériques valident la méthodologie proposée, montrant des améliorations significatives de l'EE par rapport aux approches conventionnelles et confirmant l'efficacité de l'intégration du BD-RIS dans les systèmes ISAC. Ce travail met non seulement en

évidence le potentiel du BD-RIS pour permettre des systèmes ISAC haute performance, mais souligne également le rôle transformateur de l'IA dans la résolution de problèmes d'optimisation complexes dans les réseaux sans fil de nouvelle génération.

3.3.3 Résultats

Notre analyse des schémas proposés, intitulés "TD3-BD-RIS" et "TD3-RIS", démontre que l'intégration du BD-RIS améliore considérablement l'EE par rapport au RIS conventionnel. À mesure que le nombre d'éléments RIS M augmente, les schémas BD-RIS surperforment systématiquement leurs homologues RIS diagonaux grâce à une flexibilité d'optimisation supérieure. Les éléments FC-BD-RIS améliorent encore l'EE en optimisant les conditions du canal, ce qui conduit à de meilleurs débits de données et à une consommation d'énergie réduite. Cependant, ces avantages sont atténués par les complexités, les coûts et les demandes en énergie associés à des configurations RIS plus grandes.

Lors de l'évaluation de l'impact des antennes de la BS N, le BD-RIS continue de présenter des performances supérieures par rapport aux conceptions MRT et ZF, bien que l'écart de performance se réduise à mesure que N augmente. Le schéma MRT montre de bonnes performances avec une variance de bruit plus faible, tandis que le schéma ZF est plus efficace avec une variance de bruit plus élevée. En ce qui concerne les exigences de QoS, l'augmentation de ces exigences conduit généralement à une diminution de l'EE en raison des besoins accrus en puissance d'émission. Malgré cela, le FC-BD-RIS continue de démontrer une meilleure EE par rapport aux configurations RIS diagonales conventionnelles. Le compromis entre la précision de détection et la performance de communication dans le schéma TD3-BD-RIS indique que, bien qu'une meilleure précision de détection réduise l'EE en raison de l'allocation de ressources

pour la détection, permettre une précision de détection plus faible pour améliorer la performance de communication met en évidence la capacité du BD-RIS à équilibrer efficacement ces aspects. La convergence de l'algorithme TD3 dans les scénarios BD-RIS et RIS est stable et fiable, reflétant des dynamiques d'apprentissage robustes et des performances cohérentes sur de nombreux épisodes.

En ce qui concerne la complexité totale du problème, l'utilisation de l'approche TD3 pour l'optimisation de l'EE dans les systèmes ISAC assistés par BD-RIS présente des avantages significatifs par rapport aux méthodes d'optimisation traditionnelles basées sur des modèles. La littérature existante sur les systèmes BD-RIS ISAC se concentre principalement sur la maximisation du débit ou la conception du beamforming, utilisant souvent des méthodes basées sur des modèles qui reposent sur des modèles système connus et des techniques d'optimisation linéaires ou convexes. Cependant, l'optimisation de l'EE est un problème non convexe et fractionnaire impliquant un ratio entre le débit et la consommation d'énergie, ce qui est difficile à résoudre avec les méthodes conventionnelles. En revanche, TD3 offre une solution sans modèle et évolutive qui peut optimiser conjointement le beamforming et les décalages de phase RIS sans nécessiter de modèle système explicite, ce qui en fait une solution idéale pour traiter le paysage d'optimisation non linéaire et de haute dimension de l'EE. L'algorithme TD3 peut naturellement incorporer des contraintes non linéaires (telles que SINR, CRB et limites de puissance) et optimiser directement l'objectif fractionnaire, surmontant les défis auxquels font face les méthodes basées sur des modèles. Cette approche offre une solution plus flexible, adaptable et efficace, en particulier pour les grands systèmes BD-RIS ISAC, où les méthodes traditionnelles peuvent avoir du mal à atteindre des performances optimales. Cependant, il est important de noter que, bien que TD3 offre des avantages de performance significatifs, il introduit également une complexité computationnelle

plus élevée, comme discuté ci-dessous.La complexité de la résolution du problème (??) provient à la fois de la complexité topologique du circuit de l'utilisation du FC-BD-RIS et de la complexité d'optimisation liée à l'algorithme TD3. La complexité topologique du circuit croît quadratiquement avec le nombre d'éléments RIS, $\mathcal{O}(M^2)$, car chaque élément de la matrice RIS $\mathbf{\Theta}$ est indépendamment reconfigurable. Cela contraste fortement avec les RIS diagonaux, où seuls les éléments diagonaux de $\mathbf{\Theta}$ sont contrôlés, ce qui réduit le nombre de composants reconfigurables à $\mathcal{O}(M)$. De plus, un RIS avec des décalages de phase aléatoires élimine le besoin d'optimisation, simplifiant ainsi la conception, mais au prix d'une perte de performance.

D'un point de vue optimisation, la complexité computationnelle de l'algorithme TD3 proposé pour résoudre le problème de maximisation de l'EE peut être analysée comme suit. Soit n_L le nombre de couches dans chaque réseau neuronal profond (DNN), et z_l le nombre de neurones dans la couche l. Pendant l'entraînement, l'évaluation et la mise à jour à chaque étape de temps nécessitent $\mathcal{O}(|\mathbb{B}|N_{\text{episode}}N_{\text{steps}}\sum_{l=1}^{n_L-1} z_l z_{l+1})$, où $|\mathbb{B}|$ est la taille du lot. Puisque l'algorithme TD3 implique un nombre fixe de DNNs et passe par $N_{\text{episode}} \times N_{\text{steps}}$ itérations pour terminer l'entraînement, où N_{steps} est le nombre d'étapes par épisode et N_{episode} est le nombre total d'épisodes.

3.3.4 Validation du Modèle et Limitations

Nous avons limité le travail à un modèle de système plus simple par rapport aux scénarios réels. Cependant, de meilleures performances peuvent être obtenues en prenant en compte des scénarios plus réalistes, comme suit:

- Nous négligeons les effets de couplage mutuel entre les éléments du RIS. Ce couplage se produit lorsque le champ électromagnétique généré par un

élément induit des courants dans les éléments voisins, modifiant leur excitation et compliquant le modèle de canal assisté par RIS. Souvent ignoré dans la littérature, le couplage mutuel est une propriété inhérente à la géométrie du RIS qui peut affecter les performances. Ne pas en tenir compte lors de l'optimisation du RIS peut entraîner une dégradation des résultats, ce qui rend essentielle une modélisation et une gestion appropriées pour maximiser les avantages du RIS. Les algorithmes d'optimisation prenant en compte le couplage mutuel existants souffrent d'une complexité computationnelle élevée en raison du grand nombre d'itérations nécessaires pour converger, ce qui devient prohibitif lorsque le nombre d'éléments du RIS augmente.

- Nous considérons un modèle de système à cible unique. Ce modèle peut être étendu à un cadre multi-cibles, offrant ainsi des perspectives plus approfondies sur la manière dont le BD-RIS peut simultanément gérer les interactions avec plusieurs utilisateurs et cibles, optimisant ainsi les performances dans divers scénarios. Dans des situations réelles, la position des utilisateurs et des cibles n'est pas fixe, ce qui implique que les conditions de canal dynamiques, dues à la mobilité des utilisateurs ou aux changements environnementaux, doivent être prises en compte, nécessitant ainsi l'utilisation d'algorithmes adaptatifs en temps réel.
- Bien que l'apprentissage par renforcement offre des solutions prometteuses pour les problèmes d'optimisation à haute dimension, son application en temps réel dans des réseaux à grande échelle présente des défis. Ces techniques nécessitent des ressources computationnelles considérables, ce qui peut limiter leur efficacité dans des environnements sensibles au temps. Explorer des moyens de simplifier ces algorithmes ou de les rendre plus légers, notamment par le biais de traitements distribués, pourrait constituer une piste intéressante pour les recherches futures.

Les systèmes de détection distribuée améliorent les capacités de détection en intégrant les données de plusieurs nœuds, mais ils rencontrent des problèmes tels que la synchronisation, la surcharge de contrôle et la gestion de grands volumes de données détectées. Des modèles d'apprentissage avancés, tels que l'apprentissage par transfert, l'apprentissage fédéré et les réseaux de neurones graphiques, peuvent aider à la compression des données et à la coordination. Cependant, les solutions d'IA basées sur les données rencontrent souvent des difficultés en matière de synchronisation en temps réel et d'évolutivité en raison des changements dynamiques du réseau. La découverte causale, notamment à travers des techniques comme la causalité de Granger et les modèles causaux structurels (en englais SCMs, structural causal models), est proposée comme une solution pour relever ces défis. Elle peut améliorer le suivi des faisceaux et le suivi dynamique des cibles en permettant une modélisation précise des positions des utilisateurs ou des scatterers. Grâce à des approches basées sur la théorie des jeux et au raisonnement causal, les nœuds de détection peuvent optimiser leurs stratégies, améliorer l'efficacité des communications et allouer dynamiquement leurs ressources. Ce processus soutient l'adaptabilité en temps réel et la synchronisation, éléments essentiels pour les réseaux sans fil de nouvelle génération.

- L'exploration des systèmes ISAC multi-bandes soutenus par RIS pourrait améliorer à la fois les capacités de détection et de communication en exploitant les propriétés complémentaires des différentes bandes de fréquences, ce qui pourrait également améliorer la précision du positionnement des utilisateurs grâce à l'estimation de l'CSI sur ces bandes. L'optimisation des systèmes ISAC soutenus par BD-RIS en utilisant l'OFDMA pourrait résoudre les problèmes de fading sélectif en

fréquence et améliorer l'efficacité de la détection radar et des communications. Les communications multi-porteurs offriraient des performances supérieures par rapport aux systèmes ISAC assistés par RIS utilisant une seule sous-porteuse.

3.3.5 Droits d'auteur

L'article suivant, dérivé de la thèse, est soumis [94].

AI-enabled Resource Allocation for BD-RIS Empowered ISAC Systems

Samaneh Bidabadi, Member, IEEE ,Messaoud Ahmed Ouameur, Member, IEEE ,Miloud Bagaa, Senior Member, IEEE ,Daniel Massicotte, Senior Member, IEEE ,Felipe De Figueiredo, Senior Member, IEEE ,and Anas Chaaban, Senior Member, IEEE

***Abstract*—Reconfigurable intelligent surfaces (RIS) have emerged as pivotal elements in enhancing integrated sensing and communication (ISAC) systems. Among RIS architectures, the beyond-diagonal (BD-RIS) design stands out for its advanced beamforming capabilities compared to traditional diagonal RIS. This paper investigates the deployment of BD-RIS to optimize energy efficiency through passive and active beamforming strategies while ensuring robust communication and sensing quality. The task is particularly challenging due to constraints inherent in BD-RIS configurations, including orthogonality, quartic inequalities, and the fractional nature of the objective function. To address these complexities, we employ twin delayed deep deterministic policy gradient (TD3) models, a state-of-the-art deep reinforcement learning (DRL) approach. Numerical validations confirm the effectiveness of our proposed algorithm and highlight the benefits of integrating BD-RIS into ISAC systems. Simulations demonstrate that incorporating BD-RIS leads to significant energy efficiency gains compared to benchmarks using diagonal RIS and RIS with random phase shifts.**

***Index Terms*—Reconfigurable intelligent surface, beyond-diagonal RIS, integrated sensing and communication system, deep reinforcement learning.**

I. Introduction

In the realm of next-generation wireless networks, both robust wireless connectivity and precise sensing capabilities are imperative [1]. The 6G network will act as a comprehensive sensor system, leveraging strengths such as interference management, wide area coverage, and tightly controlled operations. Integrated sensing and communication (ISAC) is a key enabling technology for 6G, building on the active localization capabilities of current 5G systems and the 3GPP standardization identifying use cases for ISAC, which enables the detection of non-network objects. Large public projects are already developing ISAC technologies and system designs for the future [3]–[5]. ISAC allows radar sensing and wireless communications to share resources like spectrum, hardware architecture, and signal processing platforms. By leveraging these congested resources, ISAC fosters mutual assistance by sharing information to enhance communication and sensing functionalities. This integration leads to improved performance in terms of spectral, energy, hardware, and cost efficiency [6], [7]. Meanwhile, reconfigurable intelligent surfaces (RIS) have emerged as a promising physical-layer technology that allows for flexible manipulation of wireless communication environments with high energy efficiency. Composed of a planar surface with numerous low-power, nearly-passive elements, RIS can reconfigure incident signals, thereby improving spectral efficiency (SE) and energy efficiency (EE) by dynamically optimizing the wireless propagation environment [9]–[12].

Recent advancements in RIS modeling underscore the need to move beyond the traditional approach, where RIS systems were modeled as ideal scatterers and relied on diagonal phase shift matrices, with each element individually controlled by a tunable impedance connected to ground. While this method was effective, it limited the flexibility of RIS operations. To address these limitations, ongoing research is focused on developing electromagnetically consistent RIS models that incorporate realistic reradiation models, taking into account mutual coupling between scattering elements and phase-amplitude correlation in reflection coefficients [9], [13], [14]. In this context, there has been a significant shift with the emergence of beyond diagonal RIS (BD-RIS) architecture. Unlike traditional RIS setups, BD-RIS incorporates tunable impedance networks that connect elements within the RIS. This advancement enables more intricate control over how signals are reflected and managed within the RIS environment. BD-RIS configurations vary in complexity. A fully-connected BD-RIS connects all elements through a reconfigurable impedance network [16]–[18], while a group-connected BD-RIS links specific groups of elements together [13], [14]. The introduction of BD-RIS, especially in fully-connected forms, has led to notable performance enhancements. Research indicates that fully-connected BD-RIS architectures can achieve maximum degrees-of-freedom, significantly improving received signal power and overall system efficiency [19].

The successful implementation of RIS in various communication contexts has sparked interest in integrating RIS with ISAC technologies [20]–[22]. ISAC represents a paradigm shift by integrating communication and sensing objectives through co-design approaches. Various advanced signal processing techniques are proposed to design dual-functional waveforms optimized for different communication and sensing metrics [25]–[29]. While typical communication metrics include signal-to-interference-plus-noise ratio (SINR) and multi-user interference (MUI), energy efficiency metrics remain underexplored in RIS-aided ISAC systems. The EE optimization problem in RIS-aided ISAC systems can address communication-centric EE, sensing-centric EE, and the trade-offs between them [15].

Meanwhile, common sensing metrics encompass beam-pattern mean squared error (MSE) and received echo power/signal-to-noise ratio (SNR). Additionally, the Cramér-Rao bound (CRB), pivotal for target parameter estimation,

warrants further exploration in ISAC-RIS aided communications [30], [31].

A. Prior Works

The related works are classified into two categories, as follows:

1) BD-RIS assisted communications systems: In [32], [33], the authors explore a multi-user multiple-input single-output (MU-MISO) downlink channel aided by a multi-sector BD-RIS, where the RIS matrices for each cell are single-connected and therefore diagonal. The optimization of multi-sector BD-RIS coefficients is conducted on the complex sphere manifold. The work in [34], examine more general BD-RIS models, including fully-connected architectures with hybrid (reflective and transmissive) BD-RIS, and optimize the BD-RIS matrix on the Stiefel manifold. Optimization techniques for BD-RIS with a group-connected architecture of group size two have been proposed in [35], employing the convex-concave procedure to convexify the unitary constraint. Closed-form solutions for fully-connected BD-RIS that maximize the equivalent channel gain for single-input single-output (SISO) and MISO/SIMO channels are presented in [36], [37].These solutions rely on different symmetric and unitary BD-RIS matrix factorizations but are otherwise equivalent. More recently, an approximate solution to maximize the sum of the equivalent channel gains when the direct channel is not blocked in an MU-MISO scenario has been described in [38]. This suboptimal solution involves solving a relaxed problem (without the unitary and symmetric constraints) and then projecting the relaxed solution onto the set of symmetric and unitary matrices, for which a closed-form solution exists. The optimization of a BD-RIS to maximize the power received by users in an MU-MISO scenario is discussed in [38]. This work adopts a frequency-dependent model for the BD-RIS, with optimization performed at a priority frequency. Furthermore, [38] does not impose the restriction of a lossless BD-RIS, so the BD-RIS matrix is symmetrical but not necessarily unitary. The work in [40] addresses the optimization of a MIMO link assisted by a BD-RIS to maximize capacity. By alternately optimizing the transmit covariance matrix and the unitary, symmetric BD-RIS scattering matrix, they develop an efficient algorithm that consistently improves capacity over diagonal RIS.

2) BD-RIS empowered ISAC systems: BD-RIS-assisted ISAC systems have been the subject of several recent studies [41]–[45]. In [41], Liu et *al.* jointly designed linear filters, transmit beamforming, and phase responses to maximize the sum rate of BD-RIS-enabled integrated sensing and communication. The work in [42] explores using BD-RIS to minimize base station transmit power in ISAC networks while maintaining communication and sensing quality, employing a penalty-dual-decomposition method to address constraints effectively. Furthermore, the BD-RIS scattering matrix for an ISAC system was studied in [43] to maximize the weighted sum of the SNR at both the radar receiver and communication users. Moreover, the work in [44] explores optimizing parameter estimation in active RIS-empowered ISAC systems through joint BS transmit precoding and active RIS reflection beamforming under SINR constraints, employing an efficient algorithm based on alternating optimization, SDR, and MM methods. In [45], a novel BD-RIS-aided transmitter architecture is proposed to enhance mmWave ISAC performance by optimizing communication sum rate and sensing CRB matrix eigenvalues through a two-stage algorithm, demonstrating significant improvements over conventional DRIS setups.

Recently, deep reinforcement learning (DRL) methods have gained substantial traction across various scientific fields as powerful tools for resource optimization. DRL has been widely utilized to optimize RIS-aided communication [46], yet its application to optimizing RIS-aided ISAC systems remains limited [47], [48], [50]. The work in [47] employing a meta-reinforcement learning (MRL) algorithm investigates STAR-RIS-aided full-duplex ISAC Systems. The aim is to optimize phase-shift matrices at STAR-RIS to maximize sum-rate amidst imperfect channel state information (CSI). The paper [48] introduces a meta-learning algorithm based on gradient descent for optimizing beamforming in RIS-assisted ISAC systems, aiming to minimize BS transmit power while adhering to SINR and CRB constraints. Furthermore, [50] proposes a novel simultaneous localization and communication (SLAC) framework leveraging RIS-aided ISAC systems and cloud radio access networks (C-RAN) to improve localization and communication efficiency. It employs a hybrid deep reinforcement learning algorithm to optimize overall system performance.

Motivated by this gap in this paper we employ DRL method to optimize EE in an BD-RIS empowered ISAC communication systems. This paper makes the following key contributions:

B. Motivation and Challenges

To address the identified research gap, this study focuses on optimizing BD-RIS-aided ISAC networks and presents the following key contributions:

- Pioneering BD-RIS Deployment for Enhanced EE Optimization in ISAC Systems: This paper is the first to integrate BD-RIS into ISAC systems with a focus on optimizing EE. Specifically, we aim to enhance communication-centric EE, defined as the ratio of achievable rate to power consumption, while ensuring target estimation and communication performance meet criteria for CRB and SINR. The complexity of our EE optimization problem is elevated by the fractional term in the objective function, distinguishing our work from previous studies, such as [41]–[45], which tackle less complex optimization challenges.
- Comprehensive Problem Formulation and Optimization: We offer a detailed physical and mathematical formulation of the BD-RIS ISAC system. Our approach uses scattering parameter network analysis to accurately model signal interactions with RIS, considering impedance mismatches and mutual coupling among the transmitter, RIS, and receiver. The model also incorporates ideal conditions with perfect matching and no mutual coupling, focusing on optimizing both transmit and passive beamforming

strategies. Additionally, we develop signal models for communication users, targets, and the base station (BS), enabling us to calculate key metrics such as SINR for communication and CRB for Direction of Arrival (DoA) estimation for radar sensing. We then combine these elements into a unified optimization problem that minimizes EE while accounting for constraints related to sensing, communication, power limits, and BD-RIS configuration, including orthogonality.

- Exploring DRL for BD-RIS Assisted Communication Optimization: DRL applications for BD-RIS-assisted communication optimization are still rare in the literature. To address the complexities involved, especially with the fractional EE term, we introduce the twin delayed deep deterministic policy Gradient (TD3) algorithm. Our extensive simulations confirm the benefits of our BD-RIS-enhanced ISAC approach and demonstrate the effectiveness of our innovative joint design algorithm.

Organization: Section II presents the system model utilized in this study. Section III delves into the problem formulation and outlines the optimization framework. Section IV introduces the TD3 algorithm and its application. Section V offers a comprehensive evaluation of the proposed method's performance, while Section VI concludes the paper.

Notations: Scalars are denoted by a, vectors by $\mathbf{a}$, and matrices by $\mathbf{A}$. The identity matrix of dimension N is $\mathbf{I}_N$, and $\mathbf{0}$ refers to an all-zeros vector. The transpose, complex conjugate, Hermitian (conjugate transpose), and inverse of $\mathbf{A}$ are denoted by $\mathbf{A}^T$, $\mathbf{A}^*$, $\mathbf{A}^H$, and $\mathbf{A}^{-1}$, respectively. The magnitude of a scalar is denoted by $|\cdot|$, while $\|\mathbf{a}\|_2$ and $\|\mathbf{A}\|_F$ denote the 2-norm of vector $\mathbf{a}$ and the Frobenius norm of matrix $\mathbf{A}$, respectively. The diagonal matrix with diagonal elements extracted from vector $\mathbf{a}$ is $\mathrm{diag}\{\mathbf{a}\}$. The trace of matrix $\mathbf{A}$ is $\mathrm{tr}\{\mathbf{A}\}$. The Hadamard product (element-wise multiplication) is denoted by $\mathbf{A} \circ \mathbf{B}$, and the Kronecker product is $\otimes$. $\mathbb{C}$ represents the set of complex numbers, $\mathrm{Re}\{\cdot\}$ and $\mathrm{Im}\{\cdot\}$ extract the real and imaginary parts of a complex number, respectively. Additionally, $\mathbf{C}_{x\times y}$ denotes an $x \times y$ complex-valued matrix, and $\mathbb{E}[\cdot]$ denotes the statistical expectation.

II. SYSTEM MODEL

In this paper, we investigate a BD-RIS-empowered ISAC system depicted in Fig. 1, where a dual-functional BS simultaneously performs multi-user communication and colocated radar sensing functions. Specifically, the BS is equipped with N transmit antennas and N receive antennas to communicate with K single-antenna users and sense potential targets in blind areas with the assistance of an M-element BD-RIS. To tackle the substantial path-loss issue between the base station (BS) and target users, we propose a sensing-enabled BD-RIS framework. This innovative approach integrates a cost-effective sensor with a uniform linear array (ULA) containing M_s elements mounted on the BD-RIS. Simultaneously, we leverage a sensing-RIS configuration, which constitutes a uniform planar array (UPA) with $M = M_y \times M_z$ reflecting elements and $M_s = M_{s_y} \times M_{s_z}$ sensing elements positioned in

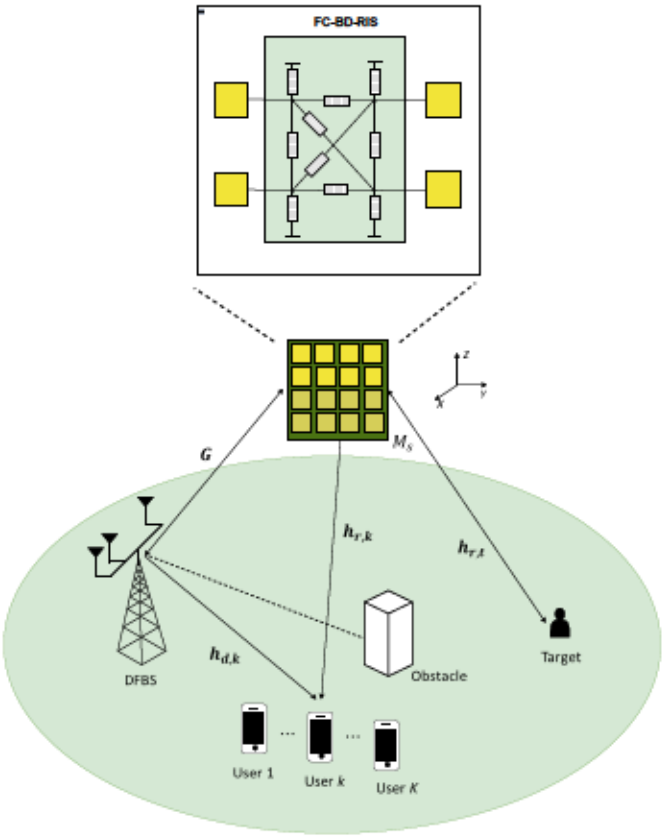

Fig. 1: An illustration of a BD-RIS-enabled ISAC system.

the $y-z$ plane. In this setup, the reflecting elements are limited to phase adjustments, thereby defining the reflection coefficient matrix $\Theta = \mathrm{diag}\{e^{\jmath\theta_1}, \ldots, e^{\jmath\theta_M}\}$, where $\theta_m \in [0, 2\pi)$ for all $m \in \{1, \ldots, M\}$.

The sensor is positioned such that its side facing the communication area is physically shielded to prevent interference from communication signals.

The entire communication subsystem of the system is represented as an L-port network, where $L = N + M + K$. This network is described by a scattering matrix $\mathbf{S} \in \mathbb{C}^{L\times L}$, which can be decomposed into sub-matrices as follows:

$$\mathbf{S} = \begin{bmatrix} \mathbf{S}_{TT} & \mathbf{S}_{TI} & \mathbf{S}_{TR} \\ \mathbf{S}_{IT} & \mathbf{S}_{II} & \mathbf{S}_{IR} \\ \mathbf{S}_{RT} & \mathbf{S}_{RI} & \mathbf{S}_{RR} \end{bmatrix}, \tag{1}$$

where the diagonal sub-matrices correspond to the scattering matrices of the transmitter, RIS, and receiver radiating elements. The off-diagonal sub-matrices represent the transmission scattering matrices between the transmitter, RIS, and receiver.

Additionally, we assume that each transmit antenna is connected in series with a voltage source and a source impedance, resulting in a source impedance matrix $\mathbf{Z}_T \in \mathbb{C}^{N\times N}$. Consequently, the reflection coefficient matrix at the transmitter is given by $\mathbf{\Gamma}_T = (\mathbf{Z}_T + Z_0\mathbf{I}_N)^{-1}(\mathbf{Z}_T - Z_0\mathbf{I}_N)$, where Z_0 denotes the reference impedance used for computing the scattering matrix.

Similarly, each receive antenna is terminated with a load impedance, resulting in a load impedance matrix $\mathbf{Z}_R \in \mathbb{C}^{K\times K}$ and a corresponding reflection coefficient matrix $\mathbf{\Gamma}_R = (\mathbf{Z}_R + Z_0\mathbf{I}_K)^{-1}(\mathbf{Z}_R - Z_0\mathbf{I}_K)$.

The M scattering elements at the BD-RIS are fully interconnected. Specifically, for each $m = 1, 2, \ldots, M$, the m-th port is connected to ground through a reconfigurable impedance $\mathbf{Z}_m$, and the m-th port is also connected to the n-th port ($n = m+1, m+2, \ldots, M$) via a reconfigurable impedance $\mathbf{Z}_{m,n}$. This configuration results in a total of $\frac{M(M+1)}{2}$ reconfigurable impedance components in the network. Therefore, $\mathbf{Z}_I$ is a full matrix, and $\mathbf{Z}_I$ can be derived from the following relationship:

$$[\mathbf{Z}_I^{-1}]_{n,m} = \begin{cases} -Z_{m,n}^{-1} & \text{if } m \neq n \\ Z_m^{-1} + \sum_{k\neq m} Z_{m,k}^{-1} & \text{if } m = n, \end{cases} \tag{2}$$

where $Z_{m,n} = Z_{n,m}$ due to the symmetry of $\mathbf{Z}_I$. The impedance matrix in Eq. 2 yields a symmetric and unitary matrix $\mathbf{\Theta} \in \mathbb{C}^{M\times M}$ of reflection coefficients, defined as:

$$\mathbf{\Theta} = (\mathbf{Z}_{TI} + Z_0\mathbf{I}_M)^{-1}(\mathbf{Z}_I - Z_0\mathbf{I}_M) \tag{3}$$

According to the network theory, $\mathbf{\Theta}$ is a full matrix satisfying the constraints:

$$\mathbf{\Theta} = \mathbf{\Theta}^T, \mathbf{\Theta}^H\mathbf{\Theta} = \mathbf{I}_M \tag{4}$$

where the off-diagonal entries of $\mathbf{\Theta}$ are generally non-zero, indicating interactions between different elements.

Using these definitions and multiport network theory based on scattering parameters, the general RIS-aided channel matrix $\mathbf{H} \in \mathbb{C}^{K\times N}$, which relates the voltages at the receiver ports to those at the transmitter ports, is expressed as:

$$\mathbf{H} = (\mathbf{\Gamma}_R + \mathbf{I}_K)^{-1}\mathbf{T}_{RT}(\mathbf{I}_N + \mathbf{\Gamma}_T\mathbf{T}_{TT} + \mathbf{T}_{TT})^{-1}, \tag{5}$$

where $\mathbf{T}_{TT} \in \mathbb{C}^{N\times N}$ and $\mathbf{T}_{RT} \in \mathbb{C}^{K\times N}$ are sub-matrices of $\mathbf{T} \triangleq \mathbf{S}(\mathbf{I} - \mathbf{\Gamma}\mathbf{S})^{-1} \in \mathbb{C}^{L\times L}$.

$$\mathbf{\Gamma} = \begin{bmatrix} \mathbf{\Gamma}_T & 0 & 0 \\ 0 & \mathbf{\Theta} & 0 \\ 0 & 0 & \mathbf{\Gamma}_R \end{bmatrix}, \tag{6}$$

and represent $\mathbf{T}$ as

$$\mathbf{T} = \begin{bmatrix} \mathbf{T}_{TT} & \mathbf{T}_{TI} & \mathbf{T}_{TR} \\ \mathbf{T}_{IT} & \mathbf{T}_{II} & \mathbf{T}_{IR} \\ \mathbf{T}_{RT} & \mathbf{T}_{RI} & \mathbf{T}_{RR} \end{bmatrix}, \tag{7}$$

The channel model in Eq. 5 is comprehensive as it incorporates the effects of antenna mismatching and mutual coupling at the transmitter, BD-RIS, and receiver. However, its complexity makes it challenging to gain insights into the specific role of the BD-RIS, which motivates us to seek further simplifications [51].

A. RIS-Aided Communication Model with Perfect Matching and No Mutual Coupling

We consider a special case where we assume that the arrays at the transmitter, RIS, and receiver are perfectly matched and have no mutual coupling, i.e., $\mathbf{S}_{TT} = \mathbf{0}$, $\mathbf{S}_{II} = \mathbf{0}$, and $\mathbf{S}_{RR} = \mathbf{0}$. In practice, this assumption can be approximated by individually matching each antenna to the reference impedance $\mathbf{Z}_0$ and ensuring that the antenna spacing is larger than half-wavelength. Additionally, we assume that the source impedance at the transmitter $\mathbf{Z}_{T,n}$ and the load impedance at the receiver $\mathbf{Z}_{R,n}$ are both reference impedances Z_0, resulting in $\mathbf{\Gamma}_T = \mathbf{0}$ and $\mathbf{\Gamma}_R = \mathbf{0}$. With these two assumptions, we can simplify

$$\mathbf{S} = \begin{bmatrix} \mathbf{0} & \mathbf{S}_{TI} & \mathbf{S}_{TR} \\ \mathbf{S}_{IT} & \mathbf{0} & \mathbf{S}_{IR} \\ \mathbf{S}_{RT} & \mathbf{S}_{RI} & \mathbf{0} \end{bmatrix}, \tag{8}$$

and

$$\mathbf{\Gamma} = \begin{bmatrix} \mathbf{0} & \mathbf{0} & \mathbf{0} \\ \mathbf{0} & \mathbf{\Theta} & \mathbf{0} \\ \mathbf{0} & \mathbf{0} & \mathbf{0} \end{bmatrix} \tag{9}$$

so that accordingly we can simplify $(\mathbf{I} - \mathbf{\Gamma}\mathbf{S})^{-1}$ as:

$$(\mathbf{I} - \mathbf{\Gamma}\mathbf{S})^{-1}) = \begin{bmatrix} \mathbf{I} & \mathbf{0} & \mathbf{0} \\ \mathbf{\Theta}\mathbf{S}_{IT} & \mathbf{I} & \mathbf{\Theta}\mathbf{S}_{IR} \\ \mathbf{0} & \mathbf{0} & \mathbf{I} \end{bmatrix}, \tag{10}$$

Making use of Eq. 9 and 10, we can simplify the expression for $\mathbf{T} = \mathbf{S}(\mathbf{I} - \mathbf{\Gamma}\mathbf{S})^{-1}$ and subsequently state that

$$\mathbf{T}_{TT} = \mathbf{S}_{TI}\mathbf{\Theta}\mathbf{S}_{IT} \tag{11}$$

$$\mathbf{T}_{RT} = \mathbf{S}_{RT} + \mathbf{S}_{RI}\mathbf{\Theta}\mathbf{S}_{IT} \tag{12}$$

Substituting Eq. 11 and 12 into Eq. 5 and making use of $\mathbf{\Gamma}_T = \mathbf{0}$ and $\mathbf{\Gamma}_R = \mathbf{0}$, we can simplify the channel matrix $\mathbf{H}$ as:

$$\mathbf{H} = (\mathbf{S}_{RT} + \mathbf{S}_{RI}\mathbf{\Theta}\mathbf{S}_{IT})(\mathbf{I} + \mathbf{S}_{TI}\mathbf{\Theta}\mathbf{S}_{IT})^{-1} \tag{13}$$

The term $\mathbf{S}_{TI}\mathbf{\Theta}\mathbf{S}_{IT}$ represents second-order reflections between the transmitter and the RIS, and back to the transmitter. However, in many practical applications, these second-order reflections are negligible due to their extremely small power, which is proportional to the square of the distance between the transmitter and the RIS. Therefore, in most cases, we can approximate $(\mathbf{I} + \mathbf{S}_{TI}\mathbf{\Theta}\mathbf{S}_{IT})^{-1}$ as $\mathbf{I}$ without significant loss of accuracy. Consequently, we can simplify $\mathbf{H}$ as:

$$\mathbf{H} = \mathbf{S}_{RT} + \mathbf{S}_{RI}\mathbf{\Theta}\mathbf{S}_{IT} \tag{14}$$

The transmission scattering matrices $\mathbf{S}_{RT}$, $\mathbf{S}_{IT}$, and $\mathbf{S}_{RI}$ correspond to the channel matrices from the transmitter to receiver, from the transmitter to RIS, and from the RIS to receiver, respectively. To demonstrate this equivalence, we consider the impedance matrix of the N-port network

$$\mathbf{Z} = \begin{bmatrix} \mathbf{Z}_{TT} & \mathbf{Z}_{TI} & \mathbf{Z}_{TR} \\ \mathbf{Z}_{IT} & \mathbf{Z}_{II} & \mathbf{Z}_{IR} \\ \mathbf{Z}_{RT} & \mathbf{Z}_{RI} & \mathbf{Z}_{RR} \end{bmatrix} \tag{15}$$

Since we assume perfect matching and no mutual coupling, we have $\mathbf{Z}_{TT} = \mathbf{Z}_{II} = \mathbf{Z}_{RR} = Z_0\mathbf{I}$, and following [52], we can derive

$$\mathbf{S}_{ij} = \frac{\mathbf{Z}_{ij}}{2Z_0} \tag{16}$$

for $ij \in \{RT, RI, IT\}$. Taking $\mathbf{Z}_{RT}$ as an example, from Eq. 16, we demonstrate that $\mathbf{S}_{RT}$ is equivalent to the channel matrix from the transmitter to the receiver. Similarly, $\mathbf{S}_{IT}$ and $\mathbf{S}_{RI}$ represent the channel matrices from the transmitter to the RIS and from the RIS to the receiver, respectively.

To clarify, we introduce auxiliary notations $\mathbf{h}_{d,k} = \mathbf{S}_{RT}$, $\mathbf{G} = \mathbf{S}_{IT}$, and $\mathbf{h}_{r,k}, \mathbf{h}_{r,t} = \mathbf{S}_{RI}$. . This allows us to rewrite Eq. 16 as

$$\begin{aligned} \mathbf{h}_k^H &= \mathbf{h}_{d,k}^H + \mathbf{h}_{r,k}^H \mathbf{\Theta} \mathbf{G}, \\ \mathbf{h}_t &= \mathbf{h}_{r,t}^H \mathbf{\Theta} \mathbf{G}. \end{aligned} \tag{17}$$

Furthermore, considering the presence of both Line-of-Sight (LoS) and Non-Line-of-Sight (NLoS) paths in Eq. 17, we model $\mathbf{h}_{d,k} \in \mathbb{C}^{N\times 1}$, $\mathbf{h}_{r,k} \in \mathbb{C}^{M\times 1}$, and $\mathbf{G} \in \mathbb{C}^{M\times N}$ using Rician fading. The vector $\mathbf{h}_{r,t} \in \mathbb{C}^{M\times 1}$ represents the steering vector from the BD-RIS to the targets and is defined as:

$$\mathbf{h}_{r,t} = \begin{bmatrix} 1 \\ e^{\frac{-j2\pi d_x(1)\sin\Theta_{v_t}\cos\Theta_{h_t}}{\lambda}} \\ \vdots \\ e^{\frac{-j2\pi d_x(M_x-1)\sin\Theta_{v_t}\cos\Theta_{h_t}}{\lambda}} \end{bmatrix} \otimes \begin{bmatrix} 1 \\ e^{\frac{-j2\pi d_y(1)\sin\Theta_{v_t}\sin\Theta_{h_t}}{\lambda}} \\ \vdots \\ e^{\frac{-j2\pi d_y(M_y-1)\sin\Theta_{v_t}\sin\Theta_{h_t}}{\lambda}} \end{bmatrix} \tag{18}$$

where M_x and M_y denote the number of elements along two dimensions of RIS, and the total number of RIS' elements is $M = M_x \times M_y$. Besides, $\lambda = \frac{c}{f_c}$ is the carrier wavelength and the parameters $d_x = d_y$ represent the inter-element spacing.

Additionally, $\mathbf{\Theta}_{v_t}$ and $\mathbf{\Theta}_{h_t}$ denote the elevation and azimuth angles, respectively, for the t-th target.

Assuming that users and targets are located in a 3-dimensional space (x, y, z), the channel between the BS and the k-th user, represented by $\mathbf{h}_{d,k} \in \mathbb{C}^{N\times 1}$, is modeled as a Rician channel. It is assumed that the BS, users, BD-RIS, and targets are located at (x_B, y_B, z_B), (x_k, y_k, z_k), (x_R, y_R, z_R), and (x_t, y_t, z_t) respectively. Therefore, $\mathbf{h}_{d,k}$ is modeled as follows:

$$\begin{aligned} \mathbf{h}_{d,k} = &\sqrt{C_0\left(\frac{d_{B,k}}{D_0}\right)^{-\alpha_{B,k}}} \\ &\times \left(\sqrt{\frac{K_{B,k}}{K_{B,k}+1}}\mathbf{h}_{d,k}^{\text{LoS}} + \sqrt{\frac{1}{K_{B,k}+1}}\mathbf{h}_{d,k}^{\text{NLoS}}\right) \end{aligned} \tag{19}$$

where $\mathbf{h}_{d,k}^{NLoS} \sim \mathcal{CN}(\mathbf{0}, \mathbf{I}_N)$ denotes the non-line-of-sight (NLoS) component of the channel vector $\mathbf{h}_{d,k}$, which follows a circularly symmetric complex Gaussian distribution with zero mean and identity covariance matrix $\mathbf{I}_N$.

The terms $K_{B,k}$, $\alpha_{B,k}$, and $d_{B,k}$ represent the Rician factor, path loss exponent, and the distance between the BS and the k-th user, respectively.

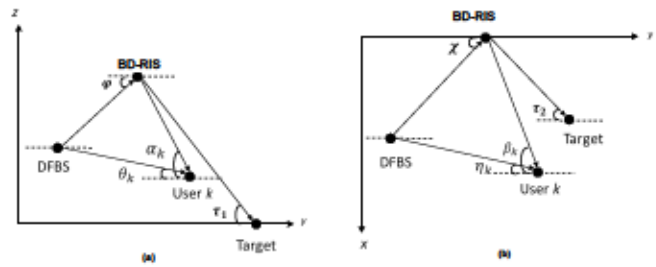

Fig. 2: (a) and (b) show the vertical and horizontal angles between the DFBS and BD-RIS

$$d_{B,k} = \sqrt{(x_B - x_k)^2 + (y_B - y_k)^2 + (z_B - z_k)^2} \tag{20}$$

Besides, the LoS channel $\mathbf{h}_{d,k}^{LoS} = \mathbf{v}_{\text{AoD,k}}$, where $\mathbf{v}_{\text{AoD,k}} \in \mathbb{C}^{N\times 1}$ denotes the vector representing the angle of departure (AoD) from the BS to the k-th user. It is defined as:

$$\mathbf{v}_{\text{AoD,k}} = [1, \cdots, e^{-j\frac{2\pi d}{\lambda}(N-1)sin(\theta_k)cos(\eta_k)}]^T \tag{21}$$

where d is the distance between BS antenna elements, and θ_k and η_k represent the vertical and horizontal angles of departure (AoD) between the BS and the k-th user, as depicted in Fig. 2. These angles are obtained as follows:

$$\begin{aligned} \sin(\theta_k) &= \frac{|z_B - z_k|}{\sqrt{(y_B - y_k)^2 + (z_B - z_k)^2}}, \\ \cos(\eta_k) &= \frac{|y_B - y_k|}{\sqrt{(y_B - y_k)^2 + (x_B - x_k)^2}} \end{aligned} \tag{22}$$

Also, the channel matrix between the BS and the BD-RIS, $\mathbf{G} \in \mathbb{C}^{M\times N}$, is defined as:

$$\begin{aligned} \mathbf{G} = &\sqrt{C_0(\frac{d_{B,R}}{D_0})^{-\alpha_{B,R}}} \times \\ &\{\sqrt{\frac{K_{B,R}}{K_{B,R}+1}}\mathbf{G}^{LoS} + \sqrt{\frac{1}{K_{B,R}+1}}\mathbf{G}^{NLoS}\} \end{aligned} \tag{23}$$

where $K_{B,R} \geq 0$ and $\alpha_{B,R} \geq 0$ represent the Rician factor and path loss exponent, respectively. C_0 and $\mathbf{G}^{NLoS}$ denote the path loss at the reference distance $D_0 = 1$ m and the NLoS component related to $\mathbf{G}$, respectively. $d_{B,R}$ indicates the distance between the BS and the BD-RIS. Additionally, $\mathbf{G}^{\text{LoS}} \in \mathbb{C}^{M\times N}$ is defined as $\mathbf{G}^{\text{LoS}} = \mathbf{v}_{\text{AoA,R}} \times \mathbf{v}_{\text{AoD,B}}$, where $\mathbf{v}_{\text{AoA,R}} \in \mathbb{C}^{M\times 1}$ and $\mathbf{v}_{\text{AoD,B}} \in \mathbb{C}^{N\times 1}$ represent the angle of arrival (AoA) and angle of departure (AoD) of the transmitted signal from the BS to the BD-RIS, respectively.

$$\begin{aligned} \mathbf{v}_{\text{AoA,R}} = &[1, \cdots, e^{-j\frac{2\pi d_y}{\lambda}(M_y-1)sin\psi cos\chi}]^T \otimes \\ &[1, \cdots, e^{-j\frac{2\pi d_x}{\lambda}(M_x-1)sin\psi cos\chi}]^T \end{aligned} \tag{24}$$

$$\mathbf{v}_{\text{AoD,B}} = [1, \cdots, e^{-j\frac{2\pi d}{\lambda}(N-1)sin\psi cos\chi}]^T \tag{25}$$

$$Sin\psi = \frac{|z_B - z_R|}{\sqrt{(y_B - y_R)^2 + (z_B - z_R)^2}} \tag{26}$$

$$Sin\chi = \frac{|z_B - z_R|}{\sqrt{(y_B - y_R)^2 + (z_B - z_R)^2}} \tag{27}$$

$$Cos\chi = \frac{|y_B - y_R|}{\sqrt{(x_B - x_R)^2 + (y_B - y_R)^2}} \tag{28}$$

in which d_x and d_y represent the distances between BD-RIS elements along the x-axis and y-axis, respectively. Additionally, ψ and χ denote the vertical and horizontal angles of departure between the BS and BD-RIS, and also the angle of arrival (AoA) between the BS and BD-RIS.

The channel between the BD-RIS and the k-th user, $\mathbf{h}_{r,k}^H$, is defined as:

$$\begin{aligned}\mathbf{h}_{r,k} =& \sqrt{C_0 \left(\frac{d_{R,k}}{D_0}\right)^{-\alpha_{R,k}}} \times \\ & \left\{\sqrt{\frac{K_{R,k}}{K_{R,k}+1}}\mathbf{h}_{r,k}^{\text{LoS}} + \sqrt{\frac{1}{K_{R,k}+1}}\mathbf{h}_{r,k}^{\text{NLoS}}\right\}\end{aligned} \tag{29}$$

where $\mathbf{h}_{r,k}^{\text{NLoS}} \sim \mathcal{CN}(\mathbf{0}, \mathbf{I}_M)$, $K_{R,k} \geq 0$, $\alpha_{R,k} \geq 0$, and $d_{R,k}$ represent the Rician factor, path loss exponent, and the distance between the BD-RIS and the k-th user, respectively.

The LoS channel $\mathbf{h}_{r,k}^{\text{LoS}} = \mathbf{v}_{\text{AoD,k}}$ where $\mathbf{v}_{\text{AoD,k}} \in \mathbb{C}^{M\times 1}$ represents the angle of departure (AoD) vector from the BD-RIS to the k-th user, and is defined as:

$$\begin{aligned}\mathbf{v}_{\text{AoD,k}} = & [1, \cdots, e^{-\jmath\frac{2\pi d_y}{\lambda}(M_y-1)\sin\alpha_k\cos\beta_k}]^T \otimes \\ & [1, \cdots, e^{-\jmath\frac{2\pi d_x}{\lambda}(M_x-1)\sin\alpha_k\cos\beta_k}]^T\end{aligned} \tag{30}$$

$$\sin(\alpha_k) = \frac{|z_k - z_R|}{\sqrt{(y_k - y_R)^2 + (z_k - z_R)^2}}, \quad \forall k = 1, 2, \ldots, K \tag{31}$$

$$\cos(\beta_k) = \frac{|y_k - y_R|}{\sqrt{(x_k - x_R)^2 + (y_k - y_R)^2}}, \quad \forall k = 1, 2, \ldots, K \tag{32}$$

$$\sin(\beta_k) = \frac{|x_k - x_R|}{\sqrt{(x_k - x_R)^2 + (y_k - y_R)^2}}, \quad \forall k = 1, 2, \ldots, K \tag{33}$$

The BS transmits information signals to the users and simultaneously receives echo signals from targets at its receive antenna. At each coherent processing interval (CPI), L information symbols are transmitted, denoted by $l = \{1, 2, \ldots, L\}$.

The transmit data stream vector at each time index l is

$$\mathbf{S}[l] = \left[s_1[l], s_2[l], \cdots, s_k[l]\right]^T \in \mathbb{C}^{K\times 1} \tag{34}$$

Before information transmission, streams are linearly precoded through a precoding matrix. It is assumed that at each CPI, the precoding matrix $\mathbf{W}$ is fixed. Therefore, the transmitted signal at the l-th time index is given by:

$$\mathbf{x}[l] = \mathbf{W}\mathbf{s}[l] = \sum_{k=1}^{K} w_k s_k[l] \tag{35}$$

where $\mathbf{W} = [w_1, \ldots, w_K] \in \mathbb{C}^{N\times K}$.

The transmitted signal $\mathbf{s}[l]$ at the l-th time index is an independent Gaussian random signal with zero mean and unit variance, so

$$\mathbb{E}[\mathbf{s}[l]\mathbf{s}^H[l]] = \mathbf{I}_K \tag{36}$$

The covariance matrix of the transmitted signal $\mathbf{x}[l]$ is obtained as

$$\mathbf{R}_x = \mathbb{E}[\mathbf{x}[l]\mathbf{x}^H[l]] = \mathbf{W}\mathbf{W}^* \tag{37}$$

Practically, $\mathbf{R}_x$ is obtained by averaging over the time indices through the following formula:

$$\mathbf{R}_x \simeq \frac{1}{L}\mathbf{X}\mathbf{X}^H \tag{38}$$

where $\mathbf{X} = [\mathbf{x}[1], \ldots, \mathbf{x}[L]]$.

The received signal at the k-th user: The received signal at the k-th user and l-th time index can be written as:

$$\begin{aligned}\mathbf{y}_k[l] &= (\mathbf{h}_{d,k}^H + \mathbf{h}_{r,k}^H\mathbf{\Theta}\mathbf{G})\mathbf{x}[l] + \mathbf{n}_k[l] \\ &= \mathbf{h}_k^H\mathbf{w}_k s_k[l] + \sum_{i=1, i\neq k}^{K} \mathbf{h}_k^H\mathbf{w}_i s_i[l] + \mathbf{n}_k[l]\end{aligned} \tag{39}$$

In Eq. 39, $\mathbf{n}_k[l] \sim \mathcal{CN}(0, \sigma_k^2)$. The SINR_k for the k-th user is given by:

$$\text{SINR}_k = \frac{|\mathbf{h}_k^H\mathbf{w}_k|^2}{\sum_{i=1, i\neq k}^{K} |\mathbf{h}_k^H\mathbf{w}_i|^2 + \sigma_k^2}, \quad \forall k \in \{1, 2, \ldots, K\} \tag{40}$$

B. Metric for sensing

The received eco-signal from the target at the BS and l-th time index is written as:

$$\mathbf{y}_s[l] = \alpha\mathbf{a}(\tau_1, \tau_2)\mathbf{b}^T(\tau_1, \tau_2)\mathbf{\Theta}\mathbf{G}\mathbf{x}[l] + \mathbf{z}_s[l] \in \mathbb{C}^{M_s\times 1} \tag{41}$$

where $\mathbf{z}_s[l] \in \mathbb{C}^{M_s\times 1}$ is the received AWGN noise at the sensing elements of the RIS. $\alpha \in \mathbb{C}$ is the complex amplitude determined by the round-trip path-loss and the complex reflection factor of the target. τ_1 and τ_2 denote the steering vectors of sensing and reflecting elements, respectively. With the BD-RIS and sensor deployed in the yz plane, the steering vectors of BD-RIS and target can be calculated as:

$$\begin{aligned}\mathbf{a}(\tau_1, \tau_2) = & \frac{1}{\sqrt{M_s}}\left[1, \cdots, e^{-\jmath\frac{2\pi d_y}{\lambda}(M_{s_y}-1)\sin\tau_1\cos\tau_2}\right]^T \\ & \otimes \left[1, \cdots, e^{-\jmath\frac{2\pi d_z}{\lambda}(M_{s_z}-1)\sin\tau_1\sin\tau_2}\right]^T \in \mathbb{C}^{M_s\times 1}\end{aligned} \tag{42}$$

$$\begin{aligned}\mathbf{b}(\tau_1, \tau_2) = & \frac{1}{\sqrt{M}}\left[1, \cdots, e^{-\jmath\frac{2\pi d_y}{\lambda}(M_y-1)\sin\tau_1\cos\tau_2}\right]^T \\ & \otimes \left[1, \cdots, e^{-\jmath\frac{2\pi d_z}{\lambda}(M_z-1)\sin\tau_1\sin\tau_2}\right]^T \in \mathbb{C}^{M\times 1}\end{aligned} \tag{43}$$

$$\sin\tau_1 = \frac{|y_t - y_R|}{\sqrt{(x_t - x_R)^2 + (y_t - y_R)^2}} \tag{44}$$

$$\sin\tau_2 = \frac{z_R}{\sqrt{(y_t - y_R)^2 + z_R^2}} \tag{45}$$

$$\cos\tau_2 = \frac{|y_t - y_R|}{\sqrt{z_R^2 + (y_t - y_R)^2}} \tag{46}$$

The echo signal at each time index is defined as:

$$\mathbf{y}_s = \left[\mathbf{y}_s[1], \mathbf{y}_s[2], \ldots, \mathbf{y}_s[L]\right]^T \in \mathbb{C}^{M_s L \times 1} \tag{47}$$

Specifically, we utilize the CRB for estimating the 2D DOAs τ_1 and τ_2 of target, which serves as a minimum limit on the variance of unbiased estimators.

Therefore, separating the noise from the signal, $\mathbf{y}_s$ can be expressed as:

$$\mathbf{y}_s = \mathbf{u} + \mathbf{z}_s \tag{48}$$

where

$$\mathbf{u} = \left[\mathbf{u}[1], \mathbf{u}[2], \ldots, \mathbf{u}[L]\right]^T \in \mathbb{C}^{M_s L \times 1} \tag{49}$$

and

$$\mathbf{z}_s = \left[\mathbf{z}_s[1], \mathbf{z}_s[2], \ldots, \mathbf{z}_s[L]\right]^T \in \mathbb{C}^{M_s L \times 1} \tag{50}$$

Here, $\mathbf{u}$ represents the signal part and $\mathbf{z}_s$ is the noise vector, where $\mathbf{z}_s \sim \mathcal{CN}(\mathbf{0}_{M_s L}, \sigma_r^2 \mathbf{I}_{M_s L})$. The echo signal $\mathbf{y}_s$ itself follows a complex normal distribution $\mathcal{CN}(\mathbf{u}, \mathbf{R}_{M_s L})$, where $\mathbf{R}_{M_s L} = \sigma_r^2 \mathbf{I}_{M_s L}$.

The estimated parameters for the target are denoted by $\bar{\phi} = \left[\bar{\tau}^T, \bar{\alpha}^T\right] \in \mathbb{R}^{4\times 1}$, where $\bar{\tau} = \left[\tau_1, \tau_2\right]^T \in \mathbb{R}^{2\times 1}$ represents the azimuth and elevation angles of departure (DoA) of the target relative to the BD-RIS. The parameter $\bar{\alpha} = \left[\mathrm{Re}(\alpha), \mathrm{Im}(\alpha)\right]^T \in \mathbb{R}^{2\times 1}$ corresponds to the real and imaginary components of the complex amplitude α.

It is required to obtain the Fisher Information Matrix (FIM) to calculate CRB for $\bar{\phi}$, defined as:

$$\mathbf{J}_{\bar{\phi}\bar{\phi}} = \begin{bmatrix} \mathbf{J}_{\tau\tau} & \mathbf{J}_{\tau\alpha} \\ \mathbf{J}_{\tau\alpha}^T & \mathbf{J}_{\alpha\alpha} \end{bmatrix} \tag{51}$$

The (i, j) element of $\mathbf{J}_{\bar{\phi}\bar{\phi}}$ is calculated as:

$$\begin{aligned} [\mathbf{J}_{\bar{\phi}\bar{\phi}}]_{i,j} &= \mathrm{tr}\left(\mathbf{R}_{M_s L}^{-1} \frac{\partial \mathbf{R}_{M_s L}}{\partial \bar{\phi}_i} \mathbf{R}_{M_s L}^{-1} \frac{\partial \mathbf{R}_{M_s L}}{\partial \bar{\phi}_j}\right) \\ &\quad + 2\mathrm{Re}\left\{\frac{\partial \mathbf{u}^H}{\partial \bar{\phi}_i} \mathbf{R}_{M_s L}^{-1} \frac{\partial \mathbf{u}}{\partial \bar{\phi}_j}\right\} \\ &\overset{(a)}{=} \frac{2}{\sigma_r^2} \mathrm{Re}\left\{\frac{\partial \mathbf{u}^H}{\partial \bar{\phi}_i} \frac{\partial \mathbf{u}}{\partial \bar{\phi}_j}\right\}, \end{aligned} \tag{52}$$

where (a) results from the fact that $\mathbf{R}_{M_s L}$ is independent of $\bar{\phi}$, hence $\frac{\partial \mathbf{R}_{M_s L}}{\partial \bar{\phi}_i} = 0$. The full derivation of the FIM elements is provided in Appendix A.

Due to the importance of estimating the target angle, the CRB matrix is considered only for $\bar{\tau}$ using the following formula:

$$\mathrm{CRB}(\bar{\tau}) = [\mathbf{J}_{\tau\tau} - \mathbf{J}_{\tau\alpha}\mathbf{J}_{\alpha\alpha}^{-1}\mathbf{J}_{\tau\alpha}^H]^{-1} \tag{53}$$

According to Eq. 53, $CRB(\bar{\tau})$ depends on angles $\bar{\tau}$. Therefore, it is necessary to determine these angles. It is assumed that the angles remain constant within coherent time blocks, since in practice, the DOAs of targets typically exhibit minimal variation between adjacent coherent time blocks. Hence, the estimated or predicted DOAs from previous coherent time blocks' estimation results suffice for system design [53]. Based on this analysis, we assume that the DOAs $\bar{\tau}$ remain constant throughout the optimization process.

III. Problem Formulation and Optimization Framework

In this section, we focus on minimizing EE of the proposed system model with respect to the design of the beamformer $\mathbf{W}$ and the FC-BD-RIS configuration $\mathbf{\Theta}$. Our goal is to ensure that the quality-of-service (QoS) for all mobile users and the sensing quality for the target remain above satisfactory levels. Subsequently, we propose to tackle this optimization problem using the TD3 algorithm.

A. Problem Formulation

The total power consumed by the system is defined as:

$$P(\{\mathbf{W}_k\}_{k\in K}, \mathbf{\Theta}) = \frac{1}{\zeta}\sum_{k=1}^{K} \|\mathbf{w}_k\|^2 + P_0, \tag{54}$$

where $0 \le \zeta \le 1$ is the power amplifier efficiency at the BS and P_0 is formulated as follow:

$$P_{\mathrm{Cir}} = P_{\mathrm{BS}} + \sum_{k=1}^{K} P_k, \tag{55}$$

where P_{BS} and P_k represent the circuit powers of the BS and the k-th user, respectively.

Besides, the feasibility set for the BD-RIS scattering matrix is defined as follows [54]–[56]:

$$\mathcal{S} = \{\mathbf{\Theta} \mid \mathbf{\Theta}^H\mathbf{\Theta} = \mathbf{I}_M, \mathbf{\Theta} = \mathbf{\Theta}^T\}, \tag{56}$$

where the unitary constraint $\mathbf{\Theta}^H\mathbf{\Theta} = \mathbf{I}_M$ indicates that the RIS is passive and lossless. The symmetry constraint $\mathbf{\Theta} = \mathbf{\Theta}^T$ arises because the RIS is a reciprocal passive network, meaning the power losses between any pair of ports are identical regardless of the propagation direction.

So, the EE can be formulated as follows:

$$\mathrm{EE}(\{\mathbf{W}_k\}_{k\in K}, \mathbf{\Theta}) = \frac{\sum_{k=1}^{K}\log_2(1 + \mathrm{SINR}_k)}{P(\{W_k\}_{k\in K}, \mathbf{\Theta})}. \tag{57}$$

Our objective is to maximize the network's EE while ensuring satisfactory radar sensing quality, leading to the following optimization problem:

$$P_0: \underset{\{\{\mathbf{W}_k\}_{k\in K}, \mathbf{\Theta}\}}{\text{Maximize}} \quad \mathrm{EE} \tag{58a}$$

$$\text{subject to} \quad C_1: \mathrm{SINR}_k \ge \gamma_{\mathrm{SINR},k}, \quad \forall k \in K \tag{58b}$$

$$C_2: \sum_{k=1}^{K} \|\mathbf{w}_k\|_2 \le P_{\mathrm{BS,max}}, \tag{58c}$$

$$C_3: \mathrm{tr}(\mathrm{CRB})(\bar{\tau}) \le \epsilon, \tag{58d}$$

$$C_4: \mathbf{\Theta} = \mathbf{\Theta}^T, \quad \mathbf{\Theta}^H\mathbf{\Theta} = \mathbf{I}_M. \tag{58e}$$

The problem is subject to several constraints: C_1 represents the SINR requirements of the users; C_2 ensures that the BS's

transmit power does not exceed $P_{\text{BS,max}}$; C_3 stipulates that the CRB for the direction of arrival estimation must be below a specified threshold ϵ; and C_4, derived from the FC BD-RIS architecture, enlarges the feasible domain of $\mathbf{\Theta}$ for greater configuration flexibility, though the orthogonality condition (i.e., the Stiefel manifold condition) introduces additional optimization challenges.

B. Optimization Framework

Model-free RL is a dynamic programming technique that learns from an uncertain dynamic environment to address decision-making problems. In this paper, problem P_0 is framed as an RL problem, and a DRL-based algorithm is developed to jointly design transmit and passive beamforming to maximize the EE.

C. Optimization Problem Transformation Based on RL

In the DRL framework, the BD-RIS-empowered ISAC communication system is viewed as the environment, while the intelligent controller coordinating with the BS is considered an agent. This agent can collect channel state information (CSI), including $\mathbf{h}_{d,k}$ and other channels. The agent interacts with the environment in discrete time slots. At time slot l, the agent obtains the current state $\mathbf{s}_l$ of the environment and selects an action $\mathbf{a}_l$ based on the policy $\pi(\mathbf{s}_l, \mathbf{a}_l)$. After executing the action $\mathbf{a}_l$, the environment transitions to a new state $\mathbf{s}_{l+1}$ and provides feedback in the form of a reward $\mathbf{r}_l$, which represents the performance of action $\mathbf{a}_l$ under the current state $\mathbf{s}_l$. The agent then selects action $\mathbf{a}_{l+1}$ for the new state $\mathbf{s}_{l+1}$. The agent uses this feedback to learn a policy that maximizes cumulative rewards. This interaction between the agent and the environment can be modeled as a Markov decision process (MDP), which consists of a tuple $(\mathbf{S}, \mathbf{A}, \mathbf{P}, \mathbf{r}, \gamma)$. The key components of the proposed DRL-based algorithm are defined as follows:

- **State Space:** The set of all states across all time slots is state space $\mathbf{S} = \{\mathbf{s}_l\}_{l \in L}$, where $\mathbf{s}_l \in S$ and $\mathbf{s}_l \in S$ represents the state observed from the environment at time slot l. The state $\mathbf{s}_l$ at time slot l is composed of information received by the agent from the environment at any time l related to problem P_0. QoS parameters such as maximum SINR of system $\{\gamma_k\}$ for all users, BS maximum power P_{BS}, the parameter ϵ related to target's maximum CRB, BS to BD-RIS and BD-RIS to users and target channel coefficients are considered part of state $\mathbf{s}_l$. Since channel coefficients are complex, they are divided into real and imaginary parts. Besides the information obtained from the environment, actions and rewards play a crucial role in enabling the agent to learn useful knowledge. State at time slot l is denoted as:

$$\begin{aligned}\mathbf{s}_l = \Big\{ &\{P_{\text{BS}}, \{\gamma_{\text{SINR},k}\}_{k \in K}, \epsilon, \\ &\left\{\mathbf{h}_{d,k}^H(l), \mathbf{h}_{r,k}^H(l)\right\}_{k \in K}, \\ &\mathbf{h}_{r,t}(l), \mathbf{G}(l)\}, \mathbf{a}_l, r(\mathbf{s}_l, \mathbf{a}_l)\Big\}.\end{aligned} \tag{59}$$

- **Action Space:** The action space A, where $\mathbf{a}_l \in A$, encompasses all possible actions across time slots. Here, $\mathbf{a}_l$ represents the set of choices available to the agent at time l, determined through interactions with the environment. In the context of problem P_0, actions involve selecting the active beamforming vectors $\{\mathbf{w}_k(l)\}_{\forall l}$ and the phase shift matrices for BD-RIS $\{\mathbf{\Theta}(l)\}_{\forall l}$. These actions can be denoted as:

$$\mathbf{a}_l = \{\mathbf{w}_k(l), \mathbf{\Theta}(l)\} \tag{60}$$

- **Policy:**Two types of action selection policies are utilized: μ and π, representing deterministic and stochastic policies, respectively. In a deterministic policy, actions are directly assigned to states, such that $\mathbf{a}_l = \mu(\mathbf{s}_l) \in \mathcal{A}$, where $\mu(\mathbf{s}_l)$ determines the action for each state $\mathbf{s}_l$. In a stochastic policy, the probability of selecting an action in a given state is defined by a probability distribution function $\pi(\mathbf{a}_l|\mathbf{s}_l)$, where $\pi(\mathbf{a}_l|\mathbf{s}_l)$ denotes the probability of choosing action $\mathbf{a}_l$ in state $\mathbf{s}_l$.
  In DRL, the goal is to design an optimal policy, wherein DNNs in DRL algorithms are trained with training data in replay buffers, comprising 4-tuples $(\mathbf{s}_l, \mathbf{a}_l, r(\mathbf{s}_l, \mathbf{a}_l), \mathbf{s}_{l+1})$. DNN parameters are set to map each state $\mathbf{s}_l$ to action $\mathbf{a}_l$ for deterministic policy or to determine action selection probabilities for stochastic policy.
- **Reward Function:** The objective of the optimization problem is to maximize EE while satisfying the constraints in problem P_0. Consequently, the reward function is designed to achieve this goal and is formulated as:

$$r_l(\mathbf{s}_l, \mathbf{a}_l) = \text{EE} + \sum_{i=1}^{4} \beta_i \times \text{EE}_i, \tag{61}$$

  where $\beta_i = 0, \forall i = \{0, \ldots, 4\}$ if constraint C_i is satisfied, and -1 otherwise. The reward function ensures no penalty if all constraints are satisfied.
- **Discount factor:** The discount factor $\gamma \in [0, 1]$ is used to weigh future rewards, reflecting the uncertainty associated with them.
- **Algorithms:** We use TD3 algorithm. TD3 is designed for continuous state and action spaces. Subsequent sections detail TD3 algorithms.

IV. TD3 Algorithm

TD3 algorithm is an advanced reinforcement learning method designed for continuous action spaces. It aims to improve performance and stability compared to previous algorithms like deep deterministic policy gradient (DDPG). TD3 leverages novel techniques and a complex neural network structure to achieve effective learning in challenging environments.

A. Overall Structure of TD3

TD3 algorithm employs a sophisticated architecture consisting of six distinct neural networks, categorized as follows:

- Two Critic Networks
- Two Target Critic Networks
- Two Actor Networks

The TD3 algorithm leverages these neural networks to enhance the efficiency and stability of the reinforcement learning process. Specifically, the critic Networks, denoted as $\mathbf{Q}_1(\mathbf{s}_l, \mathbf{a}_l; \boldsymbol{\theta}_{Q1})$ and $\mathbf{Q}_2(\mathbf{s}_l, \mathbf{a}_l; \boldsymbol{\theta}_{Q2})$, are responsible for estimating the value of taking action $\mathbf{a}_l$ in state $\mathbf{s}_l$. These networks operate independently, with $\mathbf{Q}_1$ and $\mathbf{Q}_2$ providing separate evaluations of the action's quality. This dual-critic setup is instrumental in reducing the variance of value estimates, thereby contributing to improved learning stability.

To further bolster stability, TD3 incorporates target critic networks, namely $\mathbf{Q}^1_{\text{target}}(\mathbf{s}_l, \mathbf{a}_l; \boldsymbol{\theta}_{Q^1_{\text{target}}})$ and $\mathbf{Q}^2_{\text{target}}(\mathbf{s}_l, \mathbf{a}_l; \boldsymbol{\theta}_{Q^2_{\text{target}}})$. These target networks are updated at a slower rate compared to the primary Critic Networks, which helps in maintaining stable target values during training.

In addition to the critic cetworks, TD3 employs actor networks to generate actions based on the current state, represented as $\pi(\mathbf{s}_l; \boldsymbol{\theta}_\pi)$. The primary role of the actor network is to optimize the policy by learning the most effective actions to take in various states. To ensure policy stability and mitigate excessive fluctuations, TD3 also utilizes a Target Actor Network, denoted as $\pi_{\text{target}}(\mathbf{s}_l; \boldsymbol{\theta}_{\pi_{\text{target}}})$. This network is updated slowly, serving as a stable reference for generating actions.

B. Update Procedures

a) Updating Critic Networks: The critic networks $\mathbf{Q}_1$ and $\mathbf{Q}_2$ are updated using a mean squared error loss function

$$L(\boldsymbol{\theta}_{Q1}, \boldsymbol{\theta}_{Q2}) = \mathbb{E}_{(\mathbf{s}_l, \mathbf{a}_l, r_l, \mathbf{s}_{l+1}) \in \mathcal{B}} \left[\frac{1}{2} \left(y_{Q1} - \mathbf{Q}_1(\mathbf{s}_l, \mathbf{a}_l; \boldsymbol{\theta}_{Q1}) \right)^2 + \frac{1}{2} \left(y_{Q2} - \mathbf{Q}_2(\mathbf{s}_l, \mathbf{a}_l; \boldsymbol{\theta}_{Q2}) \right)^2 \right]$$

where:

$$y_{Q1} = r_l + \gamma \cdot \min_{i=1,2} \mathbf{Q}^i_{\text{target}}(\mathbf{s}_{l+1}, \pi_{\text{target}}(\mathbf{s}_{l+1}); \boldsymbol{\theta}_{Q^i_{\text{target}}})$$
$$y_{Q2} = r_l + \gamma \cdot \min_{i=1,2} \mathbf{Q}^i_{\text{target}}(\mathbf{s}_{l+1}, \pi_{\text{target}}(\mathbf{s}_{l+1}); \boldsymbol{\theta}_{Q^i_{\text{target}}})$$

Here:

- r_l is the actual reward at time step l.
- γ is the discount factor.
- π_{target} is the target policy.
- $\mathbf{Q}^i_{\text{target}}$ are the target critic networks.

b) Updating the Policy (Actor Network): The policy π is updated using policy gradients:

$$\nabla_{\boldsymbol{\theta}_\pi} J \approx \mathbb{E}_{\mathbf{s}_l \sim \mathcal{D}} \left[\nabla_{\mathbf{a}_l} \mathbf{Q}_1(\mathbf{s}_l, \mathbf{a}_l; \boldsymbol{\theta}_{Q1}) \nabla_{\boldsymbol{\theta}_\pi} \pi(\mathbf{s}_l; \boldsymbol{\theta}_\pi) \right]$$

Here:

- $\boldsymbol{\theta}_\pi$ are the policy parameters.
- $\nabla_{\mathbf{a}_l} \mathbf{Q}_1(\mathbf{s}_l, \mathbf{a}_l; \boldsymbol{\theta}_{Q1})$ is the gradient of $\mathbf{Q}_1$ with respect to the action $\mathbf{a}_l$.
- $\nabla_{\boldsymbol{\theta}_\pi} \pi(\mathbf{s}_l; \boldsymbol{\theta}_\pi)$ is the gradient of the policy with respect to its parameters.

c) Updating Target Network Parameters: target networks are updated gradually using a soft update parameter (τ):

$$\boldsymbol{\theta}_{Q_{\text{target}}} \leftarrow \tau \cdot \boldsymbol{\theta}_Q + (1 - \tau) \cdot \boldsymbol{\theta}_{Q_{\text{target}}}$$
$$\boldsymbol{\theta}_{\pi_{\text{target}}} \leftarrow \tau \cdot \boldsymbol{\theta}_\pi + (1 - \tau) \cdot \boldsymbol{\theta}_{\pi_{\text{target}}}$$

Here:

- τ is the soft update rate.
- $\boldsymbol{\theta}_Q$ and $\boldsymbol{\theta}_\pi$ are the parameters of the main networks.
- $\boldsymbol{\theta}_{Q_{\text{target}}}$ and $\boldsymbol{\theta}_{\pi_{\text{target}}}$ are the parameters of the target networks.

d) Adding Exploration Noise: To enhance exploration and prevent getting stuck in local optima, noise is added to actions. TD3 typically uses Ornstein-Uhlenbeck noise to introduce random variations into actions [57]. The TD3 algorithm is depicted in Fig. 3.

C. Action Space for Benchmark Schemes

We use zero forcing (ZF) and maximum ratio transmission (MRT) schemes as benchmark design to compare our results in the next section. We consider that the agent is able to dynamically select ZF and MRT schemes to design the passive beamforming vectors [58].

The ZF and MRT techniques are used to design the direction of the k-th beamforming vector, which is provided by:

$$\bar{w}_k = \alpha_k \frac{\mathbf{v}_k}{\|\mathbf{v}_k\|} + (1 - \alpha_k) \frac{\tilde{\mathbf{h}}_k}{\|\tilde{\mathbf{h}}_k\|}, \tag{62}$$

The variable $\alpha_k \in \{0, 1\}$ indicates the choice of beam direction, with $\alpha_k = 1$ denoting the use of the ZF scheme and $\alpha_k = 0$ indicating the MRT scheme. The term $\tilde{\mathbf{h}}_k^H = \mathbf{h}_{d,k}^H + \mathbf{h}_{r,k}^H \boldsymbol{\Theta} \mathbf{G}$, where $\mathbf{v}_k$ represents the k-th column of the matrix $\mathbf{V} = \mathbf{H}^H (\mathbf{H}\mathbf{H}^H)^{-1}$. Here, $\mathbf{H} = [\tilde{\mathbf{h}}_1, \tilde{\mathbf{h}}_2, \ldots, \tilde{\mathbf{h}}_K]$ is constructed from the vectors $\tilde{\mathbf{h}}_k$.

The 2-norm for each beamforming vector is computed as follows:

$$P_m = \sqrt{P_{\max}} \frac{\exp(x_m) - \exp(-x_m)}{\exp(x_m) + \exp(-x_m) + 1}, \tag{63}$$

where $x_m \in (-\infty, \infty)$ and $\frac{\exp(x_m) - \exp(-x_m)}{\exp(x_m) + \exp(-x_m)} \in [-1, 1]$ are the input and the output of the output layer of the neural network, respectively, and $m \in \mathcal{K} \cup \mathcal{S}$. Then, the beamforming derived from $w_i = P_i \bar{w}_i$ $(i \in K)$.

So, the action space is given by

$$A = \{\{P_m\}, \{\alpha_i\}, \boldsymbol{\Theta}\}_{m \in K \cup S, i \in K, l \in S}. \tag{64}$$

V. PERFORMANCE EVALUATION

In this section, we evaluate the performance of the considered BD-RIS-aided ISAC system through numerical analysis.

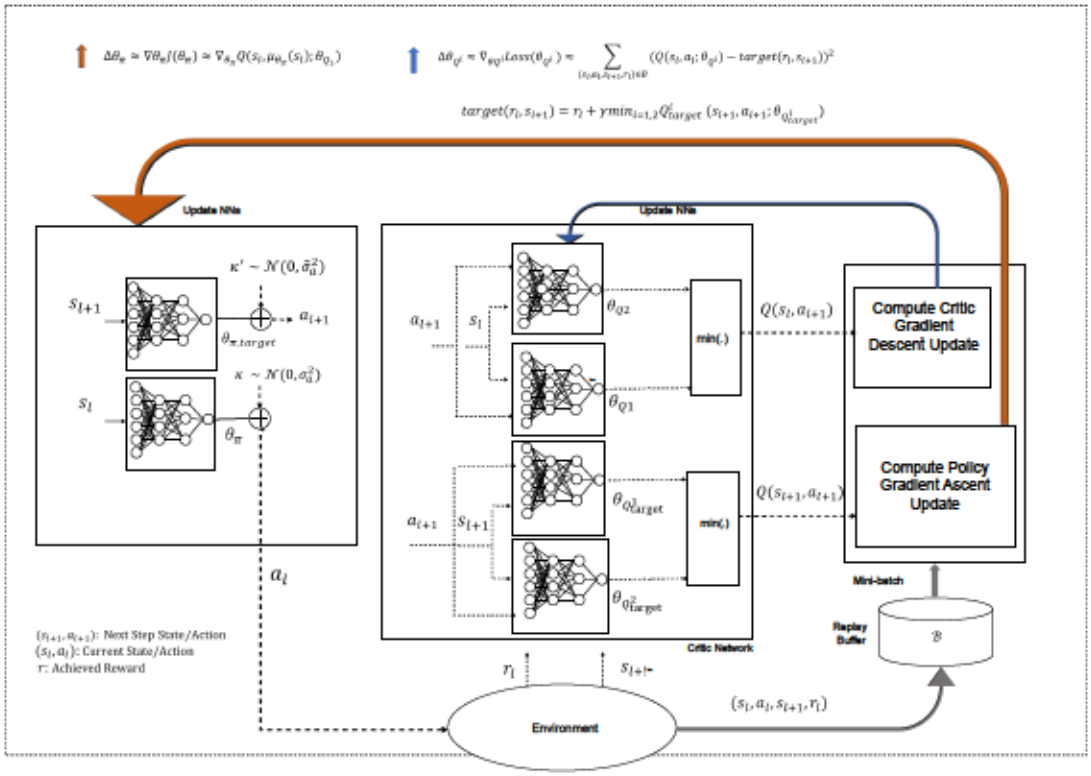

Fig. 3: Diagram of the TD3 method

A. System Configuration

We are considering a 3-dimensional scenario for a BD-RIS-aided ISAC network operating at 28 GHz. The transmitter (Tx), equipped with an 8-element array, is positioned at coordinates $(0, 0, 0)$ m. The RIS is located at $(0, 30, 30)$ m. The inter-element spacing in the BS antenna array and RIS elements is set as $\frac{\lambda}{2}$.

The network includes four users, each positioned on a circle with a radius of 4 meters, centered at coordinates $(20, 20, 0)$ m. The target is situated at $(35, 10, 0)$ m.

For channel modeling, transfer matrices such as $h_{d,k}$, $h_{R,k}$, and $h_{d,R}$ use a Rician model with parameters including the Rician factor $K_{AB} = 5$ dBm. Path loss (α_{AB}) is calculated based on the distances between points A and B, with a reference distance ($D_0 = 1$ m) and specific loss coefficients ($\alpha_{B,R} = 2.2$, $\alpha_{B,k} = 2.2$, $\alpha_{R,k} = 3.2$).

Power constraints are defined with a maximum power ($P_{\text{Max}} = 9$ W). The circuit power consumption for the BS and user devices is set at ($P_{\text{Cir}} = 1.01$ W), and the inverse of power amplifier efficiency ($\frac{1}{\xi}$) is set to 1.2. Noise power is characterized by σ_k^2, with $\sigma_s^2 = -100$ dBm for users and the target.

B. Impact of System Parameters

We compare the average EE performance of the proposed schemes, abbreviated as "TD3-BD-RIS," with "TD3-RIS." In Fig. 4, we illustrate the average EE for all considered schemes as a function of the number of RIS elements M, with $M_s = 8$ sensing elements and 5-antenna BSs. The results indicate a non-decreasing trend in performance with increasing M for all schemes. It is evident that BD-RISs outperform their diagonal RIS counterparts, demonstrating that BD-RISs provide greater optimization flexibility.

The FC-BD-RIS elements enhance EE by optimizing channel conditions for each user, which improves signal quality and reduces interference. This optimization allows the system to achieve higher data rates with lower power consumption. As M increases, the system can more effectively support a larger number of users K, leading to a significant improvement in EE. However, the benefits of increasing the number of RIS elements M may be limited due to the growing complexity, cost, and power consumption required for operating and controlling a larger RIS setup.

Besides, the diagram of EE versus the number of BS antennas is shown in Fig. 5 for three different schemes shown as: TD3-BD-RIS, MRT design, and ZF design for different values of noise variance for the users σ^2. It is observed that the MRT scheme performs well with relatively small $1/\sigma^2$, while the ZF scheme performs well with relatively large $1/\sigma^2$. Again, we can see that the schemes using BD-RIS outperform the ones with regular RIS. As observed, the EE exhibits a non-decreasing trend for all investigated schemes. It can be seen that, as N increases, the gap between the schemes with BD-RISs and those with diagonal RISs gets smaller as the effect of the BS is more pronounced combined with the fact that an RIS with $M = 16$ elements is relatively small. As N increases, the performance superiority of all schemes increases.

We examine the impact of mobile users' QoS requirements on the EE in Fig 6. As a benchmark, we also plot the

TABLE I: System Parameters

System Parameters			
Parameter	Value	Parameter	Value
Number of RIS reflecting elements	$M_y = 4$, $M_z = 4$	Number of RIS sensing elements	$M_{sy} = 2$, $M_{sz} = 4$
Power	$P_{\text{Cir}} = 1.01$ W	Maximum power	$P_{\max} = 9$ W
Noise power	$\sigma_k^2 = \sigma_s^2 = -100$ dBm	Epsilon	$\epsilon = 0.02$
Speed of light c	3×10^8 m/s	Carrier frequency f_c	28 GHz
Wavelength λ	$\frac{c}{f}$	The length of a coherent time block L	100
Reference distance	$D_0 = 1$ m	Rician factor coefficients	$K_{B,R} = K_{B,k} = K_{R,k} = 5$ dB
Path loss exponents	$\alpha_{B,R} = 2.2$, $\alpha_{B,k} = 2.2$, $\alpha_{R,k} = 3.2$	Position of the BS center	$(0, 0, 0)$
Inter-element spacing in BS	$\frac{\lambda}{2}$	Position of the BD-RIS center	$(0, 30, 30)$
RIS antenna separation	$dx = \frac{\lambda}{2}$, $dy = \frac{\lambda}{2}$	Position of target center	$(35, 10, 0)$

EE associated with conventional diagonal RIS and RIS with random phase shifts cases. As shown in Fig. 6, when QoS requirements elevate, the EE values decrease. This results from the more required transmit power consumption at the BS to meet the SINR requirement of users. Additionally, the FC-BD-RIS demonstrates superior EE compared to its diagonal counterpart. This improvement is attributed to the reduced transmit power consumption of the FC-BD-RIS, which enhances overall efficiency.

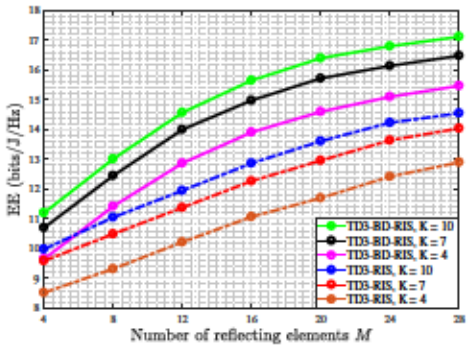

Fig. 4: Diagram of EE versus M, $\gamma_k = 3$ bits/s/Hz, $\epsilon = 0.02$, $P_{\text{BS}} = 30$ dBm, $N = 5$, $M_s = 8$, $\sigma^2 = -80$ dBm

The 7 illustrates the trade-off between sensing accuracy and communication performance in the TD3-BD-RIS scheme. CRB is used as a constraint to ensure a minimum level of sensing accuracy, impacting the overall system design. Starting with a lower value of CRB (considering lower values of P_{BS} or the lower diagram), which indicates higher sensing accuracy, EE is lower due to more resources being allocated for sensing. As the CRB increases, indicating a decrease in sensing accuracy, more resources can be reallocated to enhance communication performance, thereby improving the EE of the system. Increasing P_{BS} further increases the value of EE. The figure highlights how increasing the CRB, thus compromising on sensing accuracy, allows for better communication performance and higher EE, emphasizing the importance of balancing these two aspects to optimize overall system performance.

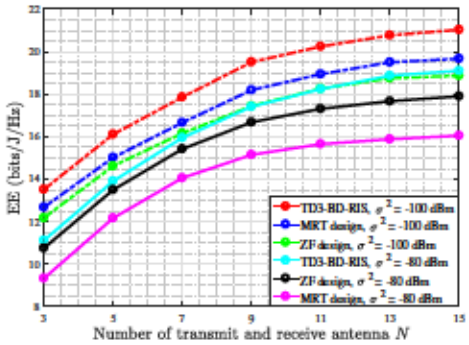

Fig. 5: Diagram of EE versus N, $\gamma_k = 3$ bits/s/Hz, $\epsilon = 0.02$, $P_{\text{BS}} = 30$ dBm, $M = 16$, $M_s = 8$, $K = 4$

As shown in the figure, even at lower CRB values (indicating higher sensing performance), the system can still achieve higher EE due to the existence of BD-RIS. This improvement underscores the potential of BD-RIS in optimizing the performance of RIS-aided ISAC systems, providing a more effective balance between sensing and communication needs.

C. Convergence Behavior

Figs. 8 and 9 illustrate the convergence characteristics of the proposed TD3 algorithm across both scenarios involving BD-RIS and RIS, over a span of 3500 episodes. The evaluation of the BD-RIS ISAC system's performance is based on the average reward and energy efficiency metrics.The consistent convergence observed in the figures for "TD3-BD-RIS" and

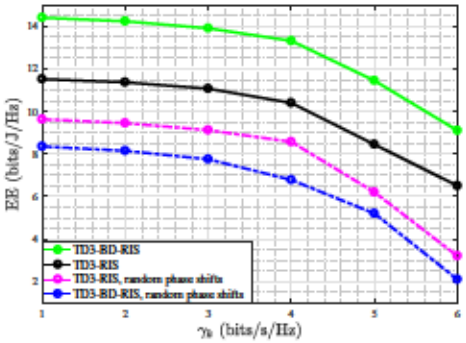

Fig. 6: Diagram of EE versus SINR, $\sigma^2 = -80$dBm, $\epsilon = 0.02$, $P_{\text{BS}} = 30$ dBm, $M = 16$, $M_s = 8$, $K = 4$, $N = 5$

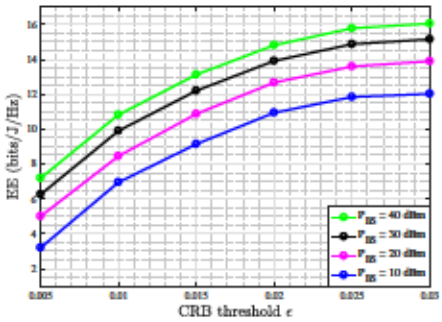

Fig. 7: Diagram of EE versus CRB threshold, $\sigma^2 = -80$dBm, $M = 16$,$M_s = 8$, $K = 4$, $N = 5$, $\gamma_k = 3$bits/s/Hz

"TD3-RIS" reflects the effectiveness of TD3's design, which, through the use of two critic networks to generate and minimize Q-value estimates, ensures stable and reliable learning dynamics, ultimately leading to higher and more stable rewards

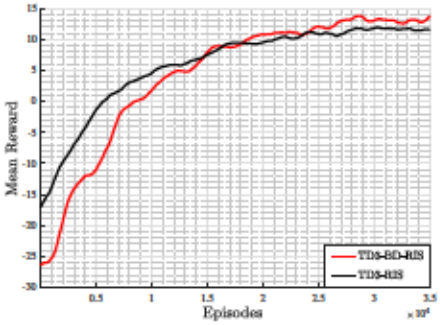

Fig. 8: Mean Reward

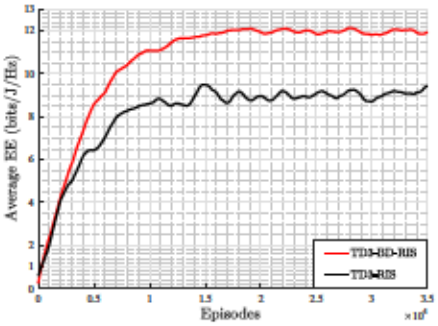

Fig. 9: Average EE

VI. Conclusion

This work shows that energy efficiency can be greatly increased by integrating BD-RIS into ISAC systems. The intricate limitations of BD-RIS, like orthogonality and fractional objective functions, are successfully addressed by our use of TD3 models. Our numerical simulation and validation results validate that BD-RIS has superior beamforming capabilities compared to conventional diagonal RIS and random phase shift RIS configurations. The capacity of BD-RIS to significantly enhance ISAC systems' sensing and communication quality is demonstrated by this work.

Appendix
Fisher Information Matrix Computation for Target Estimation

It is required to have $\mathbf{J}_{\tau\tau}, \mathbf{J}_{\tau\bar{\alpha}}, \mathbf{J}_{\bar{\alpha}\bar{\alpha}}$ for calculating $CRB(\bar{\tau})$. So, $\frac{\partial \mathbf{u}}{\partial \bar{\tau}}$,

$$\frac{\partial \mathbf{u}}{\partial \bar{\tau}} = \begin{bmatrix} \frac{\partial \mathbf{u}}{\partial \tau_1} \\ \frac{\partial \mathbf{u}}{\partial \tau_2} \end{bmatrix} = \begin{bmatrix} \frac{\partial \mathbf{u}[1]}{\partial \tau_1} \\ \cdots \\ \frac{\partial \mathbf{u}[L]}{\partial \tau_1} \\ \frac{\partial \mathbf{u}[1]}{\partial \tau_2} \\ \cdots \\ \frac{\partial \mathbf{u}[L]}{\partial \tau_2} \end{bmatrix}_{2M_s L \times 1} \tag{65}$$

To calculate the elements of Eq. 65 , the derivatives of $\frac{\partial \mathbf{u}[l]}{\partial \tau_1}, \frac{\partial \mathbf{u}[l]}{\partial \tau_2} \in \mathcal{C}^{M_s \times 1}$ for all time-indexes is required.

$$\frac{\partial \mathbf{u}[l]}{\partial \bar{\tau}_1} = \alpha \left(\frac{\partial \mathbf{a}(\tau_1, \tau_2)}{\partial \tau_1} \mathbf{b}^T(\tau_1, \tau_2) \mathbf{\Theta} \mathbf{G} \mathbf{x}[l] + \mathbf{a}(\tau_1, \tau_2) \frac{\partial \mathbf{b}^T(\tau_1, \tau_2)}{\partial \tau_1} \mathbf{\Theta} \mathbf{G} \mathbf{x}[l] \right) \tag{66}$$

$$\begin{aligned} \frac{\partial \mathbf{u}[l]}{\partial \bar{\tau}_2} = \alpha \Bigg(& \frac{\partial \mathbf{a}(\tau_1, \tau_2)}{\partial \tau_2} \mathbf{b}^T(\tau_1, \tau_2) \mathbf{\Theta} \mathbf{G} \mathbf{x}[l] \\ & + \mathbf{a}(\tau_1, \tau_2) \frac{\partial \mathbf{b}^T(\tau_1, \tau_2)}{\partial \tau_2} \mathbf{\Theta} \mathbf{G} \mathbf{x}[l] \Bigg) \end{aligned} \tag{67}$$

$$\begin{aligned} \frac{\partial \mathbf{a}(\tau_1, \tau_2)}{\partial \tau_1} = & \frac{1}{\sqrt{M_s}} \Bigg[0, -j \frac{2\pi d_y}{\lambda} (2-1) \cos\tau_1 \cos\tau_2 e^{-j \frac{2\pi d_y}{\lambda} (2-1) \sin\tau_1 \cos\tau_2}, \\ & \cdots, -j \frac{2\pi d_y}{\lambda} (M_{s_y} - 1) \cos\tau_1 \cos\tau_2 e^{-j \frac{2\pi d_y}{\lambda} (M_{s_y} - 1) \sin\tau_1 \cos\tau_2} \Bigg]^T \\ & \otimes \Bigg[0, -j \frac{2\pi d_z}{\lambda} (2-1) \cos\tau_1 \sin\tau_2 e^{-j \frac{2\pi d_z}{\lambda} (2-1) \sin\tau_1 \sin\tau_2}, \\ & \cdots, -j \frac{2\pi d_z}{\lambda} (M_{s_z} - 1) \cos\tau_1 \sin\tau_2 e^{-j \frac{2\pi d_z}{\lambda} (M_{s_z} - 1) \cos\tau_1 \sin\tau_2} \Bigg]^T \end{aligned} \tag{68}$$

$$\begin{aligned} \frac{\partial \mathbf{b}(\tau_1, \tau_2)}{\partial \tau_1} = & \frac{1}{\sqrt{M}} \Bigg[0, -j \frac{2\pi d_y}{\lambda} (2-1) \cos\tau_1 \cos\tau_2 e^{-j \frac{2\pi d_y}{\lambda} (2-1) \sin\tau_1 \cos\tau_2}, \\ & \cdots, -j \frac{2\pi d_y}{\lambda} (M_y - 1) \cos\tau_1 \cos\tau_2 e^{-j \frac{2\pi d_y}{\lambda} (M_y - 1) \sin\tau_1 \cos\tau_2} \Bigg]^T \\ & \otimes \Bigg[0, -j \frac{2\pi d_z}{\lambda} (2-1) \cos\tau_1 \sin\tau_2 e^{-j \frac{2\pi d_z}{\lambda} (2-1) \sin\tau_1 \sin\tau_2}, \\ & \cdots, -j \frac{2\pi d_z}{\lambda} (M_z - 1) \cos\tau_1 \sin\tau_2 e^{-j \frac{2\pi d_z}{\lambda} (M_z - 1) \sin\tau_1 \sin\tau_2} \Bigg]^T \end{aligned} \tag{69}$$

$$\frac{\partial \mathbf{a}(\tau_1,\tau_2)}{\partial \tau_2} = \frac{1}{\sqrt{M_s}}\Big[0, j\frac{2\pi d_y}{\lambda}(2-1)\sin\tau_1\sin\tau_2 e^{-j\frac{2\pi d_y}{\lambda}(2-1)\sin\tau_1\cos\tau_2},$$
$$\cdots, j\frac{2\pi d_y}{\lambda}(M_{s_y}-1)\sin\tau_1\sin\tau_2 e^{-j\frac{2\pi d_y}{\lambda}(M_{s_y}-1)\sin\tau_1\cos\tau_2}\Big]^T$$
$$\otimes\Big[0, -j\frac{2\pi d_z}{\lambda}(2-1)\sin\tau_1\cos\tau_2 e^{-j\frac{2\pi d_z}{\lambda}(2-1)\sin\tau_1\sin\tau_2},$$
$$\cdots, -j\frac{2\pi d_z}{\lambda}(M_{s_z}-1)\sin\tau_1\cos\tau_2 e^{-j\frac{2\pi d_z}{\lambda}(M_{s_z}-1)\sin\tau_1\sin\tau_2}\Big]^T \tag{70}$$

$$\frac{\partial \mathbf{b}(\tau_1,\tau_2)}{\partial \tau_2} = \frac{1}{\sqrt{M}}\Big[0, j\frac{2\pi d_y}{\lambda}(2-1)\sin\tau_1\sin\tau_2 e^{-j\frac{2\pi d_y}{\lambda}(M_y-1)\sin\tau_1\cos\tau_2},$$
$$\cdots, j\frac{2\pi d_y}{\lambda}(M_y-1)\sin\tau_1\sin\tau_2 e^{-j\frac{2\pi d_y}{\lambda}(M_y-1)\sin\tau_1\cos\tau_2}\Big]^T$$
$$\otimes\Big[0, -j\frac{2\pi d_z}{\lambda}(2-1)\sin\tau_1\cos\tau_2 e^{-j\frac{2\pi d_z}{\lambda}(2-1)\sin\tau_1\sin\tau_2},$$
$$\cdots, -j\frac{2\pi d_z}{\lambda}(M_z-1)\sin\tau_1\cos\tau_2 e^{-j\frac{2\pi d_z}{\lambda}(M_z-1)\sin\tau_1\sin\tau_2}\Big]^T \tag{71}$$

Also,

$$\frac{\partial \mathbf{u}}{\partial \bar{\alpha}} = \begin{bmatrix}\frac{\partial \mathbf{u}}{\partial \mathrm{Re}(\alpha)}\\ \frac{\partial \mathbf{u}}{\partial \mathrm{Im}(\alpha)}\end{bmatrix} = \begin{bmatrix}\frac{\partial \mathbf{u}[1]}{\partial \mathrm{Re}(\alpha)}\\ \vdots \\ \frac{\partial \mathbf{u}[l]}{\partial \mathrm{Re}(\alpha)}\\ \frac{\partial \mathbf{u}[1]}{\partial \mathrm{Im}(\alpha)}\\ \vdots \\ \frac{\partial \mathbf{u}[L]}{\partial \mathrm{Im}(\alpha)}\end{bmatrix}_{2M_sL\times 1} \tag{72}$$

so,

$$\frac{\partial \mathbf{u}[l]}{\partial \mathrm{Re}(\alpha)} = \mathbf{a}(\tau_1,\tau_2)\mathbf{b}^T(\tau_1,\tau_2)\mathbf{\Theta}\mathbf{G}\mathbf{x}[l] \tag{73}$$

$$\frac{\partial \mathbf{u}[l]}{\partial \mathrm{Im}(\alpha)} = j\mathbf{a}(\tau_1,\tau_2)\mathbf{b}^T(\tau_1,\tau_2)\mathbf{\Theta}\mathbf{G}\mathbf{x}[l] \tag{74}$$

Therefore,

$$\mathbf{J}_{\tau\tau} = \frac{2}{\sigma_r^2}\mathrm{Re}\left\{\frac{\partial \mathbf{u}^H}{\partial \bar{\tau}}\frac{\partial \mathbf{u}}{\partial \bar{\tau}}\right\} = \frac{2}{\sigma_r^2}\mathrm{Re}\left(\begin{pmatrix}\frac{\partial \mathbf{u}}{\partial \tau_1}\\ \frac{\partial \mathbf{u}}{\partial \tau_2}\end{pmatrix}^H\begin{pmatrix}\frac{\partial \mathbf{u}}{\partial \tau_1}\\ \frac{\partial \mathbf{u}}{\partial \tau_2}\end{pmatrix}\right) = \frac{2}{\sigma_r^2}\mathrm{Re}\left(\begin{bmatrix}\left(\frac{\partial \mathbf{u}}{\partial \tau_1}\right)^H\frac{\partial \mathbf{u}}{\partial \tau_1} & \left(\frac{\partial \mathbf{u}}{\partial \tau_1}\right)^H\frac{\partial \mathbf{u}}{\partial \tau_2}\\ \left(\frac{\partial \mathbf{u}}{\partial \tau_2}\right)^H\frac{\partial \mathbf{u}}{\partial \tau_1} & \left(\frac{\partial \mathbf{u}}{\partial \tau_2}\right)^H\frac{\partial \mathbf{u}}{\partial \tau_2}\end{bmatrix}\right) \tag{75}$$

$$\mathbf{J}_{\tau\bar{\alpha}} = \frac{2}{\sigma_r^2}\mathrm{Re}\left\{\frac{\partial \mathbf{u}^H}{\partial \bar{\tau}}\frac{\partial \mathbf{u}}{\partial \bar{\alpha}}\right\} = \frac{2}{\sigma_r^2}\mathrm{Re}\left(\begin{bmatrix}\frac{\partial \mathbf{u}}{\partial \tau_1}\\ \frac{\partial \mathbf{u}}{\partial \tau_2}\end{bmatrix}^H\begin{bmatrix}\frac{\partial \mathbf{u}}{\partial \mathrm{Re}(\alpha)}\\ \frac{\partial \mathbf{u}}{\partial \mathrm{Im}(\alpha)}\end{bmatrix}\right) = \frac{2}{\sigma_r^2}\mathrm{Re}\left(\begin{bmatrix}(\frac{\partial u}{\partial \tau_1})^H\frac{\partial \mathbf{u}}{\partial \mathrm{Re}(\alpha)} & (\frac{\partial u}{\partial \tau_1})^H\frac{\partial \mathbf{u}}{\partial \mathrm{Im}(\alpha)}\\ (\frac{\partial u}{\partial \tau_2})^H\frac{\partial \mathbf{u}}{\partial \mathrm{Re}(\alpha)} & (\frac{\partial u}{\partial \tau_2})^H\frac{\partial \mathbf{u}}{\partial \mathrm{Im}(\alpha)}\end{bmatrix}\right) \tag{76}$$

$$\mathbf{J}_{\bar{\alpha}\bar{\alpha}} = \frac{2}{\sigma_r^2}\mathrm{Re}\left\{\frac{\partial \mathbf{u}^H}{\partial \bar{\alpha}}\frac{\partial \mathbf{u}}{\partial \bar{\alpha}}\right\} = \frac{2}{\sigma_r^2}\mathrm{Re}\left(\begin{bmatrix}\frac{\partial \mathbf{u}}{\partial \mathrm{Re}(\alpha)}\\ \frac{\partial \mathbf{u}}{\partial \mathrm{Im}(\alpha)}\end{bmatrix}^H\begin{bmatrix}\frac{\partial \mathbf{u}}{\partial \mathrm{Re}(\alpha)}\\ \frac{\partial \mathbf{u}}{\partial \mathrm{Im}(\alpha)}\end{bmatrix}\right) = \frac{2}{\sigma_r^2}\mathrm{Re}\left(\begin{bmatrix}\left(\frac{\partial u}{\partial \mathrm{Re}(\alpha)}\right)^H\frac{\partial \mathbf{u}}{\partial \mathrm{Re}(\alpha)} & \left(\frac{\partial u}{\partial \mathrm{Re}(\alpha)}\right)^H\frac{\partial \mathbf{u}}{\partial \mathrm{Im}(\alpha)}\\ \left(\frac{\partial u}{\partial \mathrm{Im}(\alpha)}\right)^H\frac{\partial \mathbf{u}}{\partial \mathrm{Re}(\alpha)} & \left(\frac{\partial u}{\partial \mathrm{Im}(\alpha)}\right)^H\frac{\partial \mathbf{u}}{\partial \mathrm{Im}(\alpha)}\end{bmatrix}\right) \tag{77}$$

References

[1] Hao, Wanming, et al. "Joint Beamforming Design for Hybrid RIS-Assisted mmWave ISAC System Relying on Hybrid Precoding Structure." IEEE Internet of Things Journal (2024).

[2] T. Wild, A. Grudnitsky, S. Mandelli, M. Henninger, J. Guan, and F. Schaich, "6G Integrated Sensing and Communication: From Vision to Realization," arXiv 2305.01978, 2023. [Online]. Available: https://arxiv.org/abs/2305.01978.

[3] M. Henninger, T. E. Abrudan, et al., "Probabilistic 5G Indoor Positioning Proof of Concept with Outlier Rejection," in 2022 EuCNC & 6G Summit, IEEE, 2022, pp. 249–254.

[4] 3GPP, "Feasibility Study on Integrated Sensing and Communication," TSG SA, Technical Report 22.837, 2023, Version 1.0.0 (Rel. 19).

[5] HEXA-X-II project, https://hexa-x-ii.eu/.

[6] F. Liu, Y. Cui, C. Masouros, J. Xu, T. X. Han, Y. C. Eldar, and S. Buzzi, "Integrated sensing and communications: Towards dual-functional wireless networks for 6G and beyond," IEEE J. Sel. Area Commun., vol. 40, no. 6, pp. 1728-1767, Jun. 2022.

[7] J. A. Zhang, M. L. Rahman, K. Wu, X. Huang, Y. J. Guo, S. Chen, and J. Yuan, "Enabling joint communication and radar sensing in mobile networks - A survey," IEEE Commun. Surv. Tut., vol. 24, no. 1, pp. 306-345, First Quart. 2022.

[8] R. Liu, M. Li, H. Luo, Q. Liu, and A. L. Swindlehurst, "Integrated sensing and communication with reconfigurable intelligent surfaces: Opportunities, applications, and future directions," IEEE Wireless Commun., vol. 30, no. 1, pp. 50–57, Feb. 2023.

[9] A. Abrardo, A. Toccafondi, and M. D. Renzo, "Design of reconfigurable intelligent surfaces by using s-parameter multiport network theory – optimization and full-wave validation," 2023.

[10] H. Zarini, N. Gholipoor, M. R. Mili, M. Rasti, H. Tabassum, and E. Hossain, "Liquid state machine-empowered reflection tracking in RISaided THz communications," in GLOBECOM 2022-2022 IEEE Global Commun. Conf. IEEE, 2022, pp. 5273–5278.

[11] M. Najafi, V. Jamali, R. Schober, and H. V. Poor, "Physics-based modeling and scalable optimization of large intelligent reflecting surfaces," IEEE Trans. Commun., vol. 69, no. 4, pp. 2673–2691, 2020.

[12] Li H, Shen S, Clerckx B. Synergizing beyond diagonal reconfigurable intelligent surface and rate-splitting multiple access. IEEE transactions on wireless communications. 2024 Jan 22.

[13] S. Shen, B. Clerckx, and R. Murch, "Modeling and architecture design of reconfigurable intelligent surfaces using scattering parameter network analysis," IEEE Transactions on Wireless Communications, vol. 21, no. 2, pp. 1229–1243, 2022.

[14] M. Nerini, S. Shen, and B. Clerckx, "Closed-form global optimization of beyond diagonal reconfigurable intelligent surfaces," IEEE Transactions on Wireless Communications, vol. 23, no. 2, pp. 1037–1051, 2024.

[15] Zou J, Sun S, Masouros C, Cui Y, Liu YF, Ng DW. Energy-efficient beamforming design for integrated sensing and communications systems. IEEE Transactions on Communications. 2024 Feb 26.

[16] S. Shen, et al. "Modeling and architecture design of reconfigurable intelligent surfaces using scattering parameter network analysis," IEEE Trans. Wireless Commun., vol. 21, no. 2, pp. 1229-1243, Feb. 2022.

[17] H. Li, S. Shen, M. Nerini and B. Clerckx, "Reconfigurable intelligent surfaces 2.0: Beyond diagonal phase shift matrices," early access, 2023, doi: 10.1109/MCOM.001.2300019.

[18] M. Nerini, S. Shen and B. Clerckx, "Closed-form global optimization of beyond diagonal reconfigurable intelligent surfaces," IEEE Trans. Wireless Commun., 2023. Early Access

[19] H. Li, S. Shen, M. Nerini, and B. Clerckx, "Reconfigurable intelligent surfaces 2.0: Beyond diagonal phase shift matrices," IEEE Commun. Mag., early access, Nov. 13, 2023, doi: 10.1109/MCOM.001.2300019.

[20] R. Liu, M. Li, H. Luo, Q. Liu, and A. L. Swindlehurst, "Integrated sensing and communication with reconfigurable intelligent surfaces: Opportunities, applications, and future directions," IEEE Wireless Commun., vol. 30, no. 1, pp. 50-57, Feb. 2023.

[21] H. Luo, R. Liu, M. Li, and Q. Liu, "RIS-aided integrated sensing and communication: Joint beamforming and reflection design," IEEE Trans. Veh. Technol., vol. 72, no. 7, pp. 9626-9630, Jul. 2023.

[22] H. Luo, R. Liu, M. Li, Y. Liu, and Q. Liu, "Joint beamforming design for RIS-assisted integrated sensing and communication systems," IEEE Trans. Veh. Technol., vol. 71, no. 12, pp. 13393-13397, Dec. 2022.

[23] B. Wang et al., "A dual-function radar-communication system empowered by beyond diagonal reconfigurable intelligent surface," arXiv preprint arXiv:2301.03286, 2023.

[24] T. Esmaeilbeig et al., "Beyond diagonal RIS: Key to nextgeneration integrated sensing and communications?" arXiv preprint arXiv:2402.14157, 2024.

[25] X. Liu, T. Huang, N. Shlezinger, Y. Liu, J. Zhou, and Y. C. Eldar, "Joint transmit beamforming for multiuser MIMO communications and MIMO radar," IEEE Trans. Signal Process., vol. 68, pp. 3929-3944, Jun. 2020.

[26] F. Liu, C. Masouros, A. Li, H. Sun, and L. Hanzo, "MU-MIMO communications with MIMO radar: From co-existence to joint transmission," IEEE Trans. Wireless Commun., vol. 17, no. 4, pp. 2755-2770, Apr. 2018.

[27] F. Liu, L. Zhou, C. Masouros, A. Li, W. Luo, and A. Petropulu, "Toward dual-functional radar-communication systems: Optimal waveform design," IEEE Trans. Signal Process., vol. 66, no. 16, pp. 4264-4279, Aug. 2018.

[28] R. Liu, M. Li, Q. Liu, and A. L. Swindlehurst, "Dual-functional radar-communication waveform design: A symbol-level precoding approach," IEEE J. Sel. Topics Signal Process., vol. 15, no. 6, pp. 1316-1331, Nov. 2021.

[29] R. Liu, M. Li, Q. Liu, and A. L. Swindlehurst, "Joint waveform and filter designs for STAP-SLP-based MIMO-DFRC systems," IEEE J. Sel. Areas Commun., vol. 40, no. 6, pp. 1918-1931, Jun. 2022.

[30] F. Liu, Y.-F. Liu, A. Li, C. Masouros, and Y. C. Eldar, "Cram´er-Rao bound optimization for joint radar-communication beamforming," IEEE Trans. Signal Process., vol. 70, pp. 240-253, Dec. 2021.

[31] H. Hua, T. X. Han, and J. Xu, "MIMO integrated sensing and communication: CRB-rate tradeoff," IEEE Trans. Wireless Commun., to appear.

[32] H. Li, S. Shen, and B. Clerckx, "Synergizing beyond diagonal reconfigurable intelligent surface and rate-splitting multiple access," IEEE Trans. Wireless Commun. (DOI = 10.1109/TWC.2024.3353596), 2024.

[33] H. Li, S. Shen, and B. Clerckx, "Beyond diagonal reconfigurable intelligent surfaces: a multi-sector mode enabling highly directional full-space wireless coverage," IEEE Journal on Selected Areas on Communications, vol. 41, no. 8, pp. 2446–2460, 2023.

[34] H. Li, S. Shen, and B. Clerckx, "Beyond diagonal reconfigurable intelligent surfaces: From transmitting and reflecting modes to single-, group-, and fully-connected architectures," IEEE Trans. Wireless Commun., vol. 22, no. 4, pp. 2311–2324, 2022.

[35] M. Soleymani, I. Santamaria, E. Jorswieck, and B. Clerckx, "Optimization of rate-splitting multiple access in beyond diagonal ris-assisted URLLC systems," IEEE Trans. Wireless Commun. (DOI=10.1109/TWC.2023.3324190), 2023.

[36] M. Nerini, S. Shen, and B. Clerckx, "Closed-form global optimization of beyond diagonal reconfigurable intelligent surfaces," IEEE Trans. Wireless Commun., (DOI: 10.1109/TWC.2023.3285262), 2023.

[37] I. Santamaria, M. Soleymani, E. Jorswieck, and J. Gutierrez, "SNR maximization in beyond diagonal RIS-assisted single and multiple antenna links," IEEE Signal Proc. Letters, vol. 30, pp. 923–926, 2023.

[38] T. Fang and Y. Mao, "A low-complexity beamforming design for beyond-diagonal RIS aided multi-user networks," IEEE Comm. Letters, vol. 28, no. 1, pp. 203–207, 2024.

[39] A. S. Sena, M. Rasti, N. H. Mahmood, and M. Latva-aho, "Beyond diagonal ris for multi-band multi-cell mimo networks: A practical frequency-dependent model and performance analysis," arXiv:2401:06475v1, 2024.

[40] Santamaria, I., Soleymani, M., Jorswieck, E., and Gutiérrez, J., 2024. MIMO Capacity Maximization with Beyond-Diagonal RIS. arXiv preprint arXiv:2406.02170.

[41] Z. Liu, Y. Liu, S. Shen, Q. Wu, and Q. Shi, "Enhancing isac network throughput using beyond diagonal ris," IEEE Wireless Communications Letters, pp. 1–1, 2024.

[42] Guang, Z., Liu, Y., Wu, Q., Wang, W., and Shi, Q., 2024. Power Minimization for ISAC System Using Beyond Diagonal Reconfigurable Intelligent Surface. IEEE Transactions on Vehicular Technology.

[43] Esmaeilbeig, K. V. Mishra, and M. Soltanalian, "Beyond diagonal RIS: Key to next-generation integrated sensing and communications?" arXiv preprint arXiv:2402.14157, 2024.

[44] Q. Zhu, M. Li, R. Liu, and Q. Liu, "Cramér-rao bound optimization for active RIS-empowered ISAC systems," arXiv, 2023. [Online]. Available: https://arxiv.org/abs/2309.09207.

[45] Chen, K., & Mao, Y., 2024. Transmitter Side Beyond-Diagonal RIS for mmWave Integrated Sensing and Communications. arXiv preprint arXiv:2404.12604.

[46] H. Zhou, M. Erol-Kantarci, Y. Liu, and H. V. Poor, "A survey on modelbased, heuristic, and machine learning optimization approaches in RISaided wireless networks," IEEE Communications Surveys & Tutorials (Early access), Dec. 2023.

[47] Saikia, P., Jee, A., Singh, K., Mumtaz, S. and Huang, W.J., 2023, December. STAR-RIS-Aided Full-Duplex ISAC Systems: A Novel Meta Reinforcement Learning Approach. In GLOBECOM 2023-2023 IEEE Global Communications Conference (pp. 5086-5091). IEEE.

[48] He, X., Ye, Y., Xu, H., Liu, W. and Zhou, A., 2024. Beamforming optimization of meta-learning algorithm based on gradient descent in RIS-assisted ISAC system. Physical Communication, p.102429.

[49] Gan, X., Huang, C., Yang, Z., Zhong, C., Chen, X., Zhang, Z., Guo, Q., Yuen, C. and Debbah, M., 2024. Bayesian learning for double-RIS aided ISAC systems with superimposed pilots and data. IEEE Journal of Selected Topics in Signal Processing.

[50] Saikia, P., Singh, K., Huang, W.J. and Duong, T.Q., 2024. Hybrid Deep Reinforcement Learning for Enhancing Localization and Communication Efficiency in RIS-Aided Cooperative ISAC Systems. IEEE Internet of Things Journal.

[51] S. Shen, B. Clerckx, and R. Murch, "Modeling and architecture design of reconfigurable intelligent surfaces using scattering parameter network analysis," IEEE Trans. Wireless Commun., vol. 21, no. 2, pp. 1229–1243, Feb. 2022.

[52] K. V. Mishra, A. Chattopadhyay, S. S. Acharjee, and A. P. Petropulu, "OptM3Sec: Optimizing multicast IRS-aided multiantenna DFRC secrecy channel with multiple eavesdroppers," in IEEE International Conference on Acoustics, Speech and Signal Processing, 2022, pp. 9037–9041.

[53] F. Liu, Y.-F. Liu, A. Li, C. Masouros, and Y. C. Eldar, "Cramer-Rao ´ bound optimization for joint radar-communication beamforming," IEEE Trans. Signal Process., vol. 70, pp. 240–253, Dec. 2021.

[54] Shen, S., Clerckx, B. and Murch, R., 2021. Modeling and architecture design of reconfigurable intelligent surfaces using scattering parameter network analysis. IEEE Transactions on Wireless Communications, 21(2), pp.1229-1243.

[55] H. Li, S. Shen, and B. Clerckx, "Beyond diagonal reconfigurable intelligent surfaces: From transmitting and reflecting modes to single-, group-, and fully-connected architectures," IEEE Trans. Wireless Commun., vol. 22, no. 4, pp. 2311–2324, 2022.

[56] M. Nerini, S. Shen, and B. Clerckx, "Closed-form global optimization of beyond diagonal reconfigurable intelligent surfaces," IEEE Trans. Wireless Commun., (DOI: 10.1109/TWC.2023.3285262), 2023.

[57] . Fujimoto, H. Hoof, and D. Meger, "Addressing function approximation error in actor-critic methods," in Int. Conf. Machine Learning. PMLR, 2018, pp. 1587–1596. [39] A. S. Kumar, L. Zhao, and X.

[58] Y. Zhang, Y. Lu, R. Zhang, B. Ai, and D. Niyato, "Deep reinforcement learning for secrecy energy efficiency maximization in ris-assisted networks," IEEE Trans. Veh. Technol., pp. 1–6, 2023.

Chapitre 4 - Conclusions et recommandations

4.1 Conclusions

La technologie de la surface intelligente reconfigurable a pris une place essentielle dans le réseau de communication mobile de 6G. Récemment, les communications assistées par RIS ont attiré l'attention en ce qui concerne la gestion des ressources réseau et la conception de phases RIS.

Dans le chapitre initial, nous examinons la conception écoénergétique des réseaux MISO assistés par RIS en direction descendante. Après avoir formulé le problème, le chapitre aborde la conception des phases RIS et l'attribution de puissance en utilisant les méthodes de maximisation de l'efficacité énergétique basées sur TR et GAW. Par la suite, les résultats de simulation sont confrontés à ceux des méthodes de maximisation de l'efficacité énergétique basées sur GA et SFP, ainsi qu'à une approche conventionnelle basée sur le relais. Les résultats mettent en évidence que les approches de maximisation de l'efficacité énergétique basées sur TR et GAW sont plus efficaces que les autres approches en termes d'EE.

Dans le chapitre suivant, la technologie RIS est intégrée dans les systèmes de communication OFDMA en liaison descendante multi-utilisateurs. Cette intégration vise à optimiser les coefficients de réflexion RIS, les allocations de fréquence OFDMA et les distributions de puissance, tout en respectant les exigences rigoureuses de qualité de service et les contraintes de puissance de transmission. Ces optimisations sont systématiquement abordées par une méthodologie axée sur l'efficacité énergétique, en dérivant les limites inférieures de l'efficacité énergétique. Le problème est traité de manière efficace par l'algorithme principal, qui intègre les approches MDSA, SQP et PSO, ce qui entraîne des améliorations significatives de l'efficacité énergétique par rapport aux

scénarios sans RIS.

Au cours du troisième chapitre, nous avons examiné le terrain des systèmes de communication assistés par RIS, en mettant l'accent sur les nombreux défis et les possibilités d'amélioration qu'ils offrent en matière de conscience électromagnétique. L'une des découvertes essentielles a été la signification des modèles EM physiquement cohérents, qui constituent la fondation pour élaborer des conceptions RIS solides et performantes, garantissant un contrôle précis de la propagation des ondes EM et améliorant la fiabilité du système. En outre, nous avons abordé le nouveau domaine de l'apprentissage automatique pour l'amélioration des RIS, en soulignant son potentiel pour simplifier le processus de conception en acquérant des connaissances sur les relations complexes au sein des structures RIS et des réponses électromagnétiques. Après avoir appris ces modèles EM et repéré les lacunes présentes dans le domaine, nous avons posé les fondations du dernier chapitre.

Le chapitre final se focalise sur l'amélioration d'un système de communication ISAC renforcé par BD-RIS en employant des méthodes d'apprentissage par renforcement. L'objectif de cette approche est d'examiner les défis liés à la mise en place de solutions optimales pour de tels systèmes sophistiqués.

4.2 Recommandations

Au cours de cette partie, nous visons à identifier les domaines de recherche qui nécessitent une exploration plus approfondie et à suggérer des pistes pour les recherches à venir.

4.2.1 Communications à Large Bande Assistées par BD-RIS

La formation de faisceaux à large bande dans les systèmes assistés par RIS pose des défis majeurs en raison de l'incapacité des RIS à effectuer des décalages de phase dépendants de la fréquence, ce qui complique le traitement du signal. Bien que de nombreuses études aient démontré les avantages de la formation de faisceaux RIS pour améliorer les performances de communication et de détection, ces travaux se sont principalement concentrés sur les systèmes à bande étroite. Cependant, la demande croissante en débits de données élevés et en capacités de détection améliorées nécessite le passage à des fréquences plus élevées et à des largeurs de bande plus importantes.

Le phénomène de décalage de faisceau, où la direction du faisceau formé varie en fonction de la fréquence d'opération, rend les techniques de formation de faisceau à bande étroite inadaptées aux systèmes RIS à large bande. Cela entraîne des fluctuations de gain importantes sur la bande passante souhaitée et une distorsion de la forme d'onde dans la direction visée, réduisant ainsi la largeur de bande utilisable, les débits de données et la résolution en distance, comme souligné dans [95].

En s'inspirant des travaux fondateurs de Demir et al. [96] sur les communications large bande assistées par BD-RIS, la contribution 2 propose une extension approfondie de ce scénario. En exploitant pleinement les capacités de configuration dynamique des BD-RIS, il est possible de surmonter les effets néfastes du décalage de faisceau et d'optimiser les performances globales du système dans des environnements à large bande.

4.2.2 Modèles conformes aux EM pour les RIS

Pour que les BD-RIS soient conformes aux principes électromagnétiques, il est essentiel que leurs modèles reflètent précisément les principes électromagnétiques

régissant le système. Cela signifie que les modèles doivent capturer de manière fidèle les processus physiques de diffusion et de transformation des signaux conformément à la théorie électromagnétique. Bien que les BD-RIS offrent la possibilité d'une matrice de diffusion plus flexible et des interactions plus complexes, leur conformité aux EM dépend de la précision des modèles. Pour que les BD-RIS soient pleinement conformes aux principes électromagnétiques, leurs modèles doivent non seulement intégrer ces principes, mais aussi être pratiquement utilisables dans les simulations et les optimisations au niveau du système.

Pour analyser et optimiser efficacement les systèmes sans fil assistés par les surfaces intelligentes reconfigurables, il est essentiel de disposer de modèles de communication à la fois précis et pratiques, qui capturent fidèlement les propriétés physiques et électromagnétiques des éléments RIS ainsi que leurs transformations d'ondes. Bien que les modèles électromagnétiques complets offrent des simulations détaillées, ils sont gourmands en ressources informatiques et souvent peu pratiques pour une analyse à l'échelle du système. Actuellement, il n'existe que quelques modèles conformes aux principes électromagnétiques pour les systèmes RIS, et ces modèles tendent à se concentrer sur des aspects spécifiques sans fournir une solution exhaustive [97]. Toutefois, certaines recherches récentes [98] présentent un nouveau modèle de communication conforme aux EM, aligné sur les principes de l'électromagnétisme, qui relie explicitement les champs diffusés aux courants et à l'impédance des éléments RIS, et propose une expression pratique de l'impédance totale pouvant être facilement intégrée dans les solutions des équations d'ondes.

4.2.3 Couplage Mutuel dans les Communications Assistées par RIS

Le couplage mutuel prend une importance croissante dans les communications assistées par RIS, en particulier lorsque les éléments RIS sont densément intégrés dans des applications telles que les communications holographiques. Représenté par les paramètres **Z/S**, le couplage mutuel désigne l'interaction entre les éléments RIS, ajoutant une complexité considérable au problème d'optimisation lorsqu'il est combiné avec d'autres variables telles que les vecteurs de formation de faisceaux.

Pour gérer cette complexité, plusieurs méthodes ont été proposées dans la littérature pour mesurer le couplage mutuel:

- Simulations électromagnétiques à ondes complètes: Cette méthode offre des informations détaillées sur les interactions électromagnétiques entre les éléments RIS, permettant une mesure précise des effets de couplage mutuel [99].
- Mesures expérimentales: Les évaluations pratiques, comme celles réalisées dans [99], fournissent des données empiriques sur le couplage mutuel, validant les résultats des simulations et garantissant leur applicabilité dans des conditions réelles.
- Expressions mathématiques en forme fermée : Ces expressions facilitent le développement d'algorithmes d'optimisation et permettent une compréhension approfondie du rôle du couplage mutuel dans le motif de ré-irradiation. Des exemples incluent [33] et [100].

L'optimisation des paramètres d'impédance et de diffusion pour le couplage mutuel, ainsi que des vecteurs de formation de faisceaux, pose des défis importants en raison de la complexité des effets de couplage mutuel. De nombreuses méthodes actuelles abordent

ce problème en simplifiant l'optimisation à la configuration des faisceaux actifs et passifs, tout en ignorant le couplage mutuel. Toutefois, cette approche simplifiée peut conduire à des modèles de canal moins précis.

Dans [33], l'accent est mis exclusivement sur l'optimisation des effets de couplage mutuel. En revanche, [101] présente une nouvelle approche d'optimisation conjointe pour les systèmes de communication MIMO multi-utilisateurs assistés par des RIS non locaux, modélisés à travers des paramètres de diffusion. Cette méthode optimise le couplage mutuel, les motifs de radiation, ainsi que la formation de faisceaux actifs et passifs de manière physiquement cohérente, en prenant en compte tant les configurations réfléchissantes que transmissives des RIS. Ils proposent une méthode d'optimisation hors ligne pré-calculée pour ces deux fonctionnalités des RIS, offrant ainsi un cadre de solution robuste et efficace qui intègre l'optimisation du couplage mutuel et des motifs de radiation dans la conception du système, évitant ainsi la nécessité de réglages complexes en temps réel.

Bien que l'approche d'optimisation hors ligne propose un cadre solide, elle ne permet pas de s'adapter aux modifications en temps réel de l'environnement de communication. Les recherches futures devraient viser à intégrer des techniques d'optimisation en ligne pour ajuster dynamiquement le couplage mutuel, les motifs de radiation et les vecteurs de formation de faisceaux en fonction des conditions de canal en temps réel. Le développement d'algorithmes capables de recalculer rapidement les paramètres optimaux en réponse aux variations des états de canal permettra de tirer parti des données en temps réel pour affiner continuellement les configurations RIS, assurant ainsi que le système maintienne des performances optimales malgré les conditions changeantes.

4.2.4 Optimisation des systèmes ISAC assistés par BD-RIS avec communications multi-porteuses

Les résultats de la contribution 2 pourraient être élargis à des scénarios plus pratiques impliquant des systèmes ISAC assistés par BD-RIS utilisant des communications multi-porteuses. En effet, la majorité des recherches sur les systèmes ISAC assistés par RIS ont principalement exploré des configurations avec une seule sous-porteuse, ce qui complique la gestion de l'évanouissement sélectif en fréquence et l'égalisation complexe du signal, rendant difficile le maintien de débits élevés. L'OFDM (en anglais OFDM, Orthogonal Frequency Division Multiplexing) s'avère crucial pour résoudre ces défis. Utilisé couramment dans les systèmes radar et de communication, l'OFDM optimise l'utilisation du spectre des fréquences et minimise la dégradation du signal à différentes fréquences, le rendant particulièrement adapté à l'intégration des fonctions radar et communication. Cependant, il n'existe pas encore de recherche spécifique sur les systèmes ISAC assistés par BD-RIS dans ce contexte. En se basant sur le modèle BD-RIS dépendant de la fréquence proposé dans les travaux récents [102], il est possible d'optimiser le système OFDM-ISAC assisté par BD-RIS pour améliorer l'efficacité énergétique.

Dans le cadre de l'OFDM, un signal à haut débit est divisé en plusieurs signaux à débit inférieur, chacun étant transmis simultanément sur différentes fréquences. Cette méthode améliore considérablement l'efficacité de la détection radar ainsi que de la communication sans fil, surpassant les anciens systèmes ISAC assistés par RIS qui n'utilisaient qu'une seule sous-porteuse.

4.2.5 Systèmes ISAC Multi-bandes Assistés par RIS

Un avantage remarquable des RIS est leur capacité d'adaptation aux différentes bandes de fréquences, allant de plusieurs GHz à des centaines de GHz, voire jusqu'à la lumière visible. Cette adaptabilité rend les RIS particulièrement adaptés à la 6G, où l'utilisation conjointe de plusieurs bandes de fréquences pour fournir des services ISAC est essentielle. Quelques études ont exploré les systèmes ISAC assistés par RIS fonctionnant dans plusieurs bandes. Malgré le nombre limité de travaux existants, Les systèmes ISAC MB (en anglais MB, Multi-Band) assistés par RIS présentent une grande valeur de recherche en raison de la complémentarité des différentes bandes, ce qui peut doter les communications de capacités de détection à haute résolution et à large couverture. En utilisant les informations sur l'CSI (en anglais CSI, Channel State Information) à travers plusieurs bandes de fréquences, les systèmes ISAC multi-bandes assistés par RIS ont le potentiel de suivre les positions des utilisateurs avec une grande précision.

4.2.6 Théorie de l'Information Électromagnétique dans les Communications Assistées par RIS

La théorie électromagnétique et la théorie de l'information sont des principes fondamentaux dans le domaine des communications sans fil, avec la théorie des antennes et la modélisation des canaux de propagation sans fil. Si ces idées ont évolué de manière distincte jusqu'à l'arrivée des réseaux 5G, l'arrivée des réseaux de communication 6G, qui englobent l'espace, l'air, le sol et la mer, demande une couverture sans couture dans un espace tridimensionnel. Ceci nécessite de recueillir en permanence des informations sur l'CSI et de calculer la capacité du canal à n'importe quel endroit et à n'importe quel moment. En outre, les nouvelles technologies de la 6G telles que les MIMO ultra-massifs et les MIMO holographiques nécessitent une conception intégrée des antennes et des

environnements de propagation sans fil. Il est devenu crucial d'intégrer la théorie électromagnétique, la théorie de l'information, la théorie des antennes et la modélisation des canaux de propagation sans fil afin de faire face à ces défis, ce qui a conduit à l'EIT (en anglais EIT, Electromagnetic Information Theory) [103].

La théorie ancienne de l'électromagnétisme, basée sur les équations de Maxwell, fonctionne en temps et en espace continus, principalement en ce qui concerne les champs macro. Cependant, sur des échelles microscopiques, les variations du champ local deviennent importantes, surtout dans des situations telles que des environnements à haute mobilité millimètre wave-aided wideband. La théorie de l'information de Shannon traditionnelle, adaptée aux canaux simples, manque de précision dans les environnements complexes et non stationnaires exigés par les technologies émergentes de la 6G telles que l'ISAC, le RIS, le MIMO massif et le MIMO holographique. En intégrant la théorie électromagnétique à la théorie de l'information, celle-ci s'élargit pour englober les canaux non stationnaires, ce qui facilite le passage de la théorie de l'information à un seul utilisateur en espace discret à la théorie de l'information multi-utilisateurs/réseau en espace continu. En combinant une conception optimale des antennes avec des modèles de canaux électromagnétiques en espace continu, on peut améliorer la capacité des canaux. Les équations de Maxwell sont utilisées pour étudier l'information mutuelle entre les ondes incidentes, réfléchies, transmises et diffusées, ce qui permet de décrire précisément les performances et la capacité dans les nouvelles technologies telles que le RIS. L'idée des métamatériaux d'information intègre davantage la théorie électromagnétique et la théorie de l'information, dans le but de gérer les ondes électromagnétiques dans des structures métamatériales afin d'améliorer leur efficacité spectrale et de réduire les coûts du système. Mais les techniques de traitement du signal classiques ne parviennent pas souvent à définir de manière précise les champs électromagnétiques, ce qui met en évidence l'importance

de nouvelles approches, comme l'utilisation du RIS pour comprendre les interactions des ondes électromagnétiques et réaliser des mécanismes de transmission de l'information électromagnétique de bout en bout dans les systèmes de communication [103].

Selon [104], le concept de méta-surface numérique, également appelé IM (en anglais IM, Information Metasurfaces), est présenté. L'article examine ses utilisations dans le domaine des communications sans fil. Les IM marquent un tournant majeur, étendant la recherche sur les méta-surfaces du domaine de la physique à celui de l'information.

Il serait intéressant de mener des recherches ultérieures afin d'approfondir les possibilités et les utilisations de la théorie de l'EIT dans les scénarios RIS. Cette étude pourrait englober des avancées théoriques, des mises en pratique concrètes et des expérimentations afin de maximiser les bénéfices potentiels de l'EIT [105].

4.2.7 Applications du Machine Learning pour l'Optimisation des Communications Assistées par RIS Basées sur l'Électromagnétisme

On a largement étudié les méthodes de machine learning pour améliorer les communications assistées par RIS dans [106–109], toutes sans prendre en compte des modèles électromagnétiques physiquement cohérents. Il n'y a pas encore de recherches approfondies sur les techniques de machine learning pour améliorer les communications assistées par RIS du point de vue électromagnétique. Même si de nombreuses études se focalisent sur la conception inverse de méta-surfaces en utilisant des techniques de machine learning, l'optimisation des systèmes de communication assistés par RIS basés sur l'électromagnétisme demeure relativement inconnue dans la littérature courante. De plus, l'intégration des techniques de machine learning dans les systèmes de communication assistés par RIS basés sur la EIT (en englais EIT, théorie de l'information électromagnétique) représente un territoire de recherche inexploré. Cela constitue un écart

de recherche significatif avec un potentiel immense. Les algorithmes de machine learning peuvent jouer un rôle crucial dans l'amélioration de l'efficacité et de la précision des communications assistées par RIS en utilisant l'EIT.

4.2.8 Communications Vertes

Dans l'évolution constante de la 5G et des futures technologies 6G, la multiplication des nœuds de réseau entraîne une hausse de la consommation d'énergie et des émissions de carbone. Les quatre secteurs dans lesquels les techniques les plus couramment utilisées pour améliorer l'EE des réseaux sans fil sont classés sont l'attribution des ressources, la planification et la mise en place du réseau, la collecte et la transmission d'énergie, ainsi que les solutions matérielles.

La EH (en anglais EH,energy harvesting), qui comprend également la collecte d'énergie RF (en anglais RF,radio frequency), offre le double avantage de prendre en charge la technologie SWIPT tout en utilisant les signaux d'interférence pour la collecte d'énergie. Ce concept a été étudié dans [57]. En utilisant la technologie SWIPT, les RIS peuvent potentiellement améliorer la collecte d'énergie. En outre, lorsqu'elles sont intégrées à la technologie du OAM (en anglais OAM,orbital angular momentum), les RIS peuvent transmettre les ondes OAM bloquées par des obstacles, ce qui ouvre une voie directe pour la SWIPT basée sur un moment angulaire orbital. Par conséquent, la technologie RIS-assistée OAM-SWIPT apparaît comme une technologie prometteuse pour les communications sans fil à venir, offrant une efficacité énergétique et spectrale. Les recherches menées dans [110–112] ont examiné l'OAM dans le domaine des communications assistées par RIS. Cependant, il est évident que des études approfondies sur l'utilisation combinée des technologies RIS et OAM présentent un potentiel important pour des progrès à venir. Afin d'assurer une transmission efficace des ondes OAM par les

RIS, il est nécessaire que les RIS puissent manipuler le champ électromagnétique afin de s'adapter aux caractéristiques spécifiques des ondes OAM.

Il est important de porter une attention particulière à l'allocation de ressources consciente des aspects électromagnétiques dans les communications assistées par RIS. Comme mentionné dans le Chapitre 2, différentes approches de problèmes conscients des aspects EM pour les communications assistées par RIS ont été suggérées dans la littérature, en abordant différents aspects de cette technologie. Ces formulations ont contribué de manière significative à notre Les termes utilisés ont joué un rôle important dans notre compréhension et l'amélioration des déploiements de RIS dans différentes situations. Toutefois, un écart de recherche significatif concerne les difficultés d'accès aux ressources dans le domaine des communications à large bande. Si les travaux actuels se sont principalement focalisés sur les cas à bande étroite, les défis et les possibilités liés aux systèmes de communication à large bande n'ont pas encore été étudiés en détail. C'est un sujet essentiel pour des recherches approfondies, car les communications à large bande sont de plus en plus fréquentes dans les réseaux sans fil contemporains, et des stratégies d'allocation de ressources appropriées peuvent avoir un effet considérable sur leurs performances et leur efficacité. Dans cette optique, l'incorporation des modèles physiques des systèmes RIS dans les formulations de problèmes peut apporter des perspectives et des solutions précieuses.

By incorporating physical models, researchers can design resource allocation algorithms that take into account not only electromagnetic aspects but also the specific characteristics of RIS elements and their influence on wideband communication channels. Employing this comprehensive approach, which combines EM-awareness with physical realism, has the potential to produce more robust and efficient resource allocation

strategies for wideband RIS-assisted communications.

4.2.9 Communications Optiques

L'alliance des communications optiques avec les communications assistées par RIS offre une opportunité prometteuse pour optimiser les performances des réseaux et faire face aux défis actuels des communications. Les progrès récents, comme l'introduction de la OSTAR-RIS (en englais OSTAR-RIS, surface intelligente reconfigurable à transmission et réflexion simultanées optiques), mettent en évidence le potentiel de cette intégration [113]. Les auteurs de [114] tentent de pallier cette lacune en offrant un tutoriel exhaustif sur les systèmes de VLC (en anglais VLC, Visible Light Communications) en intérieur, en utilisant la technologie RIS. Ils étudient les principes fondamentaux des VLC et des RIS, examinent les utilisations possibles des RIS optiques pour réduire les obstacles de ligne de vue et les problèmes d'orientation des dispositifs, et suggèrent des pistes pour des études ultérieures sur l'intégration des RIS optiques avec les technologies en développement. Toutefois, l'étude des RIS dans les systèmes de OWC (en anglais OWC, Optical Wireless Communications) demeure restreinte. Il est possible d'explorer de nouvelles architectures BD-RIS en intégrant les communications optiques.

Cette intégration peut se manifester de la manière suivante :

- Consistance Physique : On peut faire appel aux communications optiques afin de modéliser avec précision le comportement des éléments RIS. La prise en considération des caractéristiques physiques de la propagation de la lumière, comme la réflexion, la réfraction et la diffraction, ainsi que des caractéristiques des surfaces RIS, permet de concevoir un modèle plus précis et physiquement cohérent des RIS. Ce modèle a la capacité de prendre en compte les interactions complexes entre les ondes lumineuses et les éléments RIS, ce qui permet d'optimiser les

prévisions de performance et les stratégies d'utilisation.

- Architectures Innovantes : En combinant les communications optiques avec les communications assistées par RIS, il est possible de créer de nouvelles architectures RIS innovantes, comme les BD-RIS. L'étude de la synergie entre les composants optiques et les éléments RIS permet de proposer des architectures innovantes qui exploitent à la fois les caractéristiques optiques et électromagnétiques. Par exemple, en incorporant des commutateurs optiques ou des modulateurs dans les structures RIS, il est possible de reconfigurer dynamiquement les éléments RIS, ce qui entraîne une plus grande souplesse et adaptabilité dans l'optimisation du réseau.

4.2.10 Communications Quantiques

L'avancement rapide de la science de l'information quantique offre une sécurité accrue grâce à la communication quantique, un pouvoir de calcul transformateur grâce à l'informatique quantique et des capacités de détection révolutionnaires [115]. La manipulation des données numériques transportées par les ondes électromagnétiques est possible grâce aux métamatériaux numériques, également appelés métamatériaux d'information, ce qui pourrait révolutionner le traitement de l'information et les systèmes d'information sans fil à haute performance. Le codage binaire est utilisé par ces métamatériaux pour gérer en temps réel les ondes électromagnétiques, créant ainsi un lien entre les domaines physique et numérique. Dans le domaine électromagnétique non classique, étroitement lié à la science de l'information quantique, ils présentent un potentiel énorme pour la science fondamentale et les applications d'ingénierie. Les métamatériaux électromagnétiques peuvent continuer à faire progresser ces avancées inspirées de la quantique, créant ainsi des métamatériaux quantiques qui étendent les concepts traditionnels pour manipuler et détecter les ondes électromagnétiques non

classiques [116].

L'approche quantique des modèles physiques des RIS apporte une dimension captivante et novatrice à la compréhension des RIS. La physique quantique offre de nouvelles perspectives et possibilités dans la conception et le fonctionnement des RIS grâce à ses principes de superposition, d'entrelacement et d'incertitude.

Pour débloquer pleinement le potentiel des environnements EM intelligents activés par les RIS, il est essentiel d'identifier rapidement les configurations optimales des RIS pour atteindre des objectifs spécifiques. Bien que les outils mathématiques tels que la loi de Snell généralisée aident à gérer la réflexion anormale, il y a un manque de solutions semi-analytiques pour certaines fonctionnalités EM telles que le beamforming multiple, la focalisation de l'énergie et la diffusion diffuse, ainsi que des fonctions sans fil comme la diversité spatiale, le taux de données et la sécurité au niveau physique. Par conséquent, différentes approches d'optimisation pour les RIS ont été suggérées, telles que les algorithmes génétiques, la synthèse basée sur l'impédance, l'inversion électromagnétique, l'apprentissage automatique et l'optimisation dynamique. Néanmoins, malgré ces progrès, l'amélioration des configurations RIS demeure un défi computationnel en raison de la multitude de possibilités, de la complexité des environnements de diffusion EM et des contraintes de temps de traitement dans les systèmes sans fil.

Les avancées récentes dans le domaine de l'informatique quantique présentent une solution prometteuse pour faire face à ces défis informatiques. Les algorithmes quantiques comme la transformée de Fourier quantique ont été utilisés pour la synthèse des réseaux d'antennes dans les applications EM, tandis que l'algorithme HHL (en anglais HHL, Harrow–Hassidim–Lloyd) est employé pour caractériser les interconnexions. Les modes de guide d'ondes ont également été calculés à l'aide

d'algorithmes quantiques variationnels utilisant la méthode des différences finies. Pour les réseaux sans fil, l'informatique quantique simplifie des tâches comme la détection MIMO multi-utilisateurs, le traitement et l'optimisation des ressources pour les réseaux sans fil 6G [117, 118].

Quelques articles récents ont examiné les communications quantiques et l'informatique quantique pour les communications assistées par RIS, tels que [119–122]. Il est intéressant d'explorer les possibilités de fusionner les modèles EM conscients des communications assistées par RIS avec les connaissances et l'informatique quantiques.

4.2.11 Communications Sémantiques Améliorées par RIS avec Modèles Physiquement Cohérents

Ces dernières années, la communication sémantique a suscité une grande attention en favorisant la transmission du sens de l'information plutôt que la reconstruction précise des bits [123]. Cette approche bouleverse la façon dont nous communiquons et interprétons les informations, en accordant une grande importance au contexte et à l'intention derrière l'échange d'informations. Certaines recherches récentes ont examiné l'utilisation des RIS afin d'améliorer les communications sémantiques, dans le but d'utiliser leur potentiel pour influencer l'environnement électromagnétique afin d'améliorer la transmission des données [123–126].

En dépit de ces progrès, une voie prometteuse qui reste largement inexplorée est l'intégration de modèles RIS physiquement cohérents, qui, basés sur les principes des interactions des ondes électromagnétiques, sont à la base d'une plus grande précision et d'une plus grande efficacité dans le cadre des communications sémantiques améliorées par RIS. En intégrant les modèles EM des RIS dans le cadre des communications sémantiques, nous pouvons avoir une meilleure compréhension de la façon dont les éléments RIS

interagissent avec les ondes électromagnétiques et, par conséquent, influencent le contenu sémantique de lacommunication.

Ce processus d'intégration présente de multiples occasions. Elle offre la possibilité d'ajuster de manière dynamique les configurations des RIS, en réponse aux évolutions en temps réel de l'industrie électromagnétique. La capacité à s'adapter assure que le sens transmis reste intact, même en cas de fluctuations de la qualité du signal et d'interférences. En outre, la cohérence physique des modèles RIS facilite l'amélioration du transfert de données, ce qui permet au contenu sémantique d'être transmis avec une plus grande clarté et fiabilité.

4.2.12 Optimisation Multi-Objectifs avec Modèles RIS Physiquement Cohérents

Une étape essentielle pour améliorer les performances des communications renforcées par RIS est de créer un cadre d'optimisation multi-objectifs qui intègre des modèles physiquement cohérents des RIS. Il est important que ce cadre vise à trouver un équilibre entre l'optimisation de la capacité, la réduction des interférences et la préservation de l'énergie, tout en prenant en considération les contraintes physiques et les caractéristiques intrinsèques des RIS, afin de garantir leur faisabilité pratique. Même si les études actuelles, comme celles de [127–132], ont avancé considérablement dans le domaine de l'optimisation multi-objectifs pour les RIS, il reste une grande opportunité d'explorer l'optimisation consciente des EM. Cette approche scientifique a pour objectif de libérer davantage le potentiel des RIS en exploitant une compréhension approfondie et une manipulation des phénomènes EM au sein du cadre, ce qui ouvre la voie à des applications RIS plus performantes et avancées dans les systèmes de communication sans fil à venir.

Références

[1] S. Jamil, M. Rahman, M. S. Abbas, and Fawad, "Resource allocation using reconfigurable intelligent surface (ris)-assisted wireless networks in industry 5.0 scenario," in *Telecom*, vol. 3, no. 1. MDPI, 2022, pp. 163–173.

[2] R. Singh, A. Kaushik, W. Shin, M. Di Renzo, V. Sciancalepore, D. Lee, H. Sasaki, A. Shojaeifard, and O. A. Dobre, "Towards 6g evolution: Three enhancements, three innovations, and three major challenges," *arXiv preprint arXiv:2402.10781*, 2024.

[3] R. Liu, R. Y.-N. Li, M. D. Renzo, and L. Hanzo, "A vision and an evolutionary framework for 6g: Scenarios, capabilities and enablers," 2024. [Online]. Available: https://arxiv.org/abs/2305.13887

[4] Q. Wu, B. Zheng, C. You, L. Zhu, K. Shen, X. Shao, W. Mei, B. Di, H. Zhang, E. Basar *et al.*, "Intelligent surfaces empowered wireless network: Recent advances and the road to 6g," *Proceedings of the IEEE*, 2024.

[5] M. Katwe, A. Kaushik, L. Mohjazi, M. Abualhayja'a, D. Dardari, K. Singh, M. A. Imran, M. M. Butt, and O. A. Dobre, "An overview of intelligent meta-surfaces for 6g and beyond: Opportunities, trends, and challenges," *arXiv preprint arXiv:2405.03356*, 2024.

[6] M. Nerini, S. Shen, and B. Clerckx, "Discrete-value group and fully connected architectures for beyond diagonal reconfigurable intelligent surfaces," *IEEE Transactions on Vehicular Technology*, vol. 72, no. 12, pp. 16 354–16 368, 2023.

[7] W. Jiang, B. Han, M. A. Habibi, and H. D. Schotten, "The road towards 6g: A comprehensive survey," *IEEE Open Journal of the Communications Society*, vol. 2, pp. 334–366, 2021.

[8] A. Bayesteh, J. He, Y. Chen, P. Zhu, J. Ma, A. Shaban, Z. Yu, Y. Zhang, Z. Zhou, and G. Wang, "Integrated sensing and communication (isac)—from concept to practice," *Communications of Huawei Research*, pp. 4–25, 2022.

[9] F. Verde, V. Galdi, L. Zhang, and T. J. Cui, "Integrating sensing and communications: Simultaneously transmitting and reflecting digital coding metasurfaces," *arXiv preprint arXiv:2406.10826*, 2024.

[10] M. Asif Haider and Y. D. Zhang, "Ris-aided integrated sensing and communication: A mini-review," *Frontiers in Signal Processing*, vol. 3, p. 1197240, 2023.

[11] A. Kaushik, R. Singh, S. Dayarathna, R. Senanayake, M. Di Renzo, M. Dajer, H. Ji, Y. Kim, V. Sciancalepore, A. Zappone *et al.*, "Towards integrated sensing and communications for 6g: A standardization perspective," *arXiv preprint arXiv:2308.01227*, 2023.

[12] C. Huang, A. Zappone, G. C. Alexandropoulos, M. Debbah, and C. Yuen, "Reconfigurable intelligent surfaces for energy efficiency in wireless communication," *IEEE transactions on wireless communications*, vol. 18, no. 8, pp. 4157–4170, 2019.

[13] Q. Wu and R. Zhang, "Intelligent reflecting surface enhanced wireless network via joint active and passive beamforming," *IEEE transactions on wireless communications*, vol. 18, no. 11, pp. 5394–5409, 2019.

[14] ——, "Towards smart and reconfigurable environment: Intelligent reflecting surface aided wireless network," *IEEE communications magazine*, vol. 58, no. 1, pp. 106–112, 2019.

[15] Y. Liu, X. Liu, X. Mu, T. Hou, J. Xu, M. Di Renzo, and N. Al-Dhahir, "Reconfigurable intelligent surfaces: Principles and opportunities," *IEEE communications surveys & tutorials*, vol. 23, no. 3, pp. 1546–1577, 2021.

[16] B. Zheng, C. You, W. Mei, and R. Zhang, "A survey on channel estimation and practical passive beamforming design for intelligent reflecting surface aided wireless communications," *IEEE Communications Surveys & Tutorials*, vol. 24, no. 2, pp. 1035–1071, 2022.

[17] O. Franek, "Electromagnetics-based ris channel model with near-field accuracy improvement," in *2024 18th European Conference on Antennas and Propagation (EuCAP)*, 2024, pp. 1–5.

[18] M. Nerini, S. Shen, H. Li, M. D. Renzo, and B. Clerckx, "A universal framework for multiport network analysis of reconfigurable intelligent surfaces," *IEEE Transactions on Wireless Communications*, pp. 1–1, 2024.

[19] M. Di Renzo, A. Zappone, M. Debbah, M.-S. Alouini, C. Yuen, J. De Rosny, and S. Tretyakov, "Smart radio environments empowered by reconfigurable intelligent surfaces: How it works, state of research, and the road ahead," *IEEE journal on selected areas in communications*, vol. 38, no. 11, pp. 2450–2525, 2020.

[20] R. K. Fotock, A. Zappone, and M. Di Renzo, "Energy efficiency optimization in ris-aided wireless networks: Active versus nearly-passive ris with global reflection constraints," *IEEE Transactions on Communications*, 2023.

[21] C.-X. Wang, X. You, X. Gao, X. Zhu, Z. Li, C. Zhang, H. Wang, Y. Huang, Y. Chen, H. Haas, J. S. Thompson, E. G. Larsson, M. D. Renzo, W. Tong, P. Zhu, X. Shen, H. V. Poor, and L. Hanzo, "On the road to 6g: Visions, requirements, key technologies, and testbeds," *IEEE Communications Surveys Tutorials*, vol. 25, no. 2, pp. 905–974, 2023.

[22] T. Gong, P. Gavriilidis, R. Ji, C. Huang, G. C. Alexandropoulos, L. Wei, Z. Zhang, M. Debbah, H. V. Poor, and C. Yuen, "Holographic mimo communications: Theoretical foundations, enabling technologies, and future directions," *IEEE Communications Surveys Tutorials*, vol. 26, no. 1, pp. 196–257, 2024.

[23] Z. Li, J. Zhang, J. Zhu, S. Jin, and L. Dai, "Enhancing energy efficiency for reconfigurable intelligent surfaces with practical power models," *arXiv preprint arXiv:2310.15901*, 2023.

[24] N. Rajatheva, I. Atzeni, E. Bjornson, A. Bourdoux, S. Buzzi, J.-B. Dore, S. Erkucuk, M. Fuentes, K. Guan, Y. Hu *et al.*, "White paper on broadband connectivity in 6g," *arXiv preprint arXiv:2004.14247*, 2020.

[25] T. Mi, J. Zhang, R. Xiong, Z. Wang, P. Zhang, and R. C. Qiu, "Toward analytical electromagnetic models for reconfigurable intelligent surfaces," *IEEE Transactions on Wireless Communications*, vol. 23, no. 5, pp. 4170–4185, 2024.

[26] N. Rajatheva, I. Atzeni, E. Bjornson, A. Bourdoux, S. Buzzi, J.-B. Dore, S. Erkucuk, M. Fuentes, K. Guan, Y. Hu, X. Huang, J. Hulkkonen, J. M. Jornet, M. Katz, R. Nilsson, E. Panayirci, K. Rabie, N. Rajapaksha, M. Salehi, H. Sarieddeen, T. Svensson, O. Tervo, A. Tolli, Q. Wu, and W. Xu, "White paper on broadband connectivity in 6g," 2020. [Online]. Available: https://arxiv.org/abs/2004.14247

[27] A. Abrardo, A. Toccafondi, and M. D. Renzo, "Design of reconfigurable intelligent surfaces by using s-parameter multiport network theory – optimization and full-wave validation," 2023. [Online]. Available: https://arxiv.org/abs/2311.06648

[28] G. Gradoni and M. Di Renzo, "End-to-end mutual coupling aware communication model for reconfigurable intelligent surfaces: An electromagnetic-compliant approach based on mutual impedances," *IEEE Wireless Communications Letters*, vol. 10, no. 5, pp. 938–942, 2021.

[29] J. A. Nossek, D. Semmler, M. Joham, and W. Utschick, "Physically consistent modelling of wireless links with reconfigurable intelligent surfaces using multiport network analysis," *IEEE Wireless Communications Letters*, pp. 1–1, 2024.

[30] H. Li, S. Shen, and B. Clerckx, "Beyond diagonal reconfigurable intelligent surfaces: From transmitting and reflecting modes to single-, group-, and fully-connected architectures," *IEEE Transactions on Wireless Communications*, vol. 22, no. 4, pp. 2311–2324, 2023.

[31] H. Li, S. Shen, M. Nerini, and B. Clerckx, "Reconfigurable intelligent surfaces 2.0: Beyond diagonal phase shift matrices," 2023. [Online]. Available: https://arxiv.org/abs/2301.03288

[32] P. Zheng, R. Wang, A. Shamim, and T. Y. Al-Naffouri, "Mutual coupling in ris-aided communication: Model training and experimental validation," 2024. [Online]. Available: https://arxiv.org/abs/2311.10544

[33] H. Li, S. Shen, M. Nerini, M. Di Renzo, and B. Clerckx, "Beyond diagonal reconfigurable intelligent surfaces with mutual coupling: Modeling and optimization," *IEEE Communications Letters*, 2024.

[34] R. Ma, J. Tang, X. Y. Zhang, K.-K. Wong, and J. A. Chambers, "Ris-assisted swipt network for internet of everything under the electromagnetics-based communication model," *IEEE Internet of Things Journal*, vol. 11, no. 9, pp. 15 402–15 415, 2024.

[35] I. Santamaria, M. Soleymani, E. Jorswieck, and J. Gutiérrez, "Snr maximization in beyond diagonal ris-assisted single and multiple antenna links," *IEEE Signal Processing Letters*, vol. 30, pp. 923–926, 2023.

[36] X. Qian and M. Di Renzo, "Mutual coupling and unit cell aware optimization for reconfigurable intelligent surfaces," *IEEE Wireless Communications Letters*, vol. 10, no. 6, pp. 1183–1187, 2021.

[37] A. Subhash, A. Kammoun, A. Elzanaty, S. Kalyani, Y. H. Al-Badarneh, and M.-S. Alouini, "Optimal phase shift design for fair allocation in ris aided uplink network using statistical csi," 2023.

[38] Y. Zhou, Y. Liu, H. Li, Q. Wu, S. Shen, and B. Clerckx, "Optimizing power consumption, energy efficiency, and sum-rate using beyond diagonal ris—a unified approach," *IEEE Transactions on Wireless Communications*, vol. 23, no. 7, pp. 7423–7438, 2024.

[39] Q. Li, M. El-Hajjar, I. Hemadeh, A. Shojaeifard, and L. Hanzo, "Coordinated reconfigurable intelligent surfaces: Non-diagonal group-connected design," *IEEE Transactions on Vehicular Technology*, pp. 1–6, 2024.

[40] M. Nerini, S. Shen, H. Li, and B. Clerckx, "Beyond diagonal reconfigurable intelligent surfaces utilizing graph theory: Modeling, architecture design, and optimization," 2024. [Online]. Available: https://arxiv.org/abs/2305.05013

[41] A. S. de Sena, M. Rasti, N. H. Mahmood, and M. Latva-aho, "Beyond diagonal ris for multi-band multi-cell mimo networks: A practical frequency-dependent model and performance analysis," 2024. [Online]. Available: https://arxiv.org/abs/2401.06475

[42] M. Nerini, S. Shen, and B. Clerckx, "Closed-form global optimization of beyond diagonal reconfigurable intelligent surfaces," *IEEE Transactions on Wireless Communications*, vol. 23, no. 2, pp. 1037–1051, 2024.

[43] X. Cheng, Y. Lin, W. Shi, J. Li, C. Pan, F. Shu, Y. Wu, and J. Wang, "Joint optimization for ris-assisted wireless communications: From physical and electromagnetic perspectives," *IEEE Transactions on Communications*, vol. 70, no. 1, pp. 606–620, 2022.

[44] Z. Mao, W. Wang, Q. Xia, C. Zhong, X. Pan, and Z. Ye, "Element-grouping intelligent reflecting surface: Electromagnetic-compliant model and geometry-based optimization," *IEEE Transactions on Wireless Communications*, vol. 21, no. 7, pp. 5362–5376, 2022.

[45] N. S. Perović, L.-N. Tran, M. D. Renzo, and M. F. Flanagan, "Optimization of ris-aided siso systems based on a mutually coupled loaded wire dipole model," 2023.

[46] J. Sang, J. Lan, M. Zhou, B. Gao, W. Tang, X. Li, X. Yi, and S. Jin, "Quantized phase alignment by discrete phase shifts for reconfigurable intelligent surface-assisted communication systems," 2023.

[47] L. Cao, H. Yin, L. Tan, and X. Pei, "Ris with insufficient phase shifting capability: Modeling, beamforming, and experimental validations," 2023.

[48] J. Xu, X. Mu, and Y. Liu, "Exploiting star-riss in near-field communications," 2023.

[49] H. Li, S. Shen, and B. Clerckx, "A dynamic grouping strategy for beyond diagonal reconfigurable intelligent surfaces with hybrid transmitting and reflecting mode," *IEEE Transactions on Vehicular Technology*, vol. 72, no. 12, pp. 16 748–16 753, 2023.

[50] A. Abrardo, D. Dardari, M. Di Renzo, and X. Qian, "Mimo interference channels assisted by reconfigurable intelligent surfaces: Mutual coupling aware sum-rate optimization based on a mutual impedance channel model," *IEEE Wireless Communications Letters*, vol. 10, no. 12, pp. 2624–2628, 2021.

[51] M. Nerini, S. Shen, and B. Clerckx, "Static grouping strategy design for beyond diagonal reconfigurable intelligent surfaces," 2024. [Online]. Available: https://arxiv.org/abs/2403.09275

[52] H. Li, S. Shen, and B. Clerckx, "Synergizing beyond diagonal reconfigurable intelligent surface and rate-splitting multiple access," *IEEE Transactions on Wireless Communications*, pp. 1–1, 2024.

[53] Z. Liu, Y. Liu, S. Shen, Q. Wu, and Q. Shi, "Enhancing isac network throughput using beyond diagonal ris," *IEEE Wireless Communications Letters*, vol. 13, no. 6, pp. 1670–1674, 2024.

[54] D. Ying, D. J. Love, and B. M. Hochwald, "Sum-rate analysis for multi-user mimo systems with user exposure constraints," *IEEE Transactions on Wireless Communications*, vol. 16, no. 11, pp. 7376–7388, 2017.

[55] P. Mursia, S. Phang, V. Sciancalepore, G. Gradoni, and M. D. Renzo, "Saris: Scattering aware reconfigurable intelligent surface model and optimization for complex propagation channels," 2023.

[56] B. Peng, K.-L. Besser, S. Shen, F. Siegismund-Poschmann, R. Raghunath, D. Mittleman, V. Jamali, and E. A. Jorswieck, "Risnet: A domain-knowledge driven neural network architecture for ris optimization with mutual coupling and partial csi," 2024. [Online]. Available: https://arxiv.org/abs/2403.04028

[57] R. Ma, J. Tang, X. Zhang, K.-K. Wong, and J. A. Chambers, "Energy efficiency optimization for mutual-coupling-aware wireless communication system based on ris-enhanced swipt," *IEEE Internet of Things Journal*, pp. 1–1, 2023.

[58] A. Zappone and M. D. Renzo, "Energy efficiency optimization of reconfigurable intelligent surfaces with electromagnetic field exposure constraints," *IEEE Signal Processing Letters*, vol. 29, pp. 1447–1451, 2022.

[59] Y. Zhu, G. Zheng, and K.-K. Wong, "Stochastic geometry analysis of large intelligent surface-assisted millimeter wave networks," *IEEE Journal on Selected Areas in Communications*, vol. 38, no. 8, pp. 1749–1762, 2020.

[60] A. D. J. Torres, L. Sanguinetti, and E. Björnson, "Electromagnetic interference in ris-aided communications," 2021.

[61] S. Bidabadi, M. Ouameur, M. Bagaa, D. Massicotte, F. Figueiredo, and A. Chaaban, "Physically-consistent em models-aware ris-aided communication —

a survey," *Computer Networks*, vol. 257, p. 110963, 2025. [Online]. Available: https://www.sciencedirect.com/science/article/pii/S1389128624007953

[62] J. Nocedal and S. J. Wright, *Numerical optimization*. Springer, 1999.

[63] H. Zhou, M. Erol-Kantarci, Y. Liu, and H. V. Poor, "Heuristic algorithms for ris-assisted wireless networks: Exploring heuristic-aided machine learning," *IEEE Wireless Communications*, 2024.

[64] S. Bidabadi, M. Ahmed Ouameur, M. Bagaa, and D. Massicotte, "Energy efficient resource allocation for re-configurable intelligent surface-assisted wireless networks," *EURASIP Journal on Wireless Communications and Networking*, vol. 2023, no. 1, p. 89, Sep 5 2023.

[65] R. Chen, M. Liu, Y. Hui, N. Cheng, and J. Li, "Reconfigurable intelligent surfaces for 6g iot wireless positioning: A contemporary survey," *IEEE Internet of Things Journal*, vol. 9, no. 23, pp. 23 570–23 582, 2022.

[66] H. Jiao, H. Liu, and Z. Wang, "Reconfigurable intelligent surfaces aided wireless communication: Key technologies and challenges," in *2022 International Wireless Communications and Mobile Computing (IWCMC)*. IEEE, 2022, pp. 1364–1368.

[67] Y. Chen, Y. Wang, J. Zhang, P. Zhang, and L. Hanzo, "Reconfigurable intelligent surface (ris)-aided vehicular networks: Their protocols, resource allocation, and performance," *IEEE Vehicular Technology Magazine*, vol. 17, no. 2, pp. 26–36, 2022.

[68] A. Anas, L. Xingwang, A. Ramez, R. Khaled, and N. Galymzhan, "Intelligent reflecting surface-aided uav communications: A survey and research opportunities," in *2022 13th International Symposium on Communication Systems, Networks and Digital Signal Processing (CSNDSP)*. IEEE, 2022, pp. 362–367.

[69] A. Alkhatieb, K. Rabie, X. Li, G. Nauryzbayev, and R. Alkhatib, "Irs-aided uav for future wireless communications: A survey and research opportunities," *arXiv preprint arXiv:2212.06015*, 2022.

[70] R. Xiong, J. Zhang, X. Dong, Z. Wang, J. Liu, T. Mi, and R. C. Qiu, "Ris-aided wireless communication in real-world: Antennas design, prototyping, beam reshape and field trials," *arXiv preprint arXiv:2303.03287*, 2023.

[71] K. Faisal and W. Choi, "Machine learning approaches for reconfigurable intelligent surfaces: A survey," *IEEE Access*, vol. 10, pp. 27 343–27 367, 2022.

[72] N. Rahmatov and H. Baek, "Ris-carried uav communication: Current research, challenges, and future trends," *ICT Express*, 2023.

[73] T.-H. Nguyen, H. Park, and L. Park, "Recent studies on deep reinforcement learning in ris-uav communication networks," in *2023 International Conference on Artificial Intelligence in Information and Communication (ICAIIC)*. IEEE, 2023, pp. 378–381.

[74] A. A. Puspitasari and B. M. Lee, "A survey on reinforcement learning for reconfigurable intelligent surfaces in wireless communications," *Sensors*, vol. 23, no. 5, p. 2554, 2023.

[75] J. Xu, C. Yuen, C. Huang, N. Ul Hassan, G. C. Alexandropoulos, M. Di Renzo, and M. Debbah, "Reconfiguring wireless environments via intelligent surfaces for 6g: reflection, modulation, and security," *Science China Information Sciences*, vol. 66, no. 3, p. 130304, 2023.

[76] S. Bidabadi, M. Ouameur, M. Bagaa, and D. Massicotte, "Energy-efficient ris-enabled siso-ofdma communication via lower bound optimization," *Electronics*, vol. 13, no. 6, p. 1040, Mar 11 2024.

[77] H. Li, S. Shen, and B. Clerckx, "Synergizing beyond diagonal reconfigurable intelligent surface and rate-splitting multiple access," 2024. [Online]. Available: https://arxiv.org/abs/2303.06912

[78] ——, "Beyond diagonal reconfigurable intelligent surfaces: A multi-sector mode enabling highly directional full-space wireless coverage," *IEEE Journal on Selected Areas in Communications*, vol. 41, no. 8, pp. 2446–2460, 2023.

[79] ——, "Beyond diagonal reconfigurable intelligent surfaces: From transmitting and reflecting modes to single-, group-, and fully-connected architectures," *IEEE Transactions on Wireless Communications*, vol. 22, no. 4, pp. 2311–2324, 2022.

[80] M. Soleymani, I. Santamaria, E. A. Jorswieck, and B. Clerckx, "Optimization of rate-splitting multiple access in beyond diagonal ris-assisted urllc systems," *IEEE Transactions on Wireless Communications*, vol. 23, no. 5, pp. 5063–5078, 2023.

[81] M. Nerini, S. Shen, and B. Clerckx, "Closed-form global optimization of beyond diagonal reconfigurable intelligent surfaces," 2023. [Online]. Available: https://arxiv.org/abs/2211.06117

[82] I. Santamaria, M. Soleymani, E. Jorswieck, and J. Gutiérrez, "Snr maximization in beyond diagonal ris-assisted single and multiple antenna links," *IEEE Signal Processing Letters*, vol. 30, pp. 923–926, 2023.

[83] T. Fang and Y. Mao, "A low-complexity beamforming design for beyond-diagonal ris aided multi-user networks," 2023. [Online]. Available: https://arxiv.org/abs/2307.09807

[84] I. Santamaria, M. Soleymani, E. Jorswieck, and J. Gutiérrez, "Mimo capacity maximization with beyond-diagonal ris," 2024. [Online]. Available: https://arxiv.org/abs/2406.02170

[85] Z. Liu, Y. Liu, S. Shen, Q. Wu, and Q. Shi, "Enhancing isac network throughput using beyond diagonal ris," *IEEE Wireless Communications Letters*, vol. 13, no. 6, pp. 1670–1674, 2024.

[86] Z. Guang, Y. Liu, Q. Wu, W. Wang, and Q. Shi, "Power minimization for isac system using beyond diagonal reconfigurable intelligent surface," *IEEE Transactions on Vehicular Technology*, 2024.

[87] T. Esmaeilbeig, K. V. Mishra, and M. Soltanalian, "Beyond diagonal ris: Key to next-generation integrated sensing and communications?" 2024. [Online]. Available: https://arxiv.org/abs/2402.14157

[88]

[89] K. Chen and Y. Mao, "Transmitter side beyond-diagonal ris for mmwave integrated sensing and communications," 2024. [Online]. Available: https://arxiv.org/abs/2404.12604

[90] H. Zhou, M. Erol-Kantarci, Y. Liu, and H. V. Poor, "A survey on model-based, heuristic, and machine learning optimization approaches in ris-aided wireless networks," 2023. [Online]. Available: https://arxiv.org/abs/2303.14320

[91] P. Saikia, A. Jee, K. Singh, S. Mumtaz, and W.-J. Huang, "Star-ris-aided full-duplex isac systems: A novel meta reinforcement learning approach," in *GLOBECOM 2023 - 2023 IEEE Global Communications Conference*, 2023, pp. 5086–5091.

[92] X. He, Y. Ye, H. Xu, W. Liu, and A. Zhou, "Beamforming optimization of meta-learning algorithm based on gradient descent in ris-assisted isac system," *Physical Communication*, vol. 66, p. 102429, 2024.

[93] P. Saikia, K. Singh, W.-J. Huang, and T. Q. Duong, "Hybrid deep reinforcement learning for enhancing localization and communication efficiency in ris-aided cooperative isac systems," *IEEE Internet of Things Journal*, vol. 11, no. 18, pp. 29 494–29 510, 2024.

[94] S. Bidabadi, M. A. Ouameur, M. Bagaa, D. Massicotte, F. D. Figueiredo, and A. Chaaban, "Ai-enabled resource allocation for bd-ris empowered isac systems," 2024, submitted to IEEE Transactions on Wireless Communications.

[95] X. Qian, X. Hu, C. Liu, and M. Peng, "Wideband beamforming with ris: A unified framework via space-frequency transformation," *arXiv preprint arXiv:2407.05293*, 2024.

[96] Ö. T. Demir and E. Björnson, "Wideband channel capacity maximization with beyond diagonal ris reflection matrices," *arXiv preprint arXiv:2404.00982*, 2024.

[97] O. Franek, "Electromagnetics-based ris channel model with near-field accuracy improvement," in *2024 18th European Conference on Antennas and Propagation (EuCAP)*. IEEE, 2024, pp. 1–5.

[98] H. Ezzeddine, A. Ourir, and J. de Rosny, "An electromagnetic-compliant scattering model for reconfigurable intelligent surfaces," in *2024 18th European Conference on Antennas and Propagation (EuCAP)*, 2024, pp. 1–5.

[99] Z. Zheng, S. Wang, Z. Fei, Z. Sun, and J. Yuan, "On the mutual information of multi-ris assisted mimo: From operator-valued free probability aspect," 2023.

[100] P. Mursia, F. Devoti, M. Rossanese, V. Sciancalepore, G. Gradoni, M. Di Renzo, and X. Costa-Perez, "T3dris: Advancing conformal ris design through in-depth analysis of mutual coupling effects," *arXiv preprint arXiv:2404.05261*, 2024.

[101] D. Wijekoon, A. Mezghani, G. C. Alexandropoulos, and E. Hossain, "Physically-consistent modeling and optimization of non-local ris-assisted multi-user mimo communication systems," *arXiv preprint arXiv:2406.05617*, 2024.

[102] H. Li, M. Nerini, S. Shen, and B. Clerckx, "Beyond diagonal reconfigurable intelligent surfaces in wideband ofdm communications: Circuit-based modeling and optimization," 2024.

[103] C.-X. Wang, Y. Yang, J. Huang, X. Gao, T. J. Cui, and L. Hanzo, "Electromagnetic information theory: Fundamentals and applications for 6g wireless communication systems," 2024. [Online]. Available: https://arxiv.org/abs/2401.08921

[104] J. Y. Dai, W. Tang, M. Z. Chen, C. H. Chan, Q. Cheng, S. Jin, and T. J. Cui, "Wireless communication based on information metasurfaces," *IEEE Transactions on Microwave Theory and Techniques*, vol. 69, no. 3, pp. 1493–1510, 2021.

[105] Z. Wan, J. Zhu, Z. Zhang, L. Dai, and C.-B. Chae, "Mutual information for electromagnetic information theory based on random fields," *IEEE Transactions on Communications*, vol. 71, no. 4, pp. 1982–1996, 2023.

[106] H. Zhou, M. Erol-Kantarci, Y. Liu, and H. V. Poor, "A survey on model-based, heuristic, and machine learning optimization approaches in ris-aided wireless networks," *IEEE Communications Surveys Tutorials*, vol. 26, no. 2, pp. 781–823, 2024.

[107] A. A. Puspitasari and B. M. Lee, "A survey on reinforcement learning for reconfigurable intelligent surfaces in wireless communications," *Sensors (Basel, Switzerland)*, vol. 23, 2023. [Online]. Available: https://api.semanticscholar.org/CorpusID:257250906

[108] S. K. Das, F. Benkhelifa, Y. Sun, H. Abumarshoud, Q. H. Abbasi, M. A. Imran, and L. S. Mohjazi, "Comprehensive review on ml-based ris-enhanced iot systems: basics, research progress and future challenges," *Comput. Networks*, vol. 224, p. 109581, 2023. [Online]. Available: https://api.semanticscholar.org/CorpusID:256175248

[109] H. Zhou, M. Erol-Kantarci, Y. Liu, and H. V. Poor, "Heuristic algorithms for ris-assisted wireless networks: Exploring heuristic-aided machine learning," *arXiv preprint arXiv:2307.01205*, 2023.

[110] R. Lyu and W. Cheng, "Joint reflection and power splitting optimization for ris-assisted oam-swipt," in *GLOBECOM 2022 - 2022 IEEE Global Communications Conference*, 2022, pp. 1073–1078.

[111] D. Shen, Z. Zhang, and L. Dai, "Joint beamforming design for ris-assisted cell-free network with multi-hop transmissions," *Tsinghua Science and Technology*, vol. 28, no. 6, pp. 1115–1127, 2023.

[112] Z. Yang, Y. Hu, Z. Zhang, W. Xu, C. Zhong, and K.-K. Wong, "Reconfigurable intelligent surface based orbital angular momentum: Architecture, opportunities, and challenges," *IEEE Wireless Communications*, vol. 28, no. 6, pp. 132–137, 2021.

[113] O. Maraqa, S. Aboagye, and T. M. N. Ngatched, "Optical star-ris-aided vlc systems: Rsma versus noma," *IEEE Open Journal of the Communications Society*, vol. 5, pp. 430–441, 2024.

[114] S. Aboagye, A. R. Ndjiongue, T. M. N. Ngatched, O. A. Dobre, and H. V. Poor, "Ris-assisted visible light communication systems: A tutorial," *IEEE Communications Surveys Tutorials*, vol. 25, no. 1, pp. 251–288, 2023.

[115] M. El MORSALANI, "Quantum sensing: Basics, algorithms, applications and the german ecosystem," 2024.

[116] J. You, Q. Ma, L. Zhang, C. Liu, J. Zhang, S. Liu, and T. Cui, "Electromagnetic metamaterials: From classical to quantum," *Electromagnetic Science*, vol. 1, no. 1, pp. 1–33, 2023.

[117] Q. J. Lim, C. Ross, A. Ghosh, F. Vook, G. Gradoni, and Z. Peng, "Quantum-assisted combinatorial optimization for reconfigurable intelligent surfaces in smart electromagnetic environments," *IEEE Transactions on Antennas and Propagation*, 2023.

[118] J. C. De Luna Ducoing and K. Nikitopoulos, "Quantum annealing for next-generation mu-mimo detection: Evaluation and challenges," in *ICC 2022 - IEEE International Conference on Communications*, 2022, pp. 637–642.

[119] T. Ohyama, Y. Kawamoto, and N. Kato, "Resource allocation optimization by quantum computing for shared use of standalone irs," *IEEE Transactions on Emerging Topics in Computing*, 2023.

[120] C. Ross, G. Gradoni, Q. J. Lim, and Z. Peng, "Engineering reflective metasurfaces with ising hamiltonian and quantum annealing," *IEEE Transactions on Antennas and Propagation*, vol. 70, no. 4, pp. 2841–2854, 2022.

[121] Q. J. Lim, C. Ross, A. Ghosh, F. Vook, G. Gradoni, and Z. Peng, "Quantum-assisted combinatorial optimization for reconfigurable intelligent surfaces in smart electromagnetic environments," *IEEE Transactions on Antennas and Propagation*, pp. 1–1, 2023.

[122] C. Ross, G. Gradoni, and Z. Peng, "A hybrid classical-quantum computing framework for ris-assisted wireless network," in *2023 IEEE MTT-S International Conference on Numerical Electromagnetic and Multiphysics Modeling and Optimization (NEMO)*, 2023, pp. 99–102.

[123] J. Shi, T.-T. Chan, H. Pan, and T.-M. Lok, "Reconfigurable intelligent surface assisted semantic communication systems," *arXiv preprint arXiv:2306.09650*, 2023.

[124] P. Jiang, C.-K. Wen, S. Jin, and G. Y. Li, "Ris-enhanced semantic communications adaptive to user requirements," *arXiv preprint arXiv:2307.16100*, 2023.

[125] Y. Wang, W. Yang, P. Guan, Y. Zhao, and Z. Xiong, "Star-ris-assisted privacy protection in semantic communication system," 2023.

[126] H. Du, J. Wang, D. Niyato, J. Kang, Z. Xiong, J. Zhang, and X. Shen, "Semantic communications for wireless sensing: Ris-aided encoding and self-supervised decoding," *IEEE Journal on Selected Areas in Communications*, vol. 41, no. 8, pp. 2547–2562, 2023.

[127] M. Li, B. Yan, and J. Zhang, "Evolutionary multi-objective optimization for ris-aided mu-miso communication systems," *Soft Computing*, vol. 27, no. 12, pp. 8091–8106, 2023.

[128] A. Azizi and A. Farhang, "Ris meets aerodynamic haps: A multi-objective optimization approach," *arXiv preprint arXiv:2301.10682*, 2023.

[129] A. Mohamed, A. Zappone, and M. Di Renzo, "Bi-objective optimization of information rate and harvested power in ris-aided swipt systems," *IEEE Wireless Communications Letters*, vol. 11, no. 10, pp. 2195–2199, 2022.

[130] K. Guo, M. Wu, X. Li, H. Song, and N. Kumar, "Deep reinforcement learning and noma-based multi-objective ris-assisted is-uav-tns: Trajectory optimization and beamforming design," *IEEE Transactions on Intelligent Transportation Systems*, vol. 24, no. 9, pp. 10 197–10 210, 2023.

[131] J. Chen, S. Wang, J. Jia, Q. Wang, L. Yang, and X. Wang, "Multi-objective oriented resource allocation in reconfigurable intelligent surface assisted hcns," *Ad Hoc Networks*, vol. 140, p. 103066, 2023.

[132] J. Chai, Y. Yi, X. He, Z. Xing, Y. Luo, and X. Zhang, "Rate optimization and interference suppression in ris-assisted mimo systems," in *Proceedings of the 2023 10th International Conference on Wireless Communication and Sensor Networks*, 2023, pp. 103–109.